Porous Silicon Carbide (SiC): A Chance for Improving Catalysts or Just Another Active-Phase Carrier?

Giulia Tuci,[#] Yuefeng Liu,[*,#] Andrea Rossin, Xiangyun Guo,[*] Charlotte Pham, Giuliano Giambastiani,[*] and Cuong Pham-Huu[*]

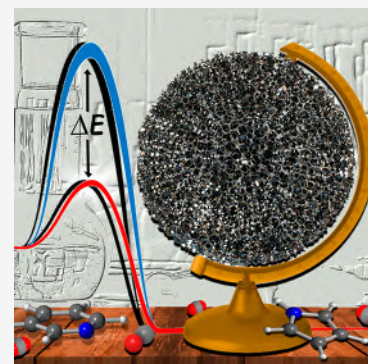Cite This: https://doi.org/10.1021/acs.chemrev.1c00269

Read Online

ACCESS | 📊 Metrics & More | 📖 Article Recommendations

ABSTRACT: There is an obvious gap between efforts dedicated to the control of chemicophysical and morphological properties of catalyst active phases and the attention paid to the search of new materials to be employed as functional carriers in the upgrading of heterogeneous catalysts. Economic constraints and common habits in preparing heterogeneous catalysts have narrowed the selection of active-phase carriers to a handful of materials: oxide-based ceramics (*e.g.* Al_2O_3, SiO_2, TiO_2, and aluminosilicates−zeolites) and carbon. However, these carriers occasionally face chemicophysical constraints that limit their application in catalysis. For instance, oxides are easily corroded by acids or bases, and carbon is not resistant to oxidation. Therefore, these carriers cannot be recycled. Moreover, the poor thermal conductivity of metal oxide carriers often translates into permanent alterations of the catalyst active sites (*i.e.* metal active-phase sintering) that compromise the catalyst performance and its lifetime on run. Therefore, the development of new carriers for the design and synthesis of advanced functional catalytic materials and processes is an urgent priority for the heterogeneous catalysis of the future. Silicon carbide (SiC) is a non-oxide semiconductor with unique chemicophysical properties that make it highly attractive in several branches of catalysis. Accordingly, the past decade has witnessed a large increase of reports dedicated to the design of SiC-based catalysts, also in light of a steadily growing portfolio of porous SiC materials covering a wide range of well-controlled pore structure and surface properties. This review article provides a comprehensive overview on the synthesis and use of macro/mesoporous SiC materials in catalysis, stressing their unique features for the design of efficient, cost-effective, and easy to scale-up heterogeneous catalysts, outlining their success where other and more classical oxide-based supports failed. All applications of SiC in catalysis will be reviewed from the perspective of a given chemical reaction, highlighting all improvements rising from the use of SiC in terms of activity, selectivity, and process sustainability. We feel that the experienced viewpoint of SiC-based catalyst producers and end users (these authors) and their critical presentation of a comprehensive overview on the applications of SiC in catalysis will help the readership to create its own opinion on the central role of SiC for the future of heterogeneous catalysis.

CONTENTS

1. INTRODUCTION

Catalysts are the engines of chemical transformations at the heart of industrial production. Nowadays roughly 85−90% of the chemical products and intermediates are generated with the contribution of at least one catalytic step among the different processes. Hence, catalysts are becoming crucial in almost all sectors of our modern society, and they are indispensable in key areas of our economy and lifestyle: from the bulk production of fine chemicals up to the abatement of pollution in end-of-pipe solutions (automotive and industrial exhaust).[1,2] They are often the key for any green and sustainable process as they can prevent pollution and avoid formation of wastes (unwanted byproducts) with crucial environmental effects. Besides being faced with these fundamental issues, a catalyst offers an energetically favorable path compared to non-catalytic transformations, hence allowing industrial processes to be accomplished under more feasible pressure and temperature conditions.[3,4] However, there are severe technical and economic constraints in catalysis that link catalyst costs to its performance and to the process choice. These constraints imply that a catalyst improvement does not necessarily occur through the development of more challenging systems from a practical viewpoint.[4]

At odds with early heterogeneous catalysts simply based on metal powders, they are now available in the form of structured composites, typically in the form of a highly dispersed catalytically active phase on a carrier (support) featured by medium-high surface area and adequate porosity for efficient mass and heat transfer. Therefore, the control of catalyst composition and size and shape of catalytically active particles, including morphology, composition, and chemical-physical properties of the carrier, become key features to be carefully addressed while searching for improved catalytic materials also in light of their final downstream applications. Through a virtually infinite combination of active phases and supports, the

last decades have witnessed a significant improvement of catalyst performance for many industrially relevant transformations.

Solid carriers for metal nanoparticles in heterogeneous catalysts are commonly selected among inert, macroscopic, and porous matrices. They are expected to play something more than the role of an innocent support for the active phase. Indeed, they should (i) ensure an optimal dispersion and stability of the nanoparticles by favoring preferential metal−support interactions, (ii) avoid the active-phase deactivation by limiting undesired leaching and/or sintering phenomena, and (iii) favor the mixing of reagents and optimize their residence time at the catalyst surface to avoid secondary reactions.[5] In addition, carriers are often required to mitigate the generation of local temperature gradients (hotspots), particularly in highly exothermic transformations where temperature swings at the catalyst bed can permanently compromise its performance and can also pose serious operational security issues.

Nowadays, heterogeneous catalysts are essentially based on a few different carriers mainly inorganic in nature such as refractory metal(s) oxides in their higher oxidation state (e.g. Al_2O_3, SiO_2, TiO_2, and aluminosilicates−zeolites)[6] and carbon in its most representative allotropic forms (activated charcoal, 1D and 2D nanocarbons, and their hierarchical composites).[7−11] Properties of these commercial carriers as such or in the form of doped samples with a variety of promoters have been widely celebrated within an impressive number of original papers and review articles that highlighted their roles in modern heterogeneous processes. The systematic improvement of their chemicophysical and morphological properties has finally contributed to their widespread application over different branches of catalysis. On the other hand, much less attention has been paid to the search of new functional carriers. Except for those listed above, it can be assumed that the number of commercialized active-phase supports from the mid-20th century up to date is quite limited in number and in nature.

At odds with more common refractory inorganic oxides, carbon and nanocarbons join relatively high specific surface areas to good thermal and electrical conductivity that have made them highly attractive active-phase supports within a relatively wide range of (electro)catalytic transformations. Moreover, their thermal conductivity has often been exploited to prevent or mitigate the formation of local temperature gradients at the catalyst bed in highly exothermic processes. However, nanocarbons suffer from technical limits that have deeply affected their practical exploitation as solid supports in catalysis. Indeed, classical nanocarbons are typical mesoporous materials with a prevalent powdery texture. This feature together with the presence of high micropore fractions in specific C networks (e.g. activated carbon)[12,13] is often at the origin of a poor diffusion of reagents and intermediates through the catalyst bed, particularly in packed-bed reactors where pressure-drop phenomena can occur and where a prolonged product residence time within the catalytic bed may result in process selectivity loss. Moreover, the essentially powdery texture of nanocarbons raises health and environmental issues,[14] other than posing serious drawbacks in terms of materials handling and transportation. Hierarchically structured C-based composites allow for combining nanosized carbons in macroscopically shaped host matrices.[15] If this approach has allowed overcoming several limits in the use of carbon-based materials in catalysis, their low resistance to

Chart 1. (A) Statistical Analysis of SiC-Based Contributions which Have Appeared Globally in the Last Four Decades (Turquoise Histograms) in Comparison with Catalysis-Related Issues (Green Histograms) in the Same Period and (B) Statistical Analysis of SiC-Based Contributions in Catalysis (Green Histograms) which Have Appeared in the Last Four Decades (and Reviewed in This Manuscript) along with the Distinction between SiC-Based Catalysts Where the Support Is Claimed to Be Innocent (Yellow Histograms) or Non-innocent (Red Histograms) in the Process[a]
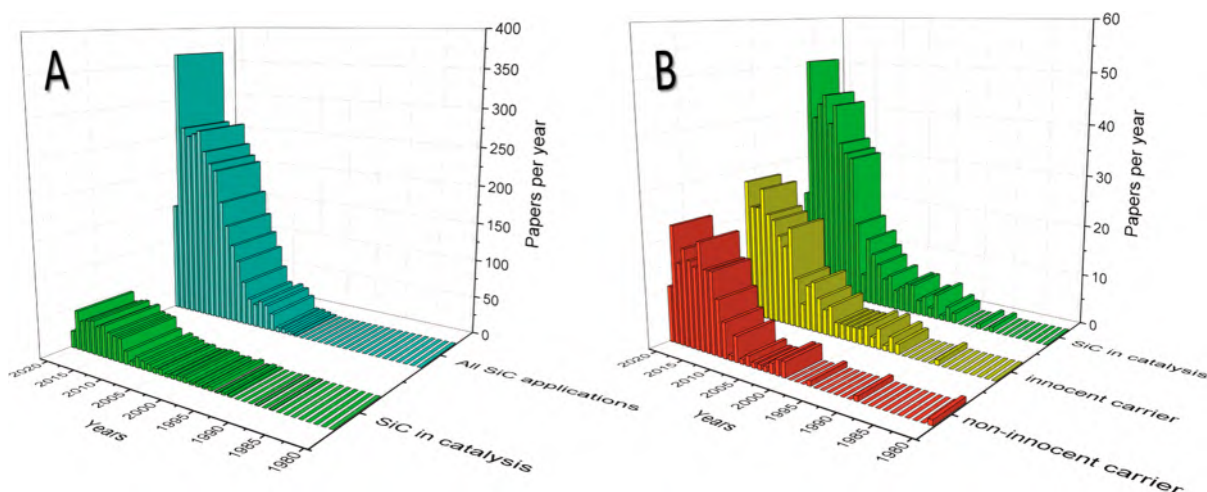
[a]Data from Web of Science (May 2021) adapted on the basis of the analyses reported hereafter.

oxidative conditions still narrows their application range. Anyway, carbon-based supports are managed under low-temperature conditions or inert/reductive atmosphere preferentially.

From all these considerations, it can be inferred that a good candidate support for catalysis should combine high chemical inertness to a (meso)porous macroscopic shape, a relatively high specific surface area, a good thermal conductivity, and a high oxidation resistance together with enough anchorage sites for the dispersion and stabilization of deposited active phases.

Silicon carbide (SiC) joins unique chemicophysical properties, such as hardness and mechanical stability, at high temperatures to a good thermal conductivity and a low coefficient of thermal expansion.[16] Its high resistance to corrosion and oxidation together with a tunable surface area featured by a prevalent meso-/macroporous character makes it an ideal alternative to classical supports within a number of catalytic transformations. The absence of micropores in SiC is particularly useful for catalytic processes where the limited diffusion of reagents, intermediates, and products may compromise the success of the process, *i.e.* fast gas-phase and liquid-phase reactions.[17] With few exceptions that will be discussed in the last section of the present review (section 4) and apart from the semiconductor nature of these non-oxide materials that makes them highly attractive samples already as such in photocatalysis, SiC chemical inertness is likely its most distinctive feature. Therefore, to exploit the fluid dynamic and structural advantages of their porous structures in heterogeneous catalysts, the generation of catalytically active sites at the SiC outer surface is generally required.[18]

Although a full account on the exploitation of these non-oxide ceramics in all their potential fields of application is really hard to address (particularly in a thematic contribution focused on catalysis), a statistical analysis on the SiC-based scientific contributions of the last three decades leaves little doubt on the steadily growing interest of the scientific community for these materials. Chart 1A (turquoise histograms) illustrates the exponential growth of publications (*i.e.* research articles,

proceedings papers, and book chapters) which have appeared in the literature and were collected from the Web of Science database in the 1980−2021 period. More than 2000 contributions have been quoted globally on SiC-based nanotechnologies, with research articles being the primary source of this statistical distribution with more than 1800 contributions (*ca.* 90%).

Green histograms (Charts 1A and 1B) illustrate the trend of SiC-based contributions in catalysis, that cover to date about 27% of the global scientific production on the SiC topic and are entirely reviewed in this contribution. Based on our scientific journey across the different applications of SiC networks in catalysis, Chart 1B also takes into account important features linked to the unique chemicophysical properties of SiC networks (*e.g.* high thermal conductivity, wide band gap) that identify SiC as an "*active player*" (red histograms) in the catalytic process rather than simple inert carriers (yellow histograms) of the umpteenth active phase. These statistical distributions (based on the experimental evidence and conclusions outlined in the papers reviewed within this manuscript) well rate the relevance and the urgency of a comprehensive contribution on the topic that offers to the catalysis community the appropriate hints to look beyond the current *state of the art*.

Accordingly, this review article aims at providing a comprehensive overview on the use of macroporous/mesoporous SiC materials, featuring from medium (10 to 70 $m^2 \ g^{-1}$) to high (400 to 650 $m^2 \ g^{-1}$) specific surface area as active-phase supports for heterogeneous catalysis. Although many seminal contributions on processing methods for the preparation of porous SiCs[19−26] have already been issued, only a few and short reports account for their application in catalysis.[17,27−29] Therefore, we will focus on the unique features of SiC samples for the design of efficient, cost-effective, and easy to scale-up catalytic materials. The manuscript will outline the success of many SiC-based heterogeneous systems where the use of other and more classical supports provided modest outcomes or even failed. It

will unveil how the rational choice of SiC as the support for the catalyst active phase ensures better stability to the latter and provides higher selectivity to the process, while reducing the environmental impact.[30] All SiC applications will be reviewed from the exclusive perspective of a given chemical reaction with the aim at highlighting all improvements rising from the use of SiC in terms of activity, selectivity, and process sustainability. A conclusive outlook will summarize the impact that a rational use of SiC materials has given to catalysis while sharing our personal opinion about the role that these non-oxide networks will have in the heterogeneous processes to come.

2. SILICON CARBIDE PROPERTIES: AN OUTLOOK IN BRIEF

SiC is a compound of Si and C in a 1:1 stoichiometry ratio. In an *on carborundum* conference proceeding presented at the World's Congress on Chemistry (Chicago, USA−1893) and published in *JACS*,[31] Otto Mühlhaeuser claimed that "*It is an American invention, having been discovered by Edward H. Acheson, of Monongahela City, Pennsylvania, who carried the invention to commercial success with extraordinary energy in the face of many obstacles*".[32] Before that time, SiC was never found on the Earth, although more recent studies on the composition of the interstellar dust leave little doubt on its presence on our planet a long time before the Acheson discovery. Evidence for the SiC presence in the cosmic space has been spectroscopically provided since the late 1970s.[33,34] Recent studies have also claimed its role in the comprehension of the prebiotic roots of life with its active participation in the abundant production of organic molecules (*i.e.* polycyclic aromatic hydrocarbons) present in the interstellar space.[35]

Undoubtedly, Acheson himself was the first who realized the importance of his discovery, and he devised a process for the commercial production of SiC (Acheson named it carborundum), whose essential features are still unchanged nowadays. α-SiC synthesized at high temperature (>1600 °C) through the Acheson process was initially appreciated for its hardness as an ideal grinding and cutting material.[36] The discovery of other distinctive chemicophysical properties of this non-oxide material (*i.e.* its high thermal conductivity, excellent thermal stability, superior stability toward oxidation compared with carbon, high mechanical strength, and chemical inertness) rapidly consolidated its use across several engineering applications:[20] from diesel particulate filters,[37,38] to solar radiation receivers,[39] porous burner systems,[40,41] molten-metal and industrial hot-gas filters,[20] or substrates for the creation of ordered organic-semiconductor interfaces to be applied from sensor technology and nanolithography up to molecular electronics,[42] just to mention a few.

As far as SiC mechanical properties are concerned, they largely depend on the sample porosity, pore size, and microstructure and on the processing/manufacturing method (*vide infra*) used to produce the SiC phase. Several review contributions which have appeared in the last two decades have pointed out the role of material porosity and SiC processing strategy on flexural or compressive strengths and fracture toughness of these ceramics.[22,25,43−45] As expected, the mechanical properties generally worsen with the increasing sample porosity; both strength and fracture toughness vary significantly with the manufacturing method and nature of additives employed for the SiC production. As an example, an excellent flexural strength of 152 MPa was obtained on a SiC

sample at 65% porosity, fabricated by the partial sintering technique (see section 2.2).[46] Depending on the processing parameters applied throughout the same manufacturing technique, the flexural strength for a SiC sample featured with a similar porosity (67%) can however drop down to 5.2 MPa (values measured at room temperature).[47] It is generally observed that the higher the SiC sample composition purity the higher the temperature value at which the sample flexural strength can be entirely retained.[25] The analysis of fracture toughness data for various SiC ceramics prepared via different processing techniques (see section 2.2) leads to the same conclusions as those reported above for flexural and compressive strengths. In particular, the fracture toughness generally decreases with increasing SiC porosity; for samples with similar porosity values (*i.e.* in the 40−70% range), the fracture toughness depends on the manufacturing method used for SiC production.[25] Silicon carbide thermal properties are also related to the material porosity and its ultimate manufacturing method. The introduction of porosity decreases the ceramic thermal conductivity (κ) whose corrected value (κ_c) is estimated from the experimentally measured one (κ_m) and the volume fraction of void (V_d) according to the following equation:[48]

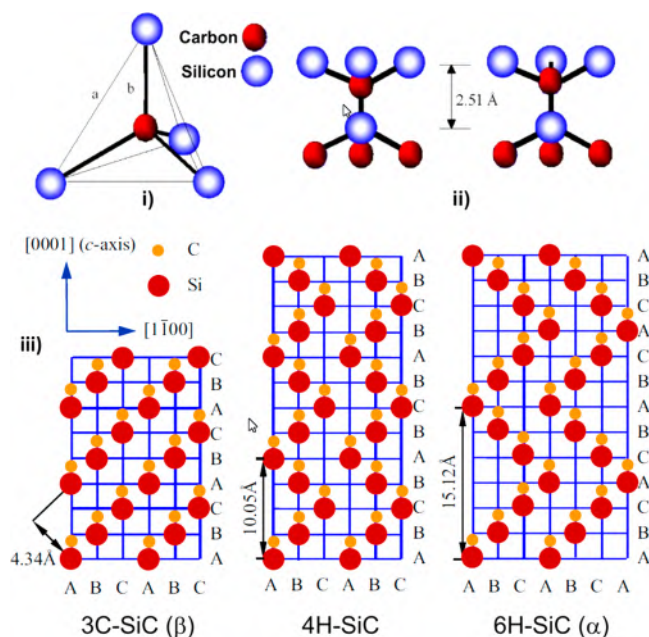$$\kappa_c = \kappa_m \left(\frac{1 + V_d}{1 - V_d} \right) \qquad (1)$$

Anyhow, other factors can deeply influence this important physical property: the choice of the manufacturing method (the use of sintering additives[49] in particular) can vary or even invert the general thermal conductivity trend based on the ultimate material porosity.

In spite of these challenging features, α-SiC prepared through the Acheson process possessed very low specific surface area (*i.e.* few square meters per gram) thus narrowing its potential application fields, especially as supports for application in heterogeneous catalysts. Only in the late 1980s, Ledoux and co-workers described the gas−solid synthesis for the preparation of porous β-SiC samples featured by medium-high specific surface areas, hence officially opening to their full exploitation as carriers for catalytically active phases.[50,51] The superior chemical inertness and resistance to aggressive media of SiC were well-known already at that time.[27,50] Lacroix and co-workers showed that the integrity of SiC extrudates was totally preserved after a long time exposure (up to 3 weeks) to harsh and oxidative chemical environments (HF 40%, HCl 37%, HNO$_3$ 68%, and NaOH 40%) where traditional catalyst supports (*i.e.* Al$_2$O$_3$, SiO$_2$, or carbon) were irremediably corrupted or even dissolved.[52] Such a feature holds important advantages for the use of SiC in catalysis. For instance, the treatment of spent SiC-based catalysts with aggressive and oxidative reagents can be used to remove the deposited active phases, hence allowing the recovery and reuse of the pristine supports. Active phases can also be recovered by a suitable chemical treatment of washing solutions. The chemical inertness of SiC also prevents undesired interactions−often encountered with classical oxide-based (*i.e.* Al$_2$O$_3$ and SiO$_2$) carriers−between active phase and support. Such solid−solid interactions are often responsible for an incomplete control of the nature, electronic properties, and oxidation state of deposited metal active phases due to the formation of complex metal aluminates or silicates at the materials interface.[53,54] The high mechanical strength of SiC

finally allows the preservation of the catalyst body during catalysis, avoiding drawbacks often encountered with lower mechanical resistant supports such as Al_2O_3 or SiO_2.[55,56] Other structural features of SiC, including its main manufacturing techniques, have systematically been addressed in a number of seminal papers, books, and review articles during the last few years. Although a complete account on these aspects is certainly out of the scope of the present contribution, the following section provides a summary of these fundamentals along with an appropriate quotation of the most relevant literature issues which have appeared so far.

2.1. SiC Polytypes

One main feature of SiC crystal structures is their existence under different polytypes.[45,57] SiC crystal units are made of covalently bonded (the nature of the bond is actually 88% covalent and 12% ionic) tetrahedral SiC_4 and CSi_4 moieties that originate different one-dimensional ordered sequences.[58] Different orientations of adjacent tetrahedrons generated by the various translations and rotations of SiC high-symmetry space groups give rise to various stacking sequences or polytypes[59] of Si–C bilayers along the c crystallographic axis (Figure 1). More than 200 SiC polytypes have been described

up to date, some with a stacking period of hundreds of bilayers.[60] The most common ones include 3C, 4H, 6H, and 15R-SiC polytypes, where (C), (H), and (R) account for the three basic cubic, hexagonal, and rhombohedral crystallographic categories, while numerical values refer to the number of layers needed to repeat the pattern[61] (Figure 1). In the face-centered cubic 3C-SiC, Si and C occupy ordered sites as in a diamond lattice. In hexagonal (nH-SiC) polytypes, C and Si layers stack in the primitive unit cell.[62] Because of the great variety of SiC polytypes, it is a normal practice to refer to cubic nC-SiC structures as β-SiC, while all noncubic ones (nH-SiC and nR-SiC) are conventionally classified as α-SiC. SiC polymorphs show similar mechanical and thermal properties but distinct band gap energies and electronic features (Table 1). In particular, at odds with other common semiconductors,[63] the band gap varies significantly with polytypes ranging from 2.4 eV for 3C-SiC to values above 3 eV for 4H and 6H polymorphs. The wide band gap makes SiC a very attractive semiconductor for optoelectronic devices,[64] while β-SiC is identified as a suitable visible-light absorption material for photocatalytic applications.
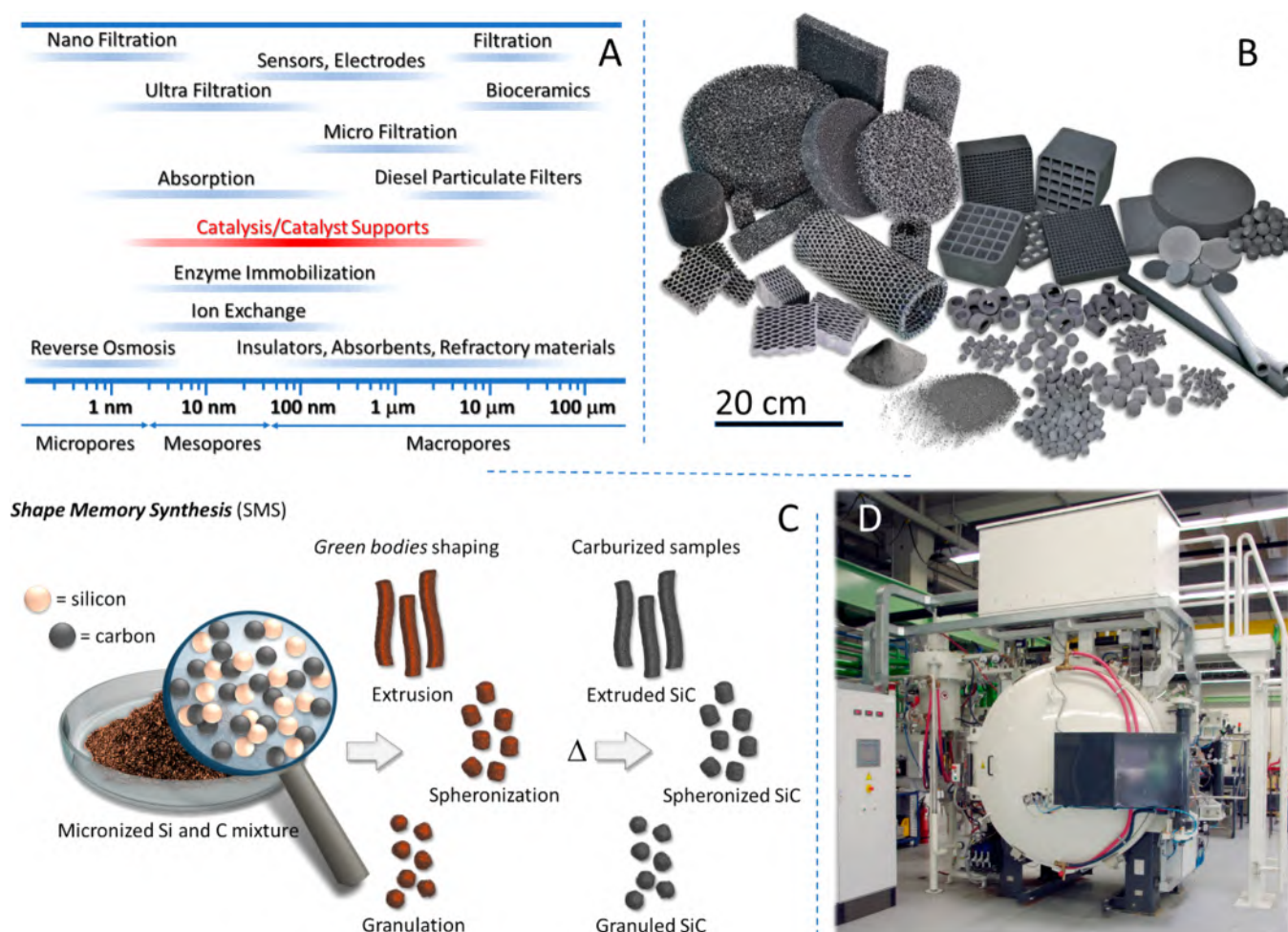
2.2. Manufacturing Methods for Porous SiC Supports

Since the pioneering Acheson process where silica sand and petroleum coke were processed together at very high temperatures (>1600 °C),[69] many other methods have been described for the preparation of large quantities of SiC powders with a variable degree of purity and polytype control. Various synthetic methodologies for the manufacturing of macroporous (with pores larger than 50 nm)[24,25] and mesoporous (with pores ranging from 2 to 50 nm)[24] SiC materials have been developed for specific applications (Figure 2A). All these protocols and their successive improvements have also been extensively reviewed in various book chapters.[26,62]

The use of hard sacrificial templates (e.g. activated charcoal or mesoporous silica) for the replication of nanoscale structures in mesoporous SiCs has sparked excellent outcomes in the field. Disordered mesoporous SiC were originally prepared using gas-phase infiltration techniques. Ledoux et al. first reported in the late 1980s on the preparation of mesoporous SiC samples with relatively high surface area ($\approx$100 m^2 g^{-1}) by reaction of the *in situ* generated gaseous SiO with activated charcoal at temperatures ranging from 1200 to 1500 °C (*shape-memory synthesis method*–SMS).[17,50,51] After successive modifications/improvements, SMS is nowadays the only synthetic method operating on an industrial scale[70] for the tons scale production of mesoporous β-SiC with controlled macroscopic shapes (*i.e.* extrudates, beads, structured foam, tubes–Figure 2B). In brief, SMS makes use of a stoichiometric mixture of micronized (<20 μm) silicon and carbon (carbon black and/or high carbon yield binder/resin–Figure 2C).

Figure 1. (i) Basic unit cell of silicon carbide and (ii) 180° rotated configurations of Si–C atoms. Reproduced with permission from ref 58. MDPI, Basel, Switzerland 2016 under [CC BY license 4.0] [https://creativecommons.org/licenses/by/4.0/]. (iii) Stacking sequence of three SiC polytypes: A denotes the first layer of atoms, while the next layers sit on position B or C. Adapted with permission from ref 43. Copyright 2015 Elsevier Ltd.

Table 1. Selected Physical and Mechanical Properties for the Most Representative SiC Polytypes

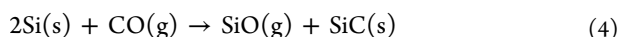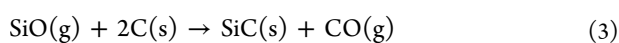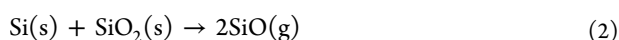| SiC polytype	peritectic decomposition temp @ 35 bar (K)[65]	thermal conductivity[66] @ 300 K (W m^{-1} K^{-1})	specific heat capacity[67] @ 300 K (J kg^{-1} K^{-1})	coeff of linear thermal expansion ×10^6 @ 300 K (K^{-1})	thermal diffusivity[66] (cm^2 s^{-1})	density[26] (g cm^{-3})	bulk modulus[66] @ 300 K (GPa cm^{-2})	band gap energy @ T < 5 K (eV)[45]
3C-SiC (β)	3100 ± 40	360		3.8[66]	1.6	3.2	250	2.40
4H-SiC	3100 ± 40	370			1.7	3.2^a	220	3.26
6H-SiC (α)	3100 ± 40	490	690	4.3[68]	2.2	3.2	220	3.02

^{a}Measured at 300 K.

Figure 2. (A) Typical application fields of micro-, meso-, and macroporous SiC matrices. (B) Digital photo of porous β-SiC samples produced through the gas–solid synthesis method. Reproduced with permission from ref 70. Copyright 2021 SICAT Sarl. (C) SMS method for the manufacturing of mesoporous SiC networks. (D) Industrial furnace for the carburization process with a 40 Mt production capacity per year. Reproduced with permission from ref 70. Copyright 2021 SICAT Sarl.

Other binders such as methyl cellulose, polyvinyl alcohol, polyethylene glycol, and silica sols can be also added to the solid mixture.[27]

The mixed solids are then shaped into "green bodies" using standard technologies such as extrusion, spheronization, and granulation. The as-processed materials are dried at room temperature before being submitted to a carburization process (Figure 2D) under an inert gas flow at ≈1400 °C, below the silicon melting point (1410 °C). At temperatures higher than 1000 °C, silicon reacts with residual traces of oxygen present in the raw materials to generate gaseous SiO (eqs 2 and 4) that further reacts with carbon to form SiC (eq 3). CO generated during the process carburizes in turn the residual silicon to form gaseous SiO and SiC (eq 4). During this treatment, the high carbon yield resin is converted into amorphous carbon binding carbon black and micronized silicon powder together.

$$Si(s) + SiO_2(s) \rightarrow 2SiO(g) \tag{2}$$

$$SiO(g) + 2C(s) \rightarrow SiC(s) + CO(g) \tag{3}$$

$$2Si(s) + CO(g) \rightarrow SiO(g) + SiC(s) \tag{4}$$

Porous carbons derived from biomass have also been employed as sacrificial templates to prepare porous SiC.

Biomass materials, such as agricultural grains, woods, and others, have formed optimized and hierarchical microstructures during the long-term natural evolution, and these optimized microstructures are favorable to the transmission of water and mineral substances.[71] Through different carbonization and subsequent siliconization processes, woods and agricultural grains such as millet, durra, and lotus root have been converted into biomorphous SiC samples.[72−74] The latter retain the initial morphologies and porous structures of biomass carbons and thus show interesting application as a catalysts supports.

Other relevant methods for the pore-size controlled preparation of mesoporous SiC samples have been successfully proposed since the beginning of this century. In particular, the sol−gel process has prevailed as a promising technique for the fabrication of tailored SiC nanostructured materials.[75−77] This technique and its successive modifications[78] have been carefully described by Guo and co-workers for the first time. They prepared nanostructured and mesoporous β-SiC samples starting from an ethanol solution of phenolic resin and nickel nitrate. In a typical procedure, tetraethoxysilane (TEOS) and oxalic acid were added into the ethanol solution in sequence to form a binary carbonaceous silica gel. Afterward, the gel was aged and dried at 100 °C to acquire a xerogel that underwent
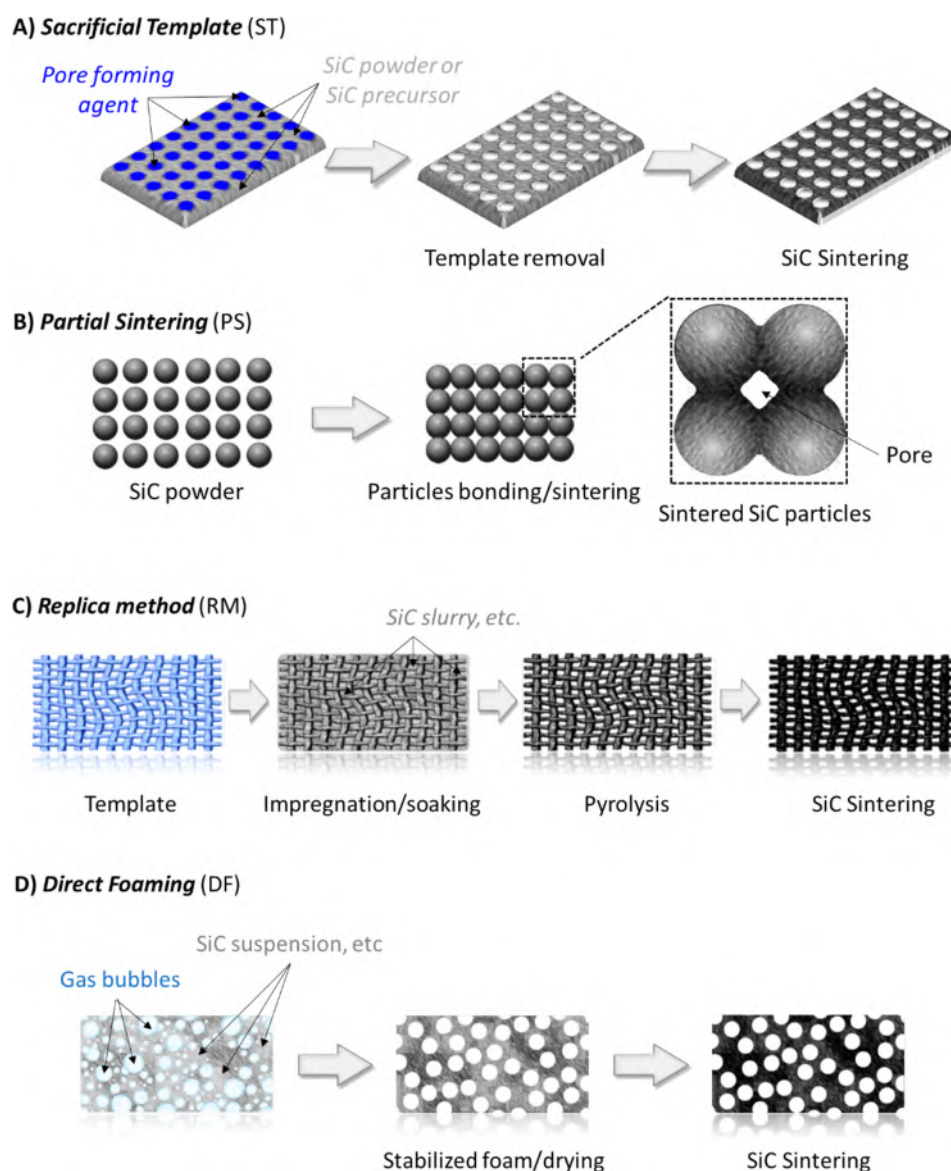
Figure 3. Main manufacturing processes for SiC macroporous networks.

heating at 1250 °C under inert atmosphere and purification by removal of residual carbon, silica, and other impurities.[78]

Another embodiment of the general sol−gel process can generate ordered mesoporous SiC carbide (OMSiC) structures exhibiting specific surface areas of 600−900 m^2/g and mesopore volumes up to 0.9 cm^3/g.[79] Such products are obtained via the formation of ordered mesoporous xerogels composed of SiO$_2$-carbon nanocomposites prepared by evaporation-induced self-assembly from a formulation comprising a phenolic resin as the carbon precursor, prehydrolyzed tetraethyl orthosilicate as the silicon precursor, and a triblock copolymer as surfactant. The xerogel is then converted into OMSiC by thermal treatment under argon at 1300 to 1600 °C.

Disordered mesoporous SiCs were also prepared via carbothermal reduction between MCM-48 silica and pyrolytic carbon[80] or by chemical vapor infiltration (CVI) of a gaseous SiC precursor into nanoporous SBA-15 silica.[81] These high-temperature processing methods gave rise to mesoporous SiC samples featuring surface areas even beyond 500 m^2 g^{-1}. Ordered mesoporous SiC samples were obtained by nano-casting polycarbosilane (PCS) on various silica templates (*i.e.*

SBA-15 and KIT-6), followed by pyrolytic etching of the latter (templating methods). All these approaches produced excellent results leading to ordered mesoporous networks in the form of inversed replica with respect to their silica templates and featured by remarkably high surface areas (up to 720 m^2 g^{-1}), large mesoporous volumes (*ab.* 0.8 cm^3 g^{-1}), and narrow pore-size distributions (2.0−3.7 nm).[82,83] Despite these excellent merits, SiC networks prepared from silica templates suffer from a relatively high degree of oxygen contamination (*i.e.* Si-oxycarbide species−SiC$_x$O$_y$) whose presence can count against their high-temperature applications. Moreover, they are prepared in the form of powders like the sacrificial templates they derive from, and this morphology makes them less attractive for any further industrial development. Accordingly, oxygen-free sacrificial templates such as mesoporous carbon remain the most promising candidates for preparing pure mesoporous SiCs.

Macroporous SiC networks hold the great advantage of reducing pressure drop phenomena whenever engaged as catalyst supports. Accordingly, they have received a great deal of attention during the last decades for application in catalysis.

A short summary on the main manufacturing techniques along with their schematic representation (Figure 3) has been reported hereafter for the sake of completeness. Each technique is specifically conceived for producing SiC samples with a controlled porosity (range of pore sizes and volume porosity).[22,24,25,44]

The *Sacrificial Template* (ST) method is one of the main approaches pursued to prepare macroporous SiC samples with ordered arrays and is featured by narrow pore size distributions.[24] It consists of mixing an appropriate template (*e.g.* synthetic and natural organics, liquids, salts, metals, and ceramics) as a pore-forming agent with a given SiC precursor. The method generates porous samples in the form of a negative replica of the sacrificial template once the latter is chemically or thermally etched off (Figure 3A). The great variety of pore-forming agents scrutinized within this method has led to the synthesis of SiC materials with an extremely wide variety of pore volumes.

Partial Sintering (PS) is another manufacturing method to acquire porous SiC samples starting from compact SiC powders.[22,25,84] Forming pressure, sintering temperature, and time along with the size of starting SiC grains control the ultimate sample porosity and pore size (Figure 3B). Here, powder grains are bonded through surface diffusion or evaporation−condensation paths enhanced by pressure and heat treatment. It is generally assumed that partial sintering gives rise to porous SiC samples with a pore size two to five times smaller than that (geometrical) of the starting raw SiC grains. Porosity of samples obtained by partial sintering is generally lower than 50%.

Macroporous, open-cell SiCs of high-volume porosity (>90%) and cell sizes ranging from hundreds of nanometers to millimeters are prepared by the *Replica* method (RM).[22,23,25] The latter consists of the impregnation of a porous template (typically a polyurethane sponge) with a ceramic slurry or a solution of a SiC precursor, followed by template pyrolysis and sintering of the ceramic layers (Figure 3C).

The *Direct Foaming* (DF) technique allows obtaining highly porous SiCs with porosity even higher than 95%.[22,23,25,85] Samples are prepared by bubbling gases (stabilized by surfactants) within ceramic suspensions that are in turn dried and sintered for consolidating the porous SiC matrix (Figure 3D). Pore sizes of the networks produced by this technique can range from dozens of μm to several mm depending on how rapidly and effectively the surfactant controls bubble coalescence phenomena.

Alternative routes to those listed above,[22,25,44,86] aimed at tailoring composition and microstructure of the porous SiCs, have contributed to these widespread materials throughout various technological areas, hence boosting their commercialization as catalytic supports, lightweight porous structures, and even biological scaffolds. Recent advances in 3D printing technologies have enabled the digital fabrication of porous scaffolds in the form of lattices, cellular structures, and foams across multiple length scales (from macroscopic dimensions down to the nanoscale). 3D printing technology is a real breakthrough toward the fast and tailored manufacturing of 3D hierarchical sacrificial templates[87,88] with porosity at the nano-, micro-, and macroscale to be employed for the bulk production of porous SiC samples exhibiting complex geometries and multiscale porosity inaccessible thus far.

3. CATALYTIC APPLICATIONS

Porous SiC materials have received a great deal of attention from the scientific community; their excellent thermal and chemical stability make them ideal candidates as supports for metal nanoparticles in heterogeneous catalysis. In addition, their large specific surface area and suitable band gap ($\sim$2.4 eV for β-SiC) have unveiled excellent properties in a number of key applications at the heart of renewable energy technology.

The following sections will provide an exhaustive overview on the main outcomes of SiC and its composites in heterogeneous catalysis. It will be a journey toward the use of SiC nanostructures in catalysis for the production of fine chemicals, synthetic fuels, as well as catalytic remediation tools for environmental protection. The performance of this non-oxide material will also be compared with more conventional conductive and non-conductive catalyst supports in a number of industrially relevant catalytic transformations. Besides providing a full account on the current *state of the art* of SiC structures in catalysis, this review article aims at highlighting the inherent potentiality of SiC to stimulate the search for new future applications. Hopefully, the reader will have an answer for our title question: *SiC, a chance for improving catalysis or just another active-phase carrier?*

3.1. Synthesis of Fine Chemicals

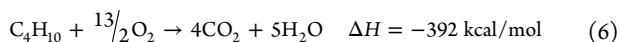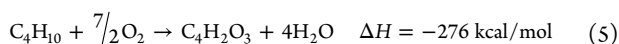**3.1.1. Oxidation Reactions.** *3.1.1.1. Alkanes Oxidation.* The controlled oxidation/dehydrogenation of saturated hydrocarbons is one of the main chemical routes of great relevance from an industrial viewpoint applied to the production of commodities and intermediates for chemical manufacturing. The high thermal conductivity, resistance to oxidation, high mechanical strength, and chemical inertness of SiC supports along with their relatively high surface area have made them very attractive tools within a number of exo- and endothermic oxidation protocols. Harlin, Ledoux, and co-workers reported on the use of SiC-supported C-modified MoO_3 for the *n*-butane dehydrogenation (DH) to C_4-alkenes.[89] They showed the SiC-supported catalyst exhibited stable butane conversion and DH selectivity to 1-butene/2-butene (20% and 70%, respectively), where the use of unsupported MoO_3 (in bulk) failed. Indeed, they showed that a progressive sintering of the unsupported active phase would have led to the rapid catalyst deactivation. A comparative study between MoO_3/SiC and Al_2O_3- or SiO_2-supported MoO_3 counterparts has finally unveiled the better performance of the former in terms of process selectivity (C_4 products) and reduced catalyst coking. Given the thermodynamic inertness of hydrocarbons, temperatures over 773 K are generally required for the process to occur. Under these conditions, the acid character of oxide supports (responsible for a higher catalyst coking degree) along with their poor thermal conductivity (responsible for a higher degree of sintering phenomena of the active phase) has highlighted the key advantages of SiC matrices as MoO_3 supports in a classical endothermic oxidation process. Later, Cao, Li et al. described a sol−gel approach to the preparation of mesostructured SiC matrices featuring relatively high surface areas (151−345 m^2 g^{-1}) along with their vanadia composites. These hybrids were tested in the oxidative (and highly exothermic) propane dehydrogenation (PODH), exhibiting higher selectivity to propylene than those obtained with conventional supports such as Al_2O_3 and SiO_2 (at the same propane conversion level).[90] The authors realized that the outstanding thermal conductivity of the SiC network was at the
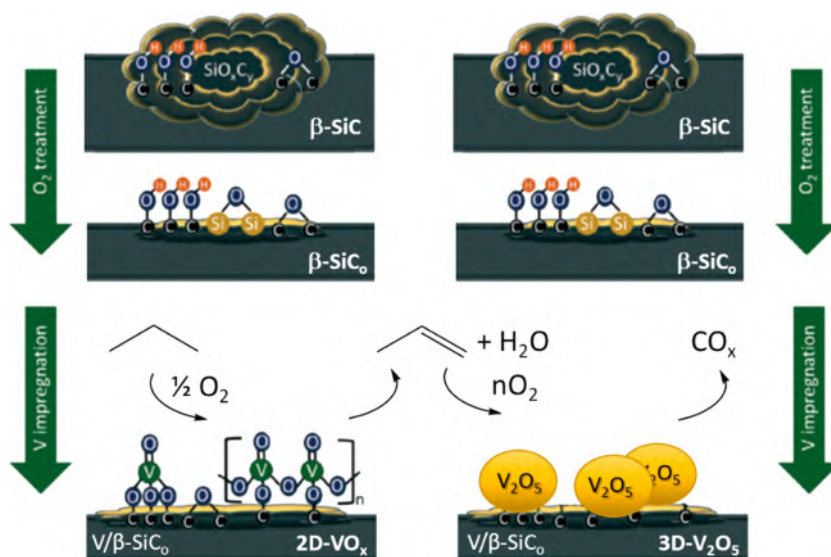
Figure 4. Two steps, nonuniform VO_x covering of preoxidized β-SiC with the formation of surface islands that represent the effective anchoring SiC surface areas for the 2D or 3D VO_x chemical grafting and their behavior in the PODH. Adapted with permission from ref 102. Copyright 2017 The Royal Society of Chemistry.

origin of its better performance. Indeed, it was supposed that the SiC support could better dissipate the heat generated from the reaction, hence avoiding local temperature gradients (hotspots) and limiting the occurrence of undesired propylene overoxidation paths. Ledoux and co-workers described another example of β-SiC-supported vanadyl pyrophosphate [VPO, $(VO)_2P_2O_7$, 30 wt %] for the direct and highly exothermic oxidation of n-butane (C_4H_{10}) to maleic anhydride (MA, $C_4H_2O_3$) (eq 5).[91]

$$C_4H_{10} + \frac{7}{2}O_2 \rightarrow C_4H_2O_3 + 4H_2O \quad \Delta H = -276 \text{ kcal/mol} \quad (5)$$

$$C_4H_{10} + \frac{13}{2}O_2 \rightarrow 4CO_2 + 5H_2O \quad \Delta H = -392 \text{ kcal/mol} \quad (6)$$

The authors claimed the superior performance of their β-SiC composite compared to the unsupported (bulk) VPO in terms of selectivity and yield of MA. If the relatively high surface area of β-SiC (>20 m^2 g^{-1}) was supposed to ensure a good dispersion of the active phase, its inherent thermal conductivity was thought to reduce the formation of hotspots at the catalytic sites, hence preventing the undesired MA over-oxidation (eq 6). VPO samples supported on SiC for the selective n-butane oxidation to MA have also been reported recently by Shcherban and co-workers. These authors claimed an appreciable reduction of the reaction temperature of their SiC composites (up to 70 °C) along with an almost twice increase of MA produced in the process and a much higher reaction rate compared to the catalytic process where the bulk VPO was used as the catalyst.[92]

Lu and co-workers described the selective propane oxidation to acrolein (C_3H_4O, ACR) with a series of metal oxides supported on SiC and doped with phosphorus (P).[93] These authors realized that P-doping of $MoTe_{0.15}V_{0.1}O_n/SiC$ catalysts favored the propane activation by fostering its methylene-H abstraction and O insertion according to the Mars van Krevelen mechanism.[94] They demonstrated that Mo-$Te_{0.15}V_{0.1}P_xO_n/SiC$ with $x = 0.05$ gave ACR selectivity up to 33.7% and yield of 10.7%. P-doping was claimed to increase the surface catalyst acidity in a controlled manner and made the redox process easier. Most importantly, they found that the

neutral character of the SiC carrier overcame the catalyst coking phenomena classically encountered with more common metal oxide (and more acidic) supports (i.e. SiO_2, Al_2O_3, and TiO_2),[95−97] whose acidic strength was also supposed to inhibit the oxidation of the reaction intermediates.

Ceramic catalytic microreactors composed of a β-SiC monolith as support for complex multicomponent MoVTeNbO oxides (as active phases) were prepared and tested as catalysts for two highly exothermic processes: the oxidative ethane dehydrogenation and propane ammoxidation.[98] Previous studies aimed at supporting selected crystalline phases of MoVTeNbO (orthorhombic M1 or pseudohexagonal M2) on classical metal oxides (i.e. Al_2O_3, SiO_2, TiO_2, or Nb_2O_5) revealed all the limits of these refractory oxides in terms of surface acidity and low/null thermal conductivity (carrier inhibition effects).[99,100] The authors' choice for SiC as support was dictated by its chemical inertness along with its high thermal stability and conductivity, porosity, and mechanical strength that made it an ideal active-phase carrier for light alkane oxidation or ammoxidation reactions. Indeed, its thermal conductivity (for radial temperature distribution) allowed a precise temperature control inside the catalytic bed, avoiding or mitigating the occurrence of detrimental temperature gradients. At the same time, the open-cell structure and high porosity of selected SiC supports allowed the prevention of pressure drop phenomena at the catalytic bed while maintaining a high diffusivity to both reactants and products throughout the reactor. Catalytic reactors were obtained by the dip-coating technique of MoVTeNbO on SiC foams using one or two active-phase deposits. Materials characterization showed that a one-layer coating contained mainly the M2 phase, whereas a two-layer coating presented a significant amount of both M1 and M2 phases. While M1 was supposed to be more efficient for the ethane oxidative dehydrogenation, a M1+M2-phase mixture was thought more suitable for the propane ammoxidation reaction.[101] The M1/M2 synergistic effect was explained as the M1 action for propane conversion to the intermediate propene followed by its subsequent readsorption on the M2 phase where it was selectively

converted to acrylonitrile. Despite these preliminary results, where only moderate improvements were achieved in terms of product selectivity and conversion compared to the use of pure M1 and M1 + M2 powdered phases, the study has given an important boost toward the preparation of microreactors and to the large-scale industrialization of both key oxidation processes.

More recently, Hermans and collaborators described the functionalization of "preoxidized β-SiC" (β-SiC$_o$) samples with medium specific surface area ($\approx$30 m^2 g^{-1}), by means of two-(2D) and three-(3D) dimensional vanadium oxide (VO$_x$) deposits.[102] Their attempts to prepare a 2D VO$_x$ coating on pristine β-SiC failed even at low V content; only V$_2$O$_5$ NPs (3D deposits) were obtained. This result revealed the absence of suitable surface anchoring sites on pristine β-SiC as to ensure an appropriate 2D growth of VO$_x$ species. The morphology of the latter and their relative abundance at the catalyst surface were known to control the activity and selectivity of supported VO$_x$ in the oxidative propane dehydrogenation (PODH). The authors found that C−OH groups in the preoxidized SiCs (instead of presumed Si−OH moieties) were directly engaged in the covalent anchoring of VO$_x$ (Figure 4).

Most importantly, they succeeded in controlling the maximum V content at which the β-SiC surface was nonuniformly coated but purely contained two-dimensional monomeric and/or polymeric VO$_x$ species. Their catalytic trials revealed that V/β-SiC$_o$ catalysts presented exactly the same trend in the PODH reaction (in terms of propane conversion and propene selectivity) of more conventional oxide-on-oxide catalysts. In addition, the interaction between vanadium and SiC ensured a more effective dissipation of the reaction heat compared to classical metal oxide supports, hence minimizing the formation of hotspots responsible for the occurrence of undesired secondary (combustion) processes and detrimental for the catalyst lifetime.

Hueso and Santamaria very recently developed a new strategy to enhance alkane oxidative dehydrogenation selectivity taking advantage of microwave (MW) heating.[103,104] To this aim, they deposited a proper catalytic active phase on SiC, selected as an efficient MW susceptor, for a preferential solid-phase heating while ensuring a relevant temperature gap with gas phases where undesired side reactions were known to occur for temperatures above 550 °C. In particular, these authors reached a 5% of selectivity increment with respect to the classical heating mode in the propane ODH to propene[104] and a remarkable 30% higher selectivity toward isobutylene in the isobutane CO$_2$-promoted ODH.[104]

3.1.1.2. Alkenes Oxidation. Alkene oxidation is a reaction of immense importance for the synthesis of chemical intermediates. In particular, the selective epoxidation of alkenes by electrophilic addition of oxygen to a carbon−carbon double bond is one of the most significant challenges in heterogeneous catalytic oxidation. In a comparative study, Hutchings and co-workers benchmarked the performance of their Au(1 wt %)/graphite catalyst with a series of Au(1 wt %)/*support* (where the *support* was selected among Al$_2$O$_3$, TiO$_2$, SiO$_2$, and SiC) for the epoxidation of *cis*-cyclooctene in the presence of catalytic amounts of a hydroperoxy species and under mild solvent-free conditions.[105] In general, the use of graphite as a support was found to give the best combination of epoxide selectivity and alkene conversions, reaching both the highest values at 80 °C.[106] The comparative study led the authors to

conclude that based on the activity of their Au(1 wt %)/support catalysts, alkene conversions varied on the basis of the support choice in the following order: graphite $\approx$ SiC > Al$_2$O$_3$ $\approx$ SiO$_2$ > TiO$_2$, while in terms of epoxide selectivity, the order was as follows: graphite $\approx$ SiO$_2$ $\approx$ TiO$_2$ > SiC > Al$_2$O$_3$.

Jang, Zhang et al. have recently described the use of a structured SiC foam catalyst for the process intensification in a highly exothermic and diffusion-controlled reaction such as the 1-butene oxidative dehydrogenation (ODH) to butadiene.[107] These authors showed the unique advantages and potentiality of their structured catalyst (ZnFe$_2$O$_4$-α-Fe$_2$O$_3$/SiC foam; ZFS) prepared by a slurry-coating technology from ZnFe$_2$O$_4$-α-Fe$_2$O$_3$ powders obtained by the coprecipitation method and a macroscopic SiC foam support prepared by polymer pyrolysis followed by sintering treatment (Figure 5).
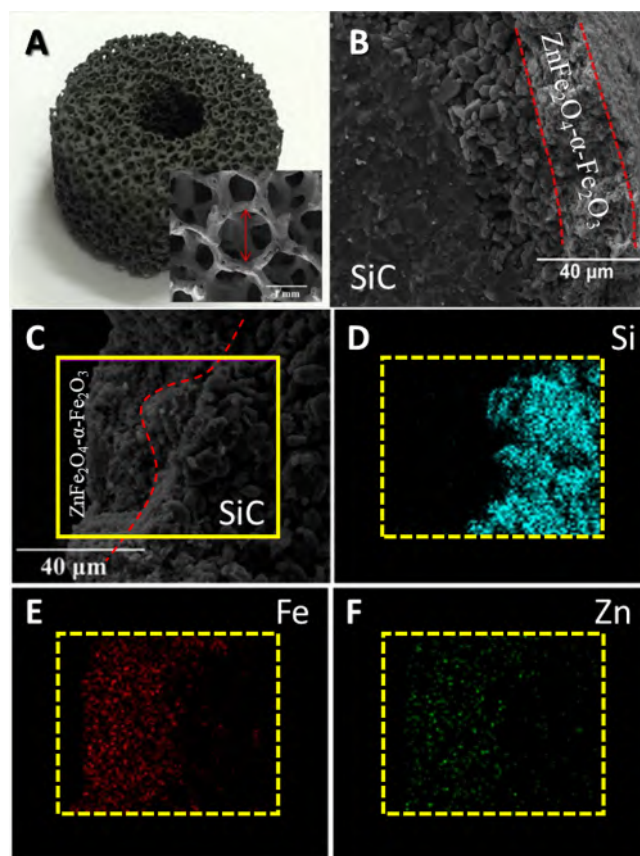
Figure 5. (A) Photo of a SiC foam and its SEM magnification, (B) cross section image of a ZFS structured catalyst, and (C−F) elemental analysis distributions for Si, Fe, and Zn. Adapted with permission from ref 107. Copyright 2019 Elsevier B.V.

According to these authors, the structured ZFS catalyst significantly intensified the process compared to particle bed catalysts, with 1-butene conversions and butadiene selectivity up to 87% and 91%, respectively (for 1-butene GHSV of 300 h^{-1}). The superior performance of the structured catalyst was unambiguously ascribed to the enhancement of heat and mass transfer together with better temperature control at the catalyst bed and a lower feed of steam that allowed the operation of the process in a wider range of the O$_2$/1-butene molar ratio and at a much higher 1-butene GHSV.

3.1.1.3. Alcohol Oxidation. The selective oxidation of alcohols to corresponding aldehydes or ketones is another
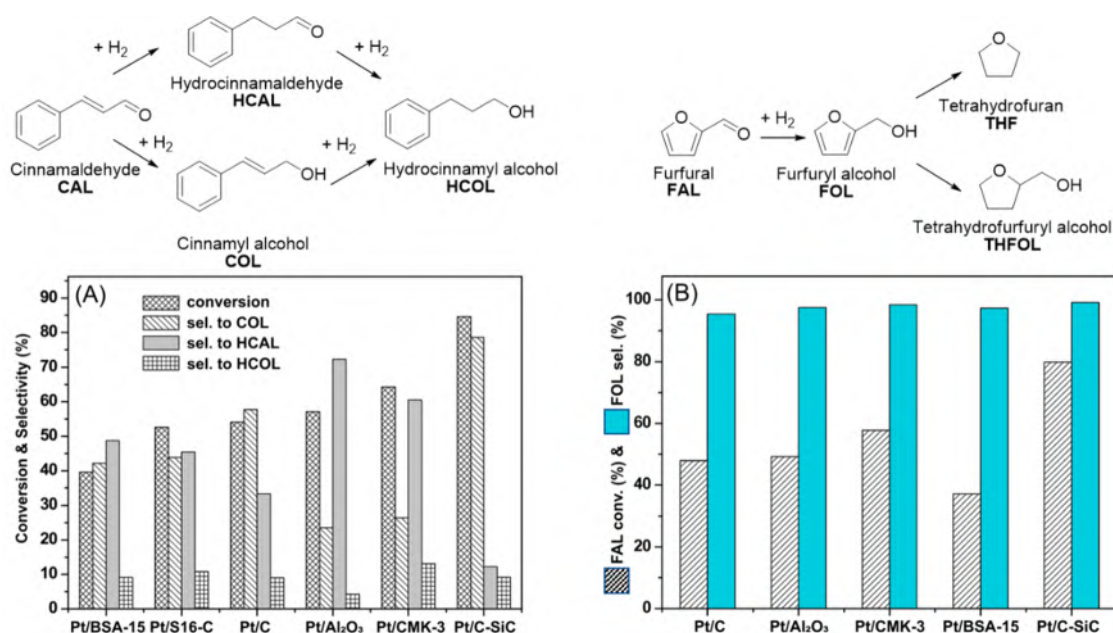
Figure 6. (A) Cinnamaldehyde hydrogenation with 5 wt % Pt supported on different carriers and a CAL hydrogenation scheme. Adapted with permission from ref 117. Copyright 2016 Royal Society of Chemistry. (B) Furfural hydrogenation with 5 wt % Pt supported on different carriers and a FAL hydrogenation scheme. Adapted with permission from ref 118. Royal Society of Chemistry 2018 under [CC BY-NC 3.0] [https://creativecommons.org/licenses/by-nc/3.0/].

process of great importance for fundamental scientific research and industrial applications.[108] In this context, the gas-phase oxidation of alcohols with molecular oxygen as oxidant has gained much attention from the scientific community due to its generally high efficiency, the easy separation process, and continuous and solvent-free operation modes. A catalyzed gas-phase alcohol oxidation is a highly exothermic process, hence catalysts with good heat-transfer capacity and preferably an ensuring low pressure drop throughout the catalyst bed are highly desirable. Wang and co-workers have recently reported on the preparation of a highly active, robust, durable, and selective bimetallic $Ag_{2.5}Cu_5$/SiC-powder catalyst for the gas-phase selective oxidation of alcohols to aldehydes or ketones (*i.e.* up to 99.3% benzyl alcohol conversion and 99.6% benzyl aldehyde selectivity).[109] In spite of these outstanding catalytic results, the practical use of these catalysts remains a challenge, since macroscopically shaped composites rather than powders are needed for real-world catalytic applications. In the same year, another Chinese team described the engineering of a SiC foam (85 vol % of void fraction) coated by the $CoO@Cu_2O$ nanocomposite (*i.e.* large CoO particles partially covered with small Cu_2O particles) and its effective use in the selective gas-phase oxidation of ethylic alcohol to acetaldehyde (AAL).[110] The authors claimed higher catalytic activity, long-term durability, and recyclability for their composite than those reported in the literature for related binary metal oxide assemblies. Worthy of note, the catalytically active composite was straightforwardly prepared *in situ* by converting the metal-nitrate precursors directly on the SiC foam during the gas-phase oxidation process. These authors operated the catalytic gas-phase oxidation under mild reaction conditions, with an ethanol conversion up to 95% and AAL selectivity of 98% in the presence of larger ethanol volumes compared to the literature (up to 20 vol %) and EtOH weight hourly space velocity (WHSV) of 8.5 h^{-1}.

More recently, the team of Lu et al. focused on the modification of surface properties of commercial SiC by preparing a series of Cu-based catalysts on SiO-enriched or C-enriched SiC matrices, respectively.[111] Their study unveiled that Cu/SiO_2/SiC and Cu/C/SiC catalysts afford higher ethanol conversion and AAL selectivity (81.4% and 99%, respectively), compared to Cu-based catalysts of the *state of the art* prepared starting from different carriers. While SiO_2 surface-enriched SiC networks favored Cu NP dispersion and accelerated ethanol conversion, the more inert C layer on SiC suppressed secondary reactions by facilitating the acetaldehyde desorption and enhancing the process selectivity.

In 2020, SiC-supported bimetallic catalysts were investigated with respect to their application in benzyl alcohol (BOL) gas-phase oxidation to benzaldehyde (BAL).[112] A Pd−Bi active phase was deposited on powdery SiC showing 92% of BOL conversion and 98% BAL selectivity already at a temperature as low as 240 °C. Given the strong exothermic character of the process, SiC was selected as an ideal support due to its outstanding thermal conductivity and oxidation resistance with respect to more common oxide-based carriers. As a matter of fact, the PdBi/SiC catalyst displayed a remarkable stability maintaining 90% of BOL conversion after 20 h of reaction, while Al_2O_3-, TiO_2-, and SiO_2-supported counterparts show high conversion values in the first 2 h (93−96%) only. However, their conversions drop down to 65−75% already after 20 h on stream.

In the same year, Parida et al. prepared a series of β-SiC-supported vanadium phosphorus oxide (VPO_x) catalysts for the liquid-phase oxidation of methanol to formaldehyde in the presence of *tert*-butyl hydroperoxide (TBHP) as oxidant.[113] Under solvent-free conditions, VPO_x/SiC reached complete methanol conversion with 89.8% of aldehyde selectivity. Moreover, the authors claimed the easy catalyst reusability up to 4 times without any loss of activity. They attributed the stability of their catalyst to the chemical inertness of SiC that
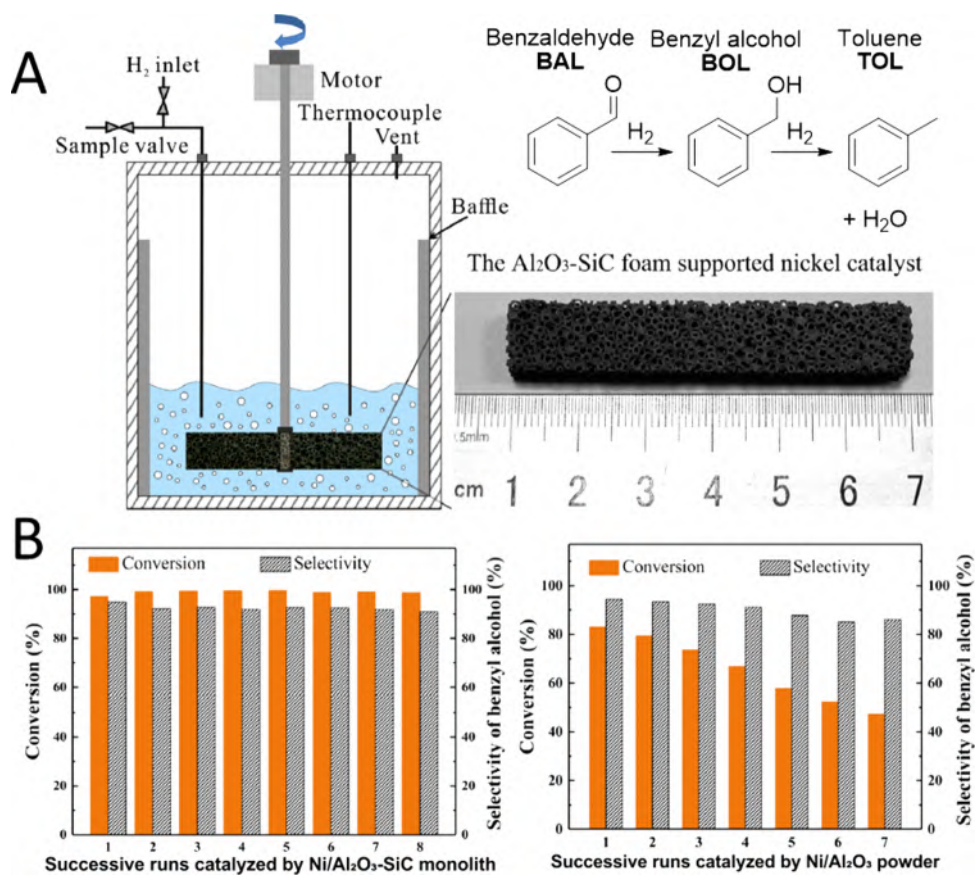
Figure 7. (A) Sketch of the rotating foam stirrer reactor (Ni/Al$_2$O$_3$−SiC) for liquid-phase hydrogenation of benzaldehyde and a BAL hydrogenation scheme. (B) Catalytic performance of 30 wt % Ni/Al$_2$O$_3$−SiC (left) and 30 wt % of Ni/Al$_2$O$_3$ powder (right) in the BAL hydrogenation in successive runs. Conditions: benzaldehyde 10 mL, isopropyl alcohol 140 mL, 90 °C, 2 MPa H$_2$, after 4 h of reaction, stirring rate: 300 rpm. Adapted with permission from ref 121. Copyright 2018 Published by Elsevier Ltd.

maintained its structural integrity also after a prolonged contact with aggressive and highly oxidant agents.

3.1.2. Reduction Reactions. This branch of catalysis covers a relatively wide range of liquid-phase and gas-phase chemical transformations of high relevance from an academic and industrial viewpoint. Scientific reports on SiC-based catalysts developed for these processes are mainly focused on the morphological and mechanical properties of these carriers. Their chemical inertness along with mechanical resistance, easy shaping, and meso-/macroporous structure are the main features that improve the performance of hierarchically structured catalysts in reduction processes. In general, SiC-based catalysts are preferentially engaged in highly exothermic gas−solid-phase reactions because of their high thermal conductivity. However, their use in traditional liquid-phase catalysis is denoted by a number of seminal examples where the SiC properties are compared with those of more traditional C and metal oxide-based carriers.

3.1.2.1. Carbonyl and CO$_2$ Hydrogenation Reactions. The research team of Pan and Bao reported a series of simply coated, low surface area SiC samples with mesoporous carbon or N-doped carbon layers prepared by thermal decomposition of various C sources (including biomasses), eventually in the presence of NH$_3$ as the N source.[114−116] The C-SiC composites showed increased specific surface area and mesoporous structure and were used to accommodate highly dispersed Pd NPs or Pd NPs dispersed among TiO$_2$ NPs.[115] All these composites were successfully tested in the model 4-

carboxybenzaldehyde (4-CBA) hydrogenation reaction to 4-carboxybenzyl alcohol with improved performance and higher stability compared to classical Pd NPs on microporous activated carbon (AC)[114,115] or Pd NPs on plain SiC,[116] respectively.

The Li team has recently reported on the preparation of highly dispersed Pt NPs on C-SiC composites featured with relatively high specific surface area and pore volume, as highly efficient catalysts for the selective liquid-phase hydrogenation of cinnamaldehyde (CAL)[117] and furfural (FAL)[118] to cinnamyl alcohol (COL) and furfuryl alcohol (FOL), respectively, at room temperature in water/alcohol media. They showed the superior performance of their Pt/C-SiC compared to other Pt catalysts supported on conventional oxide materials, such as SBA-15, CMK-3, and Al$_2$O$_3$, as well as activated carbon (AC), tested under identical experimental conditions (Figure 6). Besides the easy recovery and efficient reuse of Pt/C-SiC from the reaction media, the authors claimed the existence of an ideal interaction between Pt NPs and C-SiC capable of ensuring an optimal and uniform dispersion of metal nanoparticles along with the generation of surface Pt$^{\delta+}$ species.[117,118] The latter were supposed to foster a preferential adsorption/activation of the formyl moieties in CAL and FAL, hence driving the process selectivity toward COL and FOL mainly.

In a successive study, Hu and co-workers developed a tandem catalytic system for the conversion of FAL to cyclopentanone (CPO).[119] The first step consists of the FAL

hydrogenation to FOL promoted by a metal-supported catalyst followed by dehydration, furan ring opening, and electrophilic addition fostered by Lewis or Brønsted acids. Nickel supported on SiC was selected for the first part of the process achieving the selective production of FOL in 58% yield. Silicon carbide was rationally selected as an oxygen-free carrier because, at odds to Al_2O_3 or SiO_2, it contains negligible surface acidic sites. Accordingly, authors found it convenient for investigating the effect of external Lewis or Brønsted co-catalysts on the further conversion of FOL to the target CPO without interferences from the support.

The Zhang team described the use of a rotating stirrer reactor made of a monolith of the SiC foam (as stirring blade) that was also a porous catalyst support for an aluminum oxide (Al_2O_3) coating loaded with Pt NPs (Figure 7).[120,121] By their engineered reactor, the authors achieved a selective and highly efficient hydrogenation system for the conversion of CAL[120] and benzaldehyde (BAL)[121] to COL and benzyl alcohol (BOL), respectively. A comparison of their Ni/Al_2O_3–SiC composite with the Ni/Al_2O_3 in powder for BAL hydrogenation, under identical conditions and for identical Ni loadings, showed the outperforming behavior of the former. This outcome was ascribed to a more homogeneous dispersion of the nickel phase (with smaller NP sizes for higher nickel loadings) as well as to the invariably higher mass transfer rate ensured by the monolithic SiC foam.[121]

Guo's group recently reported a 3 wt % Ir/SiC composite prepared by the wet impregnation method as a robust, durable, and highly efficient catalyst for the aqueous hydrogenation of levulinic acid (LA) to γ-valerolactone (GVL) in a batch reactor.[122] Carbonyl reduction of LA followed by intramolecular cyclization of the 4-hydroxypentanoic acid occurred quantitatively and chemoselectively at 50 °C and 0.2 MPa of H_2 pressure, showing superior performance to those of Ir catalysts based on other carriers. Besides unveiling the high acid-resistance of their Ir/SiC composite in the process, the authors attributed its remarkable catalytic activity to the Schottky-type contacts between SiC and Ir NPs. These contacts were supposed to promote electron transfer from the carrier to the metal active phase, hence improving the catalytic activity of the latter.[122]

As a further step forward, the same group incorporated also Ru in the catalytic system obtaining a bimetallic Ru–Ir/SiC catalyst. The latter exhibited a superior hydrogenation activity with complete and selective conversion of LA to GVL already at room temperature and 0.2 MPa of H_2.[123] Its outstanding performance was attributed to a change in the SiC electronic structure induced by a synergistic effect among the support, Ir and Ru. In particular, an electron transfer from Ru NPs to Ir, together with the already observed Mott–Schottky contact between SiC and metals, contributed to enrich Ir NPs thus enhancing its activity toward H_2 dissociation. This latter was then spilled on the SiC surface where LA was adsorbed to produce the desired GVL.

Díez-Ramírez et al. have presented an interesting example of trimetallic catalyst 37.5:12.5:50 Pd:Cu:Zn (mol %) supported on β-SiC pellets for the CO_2 hydrogenation to methanol (CH_3OH) at ambient pressure.[124,125] Previous studies on the textural and morphological properties of oxide/oxide-free supports for bimetallic Cu–Zn-based active phases to be employed for the selective CO_2 hydrogenation to methanol[126] prompted the authors to explore the high thermal conductivity, mechanical strength, and chemical inertness of β-SiC matrices

as catalyst supports for the hydrogenation reactions. In particular, the chemical inertness of SiC was crucial to avoid undesired interactions between the support and the metal active phase while maximizing those synergistic interactions between different metal components in the active phase.

3.1.2.2. C–C Multiple Bond Hydrogenation Reactions. The first report on the use of Pd/SiC composites applied to the exothermic 1,3-butadiene hydrogenation is due to Berthet and co-workers.[127] These authors took advantage of the thermal conductivity of SiCs for the preparation of Pd-based composites by two different deposition techniques: the atomic beam deposition (ABD) and the plasma sputtering deposition (PSD). They showed that the morphology of metal adlayers formed on flat SiC supports was closely related to the physical deposition technique used and that PSD at higher Pd content produced catalysts working with relatively high turnover frequency (TOF) in the process.[127] Later, Garcia Cervantes et al. described the preparation of Pd (0.5 wt %) catalysts by impregnation of various thermal conductor (SiC and Si_3N_4) and insulator (SiO_2, Al_2O_3) supports and studied their catalytic performance under identical conditions for the same gas-phase hydrogenation reaction.[128] Despite a similar mean size of metal particles in all catalysts (≈ 4 nm), the authors ascribed the different behaviors of their heterogeneous systems (in terms of catalyst stabilization and/or deactivation on long-term runs) to the electronic properties underneath Pd/support interactions. Experimental evidence did not allow the drawing of any direct relationship between the support thermal properties and the catalyst deactivation. While the hydrogenation activity of Pd/SiO_2 and Pd/Si_3N_4 was found to decrease rapidly since the beginning of the process and reached a stable plateau within a few hours, Pd/Al_2O_3 and Pd/SiC showed a less pronounced but continuous decrease of their activity over time. Such a different evolution was tentatively ascribed to a different stabilization path of the catalysts on run. The authors concluded that catalyst coking, hence the formation of carbonaceous residues, whose nature and amount were dictated by the inherent properties of the metal/support couple, was at the origin of the different catalysts' performance in the process.[128]

Despite the great improvements made in selective acetylene hydrogenation to ethylene with mono- or bimetallic catalysts on classical metal oxide supports, the need to realize this technology in a fixed-bed reactor has prompted scientists to explore alternative and engineered supports for the metal(s) active phase. In 2016, Zhang and co-workers described the preparation of an α-Al_2O_3-coated, egg-shell SiC support (α-Al_2O_3@SiC) by the one-step spray coating method.[129] When used to support Pd and Pd–Ag NPs, the α-Al_2O_3@SiC was found to prevent metal precursor penetration, hence making metal active sites fully available at the outer α-Al_2O_3 surface. As compared with a conventional Pd–Ag/α-Al_2O_3 catalyst prepared from α-Al_2O_3 pellets, the egg-shell Pd–Ag/α-Al_2O_3@SiC catalyst showed improved ethylene selectivity (ca. 16% more) at the same acetylene conversion (100%). Later Guo et al. pointed out the unique properties of a low-surface area SiC support (≈ 23 m^2 g^{-1}) in the process by comparing SiC-supported Pd nanoparticles prepared by incipient wetness impregnation with the more classical Pd/TiO_2 catalyst.[130] They found that Pd/SiC was a more stable catalyst on long-term runs, more efficient, and up to 20% more selective toward ethylene than Pd/TiO_2 at the same acetylene conversion (90%) (Figure 8). The authors claimed that the
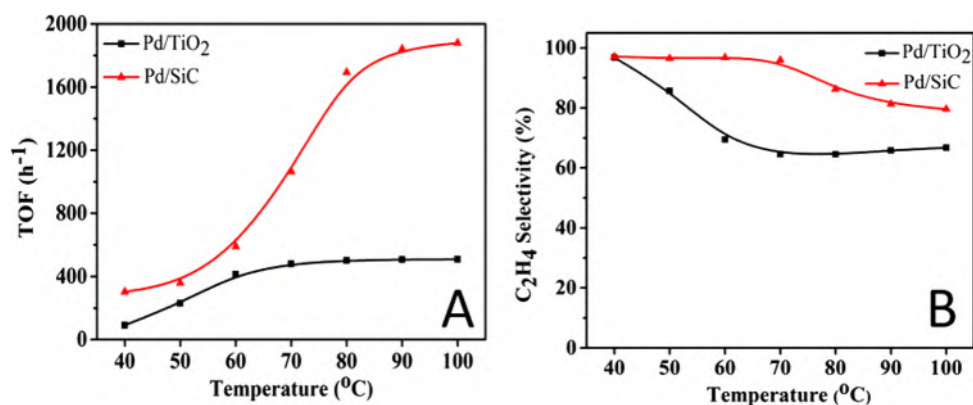
Figure 8. (A) TOF (h^{-1}) vs reaction temperature. (B) Ethylene selectivity vs reaction temperature. Reaction conditions used in a fixed-bed reactor: cat. 100 mg, GHSV of C_2H_2 30 000 mL $h^{-1}g_{cat}^{-1}$ at atmospheric pressure. Reactions were performed on a 40−100 °C temperature range with 1% C_2H_2/2% H_2/N_2 to balance. Figures adapted with permission from ref 130. Copyright 2018 Elsevier BV.

broad distribution of meso- and macroporosity in the carrier enhanced the mass transfer at high reaction rates and decreased the residence time of ethylene at the catalyst surface. Moreover, its high thermal conductivity was supposed to better homogenize temperature swings at the catalyst bed hence inhibiting overhydrogenation paths.

Finally, *in situ* XPS studies of Pd NPs on the two supports revealed the existence of stronger metal−support interactions in the Pd/TiO$_2$ catalyst responsible for a lower electronic surface density of Pd sites on the latter. Therefore, the superior chemical inertness of SiC and the consequent higher electronic surface density at the Pd sites in Pd/SiC were thought to increase the ethylene desorption rate from the catalyst surface, hence preventing undesired over-reduction processes.[130]

Chen, Si, and collaborators have recently reported on the use of Pt/SiC catalysts as excellent, highly selective, and durable systems for the 2-butyne-1,4-diol (BYD) hydrogenation to 2-butene-1,4-diol (BED).[131] SiC-based catalysts prepared by the simple wet-impregnation technique at variable Pt loading were compared with their analogues prepared on more conventional oxide-, nitride-, and carbon-based supports. As Figure 9 shows, 0.5 wt % Pt on SiC offered the best compromise in terms of BYD conversion and BED selectivity among the series of catalysts based on the same carrier. Most importantly, the highest BED selectivity measured for catalysts prepared on other supports was constantly lower than the lowest selectivity measured on the less performing Pt/SiC sample from the series. At odds with other Pt-based catalysts of the *state of the art*, 0.5 wt % Pt/SiC offered high BYD conversion and BED selectivity along with 1,4-butanediol (BDO) as the unique reaction byproduct. Other side compounds from complex BED dehydration/hydrogenation sequences, typically present in the reaction mixtures of classically Pt-based systems from the literature, were no longer detected with Pt/SiC.

They concluded that simply prepared Pt nanoparticles in the 2−3 nm size range supported on SiC provided an excellent catalyst for the highly efficient (≈96%) and selective (≈96%) BYD conversion to BED under mild conditions.

An original example of a high surface area hierarchical structured SiC-based catalyst for the highly selective cinnamaldehyde (CAL) hydrogenation to hydrocinnamaldehyde (HCAL) was prepared by the Pham-Huu team. The authors grew a dense and homogeneous layer of carbon nanofibers (CNFs) at the SiC surface by the chemical vapor
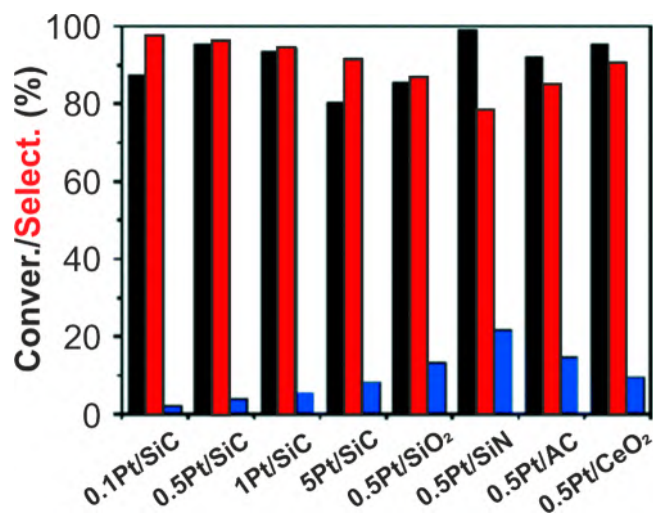
Figure 9. BYD hydrogenation with Pt-based catalysts at variable metal loading and on variable supports in comparison. BYD conversion to BED (black bars); BED selectivity (red bars); BDO selectivity (blue bars). Reaction conditions: 100 °C, H$_2$ 10 bar, water as solvent. Adapted with permission from ref 131. Copyright 2020 The Royal Society of Chemistry.

deposition (CVD) method.[132] The as-prepared CNF/SiC composite offered a higher density of anchoring sites for growing a narrower dispersion of Pd NPs (active phase) with smaller medium sizes compared to the metal dispersion obtained on the plain SiC matrix. Once applied in the liquid-phase CAL hydrogenation as a catalytic stirrer, the Pd/CNF/SiC catalyst showed higher reaction rates and stability (Figure 10A) on successive runs compared to its Pd/SiC counterpart along with a higher and constant selectivity toward HCAL (Figure 10B).

Such a behavior was ascribed to a modulation of the electronic properties of the smaller Pd NPs in contact with prismatic graphitic planes of CNFs that facilitated the desorption of the C=C hydrogenation products from the catalyst active phase before they undergo further reduction. The combination of these unique features with the high degree of radial mixing of reagents and reduced pressure drop at the catalytic bed ensured by the open-cell structure of the SiC foam together with an easier catalyst recovery and reuse at the end of each run has contributed to generate an outstanding
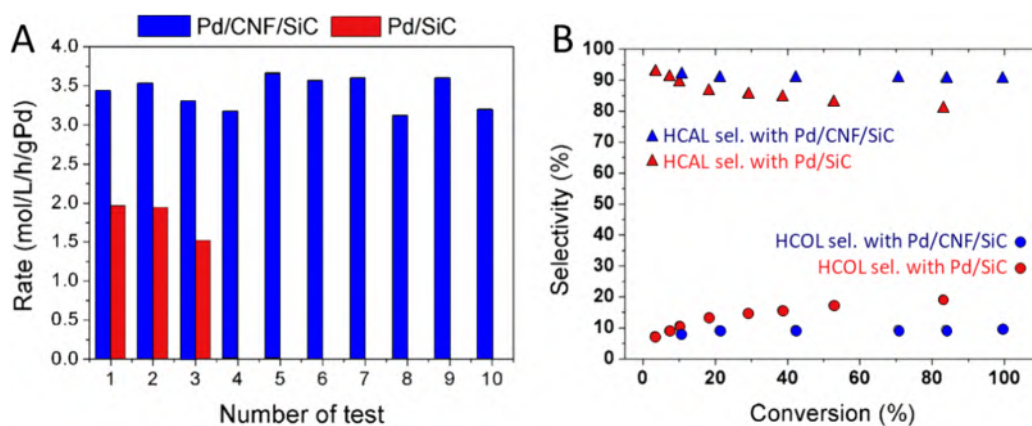
Figure 10. (A) Hydrogenation rates (expressed as mol/L/h/g_{Pd} of CAL converted) on Pd/CNF/SiC (blue bars) or Pd/SiC (red bars) catalysts. (B) Hydrocinnamaldehyde (HCAL) and hydrocinnamyl alcohol (HCOL) selectivity on the Pd/CNF/SiC (blue symbol) and Pd/SiC (red symbols) catalysts. Adapted with permission from ref 132. Copyright 2013 Elsevier B.V.
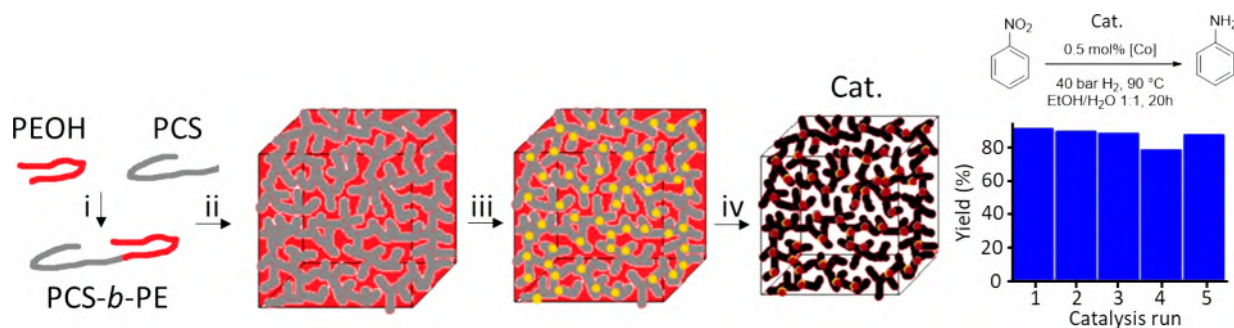
Figure 11. Synthesis of mesoporous Co@N-SiC: (**i**) block copolymer formation; (**ii**) microphase separation; (**iii**) metalation with a Co complex $[Co(L_2)(OAc)_2]$ where L = phenanthroline, OAc = acetate; (**iv**) pyrolysis. Catalyst recycling in nitrophenyl hydrogenation to aniline. Figures adapted from ref 146. Springer Nature 2018 under [CC BY 4.0] [https://creativecommons.org/licenses/by/4.0/].

hydrogenation system for the highly selective CAL conversion to HCAL.[132]

In a very recent report, Guo and co-workers described the efficient and highly selective hydrogen transfer to CAL as well as to a series of variably substituted α,β-unsaturated carbonyl and carboxyl compounds, promoted by bimetallic Pd/Ir-based catalysts on SiC.[133] They found that bimetallic catalysts remarkably enhanced their activity and selectivity toward HCAL and saturated carbonyl and carboxyl compounds due to electron transfer phenomena occurring from Pd to Ir at the SiC surface. Previous studies from the same team showed that electron transfer between metal NPs and SiC caused by the Mott−Schottky effect significantly tuned the activity and selectivity of the supported metal catalysts in a variety of catalytic applications.[134−139] Evidence for a decrease of the Pd electron density in the binary metallic system (optimal at an equimolar Pd/Ir ratio) reduced the electronic repulsion between Pd and the unsaturated C═C bond thus ensuring quantitative CAL conversions and selectivity as high as 99.2% already under very mild conditions.[133]

3.1.2.3. Miscellaneous Hydrogenation Processes. In 2009, Zheng and collaborators described the synthesis and characterization of a series of C-coated SiC networks (C/SiC) via carbothermal reduction of carbonaceous silica xerogel prepared from tetraethoxysilane (TEOS) and saccharose as the raw components.[140] The mechanical strength and chemical inertness of SiC were combined by these authors with the high specific surface area of carbon coating. Accordingly, they acquired C/SiC composites with surface areas between 329

and 849 m^2 g^{-1} and average pore diameters and total pore volumes in the range of 4.5−7.6 nm and 0.53−1.12 cm^3 g^{-1}, respectively. These composites were employed as effective supports for Ru nanoparticles, and the resulting catalysts were successfully used for the ammonia production via N_2 hydrogenation. Besides the ideal thermodynamic resistance to catalyst deactivation of selected Ru−C/SiC samples from this series, the authors realized that the combination of a mesoporous C coating with the thermally conductive SiC support not only improved the noble metal (Ru) dispersion but also enhanced the resistance of the carbonaceous phase to methanation. Indeed, a limit in the use of activated carbon (AC) as support for the process was due to its tendency to undergo methanation under harsh pressure and temperature conditions applied to N_2 hydrogenation. Under optimized conditions, the authors acquired stable Ru−C/SiC heterogeneous catalysts for N_2 hydrogenation with NH_3 content in the effluent up to 15.9%, operating the process at 435 °C, with a H_2/N_2 ratio of 3 and a flow rate of 10 000 h^{-1} at a pressure of 100 bar.[140]

The pyrolysis of self-assembly block copolymers was followed to fabricate mesoporous SiC samples with a fine-tuning of pore morphology and containing various transition-metal nanoparticles derived from the organometallic domain.[141−144] Porous SiC composites with integrated nickel nanoparticles (Ni@SiC) or N-doped mesoporous SiC cobalt nanocomposites (Co@N-SiC) were obtained through this methodology by Kempe and co-workers.[145,146] These authors demonstrated that the SiC porosity could be tailored from

O

micro- to mesoscale by modulating the molecular weight of the organic blocks. The combination of the organic copolymers with selected coordination compounds as metal sources followed by pyrolysis under neutral atmosphere gave amorphous SiC samples with integrated metal NPs (Figure 11).

This alternative way to the preparation of SiC-based metal catalysts was dictated by the need for increasing the (generally low) specific surface area of commercially available SiC samples. In terms of catalysis, Ni@SiC[145] and Co@N-SiC[146] were successfully applied as robust, highly selective (orthogonal in the presence of other hydrogenation sensitive functional groups), and reusable heterogeneous catalysts for the hydrogenolysis of aryl ethers or hydrogenation of nitroarenes to anilines, respectively.

More recently, a highly functional-group tolerant and broad substrate tolerant protocol for the reductive amination of carbonyl-containing compounds and the reductive alkylation of nitriles by carbonyl species has been described by the same team using a 4 wt % Fe/(N)SiC catalyst in the presence of aqueous NH_3[147] and a 4.7 wt % Co/(N)SiC[148] material, respectively. Their approach to the nanoparticle synthesis, using preformed N-doped SiC matrices to be impregnated in a solution of single-site complexes from the organometallic domain followed by calcination/reduction paths, provided an excellent, robust, and reusable heterogeneous catalyst for the process to occur (Figure 12).
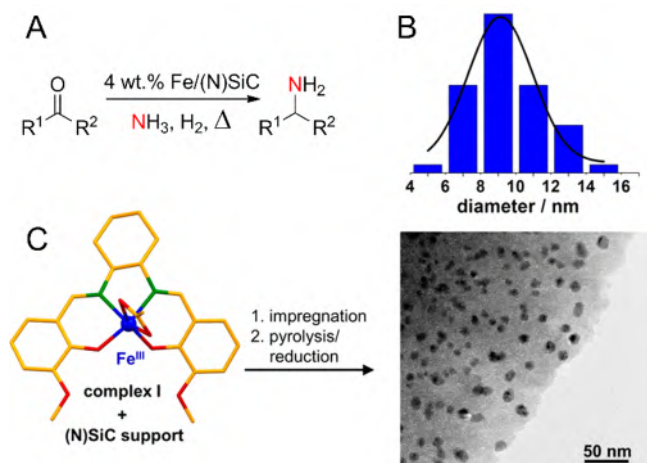
Figure 12. (A) Reductive amination scheme using NH_3, H_2, and Fe/(N)SiC as catalysts. (B,C) Synthesis of Fe/(N)SiC by wet impregnation of (N)SiC with the single-site complex I (molecular structure determined by X-ray single crystal structure analysis, color code: green = N, red = O, orange = C), followed by pyrolysis and hydrogen treatment (reduction). (B) TEM analysis suggested the presence of homogeneously distributed Fe nanoparticles with an average size of 9 nm. Adapted from ref 147. Wiley-VCH Verlag GmbH & Co. KGaA 2020 under [CC BY 4.0] [https://creativecommons.org/licenses/by/4.0/].

Most importantly, these authors found that the same impregnation/calcination/reduction scheme applied to other oxide-based supports (i.e. Al_2O_3, SiO_2, CeO_2, or TiO_2) gave rise to inactive or poorly active catalysts for the process. A similar behavior was also found when activated carbon or pyrolyzed polyacrilonitrile (PAN) matrices were selected as carriers to be impregnated for the Fe or Co NP growth.[147]

A smart approach to the catalyst active-phase tuning of SiC-supported Pd NPs has been described by Guo et al. for the highly selective aryl nitrile hydrogenation to primary or secondary amines.[149] The study took advantage of previous evidence from this team on the ability of H_2 to undergo dissociation at room temperature on Pd NPs supported on SiC and the subsequent H· spillover at the surface of the SiC semiconductor (see also section 3.5.1).[139] They showed that the Pd/SiC catalyst doped with NiO nanodots deposited by atom layer deposition (ALD) changed its selectivity for the benzonitrile (BN) hydrogenation reaction from benzylamine (BA) (94% with Pd/SiC) to dibenzylamine (DBA) (98% with NiO-Pd/SiC). They speculated on a plausible mechanism for the different selectivity with the two catalysts at work, assuming NiO nanodots as quenching sites for H·. In this way, a low H· concentration could be maintained with the NiO-Pd/SiC catalyst hence prolonging the imine intermediate (R−CH=NH) lifetime with respect to its natural reduction path to BA. The persistence of the imine at the catalyst surface was supposed to facilitate the CH=NH reaction with a second equivalent of BA to give selectively the secondary amine (DBA) (Figure 13).[149]

A bimetallic Pt−Sn/SiC catalyst was successfully employed by Zang and Wang in the last hydrogenation step of a more complex catalytic system for the ethanol synthesis with selectivity as high as 90%.[150] The authors proposed an elegant tandem protocol to the ethanol synthesis from syngas by combining a triple catalytic system for the integration of methanol synthesis with its carbonylation to acetic acid and the subsequent hydrogenation of the latter. Although SiC-supported noble metals (Rh, Pd, and Pt) were known to promote the acetic acid hydrogenation,[151] they were almost inactive in the triple tandem system proposed by these authors. Notably, they found that modification of 1 wt % Pt/SiC with 1.2 wt % Sn gave rise to well dispersed PtSn nanoalloys with a narrow size distribution of NPs and definitively changed the nature of the main product of the triple tandem system from acetic acid to ethanol.[150]

In 2020, Chu's and Liu's groups prepared a Ni/SiC catalyst for application in the hydrolytic hydrogenation of cellobiose to hexitol, a process of high importance in the field of biomass valorization.[152] Notably they found that the Ni/SiC catalyst displayed a hexitol yield as high as 64.5% that was higher than that obtained with nickel supported on more classical Al_2O_3, activated carbon, and carbon nanotubes (CNTs). Other than the higher thermal conductivity and larger mesoporosity of SiC supports, these authors attributed the better catalytic activity of Ni/SiC to a lower energy barrier for hydrogen activation as demonstrated from DFT calculations.

Very recently, Tong et al. prepared a Pd_7P_3/SiC catalyst for the total hydrogenation of phenol to cyclohexanol.[153] The authors showed that palladium phosphide was uniformly dispersed on the SiC surface and provided a pronounced hydrogenation activity already at 40 °C and 5 bar of H_2 affording an almost quantitative phenol conversion with 94% of cyclohexanol selectivity. The remarkably high catalytic activity was attributed to a synergistic effect of active phase and SiC. In particular, Pd_7P_3 activates hydrogen, and the support adsorbs the phenolic oxygen in a coplanar way with the benzene ring thus facilitating its hydrogenation to cyclohexanol.

3.1.3. C−C Bond-Forming Reactions. *3.1.3.1. Friedel−Crafts, Cross-Coupling, and Hydroformylation Reactions.*
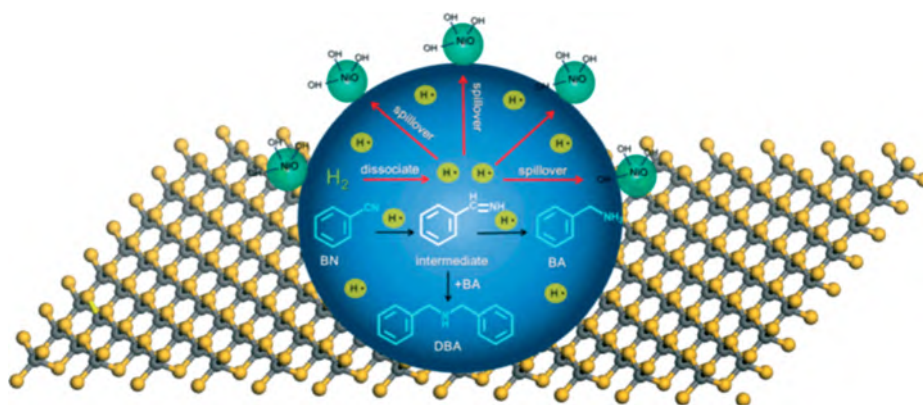
Figure 13. Sketch summarizing the speculated hydrogenation paths for Pd/SiC and NiO-Pd/SiC in the selective benzonitrile (BN) to either benzylamine (BA) or dibenzylamine (DBA), respectively. Reproduced with permission from ref 149. Copyright 2019 The Royal Society of Chemistry.
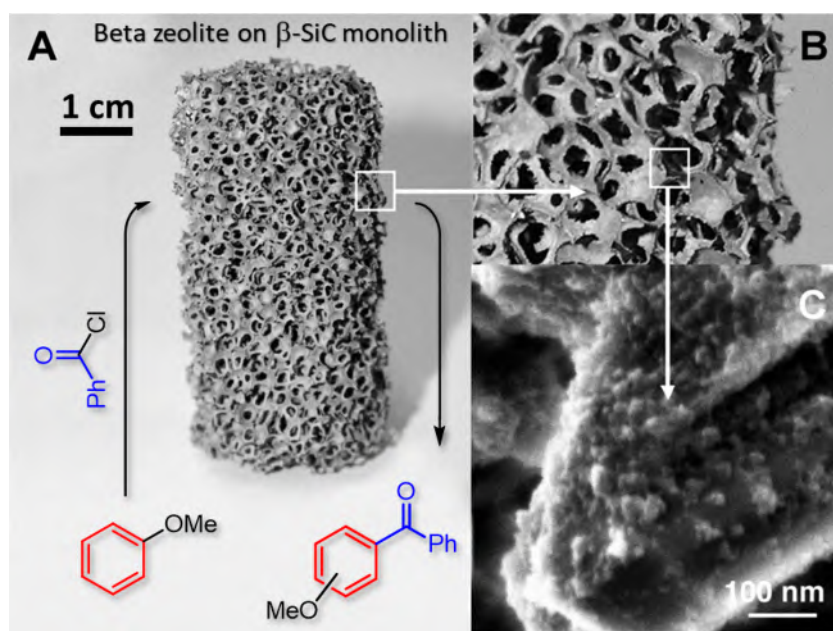
Figure 14. Optical (A and B) and SEM (C) images of the H-BEA zeolite on a macroscopically shaped SiC monolith. SEM image (C) shows the homogeneous coverage of the SiC surface by round shaped H-BEA zeolites with a mean diameter of 30 nm. Figures adapted with permission from ref 156. Copyright 2006 Elsevier B.V.

SiC networks have considerably improved the catalytic performance in Lewis acid-catalyzed processes like the Friedel–Crafts alkylation/acylation reactions. The latter is one of the most important methods for the production of key organic intermediates of great relevance in several branches of the modern chemical industry (*i.e.* pharmaceutical, agrochemical, fragrance market, etc.). Zeolites are among the most widely studied and effective catalysts for the process to occur. Pham-Huu and co-workers first described the use of SiC-supported zeolites for the process (Figure 14). Their numerous contributions on the topic have systematically outlined the unique advantages rising from the use of these porous and inert carriers in model Friedel–Crafts liquid-phase acylation reactions.[154−160] They have described the macroscopic shaping of colloidal beta zeolite using SiC matrices of various sizes and shapes. At odds with more classical binders (Al$_2$O$_3$ or Al$_2$O$_3$-silica materials) for the macroscopic shaping of beta zeolite catalysts, the choice of inert SiC matrices listed a

series of technical advantages in terms of process performance and catalyst stability on runs.

The chemical inertness of SiCs along with their meso- and macroporous open-cell structures avoided the occurrence of undesired side processes, facilitated the reactants' diffusion toward the zeolite active sites, eliminated pressure drop phenomena (typically encountered with bulk powder zeolite catalysts in fixed-bed configuration reactors),[155,158] and reduced the products residence time at the catalyst surface (generally responsible for a progressive catalyst deactivation/coking in bulk zeolite catalyzed processes). These advantages, combined with easier catalyst (zeolite) handling, recovery, and reuse, have provided extremely active, selective, and stable Friedel–Crafts acylation catalysts for fixed-bed reactors. A thorough microscopic analysis of the SiC-supported catalysts also showed a pretty homogeneous dispersion of zeolites on the SiC surface, with no traces of large aggregates. The high mechanical resistance of zeolite deposits on the SiC carriers was finally attributed to a certain degree of reactivity of zeolites

with SiO_xC_y functionalities at the SiC surface, potentially engaged in covalent grafting.[156,158] The ability of SiC matrices to adsorb microwaves, hence transforming radiation into heat directly at the catalyst bed, prompted these authors to demonstrate the higher efficiency and selectivity of their SiC-supported beta zeolite catalysts in the model anisole acylation reaction under a microwave-heated configuration.[160] Besides reducing the reaction times (from 2 to 7 h to 30 min), the microwave heated reactor showed improved substrate conversion and product selectivity compared to the traditional heating (Joule) scheme. Indeed, anisole benzoylation and acetylation yields improved from 13% to 57% and from 12% to 59%, respectively, with an almost complete selectivity (up to 95%) toward *p*-methoxyketone as product.

Palladium NPs supported on SiC matrices exhibited a broad scope as catalysts for fine chemical production. Guo and co-workers described the use of silicon carbides of medium surface area (50 m² g⁻¹) as Pd NP-decorated systems for the catalyzed carbonylative Suzuki cross-coupling reactions.[161] Their virtually monodispersed Pd NP system with a narrow NP size distribution ensured from good to excellent yields in the process with remarkably high selectivity (97−99%) toward diphenyl ketones as products with variably substituted aryl halides and arylboronic acids. Moreover, their heterogeneous Pd/SiC catalyst exhibited good recyclability up to five times with only a moderate decrease of iodobenzene conversions, likely due to a partial Pd NPs leaching throughout the recycling tests. Nishiwaki and co-workers also described the use of SiC-supported Pd NPs for Heck and Suzuki reactions between iodobenzene and methyl acrylate or arylboronic acids, respectively.[162] Their study pointed out the beneficial catalytic effects rising from the use of microwaves as an alternative heating scheme to the classical oil baths for the catalyst preparation. Indeed, the high thermal conductivity of SiC supports and their ability to act as susceptors for adsorbing microwave energy[163] improved the Pd NP dispersion on the SiC surface increasing remarkably the catalyst lifetime throughout successive catalyst recycling tests. According to their findings, the targeted microwave heating of the SiC susceptor increased its surface temperature much faster than conventional heating oil baths, thus causing a more rapid decomposition of the palladium salt precursor as well as the formation of more well-dispersed nanoparticles at its surface. On the other hand, heating with an oil bath increased the SiC surface temperature gradually, resulting in competitive aggregation phenomena of the formed Pd NPs. Notably, their MW-synthesized Pd/SiC catalyst showed improved stability and long-term reusability in Heck cross-coupling with only moderate activity loss even after 20 successive catalytic tests.[162]

Multichanneled, hierarchically structured monolithic SiC matrices with properly tailored macro- and mesoporous voids were selected as supports for the liquid-phase immobilization of a molecular Rh-bpp catalyst [BiPhePhos; 6,6′-[(3,3′-di-*tert*-butyl-5,5′-dimethoxy-1,1′-biphenyl-2,2′-diyl)bis(oxy)]bis-(dibenzo[d,f][1,3,2]dioxaphosphepin)].[164] The supported liquid-phase (SLP) composite was then used as a macroscopically shaped reactor for the model 1-butene hydroformylation reaction. These solid reactors hold all classical advantages of heterogeneous catalysts that authors elegantly combined with those of a homogeneous single-site catalyst (especially the specific activity and selectivity). SiC has offered to the study an ideal tool for the preparation of macroscopically shaped SLP

composites. Their channeled structures with thin walls, low void volumes, high geometrical areas per reactor volume, and short reagent diffusion paths allowed the optimization of the process kinetics while improving fluid dynamics and transportation phenomena.[165] In addition, the easy macroscopic shaping and pore-size control along with the chemical inertness of SiC walls made them ideal carriers for the liquid-phase immobilization of molecular complexes and their application as catalytic reactors. Portela, Haumann, and co-workers demonstrated the high performance of their SiC monolith-based SLP reactors and their successive technical improvements,[166] for the continuous gas-phase 1-butene hydroformylation.[164,166,167] With their SLP reactor scheme, they achieved substrate conversions higher than 98% over 85 h on stream and high selectivity toward the more challenging linear aldehyde.

3.1.3.2. Upgrading C_1 Feedstock into Low-Molecular Weight C_2 and C_{2+} Hydrocarbons and Oxygenated Hydrocarbons. Progress in the development of structured catalysts based on SiC networks has provided innovative solutions to overcome heat and mass transfer limitations in methanol-to-olefins reactions (MTO). The combination of the unique chemicophysical properties of SiC matrices (*i.e.* high chemical inertness, high thermal conductivity with low linear expansion coefficient) with their tunable morphology (*i.e.* open-cell and meso-/macroporous structures featured by high permeability, low pressure drop, and enhanced axial and radial reagents mixing) has been applied with success in processes like the methanol-to-low olefins (C_2−C_4) conversion. Short-chain olefins, extensively used in the chemical industry as building blocks to synthesize a wide range of commodities, are traditionally produced by thermal or catalytic cracking of naphtha or vacuum gas oil[168] as well as from alkane dehydrogenation paths.[169,170] The use of biomass derivatives as renewable feedstock for low-olefin production represents a challenging goal with important environmental and economic effects. Ivanova and co-workers first reported on the use of aluminosilicate crystals (ZSM-5 zeolite) supported on various SiC networks (extrudates or foam) as robust catalysts for the methanol-to-olefins (MTO) and gasoline (MTG) production (Figure 15).[171]
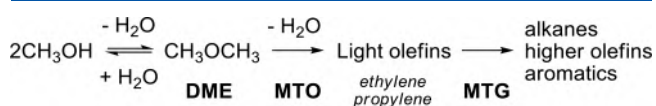
Figure 15. Reaction scheme for the methanol-to-olefins (MTO) and methanol-to-gasoline (MTG) production. Adapted with permission from ref 171. Copyright 2007 American Chemical Society.

According to their work, the high efficiency and durability of their catalytic systems were related to a thin silicon oxycarbide layer on the surface of macroscopically shaped SiC networks, which ensured the stable anchoring of microscopic prismatic aluminosilicate crystals. This aspect along with the inherent properties of SiC made it an ideal support for zeolites in a classical Lewis acid-mediated transformation. The meso-/macroporous open-cell structure of selected SiCs finally reduced the occurrence of pressure drop phenomena along the catalytic bed and contact times of reagents and products with zeolite crystals. This aspect, together with the zeolite layer thickness, was found to be crucial in the control of the process selectivity (MTO vs MTG). Compared to conventional

powdery zeolite packed catalysts, these authors claimed improved performance and higher coke resistance for their structured ZSM-5/SiC composites in MTO.[171] The same French team also described an innovative and original approach to the growing of zeolite nanocrystals whose ultimate morphology and way of growth on the bare β-SiC was controlled by the operating conditions (pH, mineralizer, time, temperature, concentration).[172] In this way, zeolite nanofibers with a regular size of about 90 nm and lengths of micrometers were grown via the so-called "in situ" SiC support self-transformation under hydrothermal conditions (Figure 16).
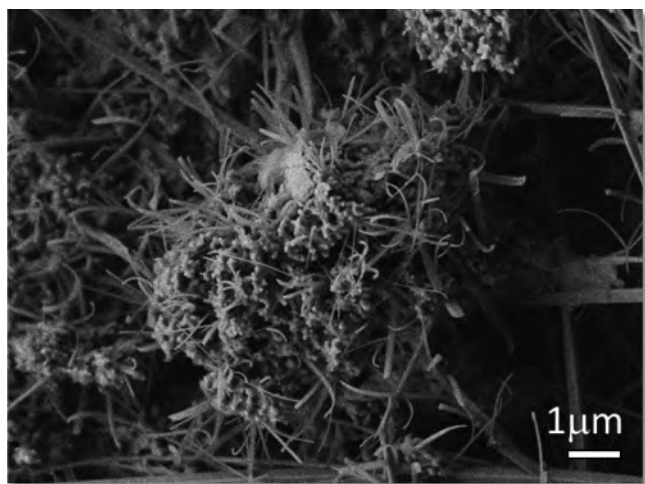
Figure 16. SEM image of alumino-silica nanowires grown on SiC after 335 h via the "in situ" hydrothermal synthesis. Adapted with permission from ref 172. Copyright 2007 American Chemical Society.

For this synthetic approach, the nanoscopic layer of silica at the β-SiC surface provided the silicon source for the alumino-silicate growth, and no other exogenous silicon sources were required. The as-obtained samples exhibited a typical silicalite-1 structure (type MFI) and acidity of ZSM-5 zeolite. Accordingly, they were scrutinized as catalysts for the methanol-to-hydrocarbon (MTG) reaction with about 38% of the MeOH conversion after 2 h on run (steady-state conditions).

A series of ZSM-5 crystal-coated SiC foams have also been prepared as structured catalysts for MTO and used to shed light on important relationships between the synthetic path used for the zeolites growth (hydroxide- or fluoride-mediated routes using either an exogenous silicon source or the above-mentioned "in situ" approach) and their ultimate catalytic performance in the process.[173] Louis et al. have compared four ZSM-5/SiC composites prepared according to the different above-mentioned synthetic routes. These authors found that the composites deeply differed from each other in terms of both crystal size, degree of crystallization, and morphology of alumino-silicate deposits (Figure 17A−D), allowing in turn different activity and selectivity in the methanol conversion to light olefins (ethylene, propylene, and other higher olefins, alkanes, and aromatics).

Ma and Bao described an original approach to the pore-shaping of SiCs starting from mixtures of SiC powder and carbon pellets of different sizes, the latter employed as hard sacrificial templates.[174] Silica and silicon oxycarbide layers formed on the SiC surface were used to fabricate ZSM-5/SiC[174] or MCM-22/SiC[175] composites, eventually applying an

alkali SiC pretreatment to improve the surface silica layer and thus facilitating the zeolites growth. The as-prepared composites were further loaded with 6 wt % Mo on the zeolite component and scrutinized as robust catalysts for the methane dehydroaromatization (MDA)[176] to BTX (benzene, toluene, and xylene isomers) and hydrogen. Their study demonstrated that Mo-ZSM-5/SiC or Mo-MCM-22/SiC catalysts offered significantly improved catalytic performance compared to the free-standing Mo-zeolite counterparts due to a better heat and mass transfer ensured by the SiC-supported systems.[174,175]

More recently, Mallada et al. supported Mo/ZSM5, the benchmark catalyst for MDA, on a SiC monolith and investigated its activity under MW irradiation.[177] SiC was selected in light of its excellent ability to absorb MW, and the catalytic activity of the sample was evaluated both under MW and conventional heating under the same experimental conditions. The authors demonstrated that methane conversion was similar in both cases, but a completely different product distribution was achieved. In particular, MW heating was found to bring a more homogeneous catalyst heating with very few productions of undesired polyaromatic hydrocarbons that are precursors of coke, whose formation was instead observed under conventional heating.

Alternative approaches to ZSM-5 coating of SiC supports,[178] including novel hierarchical SiC networks,[179,180] were also been reported later by Zhang et al. The authors described new synthetic paths toward highly loaded and homogeneously coated ZSM-5 zeolites on various SiC networks. They aimed at lowering reagent and product diffusion limits in the catalytic process to enhance the activity, selectivity, and stability of the catalysts in the methanol-to-propylene (MTP) reaction. Their ZSM-5/SiC composite showed high propylene selectivity (>45%) and a propylene to ethylene (P/E) ratio (≈6.4), while concentrations of C_1-C_4 saturated hydrocarbons (3.3%) and aromatics (2.6%) remained relatively low.[178] A hierarchical core−shell structure based on highly loaded zeolite-coated SiC nanowhiskers (SNW), grown on a SiC foam matrix (ZSM-5/SNW/SiC), was finally prepared and used in MTP by the same authors (Figure 18).[179] This engineered composite served to maximize SiC advantages as zeolite support to be employed in an exothermic catalytic transformation as the MTP reaction. ZSM-5/SNW/SiC as the fixed-bed catalyst showed reduced reagents and product diffusion limitations and controlled temperature swings at the catalyst bed thus allowing enhanced process performance and stability on run compared to either the ZSM-5/SiC foam or ZSM-5 pellets.

The ability of SiC foams to shorten diffusion path lengths and thus improve molecular diffusion and product escape from zeolite surfaces largely controlled the occurrence of secondary reactions such as aromatization and hydrogen transfer. Accordingly, ZSM-5/SNW/SiC showed the lowest average rate of coke formation (ca. 0.029 wt %/h) compared to the ZSM-5/SiC foam and ZSM-5 pellets and hence the lowest deactivation rate in the process together with the highest propylene selectivity. In an additional effort toward more stable and selective SiC-supported catalysts for the MTP reaction, Fan and Zhang added polycrystalline silicon particles to the synthesis of MFI zeolite-coated SiC foams thus creating aluminum (acidic) gradients across the MFI coating.[181] These acidic gradients in MFI coating prevented coke formation and enhanced propylene selectivity in MTP reactions. Compared to classical ZSM-5/SiC, their G-MFI/SiC composite exhibited
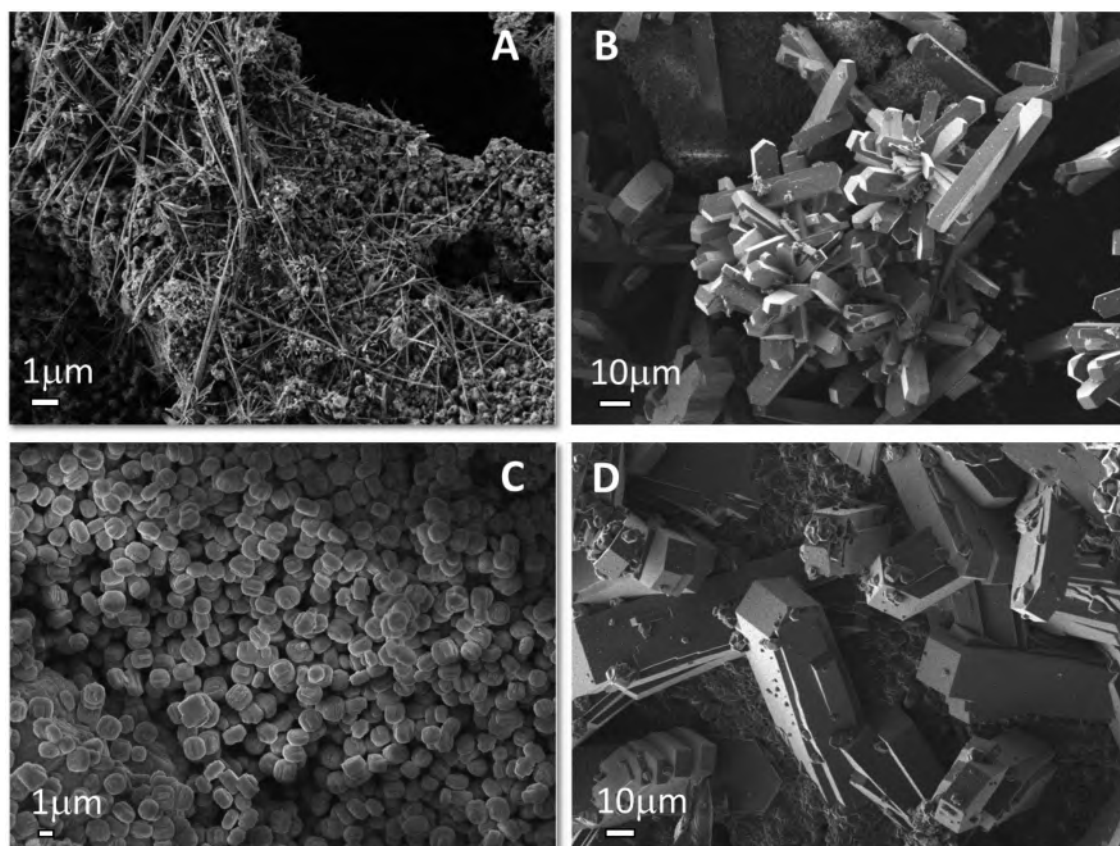
Figure 17. A−D) SEM images of alumino-silica deposits grown on SiC using different synthetic routes. **A:** "*in situ*" hydrothermal synthesis via the hydroxy-mediated route (TPAOH:NaOH:NaAlO$_2$:H$_2$O = 12:340:1:7919 molar ratio); **B:** classical fluorine-mediated route (TPABr:-TES:NH$_4$F:NaAlO$_2$:H$_2$O = 7:100:112:1:7990 molar ratio); **C:** classical hydroxide-mediated route (TPAOH:TES:NaCl:NaAlO$_2$:H$_2$O = 2.16:5.62:3.43:0.13:1000 molar ratio); **D:** "*in situ*" hydrothermal synthesis via the fluorine-mediated route (TPABr:NH$_4$F:NaAlO$_2$:H$_2$O = 7:112:1:7990 molar ratio). TES: tetraethylorthosilicate; TPAOH: tetrapropylammonium hydroxide; NaAlO$_2$: sodium aluminate; TPABr: tetrapropylammonium bromide; NH$_4$F: ammonium fluoride. Figures adapted with permission from ref 173. Copyright 2009 Elsevier, Inc.
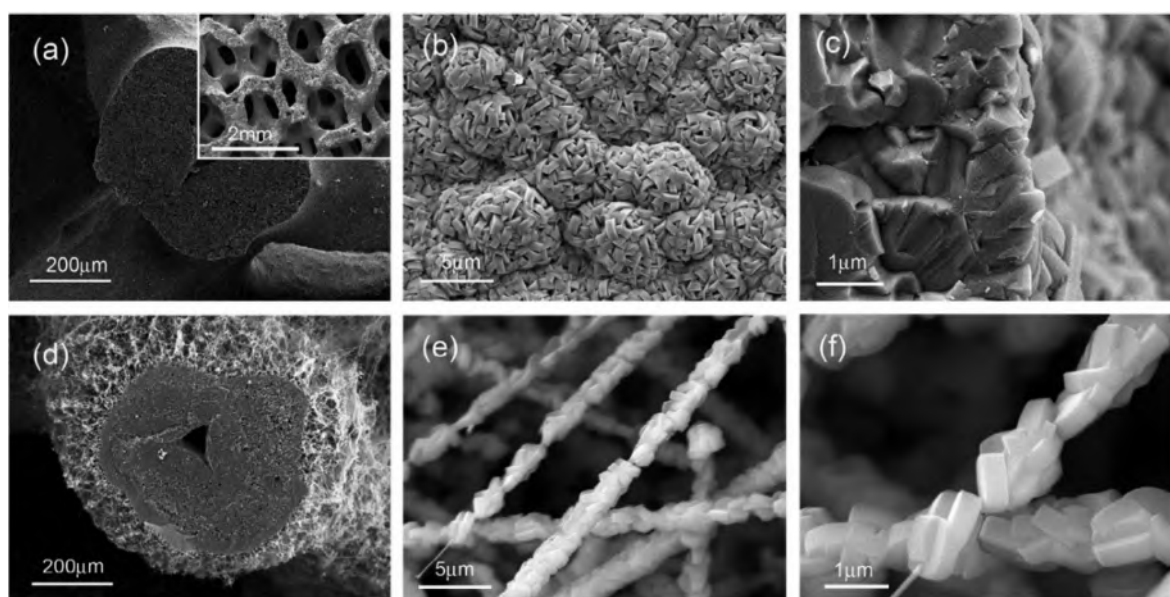
Figure 18. SEM images of (a) a typical cross section of a strut of the SiC foam support, (b,c) ZSM-5/SiC foam composite, (d) SNW/SiC foam support, and (e,f) ZSM-5/SNW/SiC foam composite. Inset in (a) presents a larger overview of the used SiC foam. Reproduced with permission from ref 179. Copyright 2015 Elsevier, Inc.

good catalytic longevity (8 h vs 76 h for >95% methanol conversion), low coke deposition (6.7 × 10^{-3} wt % h^{-1} vs 0.26 wt % h^{-1}), and higher propylene selectivity (ca. 36% vs 46%) when operated under analogous conditions. In almost the same
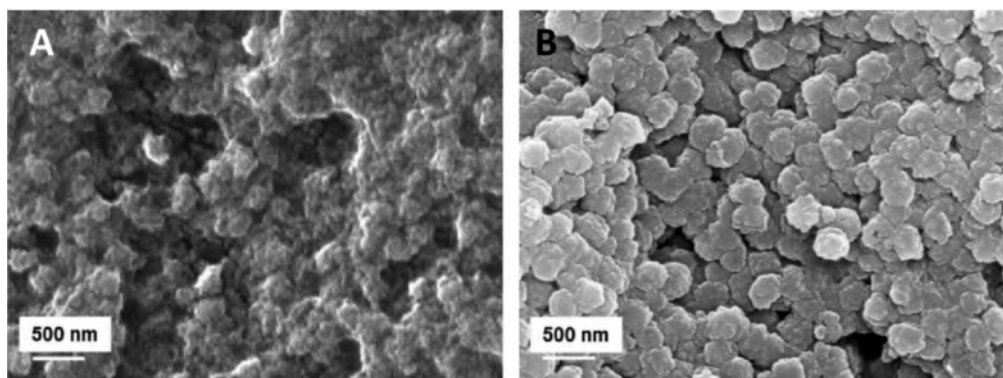
Figure 19. SEM images of (A) the reference ZSM-5/SiC foam catalysts and B) the TPAOH VPT modified ZSM-5/SiC foam catalyst obtained with a 0.5 M solution of the ammonium hydroxide. Adapted from ref 182. Published by Elsevier BV 2017 under [CC BY 4.0] [https://creativecommons.org/licenses/by/4.0/].

years, Zhang and co-workers introduced the vapor-phase transport (VPT) modification of the ZSM-5/SiC foam catalyst, using tetrapropylammonium hydroxide (TPAOH) vapors to improve the catalyst performance in MTP.[182] They realized that an optimal TPAOH concentration could deeply affect the morphology of the aluminosilicate coating, giving rise to a zeolitic phase with improved intracrystal mesopores, nanosized crystals (ca. 100 nm), and an overall higher material surface acidity (Figure 19).

Their TPAOH VPT modified ZSM-5/SiC foam catalyst represented a technical leap beyond the *state of the art* of aluminosilicate catalysts for the MTP process. Compared to ZSM-5 packed pellets, the ZSM-5/SiC obtained after TPAOH vapor VPT modification exhibited a methanol conversion per unit mass of catalyst two times higher (*i.e.* 2.9×10^3 g$_{CH_3OH}$ g$_{cat.}^{-1}$ vs 1.4×10^3 g$_{CH_3OH}$ g$_{cat.}^{-1}$), one-fifth of the pressure drop measured on zeolite pellets together with an optimal selectivity toward propylene due to the higher heat transfer property of the SiC support that guaranteed a uniform temperature at the catalytic bed throughout the whole process.[182]

More recently, Yang and co-workers investigated the performance of classical ZSM-5/SiC catalysts in a fixed-bed reactor over successive MTP catalytic runs/regeneration cycles.[183] The authors concluded that prolonged catalytic runs increased coke deposits whose burning during regeneration treatments caused the partial aluminum removal from zeolites. This phenomenon invariably changes the catalyst selectivity from a catalytic run to its successive one (in terms of propylene selectivity and propylene/ethylene ratio) up to the complete collapse of aluminosilicates and the irreversible catalyst deactivation.

In a seminal contribution by de Jong and co-workers, the authors described a direct Fischer–Tropsch route toward light olefins (FTO) from syngas (H$_2$/CO ratio of 1). They proposed the use of promoted iron nanoparticles dispersed on weakly interactive supports suitable to impart mechanical stability to the active phase without inhibiting its activation.[184] To this aim, carbon nanofibers (CNF), α-Al$_2$O$_3$, β-SiC, SiO$_2$, and γ-Al$_2$O$_3$ were scrutinized as supports for Fe, and the resulting composites were tested in FTO under industrially relevant conditions. Fe/CNF and Fe/α-Al$_2$O$_3$ exhibited selectivity as high as ≈60% toward light olefins while limiting selectivity to methane down 25%. Despite the comparable selectivity toward C$_2$–C$_4$ paraffins than Fe/CNF and Fe/α-Al$_2$O$_3$, Fe/β-SiC displayed moderately lower C$_2$–C$_4$ alkene/

C$_2$–C$_4$ alkane ratios (14.5 vs 15.25) with a CH$_4$ fraction higher than 30% C, not desirable for FTO applications. At odds with that, Fe/β-SiC presented a remarkably high stability within a long-term run (>60 h), and its catalytic activity, expressed as the number of CO moles converted to hydrocarbons per gram of iron per second (iron time yield, ITY), was among the highest measured for the Fe catalysts of this series.[184]

Stability to high temperatures, high thermal conductivity, and chemical inertness are key features that enabled SiC matrices to be used as active-phase supports for another challenging transformation: the oxidative coupling of methane (OCM) into added value C$_2$ hydrocarbons (C$_2$H$_6$ and C$_2$H$_4$).[185] Because OCM reactions are highly exothermic, temperature gradients (hotspots) can be easily formed at the catalytic bed, changing the catalyst performance over run if not altering permanently the properties of the catalyst active phase or its support. Therefore, appropriate heat management at the catalytic sites together with the selection of a catalytic active phase for the efficient and selective CH$_4$ conversion into C$_2$ products (instead of CO and CO$_2$ as CH$_4$ oxidation byproducts) is a mandatory issue to be addressed while developing a good OCM catalytic system. Liu et al. studied the effect of the reaction exothermicity on a benchmark 5% Na$_2$WO$_4$-2%Mn/SiO$_2$ catalyst[186] with its SiC (monolith foam)-supported counterpart, during the OCM reaction.[187] Both systems showed similar and high activity at 850 °C under nondiluted conditions but a different temperature control at the catalytic bed. In a model experiment, the authors recorded the temperature profiles of the two catalysts at work by sliding the internal thermocouples (Figure 20). They clearly showed significantly higher temperature swings (particularly for high GHSVs) on the SiO$_2$-supported catalyst compared to that on SiC because of the higher thermal conductivity of the latter. Arndts et al. studied the innocent or non-innocent role of the support for a Mn$_x$O$_y$-Na$_2$WO$_4$ active phase in the preparation of catalysts for the OCM.[188] Their comparative study with the benchmark Mn$_x$O$_y$-Na$_2$WO$_4$/SiO$_2$ system indicated that SiC, Fe$_2$O$_3$-based oxides and TiO$_2$-rutile were promising and alternative support materials to SiO$_2$ for the catalytic process to occur.

Later, Schuurman et al. demonstrated that the replacement of SiO$_2$ with SiC supports could have beneficial effects on the catalyst performance, preventing (in part at least) the carrier alteration under OMC conditions. Indeed, the collapse of the SiO$_2$ porous structure at the high OMC temperatures
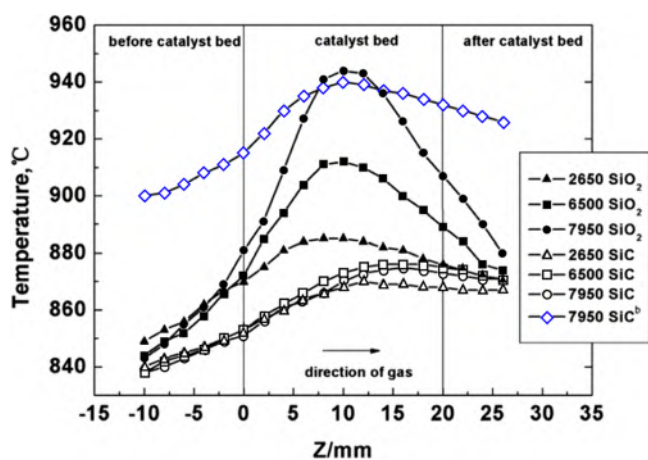
Figure 20. Temperature profiles at the catalytic beds of Na_2WO_4–Mn/SiC and Na_2WO_4–Mn/SiO$_2$ during the OCM reaction at variable methane GHSVs (from 2650 h^{-1} to 7950 h^{-1}). Reaction conditions: CH_4:O_2 = 4:1; reactor temperature 850 °C. ^{b}Reactor temperature 900 °C. Adapted with permission from ref 187. Copyright 2007 Elsevier B.V.

generated polymorph silica layers of cristobalite.[189] The formation of the latter was found to drastically decrease the surface area of SiO$_2$ with the subsequent catalyst deactivation. Although this phenomenon cannot be definitively ruled out on SiC supports, they maintained relatively high surface areas, providing C$_2$-selective catalysts (60–65%) with activity up to 12 times higher than those of the reference Mn–Na–W/SiO$_2$ catalyst under identical conditions. First, Kraehnert[190] and then later Park[191] reported on the causes for the alteration of porous SiC supports in Mn–Na–W/SiC catalysts and how to prevent them in order to maintain high methane conversions and C$_2$ selectivity in the process. The Korean team found that SiC in a nanosized SiC-supported Mn$_2$O$_3$–Na$_2$WO$_4$ catalyst (Mn$_2$O$_3$–Na$_2$WO$_4$/n-SiC) was completely converted into α-cristobalite thus showing performance and stability under OCM conditions similar to its SiO$_2$-supported counterpart. On the other hand, a microsized SiC-supported catalyst (Mn$_2$O$_3$–Na$_2$WO$_4$/m-SiC) showed higher methane conversion and C$_2$ selectivity (at 800 and 850 °C) than its Mn$_2$O$_3$–Na$_2$WO$_4$/SiO$_2$ analogue.[191] Indeed, only the surface of microsized SiC networks was converted into cristobalite thus giving rise to a SiC@-cristobalite core–shell structure where the SiC core was entirely retained. This evidence suggested that methane conversion and C$_2$ yield in OCM depended critically not only from the inherent thermal conductivity of the carrier but also from its stability under the operative conditions, i.e. how the support surface area was retained under the reaction conditions.[190,191]

Sigaeva et al. studied the dynamics of CH$_4$ pyrolysis on MgO/SiC[192] and ZrO$_2$/SiC[193] catalysts at various operative temperatures. In these experiments, the catalysts were heated by an external alternating current (hence by the electrical resistivity of SiC supports) at temperatures comprised between 700 and 1400 °C. Depending on the metal oxide used, the authors claimed methane conversions between 55% (with ZrO$_2$) and 60% (with MgO) with a prevalent selectivity toward acetylene (C$_2$H$_2$; ≈22% with MgO and 17% with ZrO$_2$) for reactions operated at 1300 °C at a reagent's (CH$_4$/N$_2$: 15/85 v/v%) flow rate of 100 mL min^{-1}. Under these conditions, they observed a progressive catalyst layering by

carbon deposits whose nature was claimed as catalytically active for the process and selective toward acetylene.[193]

Catalytic production of C$_2$ oxygenates (i.e. ethanol, acetaldehyde, and acetic acid) from syngas (CO/H$_2$) is another challenging C–C bond-forming reaction that has attracted interest worldwide[194,195] and where supported Rh-based catalysts are recognized as the most performing systems. Extensive studies have been carried out to shed light on the effects of promoters and supports[196] as to improve activity and selectivity toward C$_2$ oxygenates. Ding and co-workers studied a Rh-based catalyst prepared on calcinated β-SiC matrices as a highly effective CO hydrogenation system for the process.[197] With only 0.5 wt % of Rh on the thermal conductive SiC support, they succeeded in managing the temperature at the catalytic bed throughout the whole exothermic process (particularly at high CO conversions), preventing undesired metal particles sintering phenomena. Moreover, they ensured space-time yields (STY) toward C$_2$ oxygenates as high as 97.2 g$_{C2+}$ g$_{Rh}$$^{-1}$ h^{-1} compared to the 68.2 g$_{C2+}$ g$_{Rh}$$^{-1}$ h^{-1} obtained with the classical 1.5 wt % Rh/SiO$_2$ catalyst. In addition, they found that SiC precalcination was an essential step to increase the number of surface oxygen-containing groups[27] hence improving metal NP stabilization.[197]

3.1.3.3. Catalytic Growth of Macromolecular C Networks. SiCs are widely used materials with potential applications in the field of high-temperature, high-frequency and high-power electronic devices. Accordingly, their combination with carbon nanotubes (CNTs) or carbon nanofibers (CNFs) has attracted the interest of the scientific community for a long time toward the potential exploitation of these engineered composites in the field of structural materials (hybrid reinforcement fillers) and electronic devices. The growth of CNTs directly at the surface of micrometer-sized SiC particles generates micro-meter-scaled fillers for the improvement of composites' physical properties. These hybrid fillers often guarantee a higher compatibility and homogeneous dispersion of the guest ceramic (reinforcements) throughout the whole hosting matrix of the composite, hence avoiding undesired fillers' segregation phenomena.

Based on the floating catalyst CVD method, in which a ferrocene and xylene mixture was used, Bai and co-workers first reported on the synthesis of an aligned CNT layer at the surface of SiC particles (17 μm) and demonstrated their potential application as reinforcement fillers in structural composites.[198] Besides improving the interfacial properties between SiC particles and hosting matrices, both CNT and SiC have excellent thermal stability, and their combination in a composite can improve the mechanical properties of the hosting matrix without lowering its resistance to oxidation. These authors demonstrated that density and length of grown CNTs was easily tuned by adjusting the experimental parameters, such as the growth time and the ferrocene content in the xylene solution. Since their seminal contribution, other engineered CNTs/SiC[199−202] or CNFs/SiC[203] composites have been prepared by related CVD techniques and successfully employed for a number of technological applications beyond the classical use as reinforcement fillers in composite materials. Ajayan et al. reported on the preparation of multifunctional, conductive brushes grown on properly Au-masked SiC fibers and demonstrated their several unique tasks ranging from cleaning of nanoparticles on planar/rough surfaces, painting inside capillary, adsorption of organic
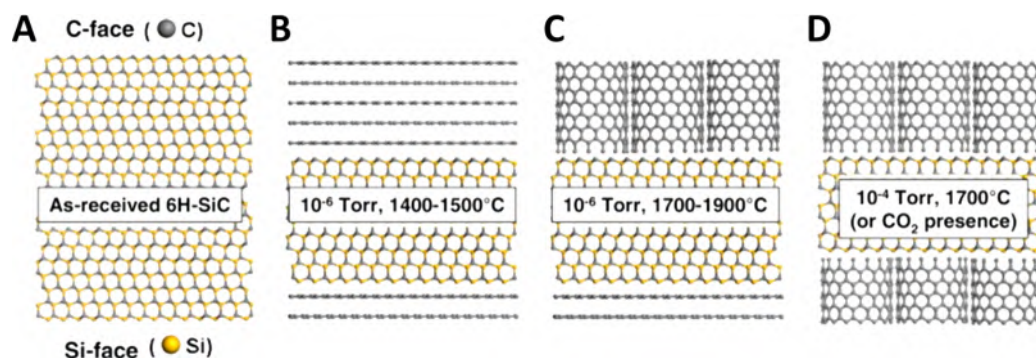
Figure 21. (A) Model of the atomic structure of a SiC crystal, (B) graphite growing on both faces at moderate temperatures, (C) CNTs growing on the C face at high temperatures, and (D) oxygen-assisted CNT formation on both faces of SiC. Adapted with permission from ref 205. Copyright 2008 Elsevier Ltd.
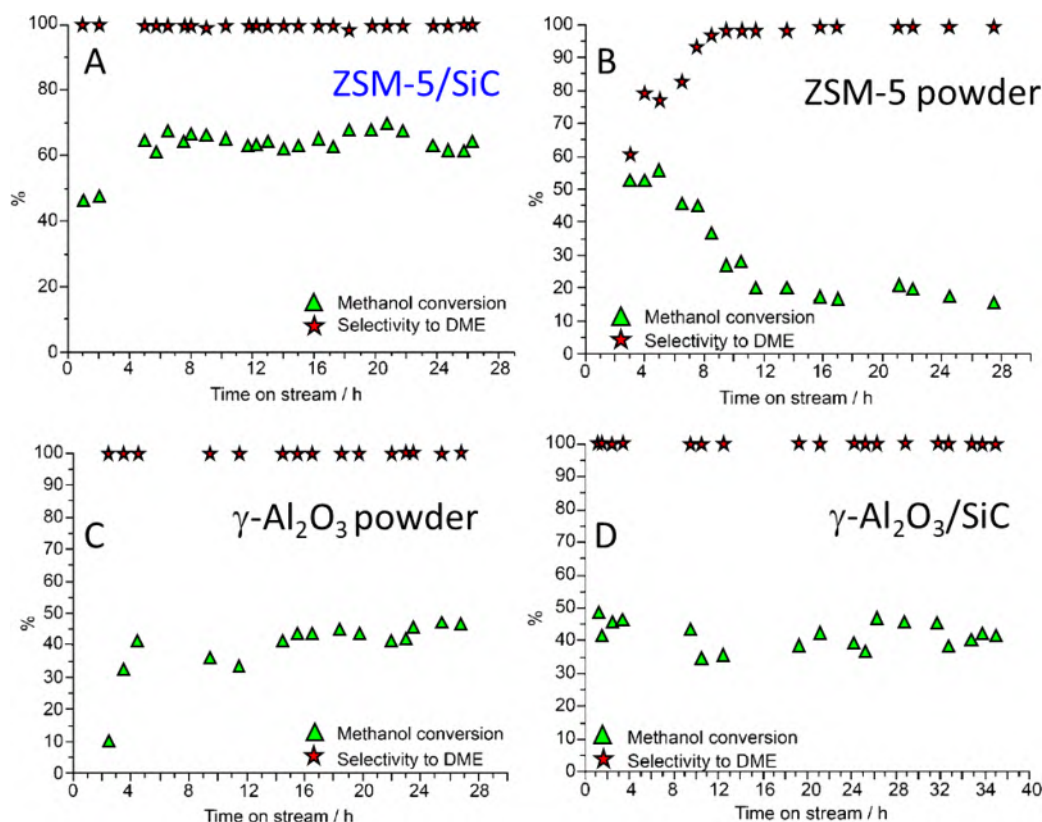
Figure 22. Methanol dehydration to DME catalyzed by (A) ZSM-5/SiC, (B) bulk, unsupported powdery ZSM-5 zeolite, (C) bulk, unsupported γ-Al$_2$O$_3$, and (D) γ-Al$_2$O$_3$/SiC. All runs were conducted at 543 K, under atmospheric pressure with a MeOH space velocity of 240 h^{-1} (STP). Adapted with permission from ref 209. Copyright 2008 Wiley-VCH Verlag GmbH& Co.

solvents, and removal of metal ions up to versatile electromechanical brush contacts and switches.[204]

Gogotsi and co-workers have systematically studied the ability of SiC networks at producing catalyst-free CNTs and graphene through their vacuum decomposition under relatively severe conditions.[205]

They showed that graphene (or relatively thick graphite) films or CNTs carpets were produced on C and Si faces of SiC leading to the almost complete transformation of the low-cost 6H-SiC wafer or 6H-SiC particles into pure and catalyst-free CNTs. Thin wrinkled graphene/graphite films were produced on the C face of a SiC wafer at 1400−1500 °C as well as its Si face when the process was operated at higher temperatures in high vacuum (Figure 21B). Small-diameter CNTs featured by

1−4 graphene walls were grown on either the C face in high vacuum (Figure 21C) or both faces of SiC wafers under low vacuum conditions (Figure 21D) and temperatures comprised between 1600 and 1900 °C. The as-obtained CNT brushes presented a nanotube density much higher than that of CVD-prepared samples. Moreover, the catalyst-free CNTs showed a significantly higher oxidation resistance upon heating in air compared to their CVD-produced counterparts.[205]

3.1.4. SiC-Based Catalysts for C−X Bond-Forming Reactions (X = O, S, Cl). Keller and collaborators described the use of thermoconductive β-SiC grains for the chemical grafting of Cu-exchanged Y zeolites and their use as heterogeneous catalysts for the vapor-phase oxidative carbonylation of methanol into dimethyl carbonate (DMC).[206] DMC

is a high oxygen-containing compound and holds potential for use as an additive in gasoline. Moreover, it can also be used as an intermediate to substitute phosgene and dimethyl sulfate for a number of applications.[207] The Cu−Y zeolite/SiC composite ensured optimal control of the temperature swings at the catalytic bed throughout the whole exothermic process, limiting the generation of local temperature gradients while affording interesting space time yield to DMC. Only a limited amount of dimethyl ether (DME) and CO_2 byproducts were detected even when the process was operated at higher temperatures.

In contrast, DME − another important oxygenated compound for the chemical industry was the target product for a series of acid catalyzed alcohol dehydration processes. Ivanova and co-workers first reported on the use of ZSM-5 zeolite crystals supported on an open-cell SiC monolith as efficient and stable catalysts for the conversion of methanol and ethanol (or a mixture thereof) into the corresponding dehydration products, mainly dimethyl ether (DME) and ethylene (C_2H_4).[208] For both dehydration processes, they found a negligible catalyst deactivation due to coke formation whose effect was claimed to slightly affect the product selectivity only. The same group reported that the formation of a strong interface between zeolite microcrystals and the SiC support improved significantly the mechanical resistance of their composite throughout the dehydration process thus preventing undesired zeolite losses during the reactions. As far as the benefits derived from the employment of the porous SiC foam is concerned, they found that the size of zeolite crystals was significantly reduced in the presence of SiC supports, and formation of large aggregates (≥ 10 μm) was substantially inhibited.[209] As a result, SiC-based composites offered a significantly higher surface exposure of the active phase to reagents. The high porosity of the open-cell SiC foam finally allowed operation of the process at higher GHSVs without any significant pressure drop at the catalytic bed and ensured higher desorption rates of products from the catalytic sites, hence limiting the catalyst fouling due to the formation of coke deposits. In their study, the authors have also demonstrated the robustness and the effectiveness of their aluminosilicate composites in the methanol dehydration to DME by comparing ZSM-5/SiC with the activity of the unsupported zeolite and γ-Al$_2$O$_3$/SiC counterpart, under identical conditions.[209] As Figure 22A−D shows, the SiC-supported aluminosilicate (ZSM-5/SiC, Figure 22A) outperformed−in terms of methanol conversion−the unsupported powdery zeolite and γ-Al$_2$O$_3$ catalysts (Figure 22B,C), as well as the γ-Al$_2$O$_3$/SiC composite. At the same time, ZSM-5/SiC was as selective as the benchmark alumina-based catalysts toward DME and ensured a markedly higher coke resistance on long-term runs. Taking advantage from the easy shaping of SiC networks, the same French team prepared ZSM-5-coated SiC foam platelets to be arranged within a milli-structured reactor.[210] They realized a highly efficient, stable and selective dehydration system for operating the process in continuum and under higher space methanol velocities compared to traditional fixed-bed configurations. Their structured reactor ensured high mixing efficiency and reagent accessibility to the catalytic active phase along with low pressure drop and negligible catalyst coking also due to the relatively low diffusion length of the foam strut.[210]

Following a similar reaction scheme, Muraza and co-workers proposed the microwave-assisted hydrothermal synthesis and grafting of the silico aluminophosphate SAPO-34 on a template pretreated (with tetraethylammonium hydroxide solution, TEAOH, 25 wt % in water) SiC foam.[211] The as-obtained composite exhibited similar dehydration activity and selectivity to that obtained with the unsupported silico aluminophosphate, operated under the identical conditions. Given the open porous structure of these composites that ensured a high reagent mixing and contact surface area between reagents and catalyst active phase, the authors operated the alcohol dehydration under relatively high gaseous space velocity (up to 4500 h^{-1}) with MeOH conversion as high as 68% and 75% and DME selectivity of 95% and 90% for processes conducted at 350 and 400 °C, respectively. Moreover, almost no appreciable catalyst deactivation due to the generation of coke was observed on the SiC-supported zeolite as a function of time on stream.[211]

More recently, Wang et al. described the synthesis of cubic Cu$_2$O nanoparticles on a medium surface area β-SiC support and their use as highly active heterogeneous catalysts for Ullmann-type C−O and C−S cross-coupling reactions in liquid phase.[212] In spite of a moderate recyclability of their composite, under optimized conditions (solvent, temperature, and base), the Cu$_2$O/SiC catalyst showed from good to excellent TOFs (h^{-1}) for the cross-coupling reaction between variably substituted aryl halides and phenols or thiophenols. The authors speculated on the non-innocent role played by the SiC support in the process. They attributed the relatively high TOF values measured in C−O and C−S cross-couplings to the formation of a p−n junction between the p-type Cu$_2$O semiconductor and the n-type SiC support.

Tungstate oxide-promoted β-SiC powders (5−20 wt % WO$_3$/β-SiC), prepared by the wetness impregnation method, were successfully employed as acid catalysts for another challenging liquid-phase reaction: the carboxylic acid ester-ification. Parida et al. demonstrated that $(WO)_x$ extended networks at the β-SiC surface facilitated the interaction of acid protons of carboxylic acids with the catalyst active phase.[213] Accordingly, WO$_3$/β-SiC exhibited more efficient esterification processes compared to other WO$_3$-supported materials like carbon, alumina, and zirconia.[214−216] They assumed the existence of positive synergistic interactions responsible for the higher esterification performance of their 20 wt % WO$_3$/β-SiC (88% of acetic acid conversion to butyl acetate with 100% selectivity toward the ester). Moreover, they showed an excellent stability of their catalytic system throughout relatively long-term runs (up to 6 h) as well as the almost complete retaining of its pristine performance after 4 successive catalytic cycles. More recently, Jiao's and Li's groups developed a structured catalyst taking advantage of a cylindrical SiC foam that they coated with ZSM-5 zeolite.[217] The authors investigated the activity of the as-prepared macroscopic catalytic system in the esterification of acetic acid with amyl alcohol and highlighted the primary role of the structured foam in controlling the kinetics of the process exhibiting a strong fluid flow characteristic dependence.

The team headed by Zhang described the synthesis of structured catalysts prepared by loading AuCl$_3$ on activated carbon-coated SiC foams as durable and highly effective heterogeneous catalysts for the exothermic hydrochlorination reaction of acetylene.[218] They proposed an original and greener alternative to the industrial production of vinyl chloride monomers (VCM) as the main component of one of the five most widely employed plastic material: polyvinyl
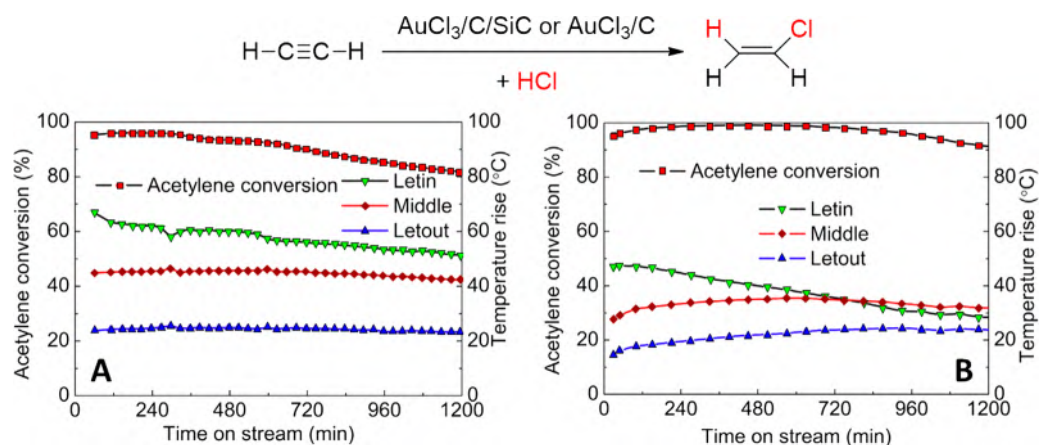
Figure 23. Temperature swings at the inlet, middle, and outlet of the fixed-bed reactor for (A) 1 wt % $AuCl_3$/C and (B) 0.2 wt % $AuCl_3$/C/SiC (with 7.5 wt % of C coating). Measurements were conducted for the acetylene hydrochlorination reaction to acquire VCM, and processes were operated at 165 °C (initially set reactor temperature) at an acetylene GHSV of 240 h^{-1}. Adapted with permission from ref 218. Copyright 2014 by Elsevier Limited.
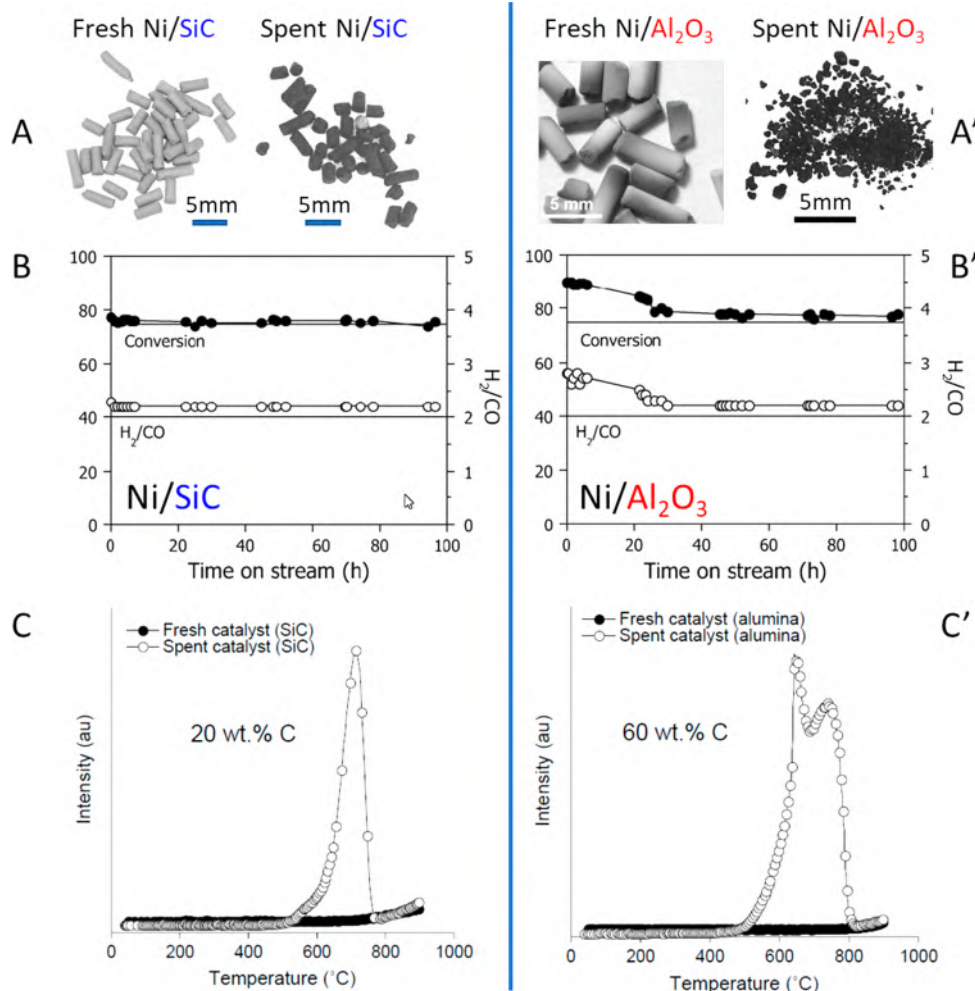
Figure 24. Optical pictures of Ni/SiC (A) and Ni/Al_2O_3 (A′) catalysts before (Fresh) and after (Spent) the methane CatPOx reaction. Catalytic partial methane oxidation to syngas with Ni/SiC (B) and Ni/Al_2O_3 (B′). Temperature-programmed oxidation (TPO) spectra of the carbon deposits on Fresh and Spent Ni/SiC catalysts (C) and the Ni/Al_2O_3 catalyst (C′) in the POM reaction. Adapted with permission from ref 55. Copyright 2004 Elsevier BV.

chloride (PVC).[219] They compared the activity and stability of their structured catalyst $AuCl_3$/C/SiC with a benchmark $AuCl_3$ loaded on extruded activated carbon pellets in a fixed-

bed reactor. They realized that the SiC foam-based catalyst loaded with one-fifth only of the Au amount used in the reference catalyst ($AuCl_3$/C) exhibited even higher HC≡CH

conversions and improved catalyst stability whatever the acetylene GHSV applied to the system (Figure 23).

Their outcomes clearly indicated a more effective and homogeneous distribution of AuCl₃ NPs on the structured catalyst. This feature together with better temperature control at the catalytic bed due to the higher SiC foam thermal conductivity as well as lower pressure drop encountered with the macroporous support served to improve both the catalyst efficiency and its lifetime on stream. As Figure 23 shows, the temperature swings recorded at the inlet, outlet, and in the middle of the fixed-bed reactor for the two catalytic systems in comparison (in particular "LetIn" and "Middle" values measured at the steady-state conditions) were appreciably lower on the structured catalyst than on the AuCl₃/C system. Besides the poorer performance of the metal richer AuCl₃/C catalyst, the higher temperature increase measured at the reactor inlet (Figure 23A vs 23B) reduces the catalyst lifetime. Indeed, the higher the local temperature caused by the process exothermicity, pressure drop phenomena at the high GHSVs, and the poor material heat-dissipation capacity, the faster the AuCl₃ decomposition to Au and the irreversible catalyst deactivation.[218]

3.1.5. Processes for Syngas Production.

Syngas, or synthesis gas, is a fuel mixture consisting primarily of H_2 and CO in variable ratios, and it represents a key feedstock for the production of hydrogen, ammonia, and methanol as well as synthetic hydrocarbon fuels.[220] It is commonly obtained as a product of coal gasification, and it is industrially produced with a relatively high H_2/CO ratio via the highly endothermic methane steam reforming (MSR) process (eq 7).

$$CH_4 + H_2O \rightarrow CO + 3H_2 \quad \Delta H = +225.4 \, KJ/mol \quad (7)$$
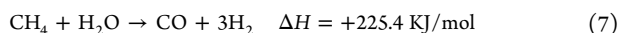
Lower H_2/CO ratios, more suitable for other industrially relevant processes like methanol and Fischer–Tropsch syntheses, have been conveniently obtained through either the catalytic partial oxidation (CatPOx) of methane (POM, eq 8) or dry methane reforming (DRM, eq 9).

$$CH_4 + \tfrac{1}{2}O_2 \rightarrow CO + 2H_2 \quad \Delta H = -38 \, KJ/mol \quad (8)$$

$$CH_4 + CO_2 \rightarrow 2CO + 2H_2 \quad \Delta H = +247 \, KJ/mol \quad (9)$$

POM (eq 8) to acquire syngas with a H_2/CO ratio of 2 is therefore a process of great commercial relevance that has attracted the interest of many research teams worldwide as to solve the many technical problems related to the development of sustainable, active, selective, and robust catalytic materials for the process. Among the drawbacks associated with this exothermic transformation, the generation of local temperature gradients within the fixed catalytic bed along with the formation of important coke deposits constitutes the main problems linked to the development of durable catalysts and represents a limit to the effective industrial exploitation of methane CatPOx.

Choudhary and co-workers were the first to perceive the importance of studying the effects of various parameters (i.e. use of different low surface area porous carriers including SiC, method of metal nanoparticle deposition, use of precoating agents and their loading, catalyst calcination temperatures) in the preparation of nickel-supported catalysts for an effective partial methane oxidation reaction.[221] However, a more complete account on the key advantages rising from the use of SiC matrices for Ni-based catalysts in the reaction was given later by Leroi and collaborators.[55] The French team concluded

that Ni/SiC was an excellent catalyst for the methane partial oxidation to syngas under medium pressures. At odds with classical insulator metal oxide supports, they demonstrated the excellent control of thermally conductive SiC toward the generation of hotspots at the catalyst surface along with its higher mechanical resistance to long-term reaction conditions (Figure 24A, A'). These features also reflected a higher coke resistance of Ni/SiC compared to the Ni/Al₂O₃ counterpart under identical conditions (Figure 24B, B'). A careful analysis of coke deposits on the two catalytic systems showed different morphologies for the grown carbons. While the alumina-based catalyst was essentially coated by C deposits in the form of high-aspect ratio nanofilaments with an average diameter of about 50 nm and length on the micrometer scale, the SiC-based catalyst presented either turbostratic or amorphous carbon structures. If different C morphologies of coke in the two samples were attributed to different Ni support interaction strengths (stronger on Al₂O₃ and lower on the more chemical inert SiC), the different amounts of coke deposits including the different graphitization degrees in the two samples (Figure 24C, C') were unambiguously ascribed to a more rapid heat evacuation from the catalytic bed ensured by the thermally conductive support.[55] The low mechanical stability of the alumina-based support also led to a complete disintegration of the catalyst after the reaction (Figure 24A'), while the SiC-based catalyst retains its morphology due to its high mechanical resistance (Figure 24A).

The Chinese team of Guo and co-workers came to similar conclusions later while studying 10 wt % Ni/SiC catalysts in the POM reaction.[222] They showed the effectiveness of their catalytic system in long-term (100 h) CH_4 conversion (≈75%) to syngas without requiring any catalyst H_2 preactivation and with an almost complete recovery of its catalytic performance after regeneration (burning of coke deposits) in air. The same team reported on catalyst modifications aimed at preparing more active, robust, and coke-resistant catalytic material for the process. They showed that pelletized, alumina-modified biomorphic SiC networks (Ni/bioSiC−Al₂O₃) exhibited high activity and stability in the POM reaction operated in a fixed-bed quartz reactor at 800 °C, under relatively high GHSVs.[223] They argued that the bioSiC surface modification with alumina (10 wt % NiO and 15 wt % Al₂O₃) strengthened the metal NP-support interactions thus reducing NP migration and sintering phenomena throughout the reaction. Similarly, N-doped SiC networks prepared by a nitridizing treatment of a plain SiC support were used by this team to increase the catalyst performance and stability on run.[224] High-temperature SiC nitridization was found to produce surface thin films consisting of Si−N−C or Si−C−N phases. The as-prepared SiC-N carriers offered preferential sites for the Ni-NP stabilization and a coke resistance from good to excellent depending on the support nitridization degree. The higher the support nitridization degree the higher the catalyst coke resistance but the lower the CO and H_2 selectivity in the process.

Al₂O₃-coated SiC foam monoliths decorated with Ni NPs were used as catalysts for the syngas production using a combined methane reforming process (MSR, eq 7 and POM, eq 8). Li, Xu et al. demonstrated the excellent structural stability (up to 900 h on run) of their SiC-based monolithic catalyst along with activity in the process close to the thermodynamic equilibrium (CH_4 conversion ≈96%), for the first 500 h on stream.[225] Most importantly, a comparison of the Ni−Al₂O₃/SiC catalyst with a Ni/Mg−Al spinel clearly
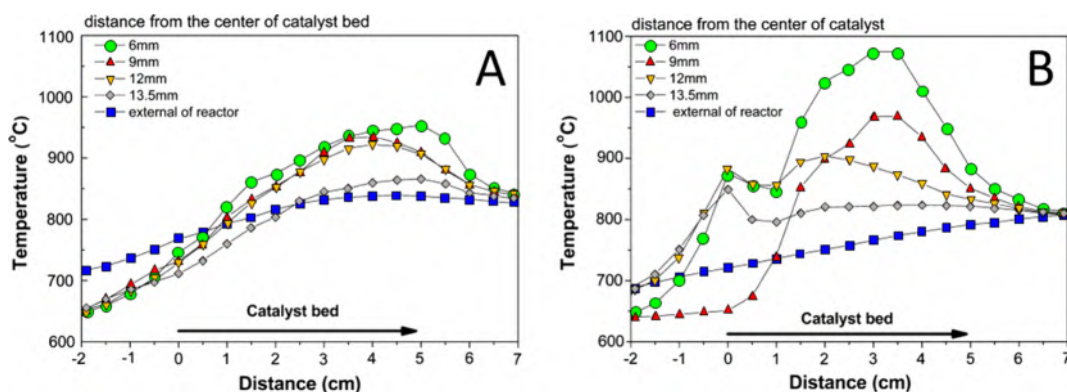
Figure 25. Temperature distribution profiles at the catalytic bed of Ni–Al$_2$O$_3$/SiC (A) and Ni/Mg–Al spinel (B) catalysts during syngas production by the combined MSR/POM reforming process. Adapted with permission from ref 225. Copyright 2013 Elsevier Ltd.
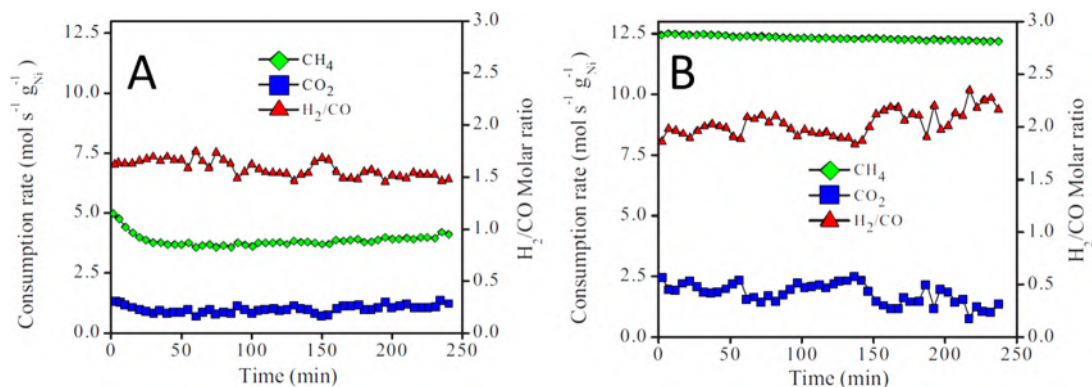
Figure 26. Catalytic activity of 5 wt % Ni/CeO$_2$ (A) and 5 wt % Ni/SiC (B) at 800 °C in the CH$_4$ tri-reforming. Ni NPs were prepared from Ni(OAc) as metal precursors, and catalysis conditions are CH$_4$ = 6%, CO$_2$ = 3%, H$_2$O = 3%, O$_2$ = 0.6%, N$_2$ balance, and total flow rate = 100 mL min^{-1}. CH$_4$ and CO$_2$ consumption rates vs time on stream (left axis) and H$_2$/CO ratio vs time on stream (right axis). Adapted with permission from ref 233. Copyright 2012 Elsevier BV.

showed that the former improved POM and MSR by intensifying heat and mass transfer phenomena. The study of temperature distribution profiles at the catalytic bed of the two Ni-based catalysts at work (Figure 25) clearly showed the considerably lower axial and radial temperature gradients measured at the SiC-based catalyst than those measured on the spinel-based one. The higher control of temperature runaway phenomena at the catalyst bed together with the SiC structural stability prompted these authors to build up a pilot-scale plant for the syngas production via POM/MSR coupling based on their catalyst technology.

Wei and co-workers have proposed a similar approach to syngas production by designing novel catalytic reactors based on surface modified monolithic SiC foams as to maximize mass and heat transfer phenomena in the combined POM (eq 8)/DRM (eq 9) process.[226,227] They reported on different SiC surface coatings as supports for Ni NPs, based on highly mesoporous Al$_2$O$_3$ layers[226] or silicate-1 zeolite (S-1).[227] In this way, they increased the poor specific surface area of the pristine carriers, improved the nickel active-phase dispersion, and strengthened its interaction with the support. Similar to the above,[225] SiC matrices ensured excellent control of the temperature at the catalytic bed, limiting hotspots formation and metal-NP sintering phenomena throughout the process. Overall, Ni–Al$_2$O$_3$/SiC and Ni–S-1/SiC have shown a far better catalytic performance and coke resistance compared to the simplest Ni/SiC and Ni/S-1 counterparts in the combined methane reforming reaction.

Garcia-Vargas and co-workers have systematically investigated the influence of various catalyst parameters and processing methods (*e.g.* feed composition,[228] copresence of alkaline and alkaline earth promoters,[229] order of metal impregnation in the catalyst synthesis,[230] and process operative temperatures[231]) on CH$_4$ conversion and the H$_2$/CO molar ratio in Ni/SiC catalysts for CH$_4$ tri-reforming. The latter, a synergistic combination of dry reforming (eq 9), steam reforming (eq 7) and the partial methane oxidation (eq 8) reaction,[232] allows for better control on energy issues related to syngas production as well as catalyst coking deactivation phenomena (eqs 10 and 11). Indeed, coke formation can be reduced by the presence of oxidants such as H$_2$O (eq 12) and O$_2$ (eq 13).

$$2CO \rightarrow C + CO_2 \quad \Delta H = -172 \text{ KJ/mol} \quad (10)$$

$$CH_4 \rightarrow C + 2H_2 \quad \Delta H = +75 \text{ KJ/mol} \quad (11)$$

$$C + H_2O \rightarrow CO + H_2 \quad \Delta H = +131.4 \text{ KJ/mol} \quad (12)$$

$$C + O_2 \rightarrow CO_2 \quad \Delta H = -393.7 \text{ KJ/mol} \quad (13)$$
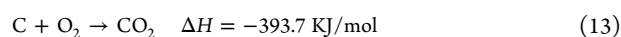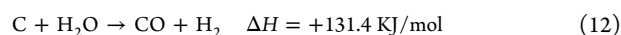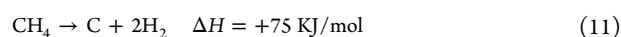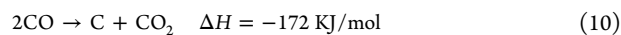
As far as the role of SiC is concerned, these authors demonstrated a higher consumption rate for methane and CO$_2$, improved catalyst stability, and higher H$_2$/CO molar ratios when tri-reforming was accomplished on SiC-supported Ni NPs instead of its CeO$_2$-supported counterpart (Figure 26).[233]
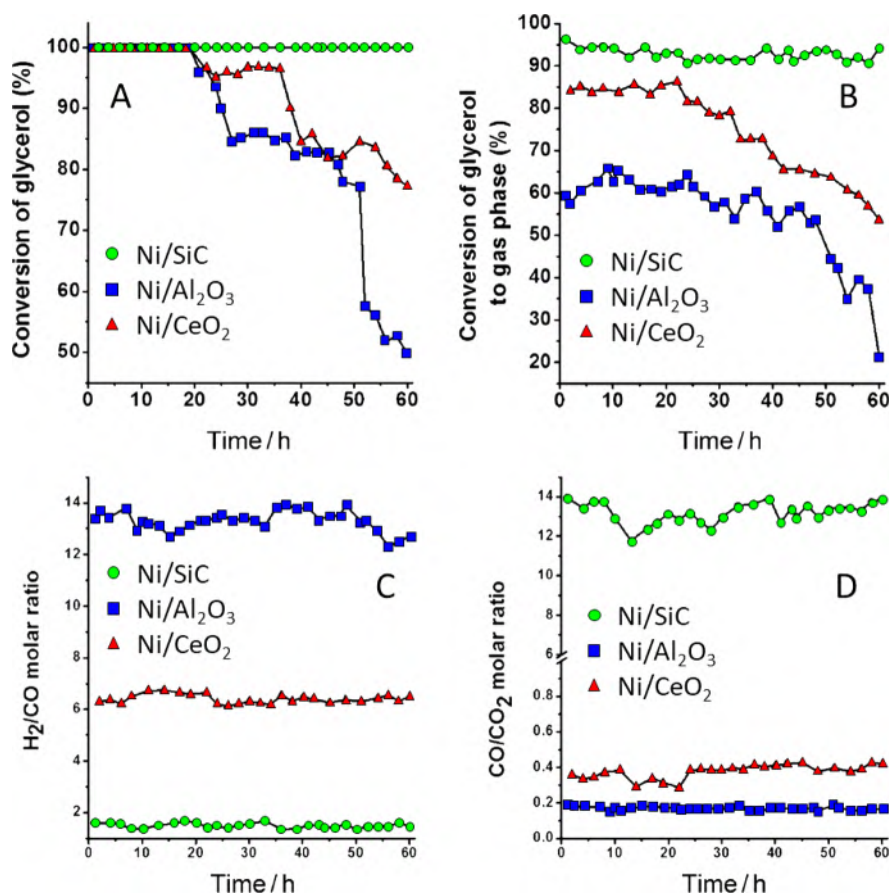
Figure 27. Glycerol steam reforming on Ni/SiC (●, green), Ni/Al$_2$O$_3$ (■, blue), and Ni/CeO$_2$ (▲, red) catalysts in comparison. Reactions conditions: Ni: 10 wt %, 400 °C, water to glycerol molar ratio (WGMR) of 9:1, feed flow rate (FFR) of 0.15 mL min^{-1} at atmospheric pressure. **A**: Catalyst stability vs time on stream in the glycerol conversion; **B**: Conversion of glycerol to gaseous products; **C**: syngas H$_2$/CO molar ratios; **D**: CO/CO$_2$ molar ratios. Figures adapted with permission from ref 239. Copyright 2012 Wiley-VCH Verlag GmbH& Co.

SiC ensured smaller Ni NP sizes, hence strengthening their interaction with the support. The smaller the Ni particles size, the lower the catalyst deactivation rate[234,235] and the higher the CH$_4$ consumption. In addition, catalysts on CeO$_2$ were found to increase CO$_2$ adsorption due to the higher basicity of the support. The higher basic character of the oxide support together with the larger size of the deposited Ni NPs accounted for a reduced H$_2$/CO ratio at the reactor outlet.[233] In a comparative study with Ni/SiC, the same team discussed the non-innocent role played by a series of oxide-based supports [*i.e.* CeO$_2$, γ-Al$_2$O$_3$, and yttria-stabilized zirconia (YSZ, with a Y$_2$O$_3$/ZrO$_2$ molar ratio of 0.08)] in the stabilization of Ni NPs.[236] They realized that metal dispersion, average Ni particle size, and their reducibility linked to the different interaction modes with the oxide-based carrier had important and disadvantageous effects on the ultimate catalyst performance in dry- and tri-reforming of methane. With the only exception of CeO$_2$, whose more basic surface character gave rise to a better performing catalyst for methane dry reforming (DRM, eq 9), Ni NPs on the chemical inert SiC showed the best performance in the tri-reforming reaction with a high methane reaction rate and without any significant deactivation.[236] Besides evident catalytic advantages of SiC-supported Ni catalysts for syngas production, the high mechanical strength and chemical inertness of this ceramic allow its easy recovery and reuse. Indeed, simple acidic or basic washings, eventually followed by thermal treatment of the spent catalysts, reduced the investment costs of the process for the final spent catalyst disposal and allowed the full reuse of the support.[237] Bae and collaborators studied LaSrNiO$_x$ mixed oxides supported on Al$_2$O$_3$-modified β-SiC networks as catalysts in the combined steam (SR) and dry reforming (DR) of CH$_4$ (CSCR).[238] Although DRM is generally considered one of the best ways to employ and convert CO$_2$ efficiently for the syngas production, its commercialization still appears limited by the severe drawbacks associated with the catalyst coking and its subsequent active-phase plugging on long-term runs. The CSCR reaction (eq 14) was then selected to skip over these kinds of technical limits while ensuring a desirable syngas composition (H$_2$/CO molar ratio of ≈2) for its subsequent utilization in methanol or Fischer–Tropsch synthesis.

$$3CH_4 + CO_2 + 2H_2O \rightarrow 8H_2 + 4CO \ (CSCR) \quad \Delta H = 659 \ kJ/mol \tag{14}$$
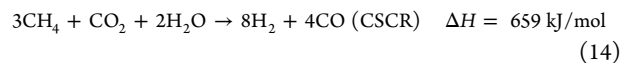
While the optimal loading of the Al$_2$O$_3$ phase on the SiC support was found to strengthen the interaction with LaSrNiO$_x$ crystallites and reduce the aggregation of Ni crystallites during the high-temperature reforming processes, the higher basicity of lanthanum and strontium oxides was supposed to foster the generation of local CO$_2$ concentration gradients proximal to the active sites for its conversion.[238]

The Korean team of Woo et al. discussed the advantages of SiC-supported Ni NPs for syngas production from glycerol steam reforming at temperatures below 500 °C.[239] Glycerol is
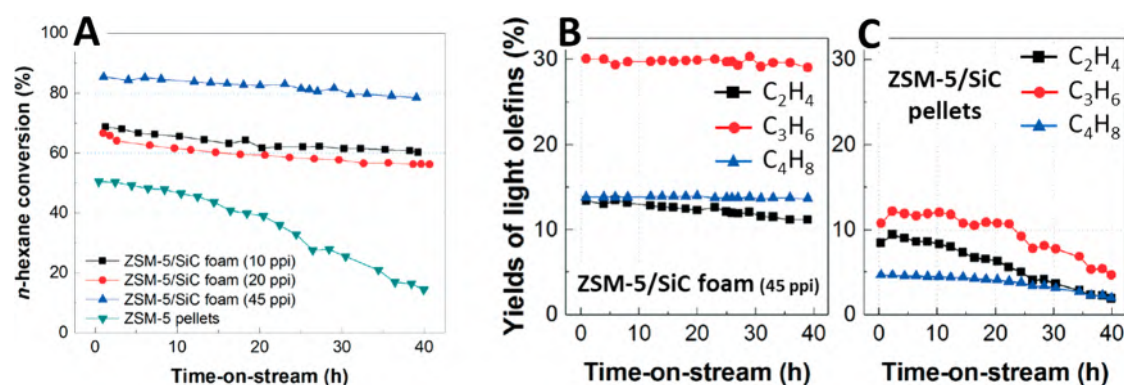
Figure 28. (A) *n*-Hexane conversion over ZSM-5/SiC foam catalysts (with different foam cell densities: 10−45 ppi) and ZSM-5 pellets (as a fixed bed) at a WHSV of 16 h^{-1}. Yields of light olefins in long-term catalytic runs conducted at WHSV of 16 h^{-1} by means of (B) the most performing ZSM-5/foam catalysts (45 ppi) and (C) a ZSM-5 pellet packed bed. Adapted with permission from ref 242. Copyright 2019 The Royal Society of Chemistry.

a byproduct of the biodiesel production.[240] Despite its fundamental use as raw material in various sectors of the modern industry,[241] its supply generally exceeds the market demand. This has moved research toward new horizons for a glycerol wider exploitation in different areas of the chemical industry. Given the large quantities of water in crude glycerol, these authors demonstrated its complete and stable reforming in the presence of steam to gaseous products (mainly syngas) with chemical yields higher than 90%, using a Ni/SiC catalyst containing a nominal 10 wt % metal loading.[239] To highlight the advantages of their carrier compared to more conventional metal oxides, they scrutinized the Ni/SiC catalytic performance and durability on stream versus Ni/Al$_2$O$_3$ and Ni/CeO$_2$ counterparts under identical conditions (Figure 27). At odds with the outstanding stability for tenths hours of Ni/SiC in glycerol conversion, Ni/Al$_2$O$_3$ and Ni/CeO$_2$ showed rapid and progressive deactivation. Such trends were unambiguously ascribed to the rapid generation of coke deposits deriving from glycerol byproduct cracking. Their formation was boosted by dehydration or condensation secondary reactions taking place on the more acidic or more basic surfaces of alumina and ceria, respectively. Moreover, Ni/SiC produced syngas with a 1.0− 1.9 H$_2$/CO ratio that was ideal for the direct use in other industrially relevant transformations (*i.e.* Fischer−Tropsch synthesis).

On the contrary, H$_2$/CO higher than 3 was obtained with Ni/Al$_2$O$_3$ or Ni/CeO$_2$ because of the higher hydrophilicity of metal oxide supports that was supposed to promote the occurrence of the water−gas shift side reaction (WGS, eq 15).

$$CO + H_2O \rightarrow CO_2 + H_2 \quad \Delta H = -41.1 \text{ KJ/mol} \quad (15)$$
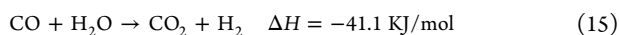
3.1.6. Other Processes for Fine Chemical Production.
Progress in the area of zeolite-based engineering of catalysts for MTO production (see also section 3.1.3.2) has strengthened the importance of increasing heat and mass transfer across alumino silicate layers, ensuring an optimal mixing of reagents and making products desorption from the catalyst as fast as possible. To this aim, the employment of SiC for catalyst production has marked a technological leap beyond the use of more conventional oxide- or carbon-based active-phase supports. Fan and co-workers have recently described the use of homogeneously coated SiC foams with a thin ZSM-5 zeolite layer as highly effective, robust, and selective cracking catalysts for *n*-hexane conversion to light (C$_2$−C$_4$) olefins.[242] In a comparative study with unsupported ZSM-5 pellets, they

demonstrated the higher performance of their SiC-structured catalyst (particularly for reactions operated at high weight hourly space velocity (WHSV), *i.e.* >10 h^{-1}), *e.g.* the olefin production per unit volume of reactor in the ZSM-5/SiC foam (45 ppi) catalyst was up to five times higher compared to ZSM-5 pellets (Figure 28A). Moreover, the structured catalyst showed a significantly improved antifouling behavior compared to plain zeolite pellets (Figure 28B vs 28C) and markedly higher selectivity toward target light olefins. SiC foams enabled a real catalytic process intensification, improving the global mass and heat transportation phenomena, maximizing the active-phase exposure to reagents and reducing the extent of pore clogging caused by coke deposits.

Successively, another zeolite-supported SiC catalyst was prepared by an Arabian research team with the assistance of a polymeric cationic template.[243] This latter induced a positive polarization on the SiC surface that attracted a negatively charged aluminosilicate and promoted the uniform growth of a zeolite (ZY) hence leading to stable ZY@SiC catalysts. The as-prepared hierarchical material showed remarkable activity in the *n*-heptane cracking process with reaction rates up to 3.5 times higher with respect to unsupported ZY and increased resistance toward deactivation. Moreover, ZY@SiC displayed a higher selectivity toward light olefins (24−36% yield) with respect to the ZY reference (7−17%). The better performance was ascribed to the homogeneous ZY dispersion on SiC that favored both reactants and products diffusion at the active sites hence increasing reaction rates while limiting the occurrence of undesired side reactions.

Nie et al. have proposed a highly efficient and selective reaction scheme for the microwave-assisted glycerol (C$_3$H$_8$O$_3$) dehydration to acrolein (HCOCH=CH$_2$) using SiC-supported WO$_3$ acid catalysts.[244] They proposed a sort of WO$_3$-decorated, ZrO$_2$@SiC core−shell particles (WO$_3$/ ZrO$_2$@SiC) as a microwave (MW) absorbing catalyst for the process. Joining the heat-dissipation properties of the catalyst SiC-core with a more rapid and accurate temperature tuning ensured by the microwave heating setup, they got complete glycerol conversion and selectivity to acrolein higher than 70%, operating the process at the nominal temperature of 250 °C. They also argued on the important advantages of MW-heating (compared to more conventional electric heating schemes) on the catalyst stability due to the more uniform temperature distribution as well as on the effectiveness of this heating technology for the regeneration of exhaust catalysts. As for the

first point, the virtual absence of important temperature gradients within the catalytic bed throughout the process was highly beneficial for the catalyst stability and lifetime on stream. Indeed, it limited catalyst fouling phenomena, particularly important in the case high-temperature processes, due to the generation of coke deposits.[244]

3.2. Fuels Production

3.2.1. Liquid Fuels. *3.2.1.1. SiC-Based Catalysts in the Fischer−Tropsch Process.* The Fischer−Tropsch process can be defined in brief as a catalytic technology used to convert syngas (H_2 + CO) to clean hydrocarbons from coal, natural gas, and biomass by means of a metal catalyst.[245−249] Hydrocarbons produced are prevalently liquid at ambient conditions, but some of them can also be gaseous or even solids in nature (eq 16).

$$nCO + (2n + 1)H_2 \rightarrow C_nH_{2n+2} + nH_2O \qquad (16)$$
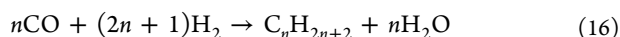
The Fischer−Tropsch process has rapidly gained the interest of the catalysis community as it conveniently links to the gas-to-liquids (GTL) industry,[250] hence to the production of added value fuels from stranded natural gases. One key feature of this technology is the ability to diversify its products from fuels to higher value chemical products. Nowadays, there are two main Fischer−Tropsch operating modes: 1) a low-temperature (200−240 °C) process catalyzed by either iron or cobalt catalysts for the production of high molecular mass linear waxes and 2) a high-temperature (300−350 °C) process promoted by iron-based catalysts and used for the production of gasoline and linear low molecular mass olefins.[248]

Fischer−Tropsch synthesis (FTS) is a highly exothermic process. Therefore, it is mandatory to adopt solutions to rapidly remove the reaction heat from the catalytic bed thus avoiding catalysts overheating that would accelerate their deactivation through sintering and fouling phenomena as well as favor the undesired production of light hydrocarbons and methane.[246,251] Avoiding temperature swings at the catalytic bed of a FT reactor is then crucial to control the process selectivity and hence the downstream application of its products. Possible products from FTS are gasoline, diesel, jet fuel, paraffinic waxes, lubricants, or petrochemical base products, just to mention a few.[252] Philippe and co-workers first figured out the importance of thermal properties and morphology of a catalyst support in such an exothermic transformation.[253] They studied a fixed-bed reactor model for the Fischer−Tropsch reaction using a cobalt catalyst over foam or extruded ceramics (*i.e.* Al_2O_3 and SiC) and observed that the thermal parameters of the catalytic bed along with the radial and axial temperature profiles of the reactor affected the catalyst performance in terms of yield, productivity, and selectivity.

A systematic study of heat transfer properties of SiC and other more classical oxide-based supports (*i.e.* SiO_2 and TiO_2) for Co catalysts in FTS was addressed later by Zhu and co-workers.[254] The authors' conclusions were a public endorsement to the merits of SiC matrices as supports for Co NPs while setting up a fixed-bed reactor for the process. Besides stressing the inherently superior heat transfer coefficient (K_{eff}) of silicon carbides compared to that of SiO_2 and TiO_2, their study unveiled that K_{eff} values increased by twice or three times during the FT reaction when SiC was used as a support. Indeed, the presence of variable amounts of liquid hydrocarbons formed throughout the process and soaking the

catalytic bed led to the increase of its heat transfer capacity. This was an extremely important finding, particularly in the case of highly exothermic processes, because it improved the control of the temperature runaway at the catalytic bed. In addition, they realized that K_{eff} values grow almost linearly with the hydrocarbon chain growth probability (α, Figure 29),[254] the latter being typically higher on chemically inert and micropore-free SiC matrices.
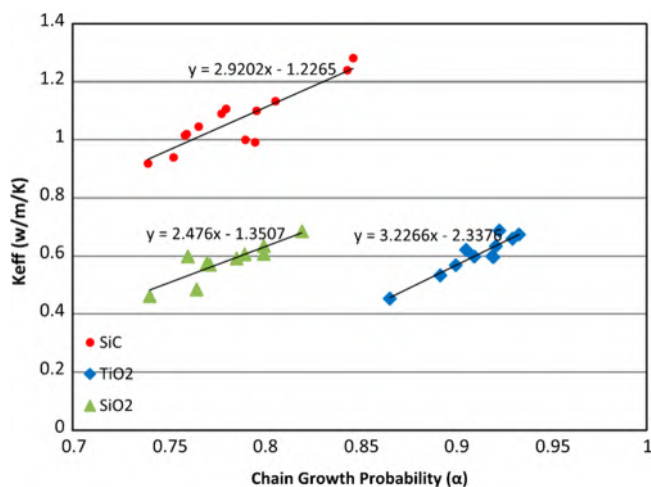
Figure 29. Linear correlation between the K_{eff} value and hydrocarbon chain growth probability (α) measured for three Co catalysts on different supports (SiC, SiO_2, and TiO_2) during FTS under comparable experimental conditions. Reproduced with permission from ref 254. Copyright 2014 Elsevier B.V.

From a chronological viewpoint, the first reports describing the technical advantages rising from the use of SiC foams in the preparation of Co catalysts for FTS were independently discussed in 2011 by Pham-Huu[52] and de la Osa.[255] The French team demonstrated the higher efficiency of SiC matrices in reducing the generation of local temperature gradients throughout the reaction course.[52] The higher the thermal conductivity of the active-phase support, the higher the catalyst performance. The higher thermal conductivity of SiC foams compared to that of Al_2O_3 foams along with the prevalently meso- and macroporous nature of the former was indicated as the main features responsible for the higher performance of Co/SiC catalysts when FTS was operated at high CO conversion rates (≥70%). Under relatively severe FTS conditions, selectivity to C_{5+} hydrocarbons on Co/SiC reached up to 88% at the steady-state conditions compared to 52% of its Co/Al_2O_3 counterpart. Similarly, the hydrocarbon chain growth probability (α), calculated from the portion of linear hydrocarbons produced in the process was found to be affected by the choice of the support and its ability to evacuate/dissipate the excess of heat generated during FTS (α = 0.91 and 0.85 for Co/SiC and Al_2O_3/SiC, respectively). The higher the local temperature gradient formation, the more likely the occurrence of undesired cracking processes and the consequent higher concentration of lighter hydrocarbons generated from these cracking side reactions.

To guarantee a higher dispersion of Co NPs on their structured catalysts, the same authors reported on the preparation of an Al_2O_3-coated SiC carrier and its use as the Co-decorated catalyst for FTS (Co/Al_2O_3−SiC). They found that the thermal conductivity of the underneath SiC core was
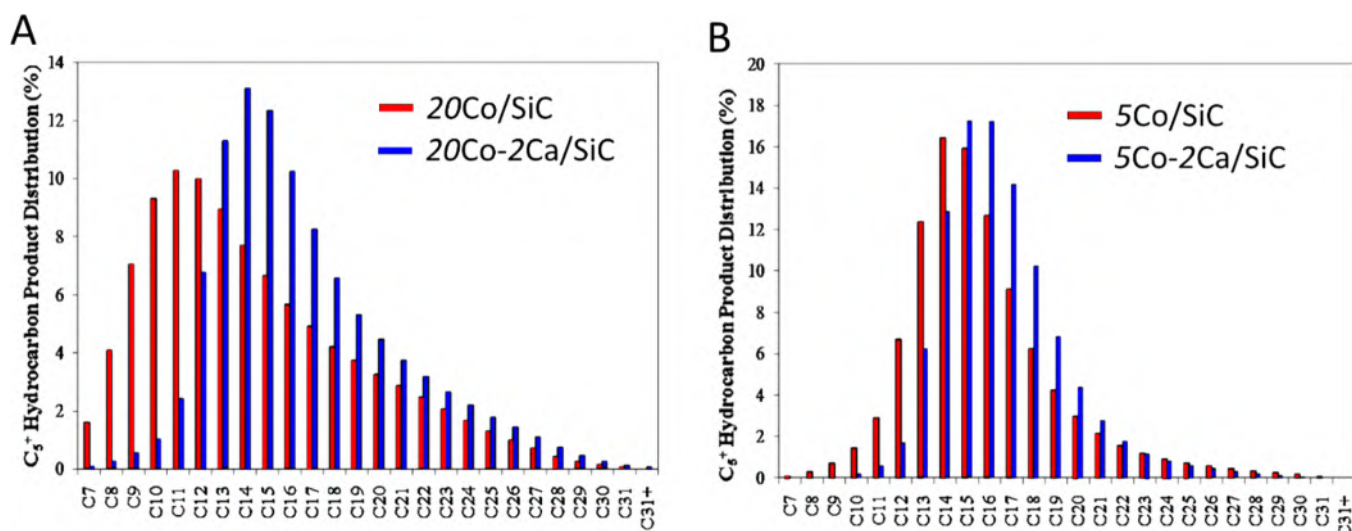
Figure 30. C_{5+} hydrocarbon distribution in a Fischer–Tropsch process catalyzed by an alkaline earth predoped Co/SiC catalyst of general formula mCo-nCa/SiC; m = 5–20 wt %; n = 0 or 2 wt %. Other experimental conditions: GHSV: 6000 Ncm^3 g^{-1} h^{-1}. H$_2$/CO: 2; reaction temperature: 250 °C. (A) Cat. 20Co/SiC vs 20Co-2Ca/SiC; (B) 5Co/SiC vs 5Co-2Ca/SiC. Adapted with permission from ref 258. Copyright 2012 Elsevier B.V.

still crucial for ensuring a better catalytic performance of the composite (C_{5+} select. 87%, α = 0.89) compared to the plain Co/Al$_2$O$_3$ system.[52] The Korean teams of Park and Bae also discussed the beneficial effects coming from alumina modifications (ideal in the amount of ≈10 wt %)[256] of SiC supports in terms of cobalt crystallite size control (larger on plain SiC matrices) and their deactivation rate due to the generation of carbon filaments (catalyst coking). They found that the rate of filamentous carbon formation was accelerated on FTS catalysts possessing large cobalt crystallites and featuring weaker metal–support interactions as in the case of NPs grown on the bare SiC network.[256,257]

de la Osa and co-workers came to similar conclusions with their Co/SiC catalyst showing higher CO conversions, improved FTS rates, and product shifting toward higher molecular weight hydrocarbons compared to the benchmark Co/Al$_2$O$_3$ system as well as related Co/TiO$_2$ and Co/bentonite catalysts.[255] By studying different formulations of a FT Co catalyst prepared from predoped SiC matrices with variable percentages of an alkaline earth promoter (mCo-nCa/SiC; m = 5–20 wt %; n = 1–2 wt %), this team also showed that the calcium doping increased the basic surface properties of the samples, improved Co NP dispersion, and finally affected CO conversion and C_{5+} hydrocarbon selectivity.[258] They reported that a Ca-promoted catalyst shifted C_{5+} distribution toward higher molecular weight hydrocarbons, especially in the case of catalysts with higher Co content and thus featured by typically larger metal particle sizes. Hence, doping the 20 wt % Co/SiC catalyst with 2 wt % of calcium (20Co-2Ca/SiC) shifted the FT hydrocarbon product distribution from a typical gasoline-kerosene formulation to a kerosene-diesel formulation mainly (Figure 30A). On the contrary, with catalysts featuring a lower Co content (5 wt %, 5Co/SiC) and thus lower metal particle sizes, the addition of a promoter (5Co-2Ca/SiC) shifted an already selective kerosene-diesel FT catalyst to a catalyst for diesel production with only negligible amounts of heavier hydrocarbons (Figure 30B).[258]

A systematic investigation of the catalyst configuration (wt % cobalt and wt % calcium as promoter) along with careful

control of all other variables (i.e. metal particle size, basicity, and extent of metal reduction) led to the optimal catalyst composition (12.5Co-2Ca/SiC) suitable to ensure the best compromise between CO conversion and C_{5+} selectivity.[259] Later on, the same Spanish team also reported on the selective production of C_{5+} middle distillates from syngas using a Co/SiC catalyst in an *ad hoc* engineered FT reactor for the "cascade waxes hydroprocessing" promoted by proton-type zeolites (i.e. H-ZSM-5 and H-βeta zeolites).[260]

A series of commercial SiC samples in the form of either grains or pellets were tested as supports for a 12.5 wt % of a Co active phase, eventually codoped with alkali and alkaline earth elements. These composites were scrutinized by a Norwegian team as catalysts for FTS, and their performance was compared with the benchmark Co/Al$_2$O$_3$ catalyst.[261] The authors pointed out the much lower activity per gram of catalyst of their SiC-based systems compared to Co/Al$_2$O$_3$, due to lower site-time yields (STYs, s^{-1}), larger Co particles, and lower Co loadings obtained with non-oxide supports. Partially in contrast with previous reports,[258,259] they argued about the detrimental effect rising from the presence of alkali or alkaline earth metal contaminants in SiC matrices. Their presence translated into an appreciable decrease of the catalyst activity (STY), whereas only moderate effects were observed on the products selectivity. In line with previous contributions from the literature, they concluded that FT selectivity toward heavier hydrocarbons was a common feature for almost all of their SiC-based catalytic materials. The observed selectivity was due to the higher ability of SiC to dissipate heat from the catalytic bed and to the non-microporous nature of these non-oxide materials.[262] Similar conclusions were drawn later by Diaz and collaborators. These authors described the beneficial effects rising from an acid treatment of β-SiC extrudates on the performance of their Co composites in FTS.[263] In this way, they claimed a reduction of metal impurities (detrimental for the FT process) in SiC networks while increasing SiC surface acid sites which seemed to facilitate the reducibility of Co oxide particles hence fostering higher CO conversions.

Playing with the effect of metal promoters, the Hungarian team of Li confirmed later the detrimental effect of an alkaline
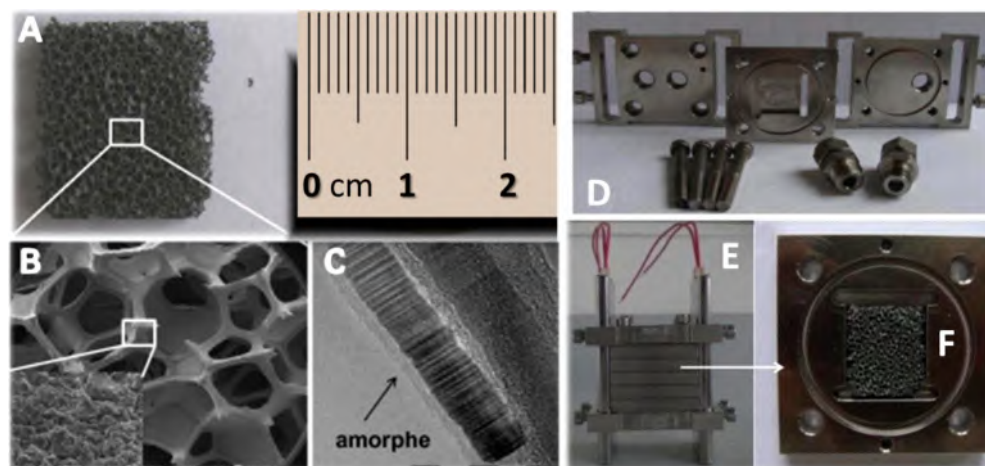
Figure 31. (A) Optical photo of an open-cell SiC foam used in the PSR setup. (B) SEM micrographs at different magnifications showing the strut size and porosity of the SiC foam and (C) HR-TEM image showing the presence of an amorphous SiO_2/SiO_xC_y layer at the SiC topmost surface; the latter was supposed to facilitate and stabilize the metal active phase. (D−F) Optical photos of PSR and reactor details. (F) Open-cell Co−Ru/SiC-E foam catalyst inside the reaction chamber. Adapted with permission from ref 266. Copyright 2013 Elsevier BV.

earth codoping (5 wt % of Ca) on the performance of a 15 wt % Co/SiC catalyst.[264] In their contribution, these authors compared various metal dopants selected among Ca, Zr, and Mn and studied their effect in Co/SiC FT catalysis. While Zr and Mn codoping gave catalysts with superior CO conversions and higher hydrocarbon chain growth probability (α), Ca doping inhibited the catalyst performance and favored the generation of lighter products.

The Pham-Huu team first reported on the preparation of a 30 wt % Co/SiC catalyst doped with 0.1 wt % of Ru by incipient wetness impregnation using ethanol as the solvent.[265] The authors demonstrated the advantages rising from the use of an alcohol in the place of water for the preparation of the FT catalyst. In this way, they got a robust SiC-E-based catalyst (E = ethanol) made of Co NPs with a larger surface-to-volume ratio, containing a higher degree of Co−Ru alloys, and with excellent FTS performance (up to a rate of 0.54 $g_{CH_2} \, g_{cat.}^{-1} \, h^{-1}$) toward the C_{5+} hydrocarbon production ($\approx$90%).[265] An additional step forward toward the preparation of a more efficient and C_{5+} selective FTS setup was made through a formulation in a platelet structured milli-reactor (PSR−Figure 31), using open-cell SiC foams of variable morphology (cell size, macroscopic porosity, strut diameter).[266]

They showed that larger pore sizes of meso- and macroporous SiC networks, besides favoring heat transfer, ensured an optimal axial and radial flow pattern of gaseous reagents and liquid products throughout the catalytic bed. The large pores of the SiC matrix were claimed to allow a rapid evacuation of the liquid hydrocarbons from the catalytic bed. This ensured a higher accessibility of reactants to the active phase (hence favoring higher FTS activity−up to 0.7 $g_{CH_2} \, g_{cat.}^{-1} \, h^{-1}$) and reduced the hydrocarbon resident time in contact with the catalyst (hence improving the selectivity toward heavier hydrocarbons−up to 95% at 220 °C under a relatively high GHSV of 3800 h^{-1}−and reducing the occurrence of side-cracking processes responsible for the catalyst fouling). The authors clearly demonstrated the improved robustness and catalytic performance of their SiC foam-based PSR in FTS compared to a more traditional microtubular fixed-bed reactor and paved the way for the study of the influence of SiC morphology on the design and up-scale

production of more performing FT catalysts.[266] Diaz and collaborators came to similar conclusions by studying the effects of a porogenic agent on a series of commercially available β-SiC extrudates.[263] The higher macropore volume of SiC supports the faster evacuation of products from the catalyst active sites with important benefits in terms of CO conversion, product selectivity, and catalyst stability on run.

A Ru-doped Co catalyst for FTS was recently reported by Moon and co-workers.[267] The authors described a series of SiC-modified γ-Al$_2$O$_3$ supports for a Co−Ru (15 wt %-0.3 wt %) active phase prepared by the incipient wetness impregnation method on extruded support granules obtained from acid boehmite dispersions at increasing percentages of silicon carbide (from 5 wt % to 25 wt %). They realized that increasing SiC contents in the catalyst support improved the sample thermal conductivity and enhanced the catalyst performance (CO conversion). On the other hand, the higher the SiC content the weaker the metal−support interactions, the larger the size of cobalt crystallites and thus the lower the CO conversion in FTS. They compared the increase of SiC content beyond a certain extent to the sintering effect often responsible for a decrease of the catalyst performance. Anyhow, they concluded that Co−Ru (15 wt %-0.3 wt %)/SiC-γ-Al$_2$O$_3$ was the best compromise between the positive effect rising from the enhanced thermal conductivity of the support and the negative effect resulting from the decrease of metal−support interactions and hence from the increased Co particle sizes.[267]

Solomonik et al. studied the Co active-phase composition and dispersion on the ultimate catalytic properties of their SiC composites in FTS.[268] Their study pointed out how different SiC support genesis and catalyst manufacturing procedures translated into different materials porosity, Co phase composition, and hence catalytic performance in the process. In line with previous achievements, they confirmed the role of ethanol as a metal precursor solvent, for the generation of highly dispersed and uniformly fixed Co NPs at the carrier surface. In the same year, the Korean team of Moon came across similar conclusions: the existence of a tight relationship between the average pore size of SiC supports, the surface density of Co NPs, their sizes and interaction with the support,
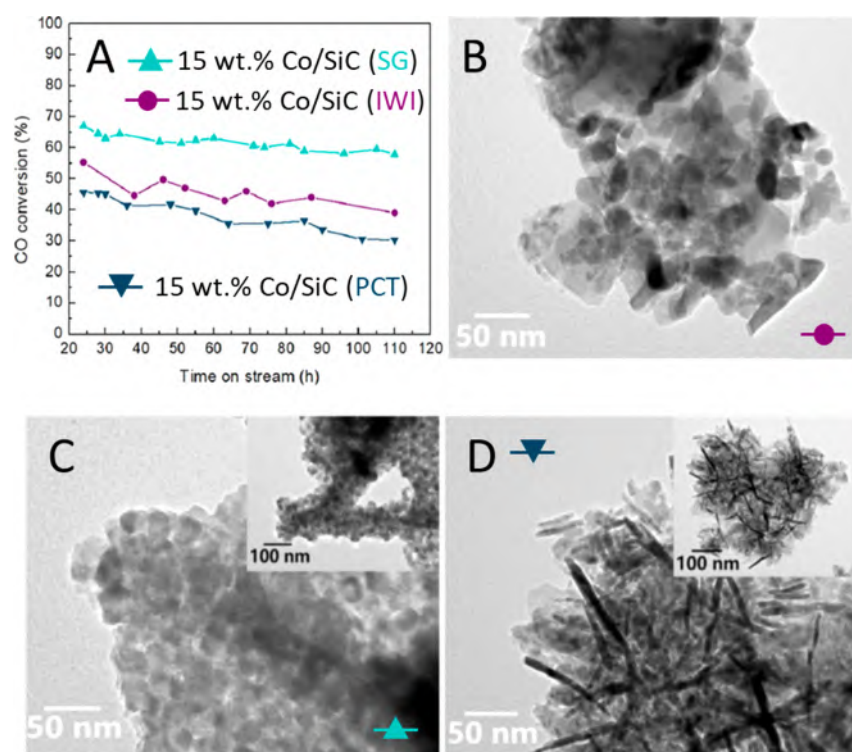
Figure 32. (A) CO conversions and catalyst stability reported as time on stream for 15 wt % Co/SiC catalysts in FTS, prepared by different preparation methods. Other experimental conditions: (precat. 2 g of Co_3O_4/SiC; T = 220 °C, H_2/CO = 2, P = 20 bar). TEM images of the freshly prepared 15 wt % Co/SiC by IWI (B), SG (C), and PCT (D) methods. Adapted with permission from ref 271. Copyright 2018 Elsevier Ltd.
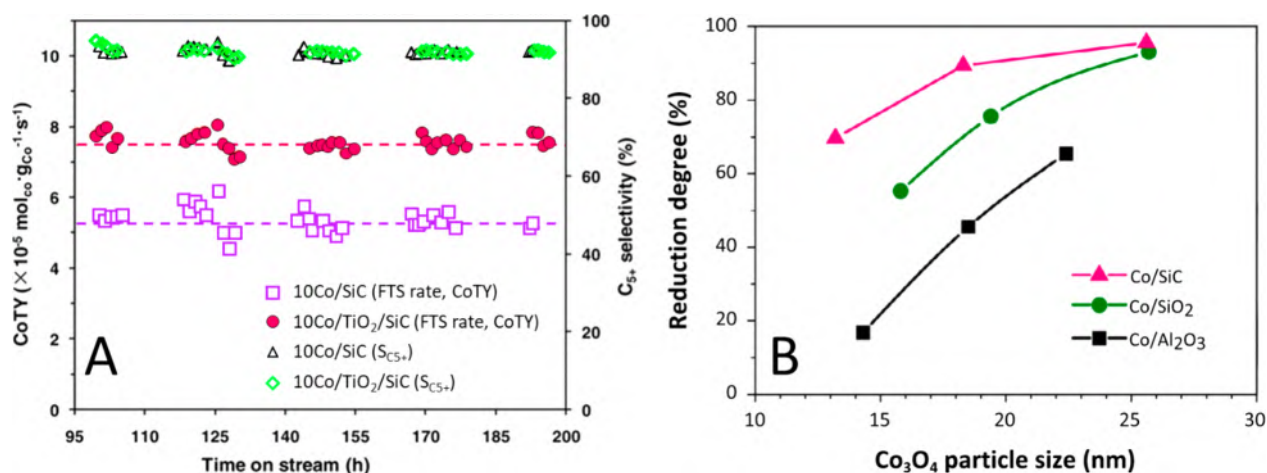
Figure 33. (A) FTS performance and stability of 10 wt % Co/SiC and 10 wt % Co/TiO_2/SiC catalysts as a function of time on stream at 230 °C. Reaction conditions: H_2/CO molar ratio = 2, pure syngas, total pressure = 40 bar, GHSV (STP) = 2850 h^{-1}. FTS rates are expressed as cobalt time yield (CoTY, mol of CO converted per gram of Co per hour). Adapted with permission from ref 275. Copyright 2013 American Chemical Society. (B) Reducibility of Co_3O_4 nanoparticles as a function of the NP size and nature of the support between SiC, SiO_2, and Al_2O_3. Adapted with permission from ref 281. Copyright 2013 Elsevier Ltd.

and the ultimate catalytic performance of the composites in FTS.[269] They demonstrated that 15 wt % was the optimal Co loading for SiC-based composites prepared via a dry impregnation technique as to maximize their catalytic performance in FTS while guaranteeing high C_{5+} hydrocarbon selectivity. de la Osa and co-workers also showed the direct influence of Co-metal precursors on the ultimate catalytic performance of Co/SiC catalysts in FTS prepared by vacuum-assisted impregnation.[270] They found that the metal precursor choice, selected among nitrate, acetate, chloride, and citrate

salts, influenced both catalyst basic properties, the extent of cobalt oxide spinel phase (Co_3O_4) reduction, and finally the metal particle sizes. Their conclusions unveiled that cobalt nitrate $[Co(NO_3)_2]$ could provide a Co/SiC catalyst with superior activity and C_{5+} selectivity [centered in the kerosene-diesel fraction (α = 0.90)] in the FT process. Later, Luo and co-workers referred to the effects of the Co phase preparation methods [i.e. incipient wetness impregnation (IWI), sol–gel (SG), and precipitation (PCT) methods] on the final performance of 15 wt % Co/SiC FT catalysts.[271] Using
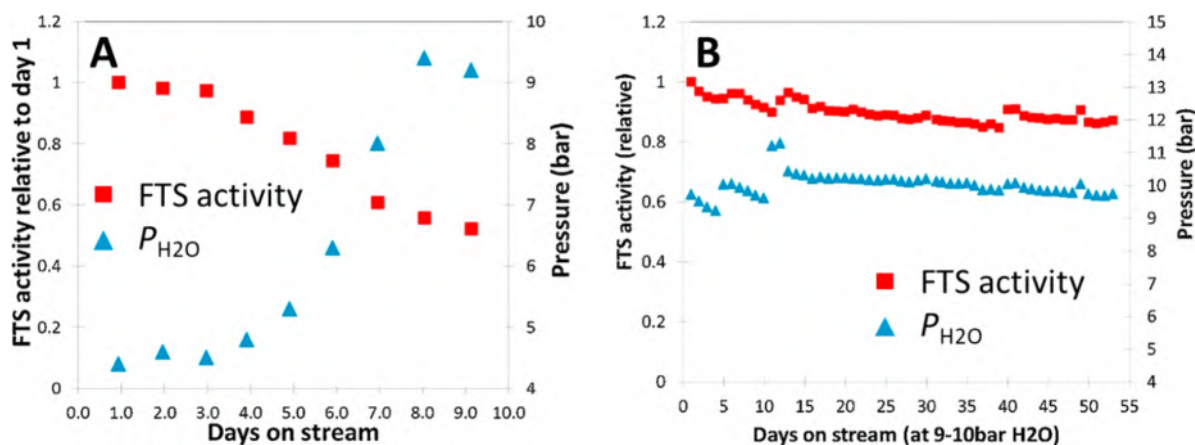
Figure 34. (A) Long-term FTS performance of a benchmark 20 wt % Co/Al_2O_3 catalyst as a function of a water partial pressure (P_{H_2O}) in the 4−9 bar range. (B) Long-term performance of a 15.9 wt % Co/β-SiC catalyst at the water partial pressure (P_{H_2O}) of 9−10 bar. The catalyst was prepared by aqueous slurry-phase impregnation and calcined at 550 °C before activation. Adapted with permission from ref 288. Copyright 2016 Elsevier B.V.

aqueous solutions of $Co(NO_3)_2 \cdot 6H_2O$ as the salt precursor, they showed that the SG method produced a Co/SiC catalyst with the highest activity, C_{5+} selectivity, and stability in long-term FT runs (Figure 32A). On the other hand, the PCT method gave rise to the worst Co/SiC catalytic system. The authors ascribed the higher performance of the Co/SiC catalyst prepared by the sol−gel method to a higher degree of reducibility and dispersion of obtained Co oxide particles, including a more appropriate size of spinel grains that fosters ideal metal−support interactions (Figure 32).[271]

Romar et al. outlined the effect of noble metal doping (*i.e.* 0.2 wt % Ru and/or Re) on the mean NP size and metal dispersion of Co catalysts for Fischer−Tropsch synthesis.[272] Their study remarked the importance of controlling the mean particle size and distribution of a Co active phase whatever the nature of oxide or oxide-free support used.[273] The noble metal doping of Co catalysts with a loading between 15 and 20 wt % deeply affected the resulting Co metal surface area by reducing the average Co NP size. In the case of a 20 wt % Co/SiC catalyst, doping with 0.2 wt % of Ru or Re translated in a reduction of the mean Co particle size by 40 and 62%, respectively. They finally showed that such a size control had important implications on the catalysts' preparation and their performance in FTS.[272] In this regard, they also demonstrated the role of noble metal promoters in decreasing the reduction temperatures needed for the conversion of Co_3O_4 to CoO up to its metallic form (Co^0). They realized that a significant decrease in the reduction temperature was possible especially when Ru was used as a promoter. For instance, for the above-mentioned 20 wt % Co/SiC catalyst, 0.2 wt % of Ru decreased the reduction temperature of the mixed Co^{II}/Co^{III} tetraoxide (Co_3O_4) to CoO from 698 to 573 K and that of CoO to Co^0 from 793 to 743 K.[274]

The Pham-Huu team also unveiled the benefits rising from the use of TiO_2-decorated SiC networks as supports for the Co active phase in the low-temperature fixed-bed FTS.[275] A careful spectroscopic[276] and advanced electron microscopy characterization of their new catalyst[277] unveiled that TiO_2 doping of β-SiC matrices created a highly favorable and homogeneous environment to grow small-medium sized Co NPs (<15 nm) thus contributing to the enhancement of CO conversion and hence to the increase of the reaction rate compared to the plain Co/SiC system (Figure 33A). They also showed that $Co-TiO_2/SiC$ outperformed similar catalytic systems of the *state of the art* prepared from different supports or catalyst formulations,[259,262,278−280] including their previous Ru-promoted Co/SiC system (Co−Ru/SiC-*E*).[265] As far as a comparison with the plain Co/SiC is concerned, $Co-TiO_2/SiC$ at 230 °C showed markedly higher reaction rates [from 5.3 × 10^{-5} for 10 wt % Co/SiC to 7.5 × 10^{-5} mol_{CO} g_{Co}^{-1} s^{-1} (cobalt-time-yield, CoTY) for 10 wt % $Co-TiO_2/SiC$] and comparably high C_{5+} selectivity (91.7% for 10 wt % Co/SiC vs 91.6% for 10 wt % $Co-TiO_2/SiC$) (Figure 33A). Once again, the authors pointed out the remarkable contribution to FTS performance rising from the unique properties of the non-oxide matrices. Their physical properties along with their easy tunable meso- and macroporous morphology made them ideal candidates for FT catalysts, ensuring adequate heat and mass transfer control across the catalytic bed.

Liu and co-workers proved the higher performance of Co/SiC catalysts in FTS with respect to related Co/Al_2O_3 and Co/SiO_2 counterparts as a consequence of the less size-dependence and easier reducibility of Co_3O_4 NPs before the FT catalytic run.[281] Indeed, the inertness of silicon carbides and the subsequent weak Co_3O_4−SiC interactions were found to be a smart and sustainable alternative to the use of noble metals as promoters for the Co oxide reduction.[282−286] As Figure 33B shows, reduction of Co_3O_4 in a H_2 flow at 400 °C and constant GHSV was much higher and less NP-size dependent in the case of SiC compared to SiO_2 and Al_2O_3. On the other hand, the weaker Co-SiC interactions were found to be responsible for a faster catalyst deactivation favored by active-phase leaching and sintering phenomena. Similar to the use of TiO_2-doped SiC networks,[275] these authors greatly improved the catalyst activity and stability of their Co/SiC system in FTS using a ZrO_2-modified catalyst. The addition of ZrO_2 reduced the generation of coke deposits on Co sites, and Co NP sintering was alleviated as well.[281]

Piao et al. studied the chemical state of ZrO_2 modified Co/SiC catalysts via *in situ* STEM and EELS techniques.[287] The authors found that the low content of ZrO_2 generated a single-site dispersion on the surface of Co nanoparticles (NPs) and on the SiC support. In this form, it played as the real active site to promote CO dissociation at the $Co-ZrO_2$ interface. When

the ZrO_2 content increased (1:1 Zr/Co molar ratio), ZrO_2 formed an amorphous coating on SiC, whereas it maintained monodispersion on the Co NPs. Finally, for higher ZrO_2 content (1.5:1 Zr/Co molar ratio), cobalt NPs started to be encapsulated by a ZrO_2 coating, losing its catalytic activity in FTS.

Moodley and co-workers highlighted the advantages of SiC supports for the preparation of Co-based catalysts for FTS in comparison with the more common refractory oxides by pointing out the higher stability of the former supports in more hydrothermally demanding environments.[288] At odds with the more classical fixed-bed reactor configuration, they scrutinized a series of Co/SiC catalysts prepared by aqueous slurry-phase impregnation in a continuous stirred-tank reactor (CSTR) under relatively high water partial pressures (P_{H_2O} *ca.* 10 bar). In a long-term FT comparative study (Figure 34) with the benchmark Co/Al_2O_3 catalyst, they proved the markedly higher water tolerance of Co/SiC-based systems and hence their higher stability under relatively high water partial pressures (P_{H_2O}). As Figure 34A shows, a water-induced Co/Al_2O_3 catalyst deactivation (estimated in *ca.* 50% of its pristine activity) was observed within a period of 4 days by operating the process at a P_{H_2O} between 4 and 9 bar. Remarkably, the activated and Co/β-SiC catalysts showed an activity decrease of only 10% (Figure 34B) over a 52-day period at a P_{H_2O} of about 10 bar.[288]

In line with previous reports, these authors also confirmed the beneficial effects on Co/SiC systems rising from a β-SiC surface pretreatment with an acidic-oxidizing agent or from its precoating with a homogeneous TiO_2 layer. While the former treatment was supposed to increase the thickness of anchoring SiO_xC_y sites and remove potentially detrimental metal impurities for the process, the latter ensured a better metal dispersion and stability to the Co active phase, improving the catalyst performance and its stability on run. In a very recent study, the team of Jia has systematically analyzed the effect of nitric acid SiC pretreatment on the formation of SiO_xC_y surface sites and their ultimate role on FTS performance of their Co/SiC catalysts. The study unveiled that the higher the nitric acid concentration used for the pretreatment, the larger the thickness of the surface SiC amorphous layer but the lower the content of SiO_xC_y surface sites. They finally demonstrated that a gradual decrease of SiO_xC_y sites holds beneficial effects on FTS by facilitating Co_3O_4 reduction and increasing the hydrocarbon chain growth probability.[289] In a previous report, the Hou team also shed light on the inherent nature of the surface Si_xO_y layer on SiC and its final role on the FTS performance of related Co-based catalysts.[290] These authors claimed a non-innocent role of the Si_xO_y surface groups in the Co_3O_4 reduction to Co^0 as well as on the electronic effects resulting from their interactions with metal nanoparticles. They showed that an Al_2O_3–SiC-coated sample and the respective 10 wt % Co/Al_2O_3@SiC composite behaved differently from the 10 wt % Co/SiC catalyst under identical conditions. Co/Al_2O_3@SiC showed a nearly double methane selectivity compared to Co/SiC, and C_{5+} selectivity of the latter was up to 10% higher than that measured on the Al_2O_3-coated samples. Accordingly, their conclusions were that SiC networks were excellent support candidates for Co catalysts in FTS not only for their inherently higher thermal conductivity but also because metal nanoparticle interaction with surface Si_xO_y groups maintained a key role in the process.[290] Afterward,

this research team also stressed the importance of the support thermal conductivity on the catalyst performance at high reaction rates (selectivity and stability on long-term runs) by comparing Co catalysts prepared on non-porous silicon-based samples (SiC, Si_3N_4, and SiO_2) featured with different thermal conductivities.[251] Their comparative study stressed once again that thermally conductive materials as supports for FTS Co catalysts (SiC ≫ Si_3N_4 > SiO_2) limited the generation of local temperature gradients at the catalyst bed, hence improving the process lifetime and hydrocarbon chain growth probability (α). The same group has recently reported on the influence of Co-ZrO_2 interfacial sites on Fischer–Tropsch activity. To this aim, a series of bimetallic SiC-supported materials were prepared adjusting the impregnation sequence of Zr to be added to Co/SiC.[291] The authors found that the higher the Co-ZrO_2 interfacial sites the higher the catalyst activity and selectivity toward C_{5+} products. SiC was selected as an ideal support for its high thermal conductivity but mainly for its chemical inertness that avoided strong metal–support interactions commonly observed with classical Al_2O_3 or SiO_2. It was therefore an ideal choice for investigating the effect of Co-ZrO_2 interfacial sites on Fischer–Tropsch synthesis without any interference from the support. Another group-IV promoter for Co/SiC was very recently identified by the Rosseinsky team.[292] A wide screening with six different supports and five promoters was used to demonstrate again the superior performance achieved with SiC with respect to activated carbon and oxide-based carriers, while Hf, with little amounts of Ru, was identified as a valid choice for improving both activity and stability.

In 2020, Kruse et al. investigated the Fischer–Tropsch activity of a cobalt-based catalyst prepared by deposition of colloidal Co NPs on a electrochemically derived mesoporous SiC.[293] The uniform metal dispersion and the porosity of silicon carbide allowed an ideal reactant and product diffusion to the active sites ensuring a catalytic activity as high as 117 μmol_{CO} g_{Co}^{-1} s^{-1} that was 1 order of magnitude higher than that recorded with Co NPs deposited on silica. Moreover, Co/SiC ensured a significantly higher selectivity for C_{5+} products with respect to Co/SiO_2 mainly attributed to the higher ability of SiC in dissipating heat.

Properties of SiC-based iron-Fischer–Tropsch catalysts in high-temperature processes (300−340 °C) for the production of linear low molecular weight (C_2−C_4) hydrocarbons [high molar percentage of light olefins ($C_2^=$−$C_4^=$) in the C_2−C_4 hydrocarbon range expressed as O/(O+P); O = $C_2^=$−$C_4^=$; P = CH_4 + C_2−C_4 paraffins] have recently been discussed by Liu and co-workers.[294] These authors have systematically scrutinized the effects of various oxide and oxide-free supports including promoters (*i.e.* K, Na, and S) on the performance of Fe-mediated FT catalysts. As far as the use of SiC as a support is concerned and more in general at odds with classical active-phase supports for the process (*i.e.* activated carbon, TiO_2, Al_2O_3 and SiO_2), they observed a remarkable improvement in CO conversion from 26.6% to 57.1% and the O/(O + P) from 37.6% to 77.1% upon K-doping (0.8 wt %) of their 10 wt % Fe/SiC catalyst. They also realized that thermal properties of SiC matrices favored a significant intensification of CO conversion and O/(O + P) up to 76% with an only moderate increase (ca. 5%) of methane when the process was operated at higher temperatures (340 °C). Based on their experimental outcomes, the authors also concluded that the influence of their promoters (*i.e.* K, S and Na) on the catalyst selectivity

[(O/(O+P)] and CO conversions was highly dependent from the nature of the support used. Supports featured with weak metal−support interactions, such as SiC, showed a more pronounced effect on the ultimate catalyst selectivity. This trend follows the higher Fe oxides reducibility to Fe^0 and the subsequent iron particles carburization for those composites where strong metal−support interactions were avoided or strongly inhibited by an *ad hoc* choice of the support. Hence, the promotional effect played by the various supports followed the order SiC > TiO_2 > AC > SiO_2 > γ-Al_2O_3.[294] In the same years, the Netherland team of Oschatz and de Jong came to similar conclusions by studying several ordered mesoporous materials [silica (SBA-15) or carbon (CMK-3) or SiC] with comparable pore size and pore symmetry, as supports for Fe NPs deposited by incipient wetness impregnation (IWI) with or without Na and S as promoters.[295] They found that the formation of FTO catalytically active iron carbide species was suppressed in the case of the strongly interacting mesoporous silica support. On the other hand, the weakly interacting CMK-3 and SiC supports provided highly active catalysts for the process.

The ability of iron catalysts to promote also the reverse water−gas-shift reaction (rWGS) for CO_2-to-CO conversion prompted Liu and co-workers to produce fuels by FTS using CO_2 as the raw component.[296] In a fixed-bed configuration, these authors demonstrated the effectiveness of their K-promoted iron catalysts (15Fe5K/S; S = support = activated carbon, TiO_2, SiC, γ-Al_2O_3) for the production of isoparaffins by a cascade hydroisomerization of FT products. As far as the nature of support is concerned, their results demonstrated once again that the SiC-supported catalyst was the most selective one toward lightweight $C_2^=$−$C_4^=$ olefins with [(O/(O+P)] values as high as 74.6%.[296]

3.2.1.2. SiC-Based Materials for Bio-Oil Production via Biomass Depolymerization. Biofuels are receiving a great deal of attention worldwide because their origin, biomass, is the only real renewable source of organic carbon in nature at zero greenhouse gas emissions impact throughout its whole life cycle.[297,298] One of the most challenging areas in the biomass-to-biofuel conversion is the development of robust and durable catalysts suitable to realize a high-efficiency biofuel production[299,300] (liquid components commonly named as bio-oils)[301,302] while ensuring stability to the catalyst active phase and its support throughout successive catalytic runs. Thermal resistance and chemical inertness of catalytic materials are then key features for the complete and successful catalyst regeneration and recovery by combustion of coke deposits. Silicon carbide exhibits high thermal stability, chemical inertness, oxidation resistance, thermal conductivity, and mechanical properties that make it an ideal catalyst support for harsh reaction processes like those related to biomass conversions.

Except for an early and non-catalytic application of SiC in the conversion of pyrolysis vapors of pine sawdust to yield bio-oils,[303] the first studies on its use as a catalyst support in the process can be traced to the lignin depolymerization and deoxygenation for the production of high added value aromatics as transportation fuel additives. Chen and co-workers first described the use of silicon carbide catalysts for the ethanolysis of dealkaline lignin (98%) in the production of oxygen-lean C_6−C_8 aromatics.[304] With a 50 wt % Fe/nano-SiC catalyst, they acquired from 63% to 80% (depending on the reaction time) of lignin depolymerization into liquid products whose composition was prevalently made of oxygen-lean C_6−C_8 aromatics and where ethanol was claimed to stabilize the depolymerization intermediates by suppressing their recondensation during the lignin cleavage.[304] The potentiality of SiC-based catalysts in lignin depolymerization was further investigated by the Chinese team of Fang and collaborators.[305] Despite an appreciable lignin depolymerization performance of plain SiC nanofibers as the catalyst in methanol at 320 °C and 30 bar of H_2 ($\approx$33% of a solid residue with $\approx$52% of methanol soluble compounds), their NiW/SiC composite prepared by incipient wetness impregnation with 5 wt % of NiO and 15 wt % of WO_3 resulted in a markedly higher depolymerization activity ($\approx$14% of a solid residue with $\approx$74% of methanol soluble compounds) under identical conditions. Notably, NiW/SiC also outperformed its activated carbon counterpart (NiW/AC) supplying higher liquid product yield. Most importantly, the SiC-based catalyst could be easily regenerated, and its catalytic activity was almost entirely recovered through a simple combustion of coke deposits followed by an acid washing treatment for ashes removal. Such a simple although harsh catalyst regeneration treatment − not equally applicable to either carbon or metal oxide supports - proved the unicity of SiC as the catalyst and catalyst support for the process.[305]

As far as bio-oils direct use in conventional engines is concerned, they list several limitations because of a series of quality issues raised from their high oxygen content, water content, acidity, and thermal instability[306] that make mandatory their pretreatment. Ruan, Wang et al. described the use of zeolite ZSM-5[307−309] or MCM41-coated[310,311] SiC foam matrices as catalysts for the *ex situ* catalytic and microwave-assisted fast pyrolysis (MACFP) of vapors downstream of a main pyrolysis reactor. Besides the aforementioned chemicophysical properties of SiC networks, these authors highlighted the excellent microwave absorbent properties of these materials, which ensured a more accurate temperature control at the catalytic bed when the latter was incorporated into a microwave-assisted pyrolysis (MAP) system.[312] Joining a MW-heating scheme with optimized reactors configurations from an engineering viewpoint, they have significantly increased the bio-oil quality (hydrocarbon percentages as high as 95% of which more than 71% of oxygen-free aromatics from woody oils pyrolysis over SiC/MCM41)[310] and have reduced the occurrence of fouling phenomena due to the generation of coke deposits, hence prolonging the lifetime of their SiC-based catalytic systems. Moreover, the authors stressed the remarkably higher stability of the ZSM-5/SiC and MCM41/SiC composites for the large scale catalytic fast pyrolysis of biomass vapors even after several reaction-regeneration cycles.[307−311]

Very recently, Wang and Ni reported a MW-assisted catalytic cleavage of 5−5′ C−C bonds of the 2,2′-biphenol molecule chosen as a model for lignin. SiC was selected as an efficient MW absorbent and coated with a carbide-derived carbon (CDC) further decorated with Pt. The as-prepared bifunctional catalyst exhibited high conversion (85%) and remarkable selectivity to monomers with a total mass yield as high as 49.3 wt %.[313]

3.2.2. Synthetic Natural Gas. *3.2.2.1. CO_x Methanation Reaction with SiC-Based Catalysts.* CO_x (x = 1 or 2) methanation is a well-known process of interest for the development of integrated chemical strategies for energy conversion and storage such as those related to the power-to-gas (P2G) chain.[314] Methanation represents a practical way for
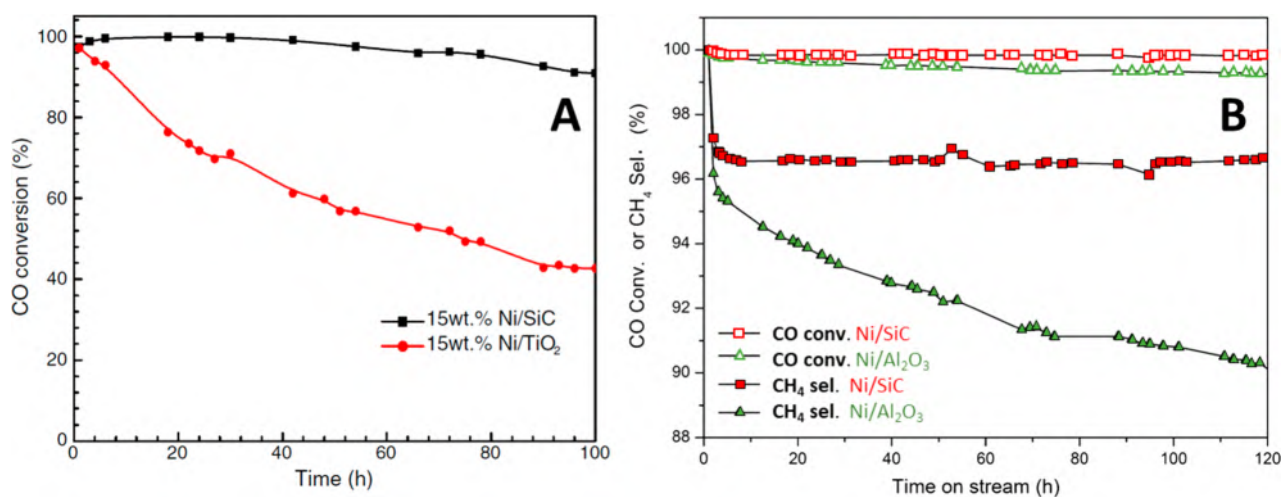
Figure 35. (A) CO methanation long-term runs with two catalysts in comparison: 15 wt % Ni/SiC (black curve) and 15 wt % Ni/TiO$_2$ (red curve). Other reaction conditions: T = 340 °C, P = 20 bar, H$_2$/CO = 3, GHSV = 4500 h^{-1}. Adapted with permission from ref 321. Copyright 2011 Elsevier BV. (B) 4.2 wt % Ni/SiC and 5.3 wt % Ni/Al$_2$O$_3$ catalysts in comparison in long-term CO methanation runs. Adapted with permission from ref 323. Copyright 2013 Elsevier BV.

the conversion of renewable energy sources into a substitute or synthetic natural gas (SNG):methane (CH$_4$). For this reason, research in the field has significantly intensified over the last decades with special attention being given to the development of effective, stable, and selective catalysts for the process.[315−318]

Methanation (eq 17) is typically operated between 200 and 450 °C depending on the catalyst nature and the experimental conditions used, and its exothermic nature has posed several concerns for a long time due to the generation of local temperature gradients (*hotspots*) that do not simply impact (detrimentally) the catalyst performance and its long-term stability on stream but often pose serious security issues in packed-bed large scale reactors.

$$CO_x + (x + 2)H_2 \rightarrow CH_4 + xH_2O \quad \begin{array}{l} \text{for } x = 1; \ \Delta H_r^0 = -49 \text{ kcal/mol} \\ \text{for } x = 2; \ \Delta H_r^0 = -39 \text{ kcal/mol} \end{array}$$

(17)
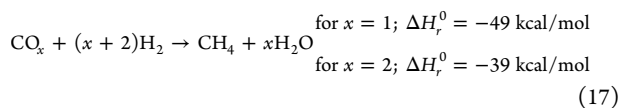
The team of Guo and co-workers first reported on the use of SiC-based catalysts for the process.[319−322] The authors' choice was motivated by the inherent thermal properties of the SiC materials, their chemical inertness, and stability under highly exothermic conditions. Indeed, their remarkable thermal conductivity was a key feature for controlling and mitigating the generation of local temperature gradients in correspondence to the metal active sites directly engaged in the CO$_x$ activation. The authors demonstrated an improvement of performance of their Ni/SiC methanation catalysts when higher metal dispersions and stronger metal−support interactions were realized. In this regard, they showed highly beneficial effects on the reaction performance when bimetallic systems Ni−La[319] or Ni−Co[320,322] were prepared and used instead of the monometallic Ni/SiC catalyst for the CO$_2$ and CO methanation, respectively. In both cases, nickel codoping was claimed to improve the metal dispersion of Ni NPs (catalyst active phase) on the support while creating an ideal electronic microenvironment for a more convenient CO$_2$ or CO activation and dissociation.[319,322] As far as the role of the active-phase carrier is concerned, their study clearly showed the higher stability and CO conversion achieved in long-term

methanation runs when a poorly conductive oxide-support (TiO$_2$) was replaced by a thermal conductive SiC (Figure 35A).

The remarkable deviation measured with the two catalysts at work (15 wt % Ni/SiC vs 15 wt % Ni/TiO$_2$) was unambiguously ascribed to the occurrence of Ni NP sintering phenomena on the less thermally conductive support (TiO$_2$). Indeed, the ignition of local hotspots generated by the process exothermicity was hardly dissipated by TiO$_2$ thus favoring the progressive nanoparticle coalescence along with a faster catalyst deactivation.[321]

A similar study was carried out by Wang and co-workers who compared the CO methanation performance between two Ni catalysts prepared by the impregnation method on either SiC or Al$_2$O$_3$ grains of 0.7−0.9 mm.[323] As Figure 35B shows, CO conversions laid on values higher than 99% whatever the catalyst used and all over the long-term tests (up to 120 h) with only minor performance discrepancies ascribed to a larger extent of coke formation and Ni NP sintering on the Al$_2$O$_3$-based system. On the other hand, while the Ni/SiC catalyst showed a stable CH$_4$ selectivity (constantly lying over 96%), it steadily decreased down to 90% over 120 h with the Ni/Al$_2$O$_3$ catalyst. The authors' conclusions outlined the progressive increase of Ni NP size on the Al$_2$O$_3$-supported catalyst, once again related to the reduced capacity of the carrier to mitigate the formation of hotspots during the process. The larger the Ni particle size the lower the catalyst performance in methanation reaction and the higher the contribution of side reaction processes (*e.g.* water gas shift reaction) with the subsequent and more appreciable decrease of CH$_4$ selectivity.[323] The same authors reported on the influence of the SiC surface oxidation degree on the ultimate methanation performance of the Ni/SiC catalysts. They offered a systematic overview on the role of SiC surface oxidation (in air at 300, 500, and 900 °C for 4 h) with respect to the Ni NP dispersion and metal−support interaction strength.[324] In agreement with related conclusions from the literature,[27,277] they concluded that a proper SiC surface oxidation enhanced the low-temperature (300 °C) catalyst activity and their stability under higher operational temperatures (*i.e.* 500 °C). A nickel active phase supported on an unoxidized SiC network resulted in a catalyst with a very
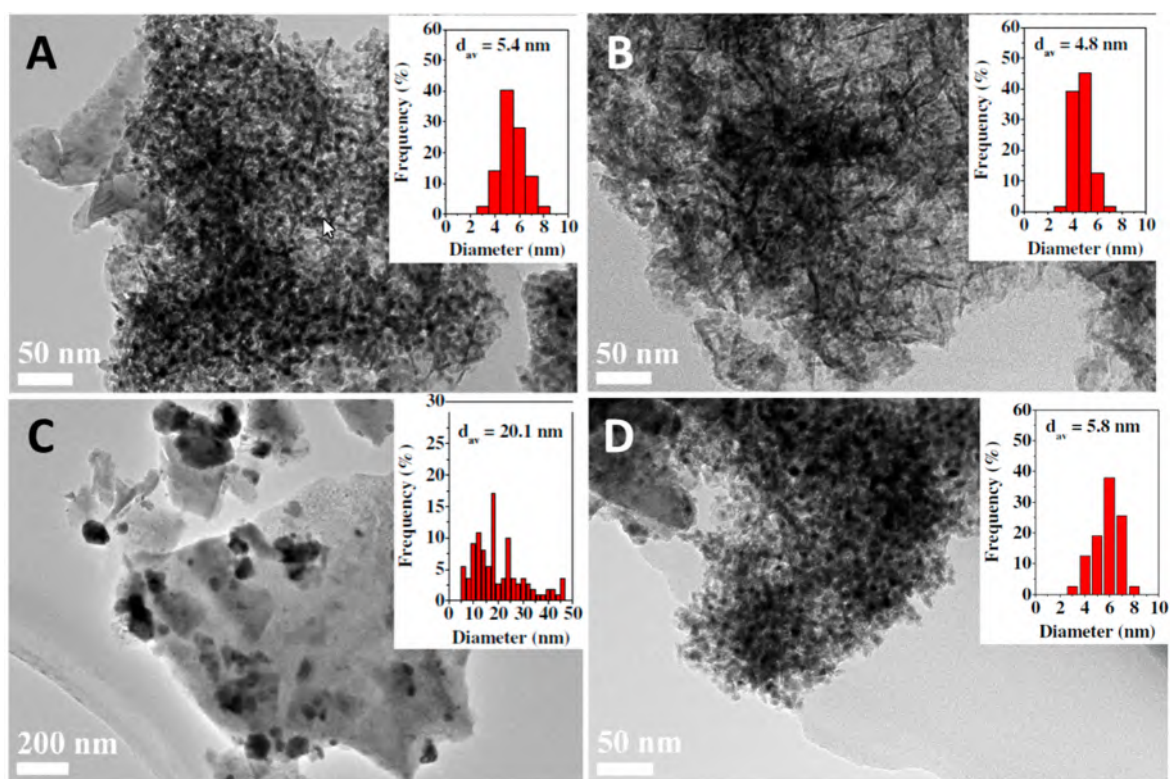
Figure 36. Transmission electron microscopy (TEM) images of the reduced NiMgAl/SiC (12.5 wt % Ni and 17.5 wt % MgAl) (A), NiMgAl (B), Ni/SiC (C), and the exhaust NiMgAl/SiC recovered after a 50 h CO_2 methanation run at 400 °C (D). The insets refer to the Ni NP size distribution determined through a statistical analysis over more than 200 NPs. Adapted with permission from ref 330. Copyright 2019 Wiley-VCH.

poor stability at the higher temperature methanation conditions. On the other hand, an overoxidation of the SiC matrix resulted in a faster catalyst deactivation already at low operative temperatures. Their ultimate finding was the generation of an ideal microenvironment at the SiC surface (oxidized but not too much) for the Ni NP anchoring and growth during the support impregnation/calcination/reduction step.[324] The effect of SiC surface oxidation was also very recently investigated by Tessonnier et al. in CO_2 methanation promoted by Ru/SiC catalysts.[325] In particular, authors took advantage of a controlled and progressive SiC surface oxidation that gradually decreased the support thermal conductivity. The authors found that a reduction of thermal conductivity by 110 W m^{-1} K^{-1} is directly correlated to a significant drop (22%) in methane selectivity. The study highlighted once again the importance of SiC ability in controlling the heat at the catalyst surface limiting the occurrence of hotspots highly detrimental for catalyst lifetime and process selectivity.

A conceptually similar approach, joining the advantages of metal oxide carriers with the thermal conductive properties of SiCs was proposed later by Gu and co-workers.[326] Their team described the uniform deposit of a proper amount of Al_2O_3 particles at the surface of SiC powder in the preparation of a variety Ni/Al_2O_3−SiC catalysts. In this way, they enhanced the Ni NP support interactions and improved their surface dispersion. At the same time, they succeeded in preventing undesired nanoparticle migration and sintering phenomena to the larger extent. While Al_2O_3 particles created an ideal environment for the dispersion, anchoring and growth of Ni NPs, the superior heat conductivity of the SiC core mitigated the generation of detrimental local temperature gradients throughout the CO methanation reaction. Wang and

collaborators came to similar conclusions while comparing CO methanation performance of nickel-based catalysts prepared from Al_2O_3-coated SiC-networks with those of plain Ni/SiC counterparts.[327] These authors also argued about the preparation method of the Al_2O_3-coated support (Al_2O_3@SiC) designed via the evaporation-induced self-assembly (EISA) method[328,329] or more trivially synthesized via deposition-precipitation technique (Al_2O_3−SiC).[223] They ascribed the superior performance and stability of the Ni/Al_2O_3@SiC catalyst to the mesoporous structure of the Al_2O_3 coating as well as to the higher dispersion and smaller NP size of the Ni active phase. Both these features that applied to EISA-synthesized supports, were claimed to enhance the anticoke and antisintering properties of the resulting Ni composites.[327] The same research team reported later on the performance of a NiMgAl/SiC catalyst synthesized via the coprecipitation method and successfully applied to CO_2 hydrogenation.[330] They showed the superior low-temperature methanation activity of their NiMgAl/SiC (12.5 wt % Ni and 17.5 wt % MgAl) catalyst compared to the simplest NiMgAl and Ni/SiC. Morphological characterization of the three systems in comparison showed the typical composite structure for the NiMgAl/SiC system resulting from that of an hydrotalcite support and a SiC network (Figure 36). Most importantly, TEM analysis unveiled a different metal dispersion and Ni NP size distribution among the three samples with that of the plain Ni/SiC catalyst being the less narrow with metal particles ranging in the wider nanometer range (≈40 nm; Figure 36C). As a matter of fact, they also demonstrated the higher performance ($X_{CO_2} \approx 77\%$ and $S_{CH_4} \approx$ 93%) and fairly good stability of the NiMgAl/SiC catalyst in a
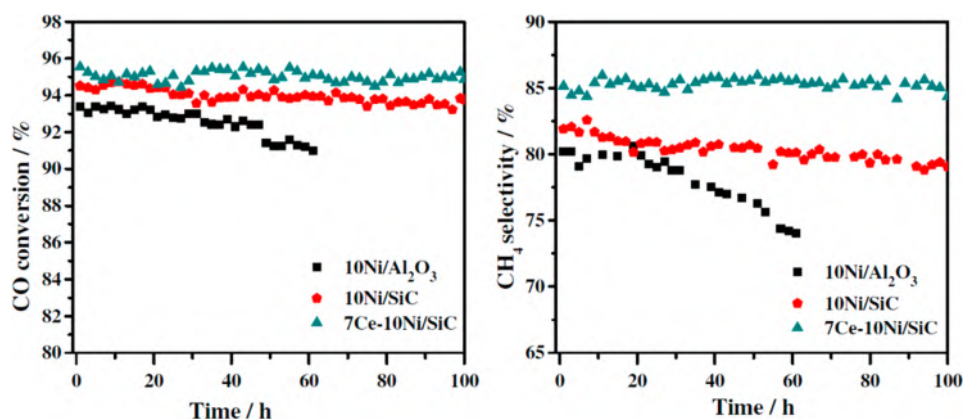
Figure 37. Long-term, high-temperature stability results in CO methanation by either 10 wt % Ni/Al_2O_3, 10 wt % Ni/SiC, or 7 wt % Ce−10 wt % Ni/SiC in comparison: (left) CO conversion and (right) CH_4 selectivity. Other reaction conditions used: H_2/CO = 3/1, GHSV = 60,000 mL g^{-1} h^{-1}, 600 °C, 10 bar. Figures adapted with permission from ref 334. Copyright 2018 Elsevier B.V.

long-term methanation run [50 h, 400 °C, CO_2/H_2 = 1:4; P = 1 bar; weight hourly space velocity (WHSV) = 60 000 mL h^{-1} g_{cat}^{-1})]. The morphological analysis of the spent catalyst confirmed the presence of well-dispersed Ni NPs with an only slight increase ($\approx 7\%$) of the mean nanoparticle diameter and a size distribution centered almost in the same narrow nanometer range (Figure 36D vs 36A).[330]

According to their experimental evidence, the superior activity of the NiMgAl/SiC catalyst, besides the thermal conductivity of the SiC core was ascribed to other two structural parameters: the small Ni NP size endowed by the hydrotalcite-based support for the active phase and the high reducibility of Ni particles species due to ideal metal−support interactions.

Frey, Edouard, and Roger studied the hydrodynamic and thermal properties of a structured SiC-based catalyst prepared by depositing a Ni/Ru active phase on an open-cell SiC foam covered with a carbon nanofiber (CNF) network, dip-coated in turn with a ceria-zirconia phase.[331−333] Their study along with various improvements and optimizations, was mainly focused on the reactor design for an effective intensification of the methanation process by means of an improved control on the (over)heat evacuation. In a seminal contribution from this team, based on the monitoring of the heat generated at the catalytic foam by infrared thermography, they concluded that the SiC covering with a CTF network did not change appreciably the hydrodynamics of a platelet milli-reactor. On the other hand, the presence of CTFs on the SiC foam facilitated the heat evacuation from the foam support, therefore intensifying the process.[332]

Ren and co-workers reported the long-term performance of methanation catalysts prepared from different supports in comparison (10 wt % Ni/SiC, 10 wt % Ni/Al_2O_3 and 7 wt % Ce −10 wt % Ni/SiC), eventually codoped with CeO_2 and operated under relatively severe CO methanation conditions.[334] Their conclusions highlighted once again the superior performance of the SiC-based catalyst where the higher thermal conductivity and reduced acid surface character of the support (compared to Al_2O_3) held important effects in terms of catalyst anticoking properties. In addition, as Figure 37 shows, the codoping of their most performing system (10 wt % Ni/SiC) with 7 wt % CeO_2 led to a catalyst with improved CO conversion degrees, higher stability on run and

selectivity to SNG up to limits of the thermodynamic equilibrium.

These authors concluded that the combination of SiC and CeO_2 codoping was essential in preventing Ni NP sintering during the catalytic process. While the former hampered the ignition of local hotspots, the latter constitute a physical barrier between the Ni NPs hence avoiding their coalescence. Moreover, CeO_2 was claimed to inhibit the generation of surface-inactive graphitized carbon, hence alleviating the problem associated with the progressive catalyst fouling and deactivation.[334] A model in silico study of the $Ni_4/3C-SiC(1\ 1\ 1)$ configuration applied to CO methanation was also proposed by the same Chinese team who investigated the presumed reaction pathway toward the generation of CH_4.[335] Their DFT calculations demonstrated that the generation of CH_4 with respect to other reaction intermediates (i.e. CH_3OH in particular) was more favorable on the $Ni_4/3C-SiC(1\ 1\ 1)$ surface compared to other Ni-based catalysts such as $Ni(1\ 1\ 1)$, Ni_4/Al_2O_3, and $Ni_4/t-ZrO_2$. This finding has further strengthened the use of these thermally conductive matrices as catalyst supports for CO_x methanation.

Chu et al. pointed out the higher reducibility of Ni-oxide NPs and anticoking properties of their bimetallic Ni−La methanation catalysts prepared on SiC networks compared to their γ-Al_2O_3-based counterparts.[336] These authors argued on the importance of weaker metal−support interactions between Ni NPs and the SiC carrier. Indeed, the chemical inertness of SiC was deemed beneficial in making the reduction step for the metallic catalyst activation easier. In this regard, they also demonstrated the influence of the Ni precursor choice on the catalyst performance in CO_2 methanation showing that Ni−La/SiC prepared from nickel acetate $[Ni(OAc)_2]$ presented higher metal dispersion and nanoparticle reducibility compared to those obtained from nickel nitrate $[Ni(NO_3)_2]$. Similar conclusions were very recently drawn by Yu's group that confirmed how the addition of a 3 wt % of La to Ni/SiC CO methanation catalysts markedly improved Ni dispersibility reducing Ni NP size with beneficial effects on catalyst activity and stability.[337]

Later, Park and co-workers concluded on the improved performance of Ni/SiC catalysts obtained from the same metal precursor $[Ni(NO_3)_2 \cdot 6H_2O]$ but using two different preparation methods: wet impregnation (WI) and deposition-precipitation (DP) methods.[338] The higher nickel active-
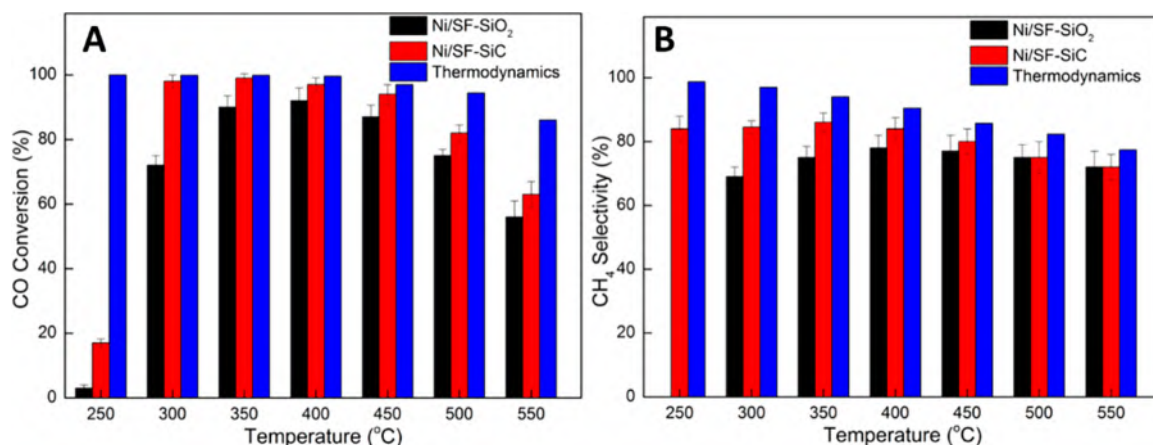
Figure 38. Catalytic performances of 10 wt % Ni/SF-SiC and 10 wt % Ni/SF-SiO$_2$ catalysts in comparison in CO methanation under different reaction temperatures. Other reaction conditions: 1 bar, GHSV = 18,000 mL g^{-1} h^{-1}: (A) histograms refer to CO conversion and (B) histograms refer to CH$_4$ selectivity. Adapted from ref 339. MDPI, Basel, Switzerland 2019 [CC BY license 4.0] [https://creativecommons.org/licenses/by/4.0/].

phase dispersion achieved by the DP method gave rise to Ni/SiC catalysts with superior performance for SNG production via CO and CO$_2$ methanation.

Recently, Zhang and co-workers have described an original and sustainable approach to the synthesis of SiCs from an industrial waste of metallic silicon production: the silica fume (SF-SiO$_2$).[339] With silica fume derived SiC matrices (SF-SiC) they prepared a 10 wt % Ni/SF-SiC composite and compared it with its 10 wt % Ni/SF-SiO$_2$ counterpart as catalysts for the CO methanation reaction. As Figure 38 shows, the two catalytic systems behaved differently throughout the whole 250−550 °C temperature range with the Ni/SF-SiC catalyst constantly outperforming its SF-SiO$_2$-based analogue in terms of CO conversion and CH$_4$ selectivity. In addition, the authors demonstrated the higher stability and antisintering properties of their Ni/SF-SiC catalyst under a long-term methanation run (50 h at 350 °C, 1 bar, GHSV = 18000 mL g^{-1} h^{-1}).

Their conclusions highlighted once again that the higher thermal conductivity of SF-SiC matrices along with stronger interactions between Ni NPs and silicon carbide were directly responsible for the superior reactivity, long-term stability and antisintering properties of Ni/SF-SiC in catalysis.

Ni catalysts supported on LTA zeolite (sodium form, NaA)-coated SiC foams (Ni@NaA-SiC) have been used as catalysts for intensifying CO$_2$ methanation reaction. Taking advantage of literature evidence for enhanced-CO$_2$ sorption properties of Ni catalysts on hydrophilic zeolite 5A,[340−344] Chen and co-workers have recently proposed the combination of SiC open-cell foams functionalized with an homogeneous hydrophilic NaA coating layer to enhance the Ni catalyzed methanation.[345] Their structured catalyst reduced the mass and heat transfer effects of the process, hence shifting the reaction equilibrium toward CH$_4$ formation. Kinetic studies shown that besides a high stability of the structured catalyst (15 wt % Ni@NaA-SiC) on long-term methanation runs (>80 h at T = 400 °C, H$_2$/CO$_2$ = 4, flow rate = 50 mL (STP) min^{-1}, GHSV = 1875 h^{-1}; CO$_2$ conversion ≈82% and CH$_4$ selectivity ≈95%), the latter exhibited an appreciably lower activation energy (E_a ≈ 30 kJ mol^{-1}) compared to its SiC-free, pelletized counterpart (15 wt % N@NaA; E_a ≈ 84 kJ mol^{-1}).[345]

3.2.3. Hydrogen Production. Hydrogen (H$_2$) is one key molecule for chemical industry and its annual worldwide

production ranks around 50 million tons. Current technologies for the industrial H$_2$ production rely on the steam reforming of natural gas[346] or coal gasification[347] mainly. Over 95% of the total hydrogen production is intended as devoted to two industrial segments: the chemical sector (≈63% for the ammonia (NH$_3$) and methanol (CH$_3$OH) synthesis and ≈2% for liquid hydrocarbons and higher alcohols), and the refining sector (≈30% for hydrotreating and hydrocracking processes aimed at producing high-grade petrochemical products).[348] The remaining 5% is devoted to other uses such as food, metallurgical and semiconductor industry, just to mention a few.

3.2.3.1. Methane Dry Reforming Process. CO$_2$ reforming of methane (see eq 9, section 3.1.5) to syngas is a key endothermic process with important environmental implications that converts two greenhouse gases into an equimolar mixture of hydrogen and carbon monoxide.[349,350] One main limit for the process is generally represented by the rapid deactivation of the catalyst due to the generation of carbon deposits (catalyst coking) and/or the sintering of its metal active phase.

In a pioneering and very preliminary approach to solar-driven hydrogen production, Tamme and co-worker argued on the advantages on the use of SiC as an alternative carrier to the classical α-Al$_2$O$_3$ for the setup of refractory, thermally resistant and Rh-doped solar light absorbers to be employed in dry methane reforming (section 3.1.5, eq 9 for DRM).[351] A similar concept was recovered and systematically exploited few years later by the Japanese team of Kodama, Gokon, and co-workers.[352,353] They described a high-temperature solar natural-gas reforming unit by means of an irradiated Ru/Ni−Mg−O−SiC foam composite as solar receiver-reactor.[352] They found the superior performance of their Ru/Ni-promoted SiC absorber along with its cost-effective use in the process with respect to the benchmark noble metal-based Rh/γ-Al$_2$O$_3$ system. Nonetheless, the same team reported few years later on the performance of a noble metal-free Ni/MgO-Al$_2$O$_3$ catalyzed SiC foam composite as one of the most promising solar absorbers for a reformer unit.[353]

Wang and co-workers reported in the same years the advantages of SiC as an active-phase carrier for non-noble metals in the process within a more classical reactor
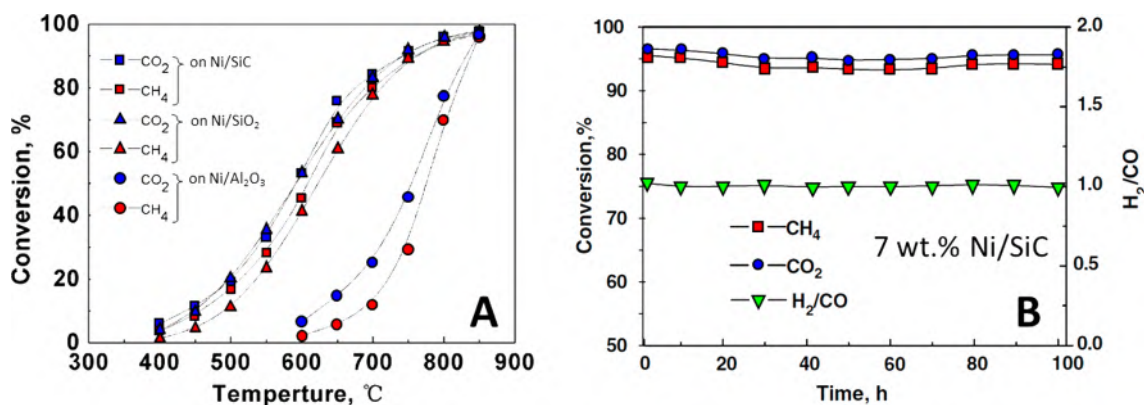
Figure 39. (A) Effect of the temperature on the catalytic performance of 7 wt % Ni/Supp (Supp = SiC$_{foam}$, SiO$_2$, Al$_2$O$_3$) in comparison. Reaction conditions: CH$_4$:CO$_2$ = 1:1, GHSV = 6.000 mL g$_{cat}^{-1}$ h^{-1}. Adapted with permission from ref 355. Copyright 2007 Springer Science + Business Media, LLC. (B) Long-term steam reforming with 7 wt % Ni/SiC. Reaction conditions: CH$_4$:CO$_2$ = 1:1, 6.000 mL g$_{cat}^{-1}$ h^{-1}, T = 800 °C. Adapted with permission from ref 354. Copyright 2007 Elsevier BV.

scheme.[354,355] They compared the performance of a 7 wt % Ni/SiC$_{foam}$ system with its Al$_2$O$_3$- and SiO$_2$-based counterparts. They monitored the effect of the temperature on reagents conversion (Figure 39A) for the three catalytic systems in comparison and realized that the SiC$_{foam}$-based catalyst was the most performing one. Besides affording higher greenhouse gases conversions at a lowest reaction temperature (Ni/SiC > Ni/SiO$_2$ ≫ Ni/Al$_2$O$_3$), 7 wt % Ni/SiC showed closer conversion values for the two gases (CH$_4$ and CO$_2$) at the same reaction temperature and within the whole temperatures range. Although these authors did not claim any reason to the closer activity profiles recorded on Ni/SiC and Ni/SiO$_2$, it seems reasonable to deduce that similarities raised from the presence of Si-oxycarbide layers (SiC$_x$O$_y$) coating the SiC surface and thus partially compromising its inherent thermal conductivity in the process. These authors highlighted another important distinctive feature between Ni/SiC and Ni on metal oxides. Indeed, the CO$_2$ conversion was generally higher than that of CH$_4$ at the same operative temperature with Ni/Al$_2$O$_3$ or Ni/SiO$_2$ at work.[355] This suggested that rWGS occurred simultaneously and more significantly on the metal oxide catalytic systems. On the other hand, the hydrophobic nature of silicon carbide was supposed to remove faster the adsorbed water at its surface,[356] thus limiting the rWGS process to occur. Finally, 7 wt % Ni/SiC did not show any appreciable catalyst coking/deactivation in a long-term catalytic run with CH$_4$ and CO$_2$ conversions remaining almost constant (≈94.0% and ≈95.0%, respectively) within more than 100 h on run (Figure 39B). On the other hand, deactivation on 7 wt % Ni/Al$_2$O$_3$ or 7 wt % Ni/SiO$_2$ occurred much faster under the same experimental conditions.[354]

More recently, Passos and co-workers came to similar conclusions for their Ni-promoted molybdenum carbide catalyst supported either on SiO$_2$, Al$_2$O$_3$ or SiC. The classical oxide carriers were not able to create a fruitful interaction with Ni/Mo$_2$C active phase hence causing a fast catalyst deactivation due mainly to a gradual Ni leaching from the surface. On the contrary, SiC-supported samples show high activity and stability in DRM process with low formation of coke deposits. The authors attributed these positive outcomes mainly to the high mechanical strength and mass transfer rate of SiC that, together with its remarkable thermal conductivity, allowed a reduction of hotspot formation and pressure drop phenomena.[357]

Nguyen, Pham-Huu et al. discussed later an interesting effect resulting from the O$_2$-pretreatment of a Ni/SiC catalyst to be employed in CO$_2$ reforming of methane.[237] These authors observed that a catalyst activation under a CO$_2$/CH$_4$ stream and in the presence of O$_2$ (during the first minutes on run only) inhibited the generation of nickel silicide species (i.e. NiSi$_2$) whose presence was found to be detrimental for the ultimate catalyst performance. Such an O$_2$-pretreatment was found to increase the CH$_4$ conversion from ≈80% (in the absence of O$_2$ activation) up to 90% at the steady-state conditions of the process promoted by a pretreated Ni/SiC catalyst.[237] The effective Ni/SiC catalyst configuration for the CO$_2$ reforming of CH$_4$ was recovered later independently by the Chinese teams of Jin and Xie who proposed an improvement of the metal active-phase stability (in terms of Ni NP sintering) and anticoking properties of their Ni/SiC catalysts prepared by the impregnation method by the addition of a proper amount of an alkaline rare earth metal oxide (i.e. Yb$_2$O$_3$,[358] Sm$_2$O$_3$,[359] or La$_2$O$_3$[360]) as the promoter. Dual support obtained by the CeZrO$_2$ surface deposit on β-SiC and Al$_2$O$_3$ was investigated as carriers for a Ni–Co active phase by Aw and co-workers.[356] These authors monitored the effects of the CeZrO$_2$ deposition method on oxide-free and oxide-based ceramics, with respect to the final stability of the metal active phase and the coke-resistant properties of the resulting catalysts employed for long-term (>550 h) for CH$_4$ dry reforming. Wang and collaborators moved on a similar ground by presenting a series of Ni-based catalysts for the process prepared by either the impregnation or coimpregnation method on C-, C,N-,[361] and carbide-derived carbon (CDC)-coated[362] SiC supports. Playing with the basic surface properties of their coated SiC carriers and with the use of CeO$_2$ as the catalyst promoter,[362] they better controlled the dispersion and size of Ni NPs thus improving the catalyst performance in terms of CH$_4$ and CO$_2$ conversion as well as the stability of the metal active phase.[361,362]

To remedy the generally moderate surface area of SiC supports, besides the solutions proposed above and based on the SiC surface coating with porous carbon or N-doped carbon layers, Tsubaki and collaborators made use of carbon nanofibers grown directly at the surface of a SiC foam monolith.[363] The nickel dispersion on the resulting CNFs-SiC support was significantly higher compared to that on the plain Ni/SiC catalyst and catalytic outcomes showed an improved
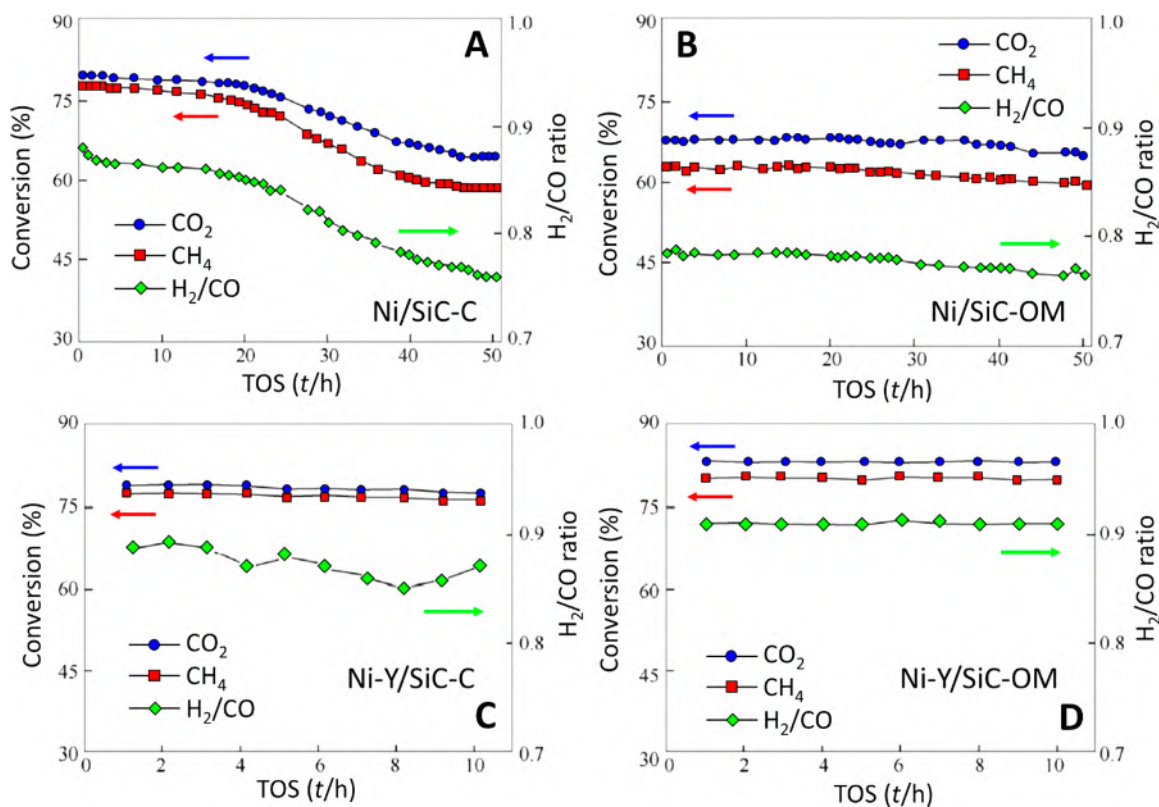
Figure 40. Catalytic performances of Ni/SiC-C (A) and Ni/SiC-OM (B) in DRM in comparison. Catalytic performances of Ni−Y/SiC−C (C) and Ni−Y/SiC−OM (D) in DRM in comparison. Reaction conditions: 700 °C, CH$_4$:CO$_2$ = 1, 1 bar, GHSV = 12.000 mL g$_{cat}$$^{-1}$ h^{-1}. Adapted with permission from ref 366. Copyright 2019 Institute of Coal Chemistry, Chinese Academy of Sciences. Published by Elsevier Limited.

sintering resistance of Ni NPs on the former system along with a considerably higher stability of the active phase on long-term methane dry reforming paths.

Kaskel and co-workers stressed the importance and the opportunity of tuning the characteristics and surface properties of nanoporous SiC networks as nickel active-phase supports in DRM.[364] The German team proposed a nanocasting protocol for the low-cost preparation of nanoporous silicon carbides using fumed silica as a hard template. By varying the pyrolysis temperature between 1000 and 1500 °C they successfully tuned the structural parameters of their SiCs thus leading to porous samples featuring with specific surface areas up to 328 m^2 g^{-1} and total pore volumes of 0.54 cm^3 g^{-1} (DUT-87; DUT = Dresden University of Technology). This team confirmed the importance of a deliberate SiC surface oxidation as to prevent the direct Ni-SiC contact, hence limiting the formation of nickel silicides responsible of a reduction/passivation of metal active species. They showed that SiC oxidation enhanced the conversions and stabilities of their 10 wt % nickel-based catalysts (Ni/SiC@SiO$_2$), unveiling at the same time the beneficial effects of their SiC@SiO$_2$ support with respect to the plain SiO$_2$ in the catalytic process.[364]

Later Wang and Xiao studied the role of ordered mesoporous SiC samples with different architectures, prepared by a nanocasting method using SBA-15, KIT-6, and MCM-41 as hard templates, on the structure-performance relationship of the corresponding Ni-based catalysts.[365] This team highlighted that the synthesized SiC samples retained the mesoporous structure of the applied silica hard template and that the latter was crucial in varying the confinement effect from the ordered mesoporous arrays on the deposited Ni NPs. The lower the

confinement effect the higher the metal particle size, the lower the metal dispersion at the SiC surface and the weaker the metal−support interactions. Low confinement effects also translated into higher catalyst coking rates and thus into their more rapid deactivation. Such a confinement effect and thus the ordered mesoporous structure of these materials was crucial in controlling the activity (CH$_4$ and CO$_2$ conversion) and stability (metal NP sintering and catalyst coking) of the corresponding Ni catalysts on run. They finally showed that Ni/SiC sample prepared with KIT-6 as hard template, exhibited the strongest confinement effect, leading to the dispersion/anchoring of metal particle inside the SiC pores, thus ensuring strong metal−support interactions, low sintering and catalyst coking phenomena.[365] Huang, Zhao, and their co-workers came to similar conclusions by comparing the Ni/SiC performance of two catalysts prepared with either an ordered mesoporous SiC (SiC-OM) material featuring with a high specific surface area (345 m^2/g) and narrow pore-size distribution or a commercial SiC sample (49 m^2/g, SiC-C) as model carriers.[366] Their results showed a significant reduction of the carbon deposition rate over the Ni/SiC-OM catalyst compared to that measured on Ni/SiC-C during 50 h on DRM (Figure 40A vs B). The authors concluded that the strong interaction between Ni NP and SiC-OM support and the confinement effect ensured by the rigid mesoporous skeleton of SiC-OM was at the origin of the improved catalyst coke resistance. In addition, they also confirmed the beneficial effects on the catalyst activity and stability of Y$_2$O$_3$-promoted Ni-based systems,[366] hence offering a hint to an optimal catalyst design aimed at fostering a concrete industrialization of the process (Figure 40C vs D).

Figure 41. Schematic representation of a flow through (A) and wall flow (B) SiC configuration. C) Methane conversion vs furnace temperature of three catalytic systems in comparison: the structured Ni catalysts with a FT SiC WF SiC configuration and the benchmark 57-4MQ catalyst provided by Katalco-JM. Common reaction conditions: GHSV = 6250 h^{-1}, 25 vol % of CH$_4$ (C) and 75 vol % of steam (S); S/C = 3. Adapted with permission from ref 376. Copyright 2017 Elsevier BV.

Fe/SiC catalysts prepared by the impregnation method were successfully used under microwave irradiation conditions for CH$_4$ dry reforming. Song and co-workers exploited the microwave absorbing properties of SiCs, highlighting the advantages of this alternative heating technology in the process.[367,368] The use of a cheap and environmentally friendly Fe-based catalyst combined with microwaves absorption properties of SiC held important effects on the dry reforming reaction. In a long-term catalytic test ($\approx$50 h), these authors observed constant reactants' conversions around 85% with negligible amount of carbon deposits at the end of the process ($\approx$0.78 wt %) and high catalyst sintering resistance ensured by the higher thermal conductivity of SiC.[367] In a very recent study, Nigar and co-workers found similar outcomes with a Ni/SiC catalyst exploited in the microwave-assisted DRM. In particular, they showed that, due to the good SiC response to MW irradiation, a CO$_2$ and CH$_4$ conversion as high as 90% can be achieved at a WHSV of 11,000 mL g^{-1} h^{-1} with no significant catalyst deactivation after 6 h on stream. On the contrary, the conventional heated catalyst achieved a 79% conversion only.[369]

3.2.3.2. Alkanes and Methanol Steam Reforming Processes. Reforming using steam is a fundamental process to produce hydrogen and synthesis gases. The most relevant alternatives are represented by the partial oxidation of fuel oil and coal gasification.[370] According to the following eqs (eq 18−20), it converts hydrocarbons into mixtures of hydrogen, carbon monoxide (eq 18), carbon dioxide (via WGS reaction, eq 19) and methane (via CO methanation, eq 20).

$$C_nH_m + nH_2O \rightarrow nCO + \left(n + \frac{m}{2}\right)H_2 \quad \Delta H^\circ = >0 \tag{18}$$

$$CO + H_2O \rightarrow CO_2 + H_2 \quad \Delta H^\circ = -41.1 \text{ kJ/mol} \tag{19}$$

$$CO + 3H_2 \rightarrow CH_4 + H_2O \quad \Delta H^\circ = -206.2 \text{ kJ/mol} \tag{20}$$

At odds with the endothermic character of the main process (eq 18), both side reactions (eqs 19 and 20) are exothermic in nature. The control of the temperature at the catalyst bed, ensured by the choice of a good thermal conductor for an optimal heat transfer from the reactor walls to the catalyst particles as well as a mitigation of local temperature gradients formed throughout the process at the catalyst bed, are key feature for guarantee optimal performance to the catalytic system.

A very preliminary contribution focused on the use of SiC networks for the support of Ni NPs and their application as effective catalytic systems for SR of methane (MSR) under conditions similar to those employed in industrial plant, was presented by the Italian team of Basile and co-workers.[371] This seminal contribution highlighted the important thermal conductivity properties of SiC as the catalyst support in the process. Anyhow, the authors also faced with the limits of this materials under conditions like those of industrial plants. In particular, they registered the SiC oxidation tendency for temperature higher than 960 °C, which caused a progressive decrease of the material surface area and consequently of the catalyst performance.

Process intensification efforts have demonstrated that high thermal conductivity supports allowed a flatter axial thermal

Figure 42. Methanol SR performance of three Cu/ZnO-based catalysts in comparison and effect of SiC fibers as a catalyst support on the process: (A) methanol conversion, (B) CO concentration, and (C) relationship between methanol conversion and CO concentration. Adapted with permission from ref 387. Copyright 2006 Elsevier BV.

profile along the catalytic bed, thus resulting in a higher average temperature at the outlet section of the reactor and consequently resulting in hydrocarbon conversions to a larger extent.[372] Moreover, highly conductive supports ensured more uniform radial temperature profiles, thus resulting in a better heat transfer and reduction of hotspot phenomena.[373] Palma, Meloni, and Ricca studied a series of Ni-loaded SiC monoliths featuring with two different geometrical configurations in the MSR and compared their catalytic outcomes with a benchmark Ni/Al$_2$O$_3$ catalyst (57−4MQ, provided by Katalco-JM).[374−377] The Italian team focused on the Flow Through (FT) vs Wall Flow (WF) SiC-monolith configuration for the performance intensification of their MSR catalytic process. The excellent heat and mass transfer properties of SiC-based monolith catalysts allowed these authors to overcome the main limitations typically encountered in SR reactors,[375] thus improving the process performance. The two proposed SiC configurations, FT and WF, present distinctive features: while the former has open channels on both sides, the latter presents alternatively closed channels and porous side walls, as showed in Figure 41 (A vs B). The WF configuration forced reagents to flow through the walls thus maximizing the contact between reagents and catalyst active phase, including that embedded in the support walls. Their study first highlighted the better catalytic activity of a WF SiC configuration with respect to the FT ones. Indeed, the former ensured a better axial and radial heat distribution compared to that on FT SiC thus leading to a higher catalytic activity up to a temperature reaction of 750 °C. The same authors also highlighted the importance of a preliminary SiC washcoating with a ceria- colloidal suspension or a ceria/alumina slurry before proceeding with the nickel impregnation.[374−376] Such a pretreatment was found to improve the Ni NP dispersion and decrease the average diameter and volume of pores in the SiC monoliths.

The performance of their structured catalysts was finally compared with a commercial catalyst (57-4MQ, Katalco-JM) and the activity tests showed that their SiC-based systems provided higher values of methane conversion for lower furnace temperatures (Figure 41C), thus providing a useful and concrete hint toward a process intensification.

In a recent contribution, the Korean team of Moon and co-workers reported on the advantages in terms of coke resistance and H$_2$ yield efficiency of structured Ni-based catalysts prepared on calcium aluminate (CA$_x$) modified SiC supports.[378] These authors argued on the beneficial effects resulting from the implementation of a thermal conductor

ceramic with a basic CA$_x$ surface porous layer. At odds with classical acid supports for the process (e.g. Al$_2$O$_3$), porous basic networks are known to reduce or even inhibit the occurrence of undesired coking phenomena at the catalyst surface while ensuring at the same time the generation of advantageous local CO$_2$ gradient concentrations close to the metal active sites for the process to occur.

Park, Bae et al. studied the effects of cobalt promoter on Ni NPs supported on a SiC-embedded MgAl$_2$O$_4$ as a catalytic material for the propane steam reforming (SRP; eq 21).[379]

$$C_3H_8 + 3H_2O \rightarrow 3CO + 7H_2 \quad \Delta H^{\circ} = 497.7 \text{ kJ/mol}$$
$$(21)$$

These authors stressed the role of SiC chemical inertness along with that of its high thermal conductivity in terms of increased dispersion of the MgAl$_2$O$_4$ phase with a subsequent higher control on the metal−support interactions during the active-phase (Ni NP) deposition. Indeed, a SiC-embedded MgAl$_2$O$_4$ carrier reduced the formation of inactive NiAl$_2$O$_4$ species whose presence was detrimental for the ultimate catalyst performance. Most importantly, they found that the addition of a cobalt promoter (ideally 5 wt %) to their Ni catalyst gave rise to improved performance and catalyst coke resistance. They clearly showed the existence of a progressive Co NP migration toward Ni NP sites throughout the SRP run. Such a phenomenon led to the Co NP segregation at the outer surfaces of Ni NPs with largely beneficial effects on the catalyst activity and stability on run.[379] Indeed, due to their higher H$_2$ spillover and oxyphilic character, the migrated Co particles enhanced the reducibility of Ni sites[380] while preventing the occurrence of Ni NP aggregation phenomena and hence reducing undesired passivation paths of the active phase (catalyst coking)[381] under the operative conditions.

When compared to other fuels, methanol lists a number of technical advantages for hydrogen production. With only one carbon atom, methanol is the simplest alcohol available and in spite of its toxicity and high miscibility in water, the absence of C−C bonds facilitates the reforming at low operative temperatures (200−300 °C).[382] This temperature range is markedly lower to that required from other fuels such as methane (reformed above 500 °C),[383] and ethanol (reformed around 400 °C).[384] Moreover, it is biodegradable, liquid at ambient conditions and possesses a relatively high hydrogen-to-carbon ratio.[385] For these reasons, methanol SR has been widely investigated for a long time as a preferential solution to

H_2 production for application in several technological fields, including that of fuel cell devices.

Copper on SiC (Cu/SiC) has been pioneered by a Japanese team at the beginning of this century as an effective catalyst for the methanol (CH_3OH) steam reforming (eq 22).[386]

$$CH_3OH + H_2O \rightarrow 3H_2 + CO_2 \quad \Delta H^{\circ} = 49.7 \text{ kJ/mol} \tag{22}$$

These authors outlined the dependency of their catalyst's performance from the calcination temperature it underwent. They found that its thermal treatment in air and at temperatures up to 1073 K led to the formation of an amorphous silica layer suitable for stabilizing copper-active species against sintering during the process.

Paper-based Cu/ZnO catalyst composites, prepared by a conventional wet papermaking technique in combination with SiC fibers (ca. 0.5 μm ⌀ and 30 μm length) were also used as effective methanol SR catalysts operating at temperatures below 300 °C.[387] The porous SiC fiber-containing catalyst exhibited a higher methanol conversion efficiency and lower CO concentration compared with the same Cu/ZnO catalyst in the form of powder or pellet. As Figure 42 shows, the paper catalyst containing SiC fibers (20% w/w) displayed the higher CH_3OH conversion efficiency and the lower CO concentration over the whole scanned temperature range compared to either the SiC-free powdered or pelleted Cu/ZnO counterparts.

These authors concluded that SiC fibers enhanced the heat transfer inside the catalyst paper thus contributing to acquire higher methanol conversion. Moreover, such a thermal effect associated with the high thermal conductivity of SiC whiskers was found to suppress the occurrence of the undesirable reverse water–gas-shift reaction (rWGS, eq 23) as a result of a more uniform heat distribution inside the catalyst paper.

$$CO_2 + H_2 \rightarrow CO + H_2O \quad \Delta H^{\circ} = 42.1 \text{ kJ/mol} \tag{23}$$

As a further step forward, Xiao and Guo reported later on a porous SiC support coated with a multicomponent CuO/ZnO/CeO_2/ZrO_2 active phase to be exploited for methanol SR in a microreactor.[388] The authors showed that rough microchannels present in SiC support favor an ideal dispersion of active phase thus producing a remarkably high catalytic activity with no deactivation observed for 30 h long-term tests, thus demonstrating the potentiality of porous SiCs for application in on-site hydrogen production. The same group also reported on a SiC pore channels modification with a uniform SiC_xO_y layer that acts as a strong binder for a nickel-based active phase. The as-prepared material showed excellent activity in ethanol steam reforming with conversion up to 95% and H_2 selectivity of 74.8% registered at 500 °C. Moreover, the strong interaction of the Ni active phase with SiC-modified support ensures a high stability on stream with only slightly loss of catalytic performance.[389]

In a very recent contribution, Green, Wilhite, and co-workers have proposed a modular approach for methanol SR (and more in general for chemicals manufacturing) based on a conceptually different way for the heating of traditional catalysts at the desired target temperatures.[390] These authors demonstrated the ability of silicon carbide fibers to act as electrically conductive susceptors for the conversion of electromagnetic energy into heat directly at the catalytic bed formed by SiC$_{fibers}$ with 1 nm Pt sputter coating. At odds with classical heating furnaces, their induction heating setup enabled smaller, safer and more sustainable reactor configurations for the on-site and on-demand production of chemicals in the absence of traditional manufacturing infrastructures[391] and with a significant CO_2 saving.

3.2.3.3. Hydrogen from Catalytic Cracking of Biomasses. A classical drawback associated with SR processes is the formation of CO_x (X = 1, 2) byproducts whose separation from H_2 is generally difficult and costly.[392] Moreover, for certain applications (*i.e.* fuel cell devices), CO needs to be completely removed from H_2 fuel as to avoid electrocatalyst poisoning/deactivation phenomena.[393] Therefore, the catalytic cracking of hydrocarbons or biomasses into H_2 and carbon (C) followed by an oxidative catalyst regeneration (C removal in the form of CO_x) represents an attractive solution to the production of a clean fuel.

The Australian team of Harris et al. has reported on the synthesis and characterization of a series of biomorphic SiCs featured by an accurate replica of the structural complexity of natural material templates both on a macro- and microscopic scale.[394] Their aim was mainly focused on broadening the scope of biotemplates for the preparation of tailored SiC networks to be used as functional catalyst supports. As a proof-of-concept, they impregnated the biomorphic SiC samples with Ni NPs (5 wt %) and the resulting composites were successfully employed for the H_2 production from the catalytic pyrolysis of cellulose with a greater H_2 peak rate than that measured on a benchmark Ni/SiO_{2gel} catalyst.[394]

More recently, the team of Song and co-workers described the synthesis of a 10 wt % Fe/SiC catalyst for the effective cracking of toluene (as a model compound from biomass tar) under microwave irradiation conditions.[395] Similarly to previous works on DRM from the same authors,[367,368] the paper outlines the excellent microwave absorption properties of SiCs in the contest of an alternative approach to H_2 production.

3.2.3.4. Hydrogen from Hydrocarbons and Alcohols Partial Oxidation. The hydrocarbons partial oxidation (P_{OX}) to syngas (CO + H_2), under a pure oxygen-lean environment, is a highly exothermic process (eq 24) occurring much faster than the endothermic SR.[396]

$$C_nH_m + \frac{1}{2}nO_2 \rightarrow nCO + \frac{m}{2}H_2 \quad \Delta H^{\circ} \ll 0 \tag{24}$$

Therefore, it lists several advantages over SR such as good response time, compactness, and less sensitivity to fuel variation.

In recent years, the team of Wang and Chen has described a series of Al_2O_3–SiC composites obtained by precipitation technique followed by high-temperature calcination treatment, to give rise stacked porous structures with a highly improved thermal conductivity compared to a plain Al_2O_3. Ni-based catalysts were prepared in turn by impregnation technique of the composites and the resulting systems (Ni/Al_2O_3–SiC) were used as effective catalysts for H_2 generation via propane partial oxidation.[397−399] According to their outcomes, local catalysts overheating phenomena, originated by the reaction exothermicity were deeply mitigated on the Al_2O_3–SiC composites due to the higher thermal conductivity of the SiC component. In particular, 8 wt % Ni/Al_2O_3–SiC (with a 30 wt % of SiC content) gave the higher hydrogen production in propane P_{OX} (*c.a.* 236 μmol g_{cat}^{-1} s^{-1}) while showing the higher stability on run (up to 26 h at 600 °C).[397,399] A better control of the temperature runaway at the catalytic bed

Figure 43. Stability and selectivity tests of Rh/CeO$_2$–SiC, Rh/SiC, and Rh/Al$_2$O$_3$ in comparison in the ethanol P_{OX}. Reaction conditions: C$_2$H$_5$OH:O$_2$ = 1:1.5 (molar ratio), WHSV = 9000 mL g$_{cat}^{-1}$ h^{-1}; catalyst temperature: 700 °C. Adapted with permission from ref 401. Copyright 2021 Elsevier, Chinese Journal of Catalysis, License no. 20210301.

translated in a reduced aggregation of Ni NPs together with an appreciable increase of the catalyst coke resistance compared to the benchmark Ni/Al$_2$O$_3$ system. In addition to that, these authors also argued on the beneficial role of SiC and its thermal conductivity with respect to the easier removal of coke deposits throughout the catalyst oxidative regeneration phase.[397,399]

As far as the alcohol partial oxidation process is concerned,[400] the pioneering work by Pan and co-workers illustrated the advantages of CeO$_2$ washcoated silicon carbide networks as structural supports for Rh NPs (Rh/CeO$_2$/SiC) in the ethanol partial oxidation.[401] These authors celebrated the advantages of the CeO$_2$/SiC support in the process by comparing the activity and deactivation paths of their Rh/CeO$_2$/SiC composite with those of Rh/SiC and benchmark Rh/Al$_2$O$_3$ (Figure 43A–C). According to their conclusions, the improved performance of the Rh/CeO$_2$/SiC catalyst in terms of higher H$_2$ selectivity (Figure 43B) and lower CO production (Figure 43C) as well as coke resistance on long-term runs were attributed to the unique thermal conductivity properties of SiC matrices and the higher C elimination capacity of the CeO$_2$ phase in the presence of active oxygen species, respectively.

3.2.3.5. Miscellaneous Processes for a Sustainable "Hydrogen Economy". Hydrogen is an attractive energy carrier with a higher energy density (142 MJ kg^{-1}) compared to that of liquid hydrocarbons ($\approx$47 MJ kg^{-1}), a lower ignition temperature value and last but not least it produces energy/heat without the formation of CO$_x$ byproducts.[402] Accordingly, its production, transportation, storage and combustion are sides of the same coin to be paid while approaching the "hydrogen economy" challenge.

The catalytic H$_2$ combustion (CHC, eq 25) is a key and highly exothermic process of a "hydrogen economy", generally associated with the CO$_x$-free production of heat for both industrial and civil purposes.

$$H_2 + \frac{1}{2}O_2 \rightarrow H_2O \quad \Delta H^\circ = -286 \text{ kJ/mol} \quad (25)$$

Regarding catalysts for the process,[403] Pt is a highly attractive candidate for CHC suitable for burning hydrogen even at room temperature.[404] From a practical viewpoint, catalysts are prepared in a supported form and the choice of the most appropriate active-phase carrier is accomplished as to

ensure the higher metal dispersion, prevent metal NP aggregation, leaching and sintering phenomena while favoring the catalyst reuse in successive cycles. SiC has been selected as one of the most appropriate catalyst supports in CHC because of its high thermal conductivity that makes it appropriate for the design of heating devices.

Fernández, Arzac, and co-workers first investigated the role of SiC networks in the form of 3D foams, powder and biomorphic monoliths as supports for Pt NPs to be applied in lean hydrogen/Air combustion ($\approx$1% v/v, H$_2$ in air),[405,406] including specific conditions like those at the outlet of a hydrogen fuel cell (3–4% v/v, H$_2$ in air).[407] Besides pointing out the thermal properties of these ceramics, the authors also investigated the advantages rising from either the SiC washcoating with alumina/ceria layers[405] or its direct oxidation in order to improve the metal active-phase dispersion at their hydrophobic outer surface. Their study demonstrated that a 0.27 wt % Pt/SiC catalytic materials was active enough to start CHC in a few seconds and at room temperature with a H$_2$ conversion as high as 18.5 L$_{H_2}$ min^{-1} g$_{Pt}^{-1}$. In a study based on the use of Pt-loaded biomorphic SiC matrices for CHC, the same authors also revealed the existence of a certain extent of anisotropy in the thermal conductivity their bio-SiC supports with a maximum temperature difference between the central material core and its periphery that can be as high as 30 °C.[407] As far as the role of SiC is concerned, the activity of Pt/SiC$_{powder}$ in CHC was compared with that of related catalysts prepared on conventional metal oxide supports (TiO$_2$, Al$_2$O$_3$, SiO$_2$). One main conclusion from these authors was that the Pt/SiC catalyst featured by a larger mean size of metal particles was also the most active in the process because of the higher metallic Pt content in its partially oxidized active phase compared to the smaller and completely oxidized Pt NPs obtained on the more traditional metal oxide carriers.[406]

The most attractive raw material for H$_2$ production remains water whose direct thermal dissociation (thermolysis) is thermodynamically challenging as it requires temperatures above 2200 °C to acquire an appreciable dissociation degree.[408] In order to accomplish the water splitting process under milder conditions, a series of indirect chemical processes whose net result is the evolution of two gases (H$_2$ and O$_2$) have been setup and named "thermochemical cycles". Sulfur-based thermochemical cycles, the sulfur–iodine (SI, eqs

Figure 44. Sulfuric acid decomposition on Pt/SiC (blue symbols) and Pt/n-SiC (red symbols) catalysts at variable reaction temperatures [650 °C (■, red; □, blue); 750 °C (●, red; ○, blue); 850 °C (▲, red; △, blue,) and GHSV = 76,000 mL g_{cat}^{-1} h^{-1}] as a function of TOS (min) (A) and as a function of GHSV (B). Adapted with permission from ref 420. Copyright 2014 Elsevier B.V.

26−29) and the hybrid sulfur cycle (HS, eqs 26−28 and 30), are among the most efficient and studied processes to acquire water thermolysis at relatively lower temperatures (<1000 °C) and with appreciably high efficiency.[409]

$$H_2SO_4 \rightarrow SO_3 + H_2O \; (\approx 400 \; ^\circ C) \tag{26}$$

$$SO_3 \rightarrow SO_2 + \tfrac{1}{2}O_2 \; (\text{up to} \approx 950 \; ^\circ C) \tag{27}$$

$$SO_2 + 2H_2O + I_2 \rightarrow H_2SO_4 + 2HI \; (\approx 120 \; ^\circ C) \tag{28}$$

$$2HI \rightarrow H_2 + I_2 \; (\text{up to } 400 \; ^\circ C) \tag{29}$$

$$SO_2 + 2H_2O \rightarrow H_2SO_4 + H_2 \; (\text{up to } 120 \; ^\circ C, \text{ electrolysis}) \tag{30}$$
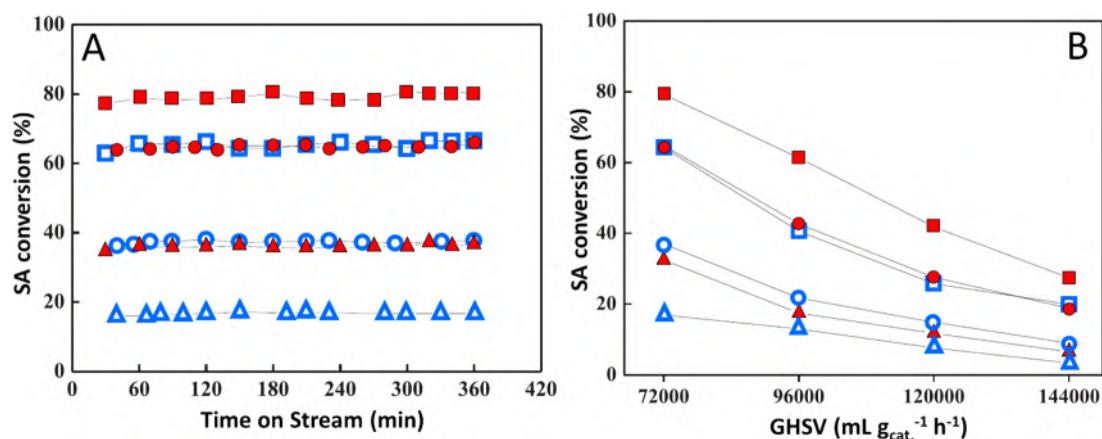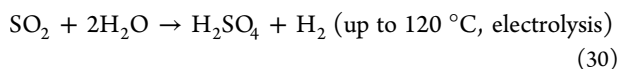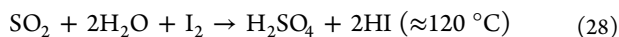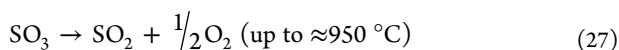
The most energy intensive step of both cycles is represented by the SO_3-to-SO_2 reduction (eq 27) that is a highly endothermic process requiring the use of a catalyst (typically a metal oxide or mixed metal oxides)[408] and taking place at relatively high temperatures. The heat required for this reaction can be supplied by concentrated solar power (CSP) devices where monolithic reactors made of catalyst-coated honeycomb supports (e.g. SiC-based networks) have found application as adsorbers for the concentrated solar irradiation. Giaconia et al. described an effective catalytic reactor suitable to operate under the environmentally harsh conditions required for the SO_3 decomposition process to occur.[410] To this aim, they tested a siliconized silicon carbide (SiSiC) honeycomb network coated with Fe^{III}-oxide as the active phase to be used as a durable and effective SO_3 decomposition catalyst under realistic sulfur thermochemical conditions (≈96 wt % H_2SO_4, temperature range 775−900 °C, pressure range 1−4 bar). The Fe_2O_3-coated SiSiC monolith showed all necessary features that an appropriate catalytic system should have for running such a challenging process efficiently (catalytic activity around 80% and close to the thermodynamic limit) without any appreciable deactivation upon exposure to the harsh reaction conditions for long reaction times (i.e. 100 h). In this regard, SiC presented excellent properties both in terms of its inherently high thermal conductivity and its chemical inertness to harsh environmental conditions that made it an appropriate choice for the preparation of a robust, cheap, and easily scalable catalyst for SO_3 splitting.[411] The limited SiC surface oxidation by SO_x species was a transitory phenomenon with no relevant effects on the ultimate performance of the catalytic system in the process. As far as the nature of the metal oxide active phases is concerned, these authors concluded that the Cr−Fe mixed oxides were among the most promising active-phase coatings for SiC supports as to acquire stable, durable, and efficient catalytic material in long-term operational reactions.[411] They also argued the close performance of their Cr−Fe mixed oxides supported on SiSiC compared to that of a benchmark and costly Pt/Al$_2$O$_3$ catalyst.

In the same years, Zhang et al. investigated a series of copper chromite ($CuCr_2O_4$) and copper ferrite ($CuFe_2O_4$) self-standing catalysts for the process and compared them with Pt/SiC.[412,413] The latter was expressly prepared and used in place of the classical Pt/Al$_2$O$_3$ as to overcome the shortcoming of instability observed with oxide-based supports in long-term catalytic runs.

Given the severe experimental conditions that catalysts undergo within sulfuric acid vaporizers and concentrators, structural materials to be exposed to high temperatures and corrosive environments need to be selected. Kubo and co-workers evaluated the corrosion resistance of SiC and exposed metal oxides to typical reaction temperatures and aqueous sulfuric acid concentrations encountered in classical operative reactors.[414] Their study highlighted the superior corrosion resistance and moderate weight loss of silicon carbide (SiC), silicon impregnated silicon carbides (Si-SiC), and silicon nitrides (Si$_3$N$_4$) once posed in direct and prolonged contact with the considered reaction environment.

Several attempts were accomplished in the following years by researchers active in the field with the aim at improving the performance and lifetime resistance of catalysts of various active-phase compositions[415,416] (including Pt/SiC), applied to sulfur thermochemical cycles for H$_2$ production from water splitting. The Korean team of Jung et al. compared the Pt-Al (1 wt % Pt/Al$_2$O$_3$) with a Pt-SiC-Al (1 wt % Pt/SiC-coated-Al$_2$O$_3$) in the sulfuric acid decomposition at ambient pressure, and temperature values comprised between 650 and 850 °C.[417] Their fundamental study revealed that the SiC-coated support (Pt-SiC-Al) was crucial in preventing the generation of sulfate species that were commonly formed on the plain alumina support (aluminumsulfate) whose presence was indicated together with Pt NP leaching and sintering phenomena,[418,419] as one of the main causes for the Pt/Al$_2$O$_3$ deactivation. The same team also compared two Pt catalysts prepared from a
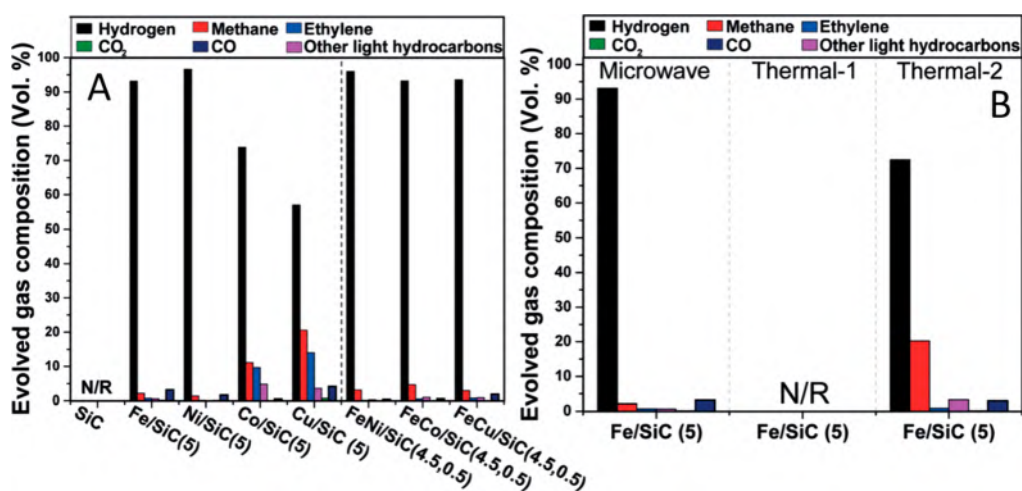
Figure 45. (A) Comparative analysis of various metals and binary metals on SiC, operating under the same dehydrogenation conditions and under microwave irradiation only for 10 min. (B) Comparison of microwave and classical conduction/convection/irradiation heating by an external furnace (Thermal-1 and Thermal-2). The number in parentheses after the catalyst's name shows the metal content, wt %. Adapted with permission from ref 429. Copyright 2017 Wiley-VCH.

commercial and crystalline, low-surface area SiC network (19.2 m^2 g^{-1}) and a homemade nano-SiC (n-SiC; 187.1 m^2 g^{-1}) prepared from nanosized silica as a hard sacrificial template.[420,421] Their study in the sulfuric acid decomposition showed the always superior performance Pt/n-SiC compared to that of the Pt/SiC sample (Figure 44A,B). The analysis of their samples led the authors to conclude that the higher activity of Pt/n-SiC was ascribed to the presence of outer n-SiC surface layers of SiO_2 and $Si_4C_{4-x}O_4$ engaged in a stronger metal NP stabilization.

Very recently, Upadhyayula and co-workers developed a series of bimetallic Cu−Fe catalysts supported on β-SiC or SiO_2 prepared by wet impregnation.[422] Both materials were tested with respect to their activity in the endothermic SO_3 decomposition reaction at high temperature (800−900 °C). Despite the harsh conditions, both materials exhibited good activity with $CuFe_2O_4$/SiC outperforming its SiO_2-supported counterpart in terms of stability for long-time experiments (120 h). The activity drop registered for $CuFe_2O_4$/SiO_2 was ascribed to the sintering of the active phase and to the lower thermal stability with respect to β-SiC. As a further step forward, the same authors deposited iron oxide NPs on SiO_2-modified SiC resulting in a highly active and stable catalyst for sulfuric acid decomposition. This study contributed to highlight once again the importance of the O−Si−O/active-phase interface for the development of high performing, sinter resistant catalytic systems.[423]

Inorganic chemical hydrides like ammonia borane and sodium borohydride are attractive precursors for H_2 production owing to some advantageous features such as 1) their easy and safe handling in aqueous solutions, 2) their easy storing at ambient conditions for relatively long periods and use on demand for the production of hydrogen, 3) their non-flammable or toxic nature, and 4) their hydrogen-rich content. A widely investigated research area deals with the development of suitable catalysts for the $NaBH_4$ (10.8 wt % of H_2) hydrolysis.[424,425] In recent years, Bernard et al. have proposed a series of 3D mesoporous non-oxide supports [*i.e.* namely mesoporous silicon carbides (SiC), carbonitrides (Si−C−N) and nitrides (Si_3N_4)] for Pt NPs to be applied in $NaBH_4$ catalytic hydrolysis under alkaline water media.[426] These non-

oxide carriers were selected as ideal active-phase supports in light of their renowned thermal, chemical, and mechanical stability in processes involving high-temperature reactions, reducing environments (*e.g.* highly alkaline media), and/or fast reaction rates. Although all Pt-based catalysts from this series collapsed after a few hydrolysis runs, the authors' findings revealed a hydrogen generation at the rate of 24.2 L min^{-1} g_{Pt}^{-1} with the mesoporous Pt/Si_3N_4 catalyst, showing markedly higher performance in the process compared to those of 3D SiC and carbonitride-based counterparts. Ammonia represents another interesting vector for H_2 production due to its low cost and high availability with an annual world production of 170 Mt registered in 2019. Moreover, its high hydrogen content (17.6 wt %) together with its carbon-free nature renders the CO-free hydrogen produced from NH_3 highly suitable for direct use in fuel cell technology.[427] As efficient catalyst systems for ammonia decomposition, the Sánchez group developed a series of Ru NPs deposited on β-SiC that revealed the ability to reach an almost complete NH_3 conversion at 623 K. In this work, silicon carbide was exploited for the first time for the process, and it was found to be an ideal support due to its high thermostability and thermoconductivity together with high mechanical strength and chemical inertness.[428]

As an alternative and highly efficient approach to the production of high-purity hydrogen fuel, Xiao, Thomas, and Edwars have proposed a microwave-promoted alkane (from C_9 to C_{17}) dehydrogenation protocol using abundant and inexpensive iron, nickel, or their alloy-based catalysts supported on silicon carbide susceptors.[429] This fundamental study demonstrated that the microwave heating of their metal rich composites promoted the deep hydrocarbon dehydrogenation process with H_2 selectivity up to 98% depending on the catalyst active-phase composition (Figure 45A). In addition, a comparative analysis of the microwave-assisted process with the classical one based on conduction/convection and radiation heat provided by an external furnace served to elucidate the importance of the adopted heating scheme with respect to the ultimate catalyst performance. As Figure 45B shows, the microwave heating scheme was from definitively outperforming (Microwave vs Thermal-1) to highly beneficial (Microwave vs Thermal-2) for H_2 production (vol %) and
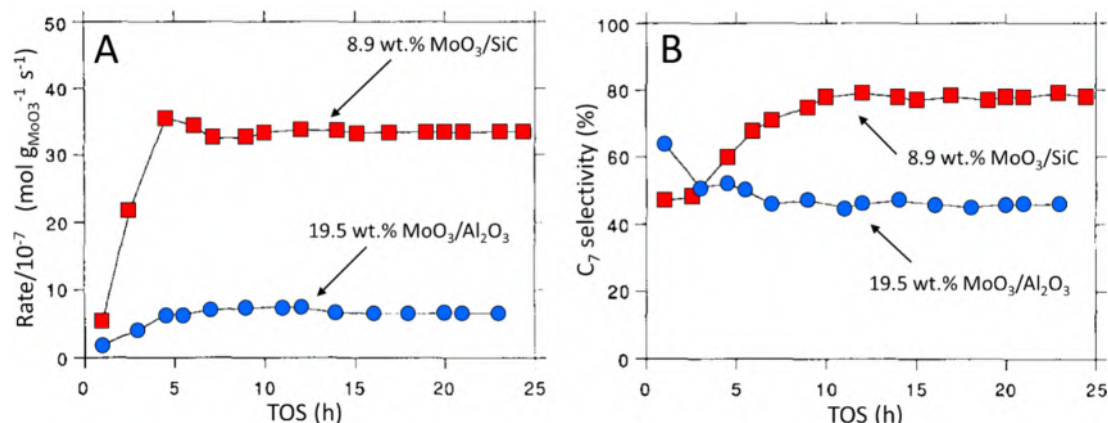
Figure 46. Comparative *n*-heptane isomerization tests (A) reaction rate vs TOS and (B) C_7 selectivity vs TOS] with two catalytic systems in comparison (8.9 wt % MoO_3/SiC vs 19.5 wt % MoO_3/Al_2O_3). Reaction conditions: catalyst: 0.3 g; reaction temperature: 350 °C; total flow rate = 40 mL/min; H_2/*n*-C_7 ratio: 60; atmospheric pressure. Adapted with permission from ref 431. Copyright 1995 Published by Elsevier BV.

process selectivity whatever the classical heating scheme applied to the process [catalyst preheated in the presence (Thermal-2) or in the absence (Thermal-1) of the reactants oils].[429]

3.2.4. Fuel Upgrading. Fuel upgrading technologies applied to the conversion of natural energy sources are key issues aimed at identifying the potential research directions to meet the energy market needs.[430] Over the last decades, such technologies have pointed out more and more the urgent need to foster the development of innovative, efficient, cost-competitive, and low-emission energy sources. The following examples offer a comprehensive overview on the use of SiC networks in catalysis for related technological purposes.

3.2.4.1. Catalytic Alkane Isomerization. The French team of Ledoux et al. focused first on the use of SiC-supported molybdenum oxycarbide catalysts for the efficient and selective alkane isomerization reaction.[431−434] The isomerization of linear saturated hydrocarbons into their branched counterparts is a fundamental process for increasing the number of octanes of unleaded gasoline while avoiding as much as possible cracking phenomena and aromatization paths because of the detrimental effects associated with the latter. While the isomerization of saturated low-molecular weight hydrocarbons (<C_6) is conveniently achieved by supported platinum catalysts (*i.e.* Pt-based catalysts on acidic alumina or zeolite), higher alkanes (>C_6) suffer from cracking side processes favored by the acid nature of commercial metal oxide supports that limit in turn the isomerization yield at high hydrocarbon conversion.[435,436] Ledoux's team reported that the MoO_3 carbon-modified phase (oxycarbide) was an efficient catalyst for C_{6+} alkane isomerization, with excellent selectivity even at high hydrocarbon conversions, particularly in combination with silicon carbide as the active-phase support.[431,432] In a comparative analysis with alumina, they showed the superior performance of MoO_3/SiC in the isomerization of model saturated hydrocarbons.[432] These authors argued the beneficial effects rising from the weak interaction between MoO_3 and the support when SiC was used in place of Al_2O_3. Indeed, the chemical inertness of SiC made easier the formation of the active molybdenum oxycarbide during the initial activation period under the hydrogen/hydrocarbon mixture, preventing stronger and catalytically detrimental interactions like those occurring on the reactive and acidic Al_2O_3. Figure 46 well outlines the two catalytic systems (8.9 wt % MoO_3/SiC vs 19.5

wt % MoO_3/Al_2O_3) in the *n*-heptane isomerization in comparison. In spite of a MoO_3 loading more than twice of Al_2O_3 compared to that of SiC, isomerization activity and C_7 selectivity at the steady-state conditions were always markedly higher on the SiC-based catalyst. In addition, the higher thermal conductivity and chemical inertness of SiC reduced the occurrence of thermal shocks during the oxidative catalyst regeneration step, thus avoiding sintering phenomena of the support and the active phase and allowing the easier recovery of the latter.

Later, the same team discussed the catalytic performance of their MoO_3/SiC catalyst (*in situ* prepared molybdenum oxycarbide) with that of the benchmark β-zeolite-supported bifunctional platinum catalyst in the *n*-octane isomerization. The study demonstrated that isomerization of high molecular weight hydrocarbons with low formation of cracking by-products and almost no aromatic compounds was possible at very high hydrocarbon conversion (close to the thermodynamic equilibrium) when a SiC-supported molybdenum oxycarbide catalyst was employed in the process.[434] The main reaction products were mono- and dimethyl isomers with a C_8 selectivity higher than 90% and *n*-octane conversion up to 75%. Their comparative analysis unveiled the higher catalytic performance of the MoO_3/SiC system and the markedly lower catalyst coking degree compared to the benchmark Pt system. In addition, they also demonstrated the markedly higher resistance of their molybdenum-based catalyst (vs Pt/β-zeolite) to sulfur- and nitrogen-containing compounds (catalyst poisons) typically available in crude natural oils. This important finding along with the cheaper and most abundant availability of Mo with respect to Pt additionally strengthens the relevance of this catalyst technology for future cleaner fuels.[434]

3.2.4.2. Catalytic Hydrodeoxygenation (HDO) Reaction. Very recently, Jiao, Fan, and co-workers reported on a high-quality ZSM-5 coating on SiC foam composites with intercrystal porosity[437] for the highly efficient bio-oil upgrading using methanol and anisole as probe molecules in the catalytic hydrodeoxygenation (HDO) reaction.[301] HDO is a complex process that may include hydrogenation, hydrogenolysis, decarbonylation, and dehydration reactions, and it has received considerable attention from the scientific community as a way for converting biomass-derived oxygenates into renewable fuels and chemicals. Jiao and Fan found a significant process
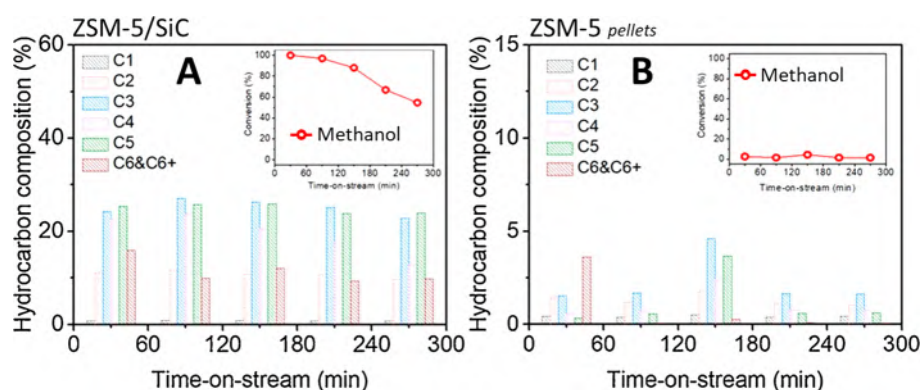
Figure 47. Hydrocarbon compositions (C6&C6+: paraffins, heavy olefins, naphthenes, and aromatics containing six and more than six carbon atoms) and methanol conversion as a function of time on stream (TOS) at WHSV of 8 h^{-1} over (A) the ZSM-5/SiC foam composite and (B) the plain ZSM-5 catalyst as pellets. Figures adapted from ref 437. Elsevier BV 2020 under [CC BY 4.0] [https://creativecommons.org/licenses/by/4.0/].

intensification when their structured ZSM-5/SiC foam composite was employed in the process in place of a classically packed-bed reactor filled with ZSM-5 pellets. While the former showed 100% of methanol and anisole conversion at the initial stage of the process, the latter gave rise to a modest 3% conversion when the reactions were operated under identical conditions (Figure 47). They concluded that the enhanced mass transfer properties along with the inherent thermal conductivity of the SiC support were at the origin of the observed process intensification. Indeed, catalyst fouling due to the generation of coke deposits was significantly higher when the reaction was operated in the packed-bed configuration with ZSM-5 pellets than in the case of their structured ZSM-5/SiC foam catalyst. Wang and collaborators came across similar conclusions with their Pd@ZSM-5/SiC composite employed in the hydrodeoxygenation of methyl oleate, a model molecule for biofuel.[438] Using an unconventional solvent-free crystallization process, this team obtained a pure SiC surface coating based on a highly crystalline zeolite sheath to be used as the catalyst in the process.

Compared to the Pd@ZSM-5 powder, their Pd@ZSM-5/SiC monolith showed a markedly improved process efficiency linked again to the fast mass and heat transfer allowed by the honeycomb SiC structure. They also showed a higher durability of their foam composite along with a higher stability at the high-temperature conditions required for the catalyst regeneration.[438]

3.2.4.3. Catalytic Oxidative Desulfurization (ODS). Another key process in the natural fuel managing deals with the removal of organic and inorganic sulfur compounds. This is a fundamental issue particularly because of their heavy environmental and health impacts once released in the atmosphere.[439,440] In this regard, hydrodesulfurization (HDS) is a widely used technique to obtain low-sulfur commercial fuels. However, HDS is a scarcely effective process to remove thiophenic compounds.[441] On the other hand, oxidative desulfurization (ODS) is a lower-energy consumption approach[442] where thiophenes can be oxidized under mild conditions into the corresponding sulfones which are removed in turn by adsorption or extraction methods.[443] Best results are generally obtained in the presence of metal oxide catalysts prevalently selected among high-valent transition metals such as Mo, W, V, Ti, etc.[444,445]

After the pioneering work by the French group of Ledoux who first employed silicon carbide doped with high-valent metal ions (*i.e.* sulfide CoMo) for the hydrodesulfurization (HDS) of thiophene,[50] recently an Iranian team has reported on the synthesis of a series of mesoporous SiCs featured by high surface area, prepared from natural biopolymers such as guar, tragacanth, Arabic, and xanthan gum.[446,447] These materials, including their N-doped counterparts, have been prepared and used as catalyst supports for high-valent Mo active phases (*e.g.* MoO$_3$[447] or MoO$_2$/Mo$_2$C/MoSi$_2$[446]) to be employed in the oxidative desulfurization (ODS) of a model fuel prepared by dissolving a certain amount of dibenzothiophene in *n*-octane. Their comparative study with plain SiC and N-doped carbons as carriers for the Mo active phase has unveiled the superior performance of the N-doped SiC network as a support for the Mo phase to be employed in ODS. Therefore, SiC structures and N-doped SiC networks, in particular, allowed an increase in the electron density on peroxo groups hence decreasing the energy barrier associated with the oxidation process.[446] To accomplish their catalytic purposes, the same group has also reported on the synthesis of SiO$_2$@SiC core—shell nanospheres and their subsequent surface engineering with WO$_3$ single-atom moieties[448] or—as an alternative—porous MoO$_3$@SiC[449] hollow spheres to be employed in ODS always with superior performance with respect to functionalized silica nanospheres[448] and MoO$_2$@C[449] counterparts, respectively.

3.2.4.4. H$_2$S Selective Oxidation to Elemental Sulfur. This selective oxidation process holds important effects on both an industrial, health, and environmental viewpoint, and thus it can be properly discussed in the section dealing with the fuel production and upgrading as well as in the successive chapter dealing with the use of SiC in processes related to the environmental protection (section 3.3). Hydrogen sulfide, H$_2$S, is a colorless chalcogen hydride gas with the characteristic foul odor of rotten eggs. It is poisonous, corrosive, and flammable, and it is normally contained in acid gases generated by oil refineries or natural gas plants. Due to its high toxicity and the need to address all restrictions posed by the legislation of fossil fuels producer-and-user countries, it is mandatory to transform/remove it from any natural source before it comes in contact with the atmosphere.[450,451] Generally, H$_2$S desulfurization is industrially addressed by the so-called Claus process[452]
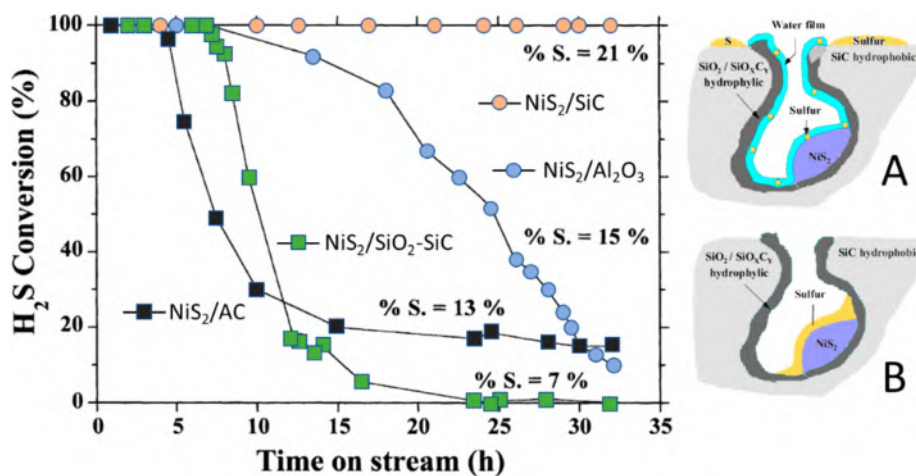
Figure 48. H_2S conversion as a function of time on stream and solid sulfur weight deposited on the catalyst. Four NiS_2-based catalysts prepared on different supports and compared in a model desulfurization process operated at 60 °C in the presence of 20 vol % of steam. A and B refer to the proposed mechanism of sulfur deposition on the SiC-based catalyst in the presence (A) and in the absence (B) of steam in the feed. Adapted with permission from ref 461. Copyright 2002 Elsevier Science BV.

that consists of treating natural gaseous effluents as to selectively oxidize H_2S into elemental sulfur (eqs 31 and 32)

$$H_2S + \tfrac{3}{2}O_2 \rightarrow SO_2 + H_2O \tag{31}$$

$$2H_2S + SO_2 \rightarrow 3S + 2H_2O \tag{32}$$
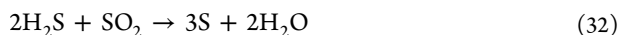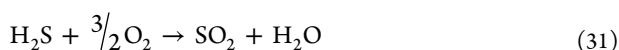
However, due to thermodynamic limitations of the Claus equilibrium, typical sulfur recovery efficiencies rank in the 90−96% range for a two-stage reactor plant and 95−98% for a three-stage reactor plant. Accordingly, additional processes dealing with the Claus tail gaseous treatment have been developed (direct H_2S oxidation with no thermodynamic limitations) as to make possible the almost complete (up to 99.9%) hydrogen sulfide conversion into elemental sulfur (eq 33)[453] and minimize SO_2 emissions from the incinerator. Among the methods for the gas tail treatment, the Superclaus process developed in 1985 has allowed for upgrading the H_2S desulfurization efficiency up to 99.5% by means of Fe and Cr catalysts supported on alumina or silica.[453,454] One main drawback of the direct catalytic H_2S oxidation is the too high efficiency of the employed catalytic systems that may favor overoxidation paths (eq 34).

$$H_2S + \tfrac{1}{2}O_2 \rightarrow \tfrac{1}{n}S_n + H_2O \tag{33}$$

$$\tfrac{1}{n}S_n + O_2 \rightarrow SO_2 \tag{34}$$
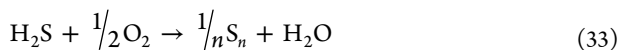
In this way, undesired SO_2 is generated, and the reaction efficiency is reduced. Moreover, classical oxide-based materials as catalyst supports can undergo sulfatation in the presence of steam and sulfur thus leading to a progressive decrease of the catalyst activity or even its complete deactivation on stream.

The use of silicon carbide as an alternative and valuable catalyst support for the process was first presented by the French team of Ledoux in 1999.[455,456] These authors reported on the use of this non-oxide material as an ideal thermally conductive and chemically inert carrier for nickel sulfide or iron oxide active phases to be employed in the process within a relatively wide range of operative temperatures (40−240 °C).[455] They found that NiS_2/SiC exhibited excellent activity and selectivity toward elemental sulfur already under moderate reaction temperatures (below elemental sulfur dewpoint), in the presence of steam and an excess of oxygen. They showed that the presence of a film of condensed water (steam) at the catalyst surface favored the formation of large sulfur deposits while preserving a regular H_2S uptake to the catalyst active sites. Indeed, the desulfurization activity was quantitative, and the catalyst performance did not show any appreciable deactivation up to 90 h on stream while forming an amount of deposited sulfur at the catalyst surface that was in accord with that expected for the process. Water was supposed to mechanically remove and transport the formed elemental sulfur from the catalyst active phase on the hydrophilic part of the support (*i.e.* oxycarbide or oxide of Si) to its more hydrophobic one (*i.e.* plain SiC), hence preventing active-phase fouling phenomena even after long-term runs when the sulfur loading at the catalyst surface becomes relatively high.[457] These authors also found that the absence of microporosity in SiC reduced the reagent contact time with the catalyst surface thus resulting in quantitative selectivity for the process without any trace of SO_2 detected at the reactor outlet. The chemical inertness of the SiC support was also found to prevent any undesired and detrimental side reaction between the carrier and its active phase.[456]

The unique properties of SiC not encountered in more classical metal oxide materials or carbonaceous supports are also at the origin of the excellent H_2S desulfurization performance reported by the French team with SiC-supported iron-based catalysts applied to the process.[458] The high thermal conductivity of the SiC support along with its essentially macroporous nature combined with the absence of acidic and/or basic surface sites potentially responsible for undesired side processes provided these authors with an extremely robust and effective catalytic system for the highly selective H_2S oxidation to elemental sulfur in the presence of a large amount of oxygen and steam in the feed. Their iron-based catalyst exhibited a high stability as a function of time on stream during several weeks in an industrial pilot plant operated at temperatures above the sulfur dewpoint without any appreciable deactivation or fouling.[458] Moreover, the absence of microporosity in the active-phase support was functional for the reduction of resident time of sulfur in
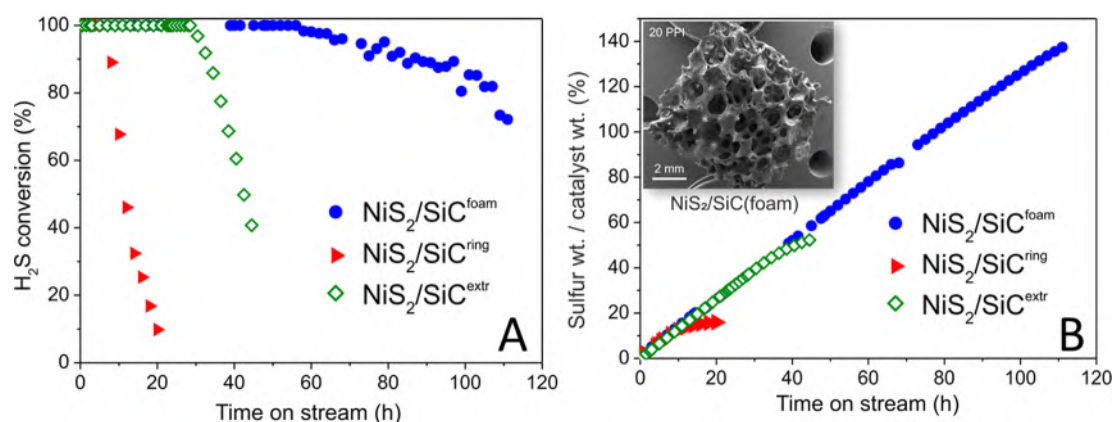
Figure 49. (A) H_2S conversion on various $NiS_2/SiCx$ catalysts (x = foam, extrudates, rings); (B) Solid sulfur deposited on the catalyst expressed as a wt % increase of the spent catalyst with respect to the initial catalyst weight. Reaction conditions: $[H_2S]$ = 0.5 vol %, $[O_2]$ = 1.25 vol %, O_2-to-H_2S ratio = 2.5, $[H_2O]$ = 30 vol %, balance helium, reaction temperature = 60 °C, GHSV (STP) = 1200 h^{-1}. Adapted from ref 462. MDPI, Basel, Switzerland 2018 under [CC BY license 4.0] [https://creativecommons.org/licenses/by/4.0/].

contact with the catalyst, hence avoiding undesired over-oxidation paths and ensuring high selectivity to the process.[459]

Remarkably, the same authors also proposed a reproducible synthesis of SiC nanotubes of different internal and external diameters by the gas—solid reaction between SiO vapors and carbon nanotubes or nanofibers (shape-memory synthesis).[460] They demonstrated interesting structure/activity relationships by preparing NiS_2/SiC nanotubes to be applied in the selective H_2S desulfurization to elemental sulfur. Indeed, a significant increase of the catalytic reaction rate, likely due to a microscopic increase of the H_2S partial pressure inside the tubes (caused by condensation and microcapillarity), was claimed to be at the origin of the observed phenomenon.[460]

The clear-cut superiority of SiC-supported NiS_2-based catalysts in terms of time on stream and solid sulfur loading in the low-temperature H_2S selective oxidation was demonstrated by Keller and co-workers in a comparative study with more classical oxides (i.e. SiO_2 and Al_2O_3) or activated charcoal as supports for the metal active phase.[461] As Figure 48 shows, these authors compared the desulfurization activity of the different nickel sulfide-supported catalysts in a process operated at 60 °C in the presence of 20 vol % of steam and measured the wt % of sulfur deposited at the end of the process.

In spite of the larger quantity of sulfur on the SiC-based catalyst (21 wt % after 35 h on run), it largely outperformed all other supported NiS_2 catalysts in comparison. The SiC superior performance was explained as the combination of the peculiar action played by steam in the process and dual hydrophilic/hydrophobic nature of the SiC surface. While the former (SiC/SiO_xC_y) was claimed to accommodate the NiS_2 active phase and undergo the continuous cleaning action of steam, the latter—typically located outside the material mesoporosity—allowed the formed sulfur to be collected and accumulated without affecting the regular H_2S uptake at the catalyst active sites even for long-term desulfurization runs (Figure 48 A vs B).[459,461]

Following the same concept, these authors have recently compared and discussed a series of NiS_2-decorated SiC catalysts prepared from non-oxide carriers of variable size and shape.[462] They have demonstrated the superior performance of a 3D open-cell SiC foam as support in the low-temperature desulfurization process compared to SiC rings and

SiC extrudates, with the foam showing a sulfur-storage capacity up to 140 wt % in a discontinuous setup for the treatment of highly H_2S-enriched (from 0.5 to 1 vol %) gas effluents (Figure 49A).

The unique chemicophysical and morphological properties of the SiC foam allowed good reagent accessibility to the catalyst active sites even when large deposits of sulfur were formed. In addition, the amphiphilic surface properties of SiC created preferential areas for the growth of sulfur deposits thus ensuring longer-term desulfurization stability to the composite (Figure 49B).[462]

Other reports from the same authors have additionally contributed to highlight the important properties of SiC supports in such a highly exothermic process.[463,464] Indeed, the ability of a mesoporous SiC support to host a homogeneously dispersed Fe_2O_3 active phase for the efficient and highly selective H_2S direct oxidation has also pointed out the ability of this thermal conductive ceramic to mitigate the generation of local hotspots during the process.[465] At odds with a more classical thermal insulator like Al_2O_3, the thermal conductivity of SiC was claimed to play a key role in the maintenance of the high process selectivity avoiding the formation of local temperature gradients even when the desulfurization reaction was operated at high reagents space velocity.[463,464]

3.3. Environmental Protection

3.3.1. Removal of Pollutants from Air. One of our era's greatest scourges and challenge for the incoming generations is air pollution, both for its impact on climate change and for its effects on public and individual health. There are different pollutants that pose serious concerns in terms of human diseases. Particulates of variable size diameter, ozone, nitrogen oxide, sulfur dioxide, volatile organic compounds (VOCs), dioxins, carbon monoxide, heavy metals, and polycyclic aromatic hydrocarbons (PAHs), are all classified among the most harmful air contaminants to human health.[466] Lastly, climate changes, resulting from environmental pollution, are already known to deeply affect the geographical distribution of several diseases as well as the widespread occurrence of intense natural atmospheric events never seen before in certain world areas. Public perception and the current worldwide legislations in terms of control of air pollutants have a fundamental role in keeping alive the interest of the scientific community on a so challenging and societal impacting matter. In this regard,
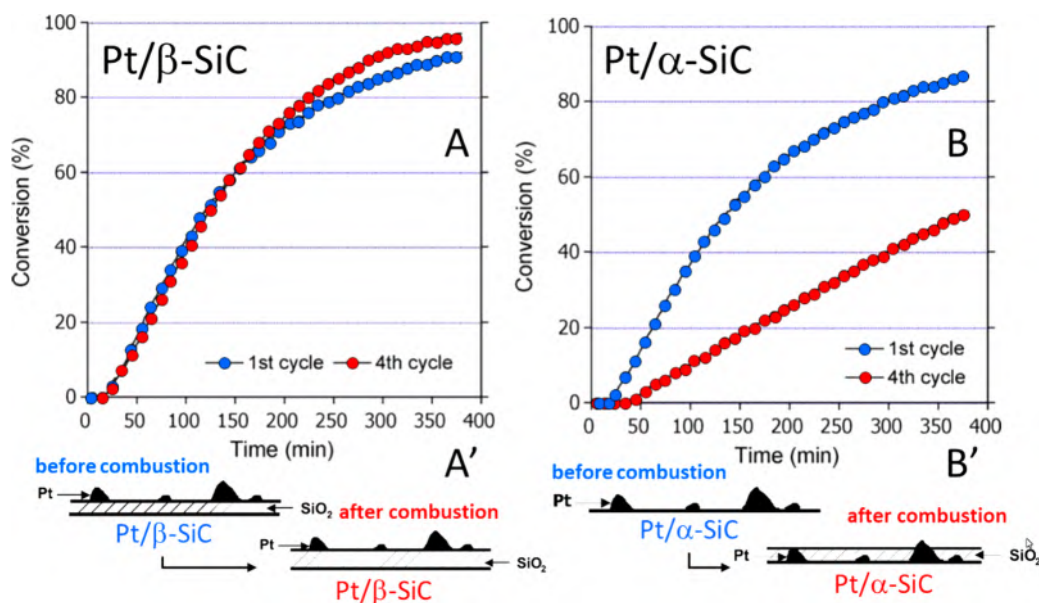
Figure 50. Combustion activity over Pt/β-SiC (A) and Pt/α-SiC (B) as a function of cycles. Different modes of silica layer growth on Pt/β-SiC (A′) and Pt/α-SiC (B′) and the supposed catalyst deactivation mechanism by metal particle encapsulation. Adapted with permission from ref 471. Copyright 2004 Elsevier BV.

catalysis plays a key role in the control of air pollutants, and silicon carbide remains one of the fundamental actors for the development of robust, stable, and effective catalytic systems.

3.3.1.1. Catalytic Filters for Diesel Particulates. The emission of particulates from diesel engines (diesel exhaust particulates—DEP) can deeply impact the quality and health-iness of the outdoor atmosphere to which all of us are constantly exposed. Diesel particulate filters (DPFs) are employed to remove soot from a diesel exhaust stream. Anyhow, their prolonged use leads to a progressive filter clogging whose regeneration is made possible by a complete soot oxidation that naturally occurs at temperatures much higher (~700 °C) than those operative in a diesel engine (~300 °C). Therefore, catalysis has been employed to promote the complete soot oxidation at the engine regime conditions. A first approach in the use of SiC-supported Pt-based catalysts was proposed by the Japanese team of Oi-Uchisawa who made use of a heat-resistive, thermal conductive, and chemically inert SiC carrier for preparing a series of Pt-based composites [Pt/MO$_x$/SiC (MO$_x$ = TiO$_2$, ZrO$_2$, Al$_2$O$_3$)] to be employed as stable and effective catalysts in the DPF regeneration.[467−469] The authors have reported a series of publications describing the indirect oxidation action of their catalysts with Pt sites oxidizing NO present in the exhaust gas to NO$_2$ and with the latter that was used in turn for oxidizing soot to CO$_2$. As far as the use of silicon carbide as support is concerned, these authors demonstrated the higher oxidation performance of their SiC composites compared to the plain Pt/MO$_x$ at work in the process. The need for reducing NO$_x$ emissions (due to more severe legislations on the matter of air pollution) has also led to rethink the assembly of catalytic reactors employed for the soot oxidation. Thus, to optimize the NO$_2$/soot ratio as to limit the emission of unreacted NO$_2$ in the atmosphere, Makkee and co-workers have demonstrated the effectiveness of the combination of a SiC foam and a SiC membrane in a so-named TU Delft (TUD) catalytic filter configuration.[470] In TUD, soot oxidation took place on the Pt/SiC foam as an integrated system and in a

SiC membrane as a continuously regeneration trap (CRT), ensuring high process efficiency at the lower rates of NO$_2$ and CO emissions.

In the same years, Pham-Huu and collaborators reported on the comparative performance of Pt-based catalysts supported on either a medium surface area β-SiC carrier or a low surface area α-SiC one.[471,472] This study devoted to the combustion of a model carbon particulate unveiled the superior performance and potentiality of the β-SiC support in the process. As Figure 50 shows, the isothermal combustion (300 °C) with the two catalytic systems in comparison was quite similar, at least for the first catalytic cycle. An opposite trend was registered between the two systems as a function of the combustion cycles. Accordingly, the catalytic combustion activity decreased gradually on the Pt/α-SiC sample with a significant reduction of NO$_2$ formation already after four successive cycles. The hypothesis for the lower performance of the α-SiC-supported catalyst in the process was ascribed to a progressive metal particle encapsulation by silica layer growth on the oxygen-free surface of α-SiC during the reaction cycles. On the other hand, metal particle encapsulation did not occur on the β-SiC sample because additional silica layers were supposed to grow inside (in the bulk) the pre-existing SiO$_x$C$_y$ and SiO$_2$ coating naturally available at the outer surface of this medium surface area carrier.[471,472]

Garcia-Garcia et al. have more recently described a simple, green but effective coating procedure for the dispersion of a 2% CuO/ceria-zirconia powder catalyst onto a SiC-based DPF (diesel particulate filter) to be employed for NO oxidation to NO$_2$ and for soot combustion under NO$_x$/O$_2$.[473] Besides getting a stable and reusable composite for the process, they also found a satisfactory activity toward NO oxidation reaction and soot combustion reaction. Moreover, the use of the 3D structured catalyst allowed the authors to operate the process under remarkably higher gas hourly space velocity (GHSV) compared to that used with the unsupported CuO/ceria-zirconia powder.

Very recently, Pilar Orihuela et al. employed a biomorphic silicon carbide monolith coated with ceria to fabricate a wall-flow filter for soot oxidation. The authors found that a synergistic effect between ceria and support allowed the reduction of soot oxidation temperature while reducing also the filter regeneration temperature.[474]

3.3.1.2. Carbon Monoxide (CO) Oxidation. Carbon monoxide (CO) is primarily formed when carbon fuels are not burned completely. Transportation sources account for the majority of CO emissions.[475] Power plants and industrial and domestic activities finally complete the list of major producers of this toxic air pollutant. Consequently, high concentrations of CO generally occur in areas with heavy traffic congestion and in overcrowded and industrialized areas mainly. CO is a colorless, odorless, and tasteless flammable gas with high affinity toward hemoglobin that makes it highly toxic and harmful for living beings. Its oxidation and hence the development of catalysts suitable for carrying out the process efficiently and under mild conditions has been therefore a challenging area for research for a long time. Accordingly, an extensive number of transition-metal-based catalysts, prevalently selected from the series of Pt group metals (PGM) or their alloys, have been studied in the process.[476] The first report on the use of the Pt-doped SiC catalyst for CO oxidation was presented by the Indian team of Singh and collaborators in 1995.[477] These authors described the synthesis of β-SiC networks with relatively high specific surface areas ($\sim$150 $m^2 g^{-1}$) from the thermal plasma processing of rice husk followed by their 1 wt % Pt doping. They reported on the high CO-to-CO_2 oxidation activity of their Pt/SiC catalyst already under relatively low operative temperatures (175 °C) together with the high thermal stability of the composite for temperatures as high as 700 °C. While the former (activity) was ascribed to a homogeneous SiC surface distribution of Pt NPs, the latter (stability) was attributed to the thermal resistance of the support. Twelve years later, Zhan and co-workers came onto very similar catalytic conclusions using a 2 wt % Pt/SiC composite prepared by simple incipient impregnation of a porous SiC network synthesized by the carbothermal reduction method.[478] Later on, the Russian team of Vershinin studied the oxidation kinetic of low CO concentration air flows (100 mg m^{-3}) at ambient conditions, promoted by either 4 nm Pt clusters on β-SiC nanoparticles, or Pt on nanodiamonds or platinum black powder.[479] They showed that the CO oxidation rate per unit weight of platinum on Pt/SiC was from 60 to 90 times higher than that measured over the 30 $m^2 g^{-1}$ platinum black powder. They argued that the higher oxidation rate was due to both the higher surface area of Pt clusters on SiC as well as to the lower CO activation energy to the surface of the composite with respect to platinum powder. They also highlighted that a 12 wt % Pt on their SiC nanoparticles satisfied the conditions for a maximum CO oxidation rate under their selected ambient conditions.[479] In a very recent contribution by Lu and collaborators, the Chinese team has pointed out the role of the high SiC surface chemical inertness on the performance of Pt-based composites in catalysis. With Pt/CeO_2 and Pt/SiC catalysts obtained from a simple Pt colloidal particles deposition method followed by calcination in a wide range of temperatures (200−800 °C), they pointed out the double-edged sword role of metal−support interactions with respect to their catalysts' performance in the CO oxidation.[480] While the oxide-based carrier after a low-temperature calcination treatment displayed beneficial Pt−O−Ce interactions for the CO oxidation process, its calcination at higher temperatures reduced the content of Pt(0) necessary to the process, thus resulting in a progressive catalyst deactivation. On the other hand, the chemically inert SiC did not show any interaction with Pt whatever the applied calcination temperature hence providing a Pt/SiC catalyst with a markedly higher thermal stability than its oxide-based counterpart.[480]

As far as the use of non-noble metal-based catalysts in the process, the Ukrainian group of Ishchenko and co-workers reported on the treatment β-SiC nanofibers with a mixture of HF and HNO_3 as to create a highly defective and oxidized carrier surface suitable to accommodate the stable and catalytically active $Cu_2(OH)_3NO_3$ phase for the low-temperature CO oxidation.[481] They realized that such an oxidative treatment of the inert silicon carbide surface created a preferential chemicophysical microenvironment for the stabilization of the above-mentioned active phase while preventing its progressive conversion into the less active CuO phase.

Landi and collaborators compared CuO/CeO_2 washcoated monoliths prepared from either Cordierite (a magnesium−iron-aluminum cyclosilicate) or SiC as active-phase carriers. Their comparative study focused on the thermophysical properties of the carrier (*i.e.* cell density and walls thermal conductivity) for the intensification of the CO oxidation process in hydrogen purification, while improving selectivity to CO_2.[482] They showed that the higher the carrier cell density and the thermal conductivity of its walls, the higher the process intensification and the selectivity to CO_2. In particular, the superior thermal conductivity of SiC flattened the axial temperature profile in the monolith, avoiding the generation of local temperature gradients (hotspots) and improving the process selectivity.

3.3.1.3. Hydrofluorocarbon (HFC) Dehydrofluorination. Hydrofluorocarbons (HFCs) are a group of industrial chemical compounds primarily used in air conditioning and refrigeration that hold high global warming potential (GWP).[483] Selected compounds from this series possess a GWP that can be orders of magnitude higher than that of more common greenhouse gases. Dehydrofluorination of HFCs to give hydrofluoroolefins (HFOs) is a thermodynamically and kinetically challenging reaction[484] that represents the most effective route for converting these gases into value-added and environmentally benign compounds to be reused in the fluorinated polymer manufacturing industry. Strong Lewis acids usually act as catalysts for the highly endothermic process although they generally suffer from deactivation paths due to either the generation of coke deposits or sintering phenomena of the active phase. Moreover, hydrofluoric acid (HF) is the major side product of dehydrofluorination, and its highly corrosive nature strongly limits the type of active phase and catalyst supports to be selected for the process. Silicon carbide has a strong corrosion resistance, including HF corrosion,[485] and possesses a high thermal conductivity[50,486] that makes it an ideal choice for the development of stable and coke-resistant catalysts for dehydrofluorination.

In a recent contribution, Han and co-workers have prepared and compared silicon carbide-supported and AC-supported aluminum fluoride (AlF_3) catalysts to be employed in the dehydrofluorination of 1,1-difluoroethane (HFC-152a).[487] As Figure 51 shows, the catalytic performance of SiC-supported AlF_3 was markedly higher than that measured on the activated carbon-supported catalyst.
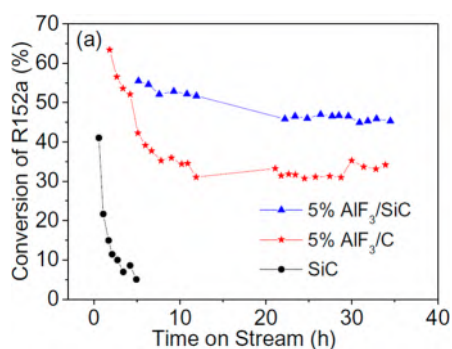
Figure 51. HFC-152a conversion rate over different catalysts as a function of time on stream. Other reaction conditions: atmospheric pressure, 300 °C, GHSV of 300 h^{-1}, feed gas composition: 50 vol % HFC-152a and 50 vol % N$_2$. Reproduced with permission from ref 487. Elsevier BV. 2020 under [CC BY-NC-ND 4.0] [https://creativecommons.org/licenses/by-nc-nd/4.0/].

Their study has pointed out the superior stability and thermal resistance of SiC to the extra heat required for the reaction to occur along with its higher thermal conductivity that was crucial in facilitating the heat reaction transfer to and from the supported catalytic active phase. Accordingly, SiC acted as a thermal regulator to disperse and homogenize the heat at the catalyst bed. Most importantly, such a more effective heat management on SiC was found to prevent the catalyst active phase from sintering and carbon deposition phenomena at high reaction temperatures.[487]

3.3.1.4. Methane Total Oxidation. Heavy-duty engines burning natural gas or biogas produce less air pollutants like soot and NO$_x$ compared to diesel engines. On the other hand, more light hydrocarbons such as methane and ethane are released in the atmosphere.[488] Due to their high global warming potential (GWP) it is crucial to control these emissions from natural gas vehicles (NGVs). Commercial catalysts suitable to provide a satisfying performance in the catalytic combustion of hydrocarbon-lean streams from NGVs are traditionally based on palladium nanoparticles supported on monolithic honeycomb networks. At odds with more classical oxide-based materials, the refractory and thermal conductive silicon carbide offers a higher thermal stability to the catalytic active phase and itself as support in reactions where high temperatures are required (*i.e.* the hydrocarbon oxidation reactions).

In a pioneering contribution on the use of SiC as support for Pd NPs engaged for the total methane oxidation, the authors studied the role of the metal-precursor decomposition method on the ultimate Pd NP size as well as on the final stability and aging of their composites.[489] Besides illustrating the advantages of SiC supports linked to their thermal stability and conductivity, the French team highlighted a faster aging and deactivation of selected composites due to a progressive metal NP encapsulation in surface grown SiO$_x$ layers.
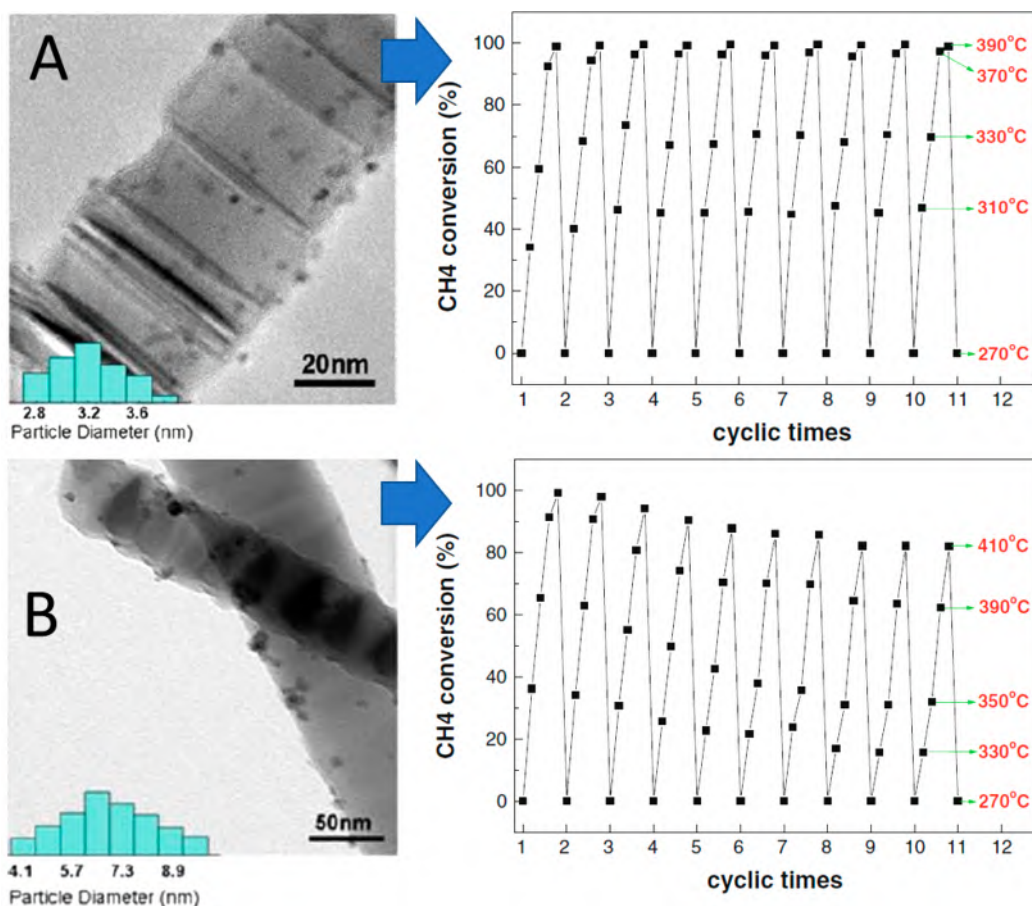
Figure 52. (A) Surface etched Pd/SiC catalyst exhibiting excellent activity and stability over ten successive runs. (B) Surface unetched Pd/SiC catalyst showing a significant activity decrease over successive runs due to NP migration and sintering. Adapted with permission from ref 491. Copyright 2009 the Authors.

Later, Ledoux et al. studied the effect of the impregnation method in the preparation of medium surface area β-SiC samples decorated with palladium particles to be employed in methane combustion under high space velocity.[490] Their study took a cue from the amphiphilic properties of SiC networks and thus from the preferential housing of NPs inside (hydrophilic part) or outside (hydrophobic part) the support mesopores as a function of the adopted one-step aqueous or two-step biphasic impregnation procedure. Their conclusion was that a two-step biphasic impregnation procedure favored the NPs growth outside the support mesopores hence reducing diffusion phenomena, improving reagents access to the material active sites, and improving the catalyst methane combustion activity.[490]

Guo, Tu, and co-workers have reported on a smart approach to the physical confinement of Pd NPs at the surface of etched SiC nanowires featured by a nanoditched structure (Figure 52). This spatial NP confinement was functional to the thermal resistivity and stability of the Pd/SiC composite in the highly exothermic methane combustion process. Indeed, the limitation posed from nanoditches to migration and sintering of Pd NPs allowed keeping the methane conversion close to 100% even after several successive catalytic cycles (Figure 52A). On the contrary, the catalyst prepared from the unetched support exhibited a progressive deactivation from 100% down to 82% conversion after ten cycles (Figure 52B).[491] A Chinese-French joint venture between Brault and Guo also referred to the structural evolution of SiC-supported Fe@Pt and Fe@Pd core−shell nanoparticles and the gradual increase of their catalytic activity upon cycling on methane combustion reaction. These authors claimed the progressive Fe−Pt and Fe−Pd surface alloying as the reason for the increased core−shell NP activity compared to their monocomponent noble metal counterparts.[492] The same team has also demonstrated the superior stability of Pd/SiC vs Pd/Al$_2$O$_3$ catalysts in the methane combustion as a function of successive cycles. While the former maintained the 100% conversion after 10 successive catalytic runs, the latter dropped down to 67% as the consequence of the γ-Al$_2$O$_3$ sintering and PdO NP coalescence.[493] They also proved the beneficial effect of a Zr$_{0.5}$Ce$_{0.5}$O$_2$-promoted SiC support for the process with a significant reduction of the T10% (temperature of 10% methane conversion) and T100% (temperature of 100% methane conversion) with respect to the unpromoted SiC support.[493]

Kinetic studies have been reported by Ordonez and co-workers on a model Pd/β-SiC foam catalyst prepared without any support washcoating and applied to the lean methane combustion.[494] Besides demonstrating the excellent catalyst stability without any appreciable activity decrease within 10 h on run, the fitting of their experimental outcomes confirmed that a first-order kinetic model applied well to the process. In the same years, Hayes and collaborators pointed out the importance of heat exchange properties of monoliths employed in the methane oxidation. These authors compared two washcoated monoliths composed of cordierite and silicon carbide, respectively, and considered the effect of layer thickness, monolith length, and GHSV, the latter defined in here as twice the total monolith flow path divided by the inlet velocity for a process operated at 400 K.[495] Their in silico model revealed that for a space velocity typically operating in a natural gas-powered vehicle, the combustion of added methane was able to elevate the reactor temperature to a level

sufficiently high to achieve catalytic combustion of methane. Their simulation unveiled how the higher thermal conductive SiC monolith required about one-half of the added energy to acquire complete methane conversion compared to cordierite (Figure 53).
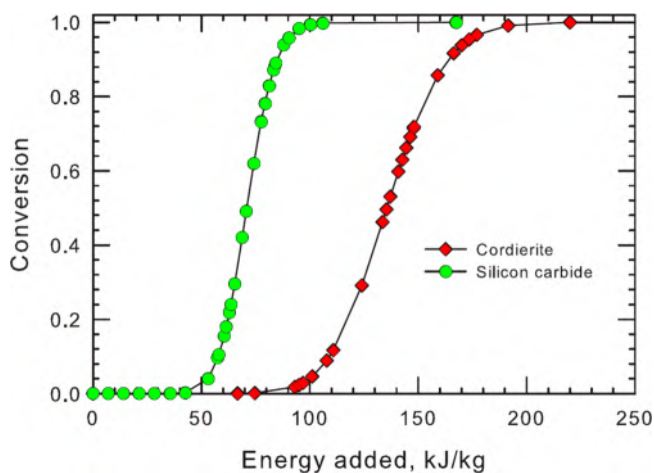
Figure 53. Conversion of methane as a function of heat added to the system for cordierite and SiC monoliths. Monolith sections and lengths were 10 mm and 15 cm, respectively. The inlet velocity was 1.5 m/s, and thus the resulting space time was 0.2 s. Adapted with permission from ref 495. Copyright 2012 Elsevier B.V.

Later, the same Spanish team discussed the performance of a Pd/(β-SiC) foam catalyst in a reverse flow reactor for the lean methane oxidation while comparing different catalyst shapes (e.g. raschig rings, honeycomb monoliths, and foams) of equivalent geometry.[496] Their theoretical simulations and experimental outcomes led these authors to conclude that the foam bed showed better mass and heat transport properties together with a competitive pressure drop with respect to the honeycomb monolith, while being less efficient than the latter for heat storage. Therefore, the use of foam beds was recommended in the catalytic bed at the center of the reactor (where fast mass and heat transfer are required), whereas the honeycomb monolith should be preferably employed in the inert beds, where higher heat storage capacity is required.

The importance of thermal properties of structured supports for the catalytically active phase was recovered later by Specchia and co-workers in a study where these authors evaluated the performance of SiC and zirconia open-cell foam (OCF) supports featured by different porosities as carriers for a 3 wt % Pd/Co$_3$O$_4$ active phase to be used in the lean methane oxidation under variable weight hourly space velocities (WHSVs).[497,498] Their conclusions were that an optimal reactor configuration and heat management along with an appropriate process intensification could be realized by housing a catalytic SiC OCF preferentially at the beginning of the reactor and a catalytic zirconia OCF featured by a lower volumetric heat exchange coefficient, afterward. In this configuration, the superior thermal conductivity of SiC OCF was helpful to retain the heat of reaction for boosting the ignition of the first reacting molecules on the surface of the catalyst, while zirconia OCF boosted the process at higher temperatures.

Kaskel and co-workers have recently reported on a new and versatile synthetic method to the generation of porous SiC
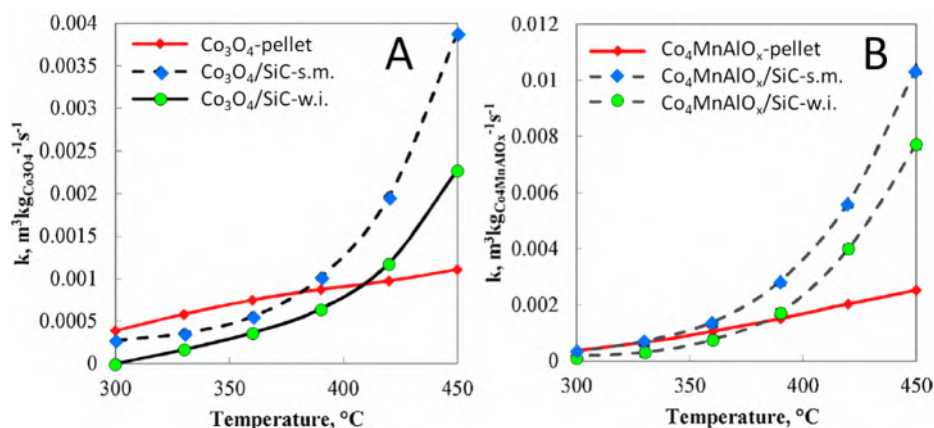
Figure 54. Temperature dependence of a specific kinetic constant for (A) Co_3O_4 deposited on the SiC foam as a catalyst for the nitrous oxide decomposition compared with the metal oxide in its pelletized form and (B) Co_4MnAlO_x deposited on the SiC foam as a catalyst compared with the metal oxide in its pelletized form. s.m. and w.i. stand for suspension and wet impregnation methods. Adapted with permission from ref 504. Copyright 2019 Elsevier BV.

samples with a tailored pore diameter in the mesopore range and containing catalytically active nanoparticles encapsulated in the templating carrier.[499] Their major achievement was demonstrated by the effectiveness of their protocol in the preparation of the CeO_x/SiC catalyst with a rare earth metal oxide content lowered by at least 80 wt % compared to the unsupported active phase and with a reduction of the onset temperature in the methane oxidation as high as 270 K. Moreover, their synthetic route to CeO_x/SiC catalysts combined for the first time the core−shell nanoparticle synthesis with the nanocasting approach for the SiC growth while giving rise to extremely stable catalytically active phases with an unprecedented resistance toward sintering. Such an achievement is extremely relevant in the light of preparing robust catalytic systems suitable to operate highly exo- or endothermic processes including those carried out under extremely harsh temperatures conditions and/or under corrosive environments.[499]

As far as the use of non-noble transition-metal-based catalysts supported on SiC in the process, Hashimoto and Kamiya have proposed an iron-based catalyst on a N-doped silicon carbide network.[500] Starting from the Fe-deposited on plain SiC, its annealing at 900 °C under ammonia atmosphere gave rise to the expected iron composite to be tested as a methane combustion catalyst. Their comparative study between Fe/SiC and Fe/N-SiC unveiled the higher performance of the latter whose improved activity was reasonably ascribed to a more favorable O_2 activation by Fe sites coordinated to N sites of the doped carrier. The authors speculated indeed on the role played by the strong π back-donation from the metal sites to the π^* orbitals of O_2^* activated molecules, thus resulting in a faster combustion acceleration.[500]

3.3.1.5. NO_x Catalytic Abatement on SiC-Based Catalysts. NO_x are among the main pollutants of the atmosphere as they take part in several environmental drawbacks such as the photochemical smog, the acid rain, the ozone layer depletion, and even the global warming caused by N_2O. Besides their environmental impact, they are also at the origin of several health problems once humans meet high concentrations of these gases.[501] The need to face more and more stringent legislation on the control of the air quality has boosted scientists to focus on various new technologies to be engaged

for NO_x removal from exhaust gases. Large efforts have been devoted to NO_x control from their primary sources such as the combustion of fossil fuels in power stations and mobile vehicles up to synthetic methodologies applied in the chemical industry. N_2O is a greenhouse gas which possesses a GWP as high as 310 times that of CO_2.[502] As far as the use of SiC in the catalytic NO_2 decomposition to O_2 and N_2, literature reports tell different stories, very likely dictated by the nature of the metal active phase employed in the process. In a first contribution which appeared in 2015, the German team of Köhler and co-workers compared the catalytic activity of Ru particles supported on various oxide and non-oxide supports for the decomposition process.[503] These authors pointed out the non-innocent role of non-oxide and C-containing networks (AC and SiC) in the process. According to their findings, both AC and SiC (the latter to a lower extent) participated as reducing agents. Indeed, both NO_2 and its decomposition product O_2 are strong oxidizing agents suitable to oxidize under the operative conditions C-containing networks (eqs 35 and 36).

$$2NO_2 + C \rightarrow CO_2 + 2N_2 \tag{35}$$

$$O_2 + C \rightarrow CO_2 \tag{36}$$

$$2NO_2 \rightarrow O_2 + 2N_2 \tag{37}$$

In Ru/SiC, the support oxidation was less evident but still present along with a partial NO_2 decomposition promoted by the Ru particles (eq 37). In addition, whatever the C-containing support employed in the process, the presence of Ru particles lowered considerably the oxidation temperature of C-containing supports.[503]

In a more recent report, Klegova et al. referred to the preparation methods of Co_3O_4 and Co_4MnAlO_x mixed oxides on SiC open-cell foams.[504] Their study focused mainly on important differences on the morphology of metal oxide deposits as a function of the deposition method used (impregnation vs suspension method) and the subsequent effect on their catalytic performance in nitrous oxide decomposition. Irrespective to the deposition method used, metal oxides on SiC foams gave rise to stable catalysts featured with higher specific kinetic constants in the NO_2 decomposition process compared to pelleted metal oxide ones (Co_3O_4 and Co_4MnAlO_x) (Figure 54).
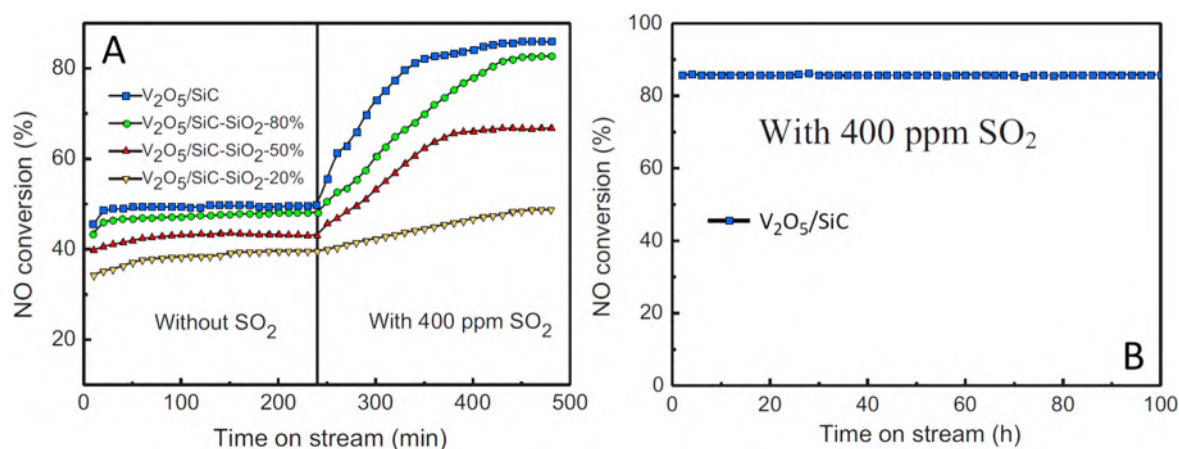
Figure 55. (A) Effect of SO_2 on the deNO$_x$ activity of V_2O_5/SiC/SiO$_2$ catalysts at a different SiC/SiO$_2$ content ratio (from 80 to 20 and with plain SiC). (B) Long-term stability test of the V_2O_5/SiC catalyst in the presence of 400 ppm of SO_2. Adapted with permission from ref 508. Copyright 2016 Elsevier Ltd.
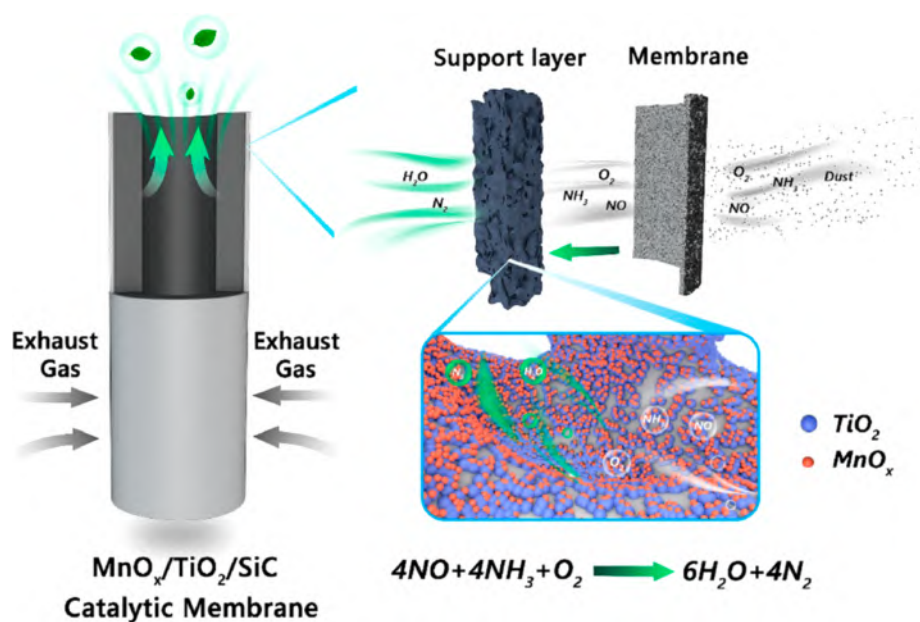
Figure 56. Schematic representation of a MnO$_x$/TiO$_2$/SiC catalytic membrane for the simultaneous NO and dust removal. Figures reproduced with permission from ref 516. Copyright 2020 Elsevier B.V.

Among the technologies applied nowadays to reduce NO$_x$ concentration, the selective catalytic reduction (SCR) in the presence of ammonia and oxygen is one of the most popular and widely investigated mainly to reduce NO$_x$ emission (deNO$_x$) from combustion processes.[505] V_2O_5–WO_3(MoO_3)/ TiO$_2$ is certainly one of the most investigated catalysts for the process.[506] However, this catalytic technology suffers from SO_2 poisoning depending on the operative temperatures applied to deNOx. Indeed, the generation of NH_4HSO_4 at the catalyst surface by reaction of SO_2 with NO$_x$ can progressively inhibit the catalyst performance once processes are operated at temperature below 350 °C. Studies based on the use of V_2O_5 as the active phase for deNO$_x$ catalysts prepared from carbon-containing supports have shed light—once again—on the active role played by the latter.[507] Bai and co-workers have systematically investigated the effect of C content in a series of V_2O_5/SiC/SiO$_2$ catalysts for deNOx under low-temperature conditions and in the presence of SO_2.[508] These authors demonstrated that SO_2 significantly promoted SCR activity

with a NO$_x$ removal efficiency as high as 86% at 250 °C in the presence of 1 wt % V_2O_5/SiC/SiO$_2$ when the carbon content in the support was higher than 15%. Thus, catalysts prepared with a SiC/SiO$_2$ ratio above 50% (Figure 55) or preferably prepared on plain SiC (V_2O_5/SiC) offered the most improvement of catalyst performance and resulted in stability for long-term deNO$_x$ runs. Although the real effect of the support carbon content on the boosting action of SO_2 toward deNO$_x$ remains still unclear, according to these authors, carbon from SiC was supposed to act as a reducing agent for promoting the decomposition of NH_4HSO_4 into SO_2.[508]

As far as high-temperature catalysts for deNO$_x$, Zhang and Dong have demonstrated the significantly higher activity and stability of a heterostructural catalyst prepared by the homogeneous growth of Cu-ZSM-5 zeolite on a silicon carbide (SiC) monolith by means of a one-pot hydrothermal method.[509] These authors pointed out that the excellent thermal conductivity of their carrier along with the effectiveness of the coating procedure described in their
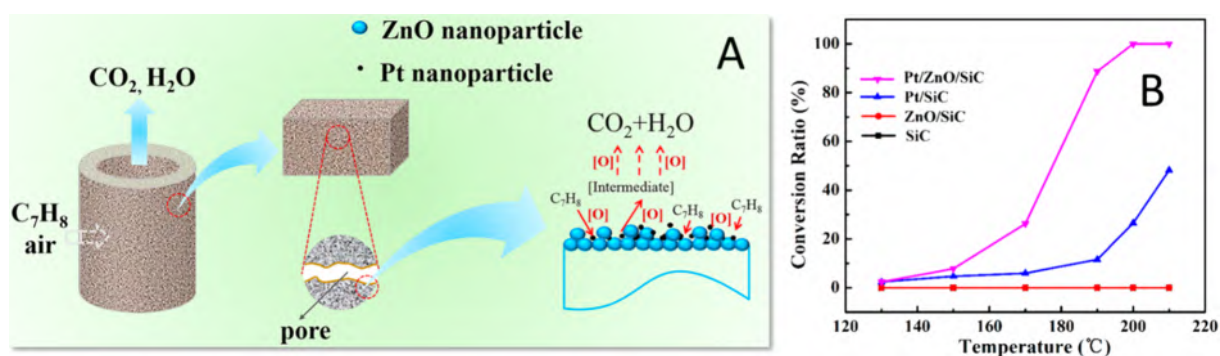
Figure 57. (A) Schematic representation of Pt/ZnO/SiC in the catalytic toluene oxidation. (B) Toluene conversions on various SiC-based filters in comparison. Reaction conditions: 210 °C, 0.72 m/min, toluene: 300 ppm. Adapted with permission from ref 523. Copyright 2017 American Chemical Society.

catalyst formulation offered significantly higher performance in NH₃−SCR at T > 350 °C than those obtained with the plain Cu-ZSM-5 catalyst. In particular, they claimed a NO consumption rate with their structured catalyst up to 7.5 times higher than that measured with the Cu-zeolite.[509]

SiCs are also employed in gas filtration due to their high mechanical strength, good chemical resistance, and excellent dust filtration efficiency.[510,511] Depending on the nature of exhaust gases sources responsible for NO_x emission in the atmosphere, these pollutants can be frequently accompanied by large quantities of dust.[512] Amal, Scott, and Choi first reported on the development of a Pt-promoted catalytic filter based on a V_2O_5−WO_3 deNO$_x$ catalyst supported on a TiO₂-coated SiC network by vacuum aided-dip coating (Pt−V_2O_5−WO_3−TiO_2/SiC).[513,514] The promotional effect played by the addition of Pt allowed these authors to reduce the working temperature of the catalytic filter from 280 to 330 °C to 180−230 °C while ensuring it with an optimal deNO$_x$ performance. Part of this team reported a few years later on the optimization of the catalytic coating deposition and V_2O_5 content in a Pt-free, V_2O_5−WO_3−TiO_2/SiC catalytic deNO$_x$ filter.[515] They demonstrated that the active-phase grinding by ball milling treatment reduced the particle size and improved the catalyst surface area thus improving its ultimate performance in the process. They also showed that a 6 wt % V_2O_5 content allowed getting a >99% NO conversion already at a reaction temperature as low as 240 °C.

Following a similar filtering strategy, Zhong and co-workers recently described an effective approach for the preparation of catalytic membranes for denitration and dust removal under low-temperature operational conditions.[516] They have proposed a novel MnO_x/TiO_2/SiC catalytic membrane prepared by coating the SiC support with TiO_2 aerogel as the transition phase between SiC and MnO_x as the active phase for the process. They demonstrated that TiO_2 increased more than twice the MnO_x loading capacity without affecting in a significant manner the gas permeance of the SiC membrane (Figure 56). The MnO_x/TiO_2/SiC composite exhibited excellent filtration performance with the dust rejection rate exceeding 99.97% and the NO conversion rate above 80% for a deNO$_x$ configuration operated in the 120−180 °C temperature range. In addition, the filtration assembly was found to maintain remarkable stability in a simulation environment with NO conversion rates ranking close to 90% within 65 h.[516]

3.3.1.6. VOC Catalytic Treatment on SiC-Based Catalysts. Volatile organic compounds (VOCs) are typical air pollutants

featured by a boiling point at ambient conditions comprised between 50 and 260 °C.[517] Besides their environmental impact, the toxic and carcinogenic nature of many VOCs threaten human health particularly in the developing countries where industrialization proceeds faster. The long-time human body exposure to VOC pollutants can be responsible in many cases of serious and irreversible damage. Therefore, the research community has focused for a long time on developing practical remediation tools and catalytic technologies to effectively remove VOCs. Nowadays, more than 300 groups of VOCs can be listed in the family of industrial volatile pollutants among which alkanes, alcohols, ketones, aldehydes, aromatics, halogenated hydrocarbons, and S/N-containing compounds are the most common.[518]

In a seminal contribution, the French team of Ledoux and co-workers has reported on the chemical inertness of silicon carbide supports in the preparation of noble metal-based oxidation/reduction catalysts to be employed for the simultaneous treatment of classical pollutants from automobile exhausts such as carbon monoxide (CO), hydrocarbons (HCs), and nitrogen oxides (NO_x).[519] In their pioneering HR-TEM study, the authors investigated the structural properties of Pt−Rh catalysts supported on Ce-doped SiC networks, and most of their conclusions have been recovered later in papers by other research teams active in the field. In particular, they demonstrated that noble metals deposited at the SiC surface did not undergo any apparent structural modifications. In this way, the noble metal active phase and the support can be easily recovered and reused upon simple acid washing of the composite. On the other hand, the direct evidence for strong noble metal associations with the cerium oxide interface in Ce-doped SiC supports was unambiguously pointed out. According to their conclusions, such an interface was directly engaged in all main oxidation and reduction processes. Accordingly, cerium oxide was supposed to easily change its oxidation state (Ce^{4+}/Ce^{3+}), while the noble metal acts as a donor or acceptor of electrons. The formation of an active interface or a buffer oxygen layer for selected oxidation processes was therefore directly related to the improved catalytic performance of these noble metal/ceria composites.[519]

In recent years, a Chinese team has reported on the remarkable adsorption performance of the odorous and volatile mercaptan CH_3SH by a hierarchical macro-, meso-, and microporous adsorber prepared by sludge-derived activated carbons coated on a silicon carbide foam.[520] These authors

proposed a simple and one-step pore-forming strategy based on the combination of the macroporous SiC network with hexadecanol micelles and $ZnCl_2$ as pore-forming agents for the generation of meso- and micropores in the sludge-derived carbon network, respectively. While the microporous SiC skeleton of the foam and mesopores formed by hexadecanol micelles contributed to the adsorbate mobility, micropores formed by $ZnCl_2$ were supposed to function as mercaptan capture sites. As an additional step forward, the same team has proposed the same 3D hierarchical network to prepare a Fenton-like catalyst (FeK-promoted) for the methyl mercaptan oxidation to sulfate.[521] Fenton-like heterogeneous catalysts are a branch of advanced oxidation processes (AOPs) applied to VOC removal as well as to the treatment of waste waters. The reaction mechanism of these AOP processes is based on the generation of ·OH radicals suitable for oxidizing a wide range of organic pollutants, including S-VOCs to SO_4^{2-}.[522] The KOH activated Fenton-like 3D porous catalyst proposed by Xia and He (SC_{FeK}-SiC) showed excellent decomposition performance of CH_3SH with its almost complete oxidation to sulfate using hydrogen peroxide (H_2O_2) as oxidant under ambient conditions.[521]

Zhong and Xing have successfully designed and prepared a Pt/ZnO/SiC filter for the catalytic VOC abatement by means of a sol−gel ZnO-coated silicon carbide filter followed by Pt NP decoration using a simple impregnation method.[523] These authors demonstrated the effectiveness of their composite for the catalytic oxidation of a probe volatile such as toluene, getting quantitative conversions of the pollutant in a remarkably stable filtering setup operated at a filtration velocity of 0.72 m/min for 240 h at 210 °C and in the presence of 300 ppm of toluene. They also pointed out the synergistic action between ZnO-coating and Pt NPs in the process (Figure 57A). Similarly to what was previously reported by Ledoux et al.,[519] such a synergistic action was claimed to improve the oxygen transfer significantly hence fostering the catalytic performance of the Pt/ZnO/SiC filter composite by 43% compared to that of its simplest Pt/SiC counterpart (Figure 57B).[523]

The existence of a cooperative synergistic action between metal oxide pairs in CO and ethene total oxidation was also claimed by Piumetti et al. while studying the catalytic performance of cerium−copper oxide catalysts in the form of powders deposited on silicon carbide monoliths.[524] It was observed that catalysts with CuO_x clusters interacting with CeO_2 were particularly effective for both the oxidation reactions, leading to higher activities because of an easier catalyst surface reducibility along with its higher defective structural nature (oxygen defect vacancies). In the same years, Bernard and co-workers proposed the use of a mixed oxides and metallic-phase membrane ($CeO_2−Fe_2O_3−Pt$/SiC) as an *in situ* prepared composite coating of a diesel particulate filter (DPF), using allylhydridopolycarbosilane (AHPCS) as precursor of the SiC network.[525] They successfully tested the performance of their catalytic filter in the CO and hydrocarbons oxidation as well as in soot combustion hence combining at the same time filtration efficiency, durability, and catalytic activity.

3.3.2. Treatment of Organic Water Pollutants.
Due to the tightening of environmental regulations and shrinking of global water resources, the need for innovative and effective solutions to treat and manage wastewaters is becoming one of the most urgent matters of our modern society. Dissolved gases and volatile organic compounds (VOCs), including

polycyclic aromatic hydrocarbons (PAHs) and phenols, are commonly available in industrial waters from the oil/gas production as well as from other manufacturing activities. Therefore, the development of innovative technologies— mostly falling in the class of the so-called Advanced Oxidation Processes (AOPs)—for the complete mineralization of these toxic and biorecalcitrant pollutants has been a matter of interest from both academia and industry for a long time.

As far as the use of SiC in this further branch of environmental catalysis is concerned, the first contribution which appeared in the literature is due to the USA team of Atwater et al., who proposed to improve the resilience of a highly active bimetallic platinum−ruthenium catalyst on AC (RP-121),[526] employed for the deep oxidation of organic pollutants, by means of a silicon carbide coating[527] upon reaction with gaseous silicon monoxide under an inert carrier gas stream.[528,529] They clearly demonstrated that the conversion of surface regions of AC support into β-SiC increased significantly the catalyst resistance to oxidation by O_2-saturated water under the operative conditions. Remarkably, the β-SiC coating was operated on the AC-based catalyst before and after impregnation with the bimetallic noble metal mixture. In spite of a reduction of the SiC-coated catalyst surface areas, their oxidation rate constants in the oxidation of an aqueous acetic acid solution were comparable irrespective to the following β-SiC coating sequence and significantly higher than that measured for the uncoated RP-121 catalyst.[527]

In recent years, microwave (MW) irradiation has been successfully employed in a series of SiC-supported catalysts for the treatment and decomposition of various cyclic pollutants and aromatic polycyclic dyes in water. Indeed, the ability of SiC matrix to adsorb and convert electromagnetic microwaves into heat acting as a responsive susceptor has improved the decomposition performance of a series of transition-metal-based catalysts applied as effective water remediation tools. Besides offering higher heating rates compared to a more traditional heating setup, MW irradiation exhibits more selective and volumetric heating properties that have particularly attracted the interest of researchers engaged in the development of AOPs in wastewater treatment. In particular, the ability of SiC supports to absorb MW and promote the generation of local temperature gradients at their surface (hotspots)[530] is conventionally claimed to foster O_2 activation, thus favoring the generation of reactive oxygen species (ROS; *i.e.* ·OH and $·O_2^-$) necessary for the mineralization process to occur.

Yang and co-workers have demonstrated the most rapid and effective degradation operated by the magnetic $MgFe_2O_4$−SiC catalyst with respect to its SiC-free counterpart in a microwave heated batch reactor for the treatment of a model of azo dye pollutant.[531] A similar SiC-supported mixed-oxide catalyst supported on the SiC foam ($CoFe_2O_4$−SiC) was proposed by Mao and co-workers as an effective and rapid degradation system for the fixed-bed treatment water flows contaminated with malachite green (MG) a silk, leather, and paper dye with a relatively high degree of toxicity.[532] Chen and Wang reported on the improved degradation efficiency of Norfloxacin (NOR)—a common antibiotic present in wastewater effluents from the aquaculture industry and livestock—[533] and oxidation of As^{3+} to arsenate[534] (As^{5+}) by a MW-heated/activated Fe/ SiC catalyst. They have also demonstrated the improved degradation efficiency of *p*-nitrophenol (PNP) by a SiC-supported Cu catalyst compared to a Cu catalyst supported on

the less thermal conductive and less MW-responsive Attapulgite (ATP),[535] a hydrous magnesium–aluminum silicate clay. Shen and co-workers have finally made use of a similar Cu/SiC catalyst under MW-assisted heating for the phenol degradation using either H_2O_2 and $Na_2S_2O_8$ as the ROS source for the degradation process,[536] showing for the persulfate a markedly higher production of free radicals and thus a higher pollutant degradation efficiency.

Other AOPs, mainly based on the use of H_2O_2 which is conventionally considered as an environmentally friendly agent, have been developed from hierarchically structured reactors based on robust, high surface-to-volume, and open-cell SiC foam networks suitable for providing the ideal hydrodynamic and pollutant resident time as to acquire optimal performance in the catalytic wet peroxide oxidation (CWPO)[537] and good longevity to systems operating under flow conditions.

Hardacre, Yan, and Fan have recently described the preparation of a hierarchical Fe-ZSM-5/SiC foam catalyst for the phenol CWPO under flow conditions.[538] They proved the excellent hydrodynamics of their structured reactor for the process along with its relatively high stability and the quantitative phenol conversion per long oxidation tests (up to 24 h). At odds with a very convenient CWPO configuration with relatively high TOC (total organic carbon) rates, Fe-leaching from the SiC-supported Fe-ZSM-5 zeolites has led these authors to propose an additional strategy to the assembly of Fe-active sites in the zeolitic coating of the SiC foam, thus mitigating the catalyst deactivation on runs.[539]

With a conceptually new vision to the design and synthesis of SiC-based structured reactors, the Spanish team of Quintanilla and Belmonte has described the preparation of 3D Fe/SiC monoliths using a three-dimensional printing technique.[540] They demonstrated the feasibility of the robocasting method for fabricating robust Fe/SiC monoliths to be employed as catalysts in the CWPO. To this aim, they made use of pseudoplastic Fe-doped SiC inks as precursors of the ceramic scaffold and tuned its density (porosity) as well as the access of reactants to the catalytically active Fe-sites by changing its final thermal treatment. They found that increasing temperature treatments decreased the SiC porosity of the printed structure, lowered the accessibility of reactants to Fe sites, but improved the catalyst mechanical strength and leaching resistance. This innovative finding to the fabrication of Fe/SiC monoliths combines the high catalytic activity and efficiency of the structured catalyst in the H_2O_2 decomposition along with a long-term stability of the system on stream (up to 350 h). Moreover, the robocasting is presented as a valuable one-step process for the development of metal-based catalysts with suitable and tunable morphology for the scaling-up of structured reactors to be applied in CWPO.[540]

SiC properties, such as its resistance to high temperatures, radiation, oxidation, and corrosion along with its low-thermal expansion rate, its good thermal conductivity, and excellent mechanical strength, make it a highly desirable carrier for the preparation of catalysts featuring with specific requirements. In particular, the use of this carrier in the form of a polytetrafluoroethylene (PTFE)-coated, open-cell foam composite has been successfully employed as a hydrophobic carrier for Pt NPs to be engaged in the water detritiation (WD) via a liquid-phase catalytic exchange process (LPCE).[541] The latter relies on the use of a hydrophobic catalyst suitable to repel water while permitting gaseous reactants and products to move

toward and from the catalyst active centers. With a 3-fold PTFE-coated SiC foam decorated with Pt NPs (Pt/PTFE/SiC foam), Wang and co-workers demonstrated that their composite had a sufficient hydrophobic character and an appropriate morphology to satisfy the requirements of a catalyst for water detritiation via the gas–liquid isotopic exchange reaction.[541]

3.4. Electrochemical Processes

3.4.1. Processes for Fuel Cell Technology.
Energy storage and conversion is a key and challenging issue of our modern society, and all related technologies include an important and timely field of research that ideally covers the energy production to the energy consumption.[542] At odds with more traditional and unsustainable fossil fuel resources, fuel cell technology has rapidly gained the attention of the research community because of its capacity to efficiently convert an oxidant and chemical energy accumulated in a fuel directly into DC electricity with heat and water as the unique byproducts and without involving any moving mechanical part.[543] Limited reserves of traditional fossil fuels along with serious pollution problems caused by their overuse have made the development of alternative and greener energy solutions one of the main and highly interdisciplinary research subjects. Although fuel cell technology is certainly out of the scope of this review paper, there is little doubt that researchers have devoted large efforts in the last decades for discovering new catalytic materials, electrodes, membranes, and sustainable manufacturing methods to enhance fuel cell performance, simplify their components, and make easier the commercialization of this technology. Up to date, commercialized fuel cells fall into three technologies mainly the polymer electrolyte membrane fuel cells (PEMFCs),[544] solid oxide fuel cells (SOFCs),[545] and direct methanol fuel cells (DMFCs).[546] The following subchapters will focus on specific aspects and electrochemical processes where the use of SiC has represented a technological step forward for the practical and efficient exploitation of this technology.

3.4.1.1. SiC-Based Electrocatalyst Supports for Improved Fuel Cells (FCs) and Membrane Electrode Assembly Performance. Attempts to employ silicon carbide networks in fuel cell devices have answered to the need for developing stable catalyst supports suitable to operate under chemical and electrochemical hostile and oxidant environments as to enhance the catalyst stability, its performance, and lifetime. This fundamental aspect was pioneered by a Japanese team who first commented on the need for using an acid resistant support for noble metal nanoparticles in place of the classical carbon black.[547] Indeed, the progressive corrosion of carbon supports in strong acid environments was claimed as the main reason for the electrocatalyst activity loss in the first fuel cell and semicell prototypes. Carbon corrosion caused the aggregation of the noble metal NPs with the subsequent irreversible decrease of their electrochemical surface area (ECSA).[548] Moreover, noble metal-based catalysts can accelerate the rate of carbon corrosion to form CO_2, which may cause permanent carbon loss, a loss of catalyst activity, and even a structural collapse of the electrode.[549,550] Anyhow, the first SiC-based electrocatalysts have seen the use of carbon-mixed Pt/SiC composites as to ensure the necessary electrical conductivity to the samples for their use in electrocatalytic transformations. The addition of carbon to a SiC-supported catalyst was conventionally used to compensate the relatively
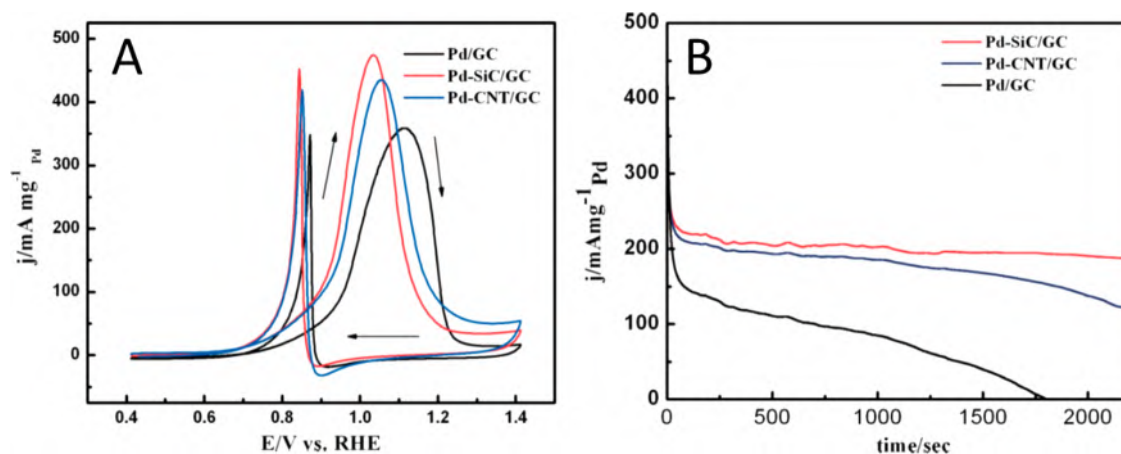
Figure 58. (A) CV tests on Pd-SiC NWs/GC, Pd-CNT/GC, and Pd/GC recorded at a potential scan rate of 50 mV s^{-1} in 0.1 M KOH added to a 0.5 M methanol solution. (B) Current density decay as a function of time on run for the three electrocatalysts in comparison. Adapted with permission from ref 560. Copyright 2011 Wiley-VCH.

low or non-electrical conductivity of the supports.[547,548] Cyclic voltammetry accelerated durability tests (ADTs) conducted in 0.5 M H_2SO_4 as an electrolyte and combined with high-resolution electron microscopy (HRTEM) studies have unambiguously showed the improved stability of the carbon-mixed Pt/SiC electrocatalysts (Pt/SiC/C) compared to the Pt/C counterpart in the face of a similar electrochemical performance of the two systems in comparison. After cycling the catalysts for 4000 runs, only 8.9% of the initial ECSA remained for Pt/C, whereas that on Pt/SiC/C was up to 22.5% of its pristine value.[548]

In the same years, the Chinese team of Niu et al. described the synthesis and use of Pt-decorated (50 wt %) macroscopic SiC nanowires (SiCNWs) as both a H_2 sensor and an effective and stable electrocatalyst for the methanol oxidation under acidic environments.[551] Whatever the application of their composite, these authors reaffirmed the high resistance to oxidation corrosion of their catalyst hence emphasizing its versatility for the development of robust and durable fuel cell devices.

A similar leitmotif and analogous conclusions go across most of the papers which appeared in the past decade and used these non-oxide carriers for electrocatalyst preparation.

Wang and co-workers reported on the synthesis of both Ti-coated SiC powders[552] and core−shell SiC@C structural composites[553] as supports for Pt NPs prepared by the microwave-assisted reduction method. Their final composites (Pt−Ti/SiC and Pt/SiC@C) exhibited improved electro-catalytic performance in the methanol-oxidation reaction (MOR) and oxygen reduction reaction (ORR) of a DMFC as well as higher stability compared to the same active phase deposited on plain SiC.[552,553] As for Pt−Ti/SiC, the authors ascribed the improved performance of their composite to a highly favorable interaction between the metallic Ti-coating and Pt-NPs that ensured a higher and homogeneous active-phase dispersion compared to the plain SiC support. In addition, the evidence for strong Ti-SiC interface interactions (i.e. the presence of Ti−Si and Ti−C bonds) conferred higher stability to the Ti-coated nano-SiC support.[552] Similarly, these authors attributed the improved performance and stability of their core−shell composite (Pt/SiC@C) to the higher affinity of the more electrically conductive carbon shell toward Pt NPs,

with the SiC core always providing a higher stability to the composite under acidic environments.[553]

SiC-supported Pt catalysts were also reported by the Danish team of Morgen and Andersen who described the synthesis of SiC nanocrystals and their homogeneous decoration with Pt NPs as robust and efficient electrocatalysts for PEMFCs.[554,555] These authors described first the higher performance and stability of their Pt/SiC composites compared to classically C-based electrocatalysts of the *state of the art*.[554] In more recent years, they also succeeded in the application of their SiC-based composite for the preparation of low-temperature PEM fuel cell electrodes and membrane electrode assemblies (MEAs).[555] Additional studies conducted on spent Pt/SiC electrocatalysts from PEMFCs confirmed the improved electrochemical stability of platinized silicon carbides over more common platinized active carbons.[556,557]

The Spanish team of Lobato and co-workers studied the stability of commercially available titanium/SiC composites (SiCTiC with a Ti content of 13.89%; SiC/TiC = 90:10 mol % approx.) as supports for Pt NPs (40 wt %) to be employed in high-temperature PEMFCs.[558,559] The authors' conclusions pointed out once again the superior stability of their 40 wt % Pt/SiCTiC compared to Pt catalysts supported on carbona-ceous materials. In particular, harsh electrolytic conditions (hot 2 M H_3PO_4) unveiled more appreciable ECSA losses for all carbon-based catalysts compared to the binary carbide support. Finally, these authors' conclusions closely meet those previously reported by Wang et al.[552] particularly for the non-innocent role played by the support (SiCTiC) in terms of active-phase dispersion and active-phase/support interac-tion.[558,559]

3.4.1.2. SiC-Supported Electrocatalysts in Semicell Oxida-tive Processes. The Chinese team of Guo and co-workers has reported on an electrochemical preparation method to acquire highly dispersed Pd NPs on SiC nanowires (SiC NWs) and their successful use in the electrochemical methanol oxidation in alkaline environments. In this way, the authors demon-strated the versatility of SiC NWs as an ideal support for highly dispersed and small sized noble metal NPs to be employed at an anode of a classical direct alcohol fuel cell.[560] As Figure 58A shows, cyclic voltammetry (CV) tests carried out in 0.1 M KOH solution in the presence of methanol (0.5 M) on Pd-SiC NWs showed its superior electrocatalytic performance (1.03 V
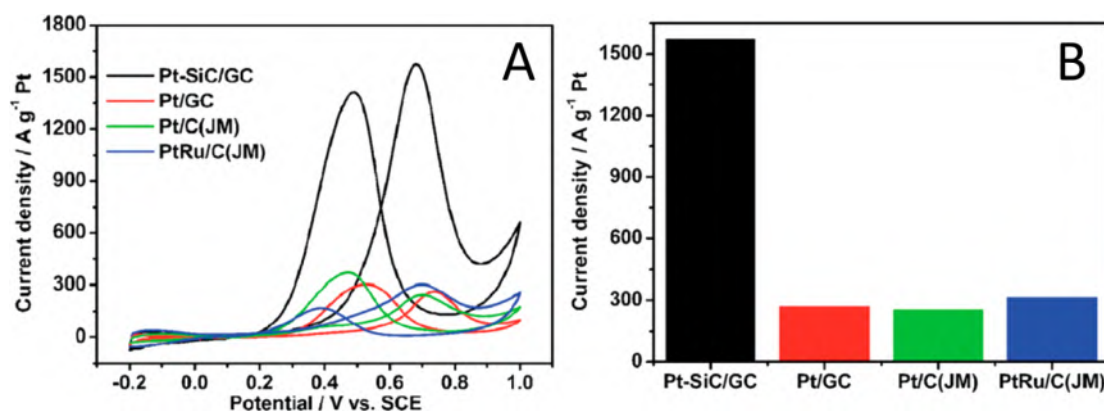
Figure 59. (A) CV curves of Pt-SiC/GC, Pt/GC, Pt/C(JM), and PtRu/C(JM) catalysts in the 0.5 M H_2SO_4 + 0.5 M CH_3OH electrolyte. (B) Mass ratio activity calculated on CVs in A. Adapted with permission from ref 566. Copyright 2015 The Royal Society of Chemistry.

vs RHE) compared with Pd-CNT (1.05 V vs RHE) and plain Pd deposited on the glassy-carbon (GC) electrode (1.11 V vs RHE). Moreover, the current density at the Pd-SiC NWs/GC electrode was systematically higher than that measured on the Pd-CNT/GC electrode, and it was ca. 45% (500 s) higher than that on the Pd/GC electrode when the electro-oxidation process reached the steady state (Figure 58B). Finally, Pd-SiC NWs/GC showed superior stability in the process without any fouling effect in the time frame, hence indicating its improved tolerance to deactivation/poisoning phenomena.

Dai and Chen came to similar conclusions on an independent research paper where highly and uniformly dispersed Pd NPs supported on silicon carbide were straightforwardly synthesized and applied with success to the electro-oxidation of alcohols with different lengths of carbon chains.[561] Their study confirmed the excellent performance of these composites in the process by presenting nanocomposite films featuring very good stability, notable electroreduction peak currents, low anodic oxidation potential, and convenient operational conditions.

Pt-based SiC-supported electrocatalysts engaged in alcohol oxidation have attracted the interest of several research team due to their superior performance compared to electrocatalysts of the same type but supported on classical conductive carbon networks. Fang and co-workers reported on the superior performance and CO tolerance of their 5 wt % Pt/SiC electrocatalyst in the ethanol electro-oxidation, compared to its Pt/C counterpart.[562] In the same years, Chen et al. described an elegant approach for the preparation of a SiC hetero-architecture formed by growing edge-oriented SiC nanowalls on a Si substrate, followed by a graphitization step as to acquire sheathed SiC matrices by few-layer strained graphene layers.[563] Their composites decorated with Pt NPs showed remarkably high catalytic activity, low onset potential, and high CO poisoning tolerance once employed as methanol electro-oxidation catalysts. The observed superior performance in the process was ascribed to the good dispersion and small size of Pt NPs as well as by enhanced catalyst−support interactions induced by surface strain of graphene.

Some years later the group of Guo described an interesting step forward in the preparation of Pt-based SiC composites for the electrochemical alcohol oxidation in acidic media. They demonstrated the ability of boron-doped SiC networks (Pt/$B_{0.1}$SiC) to host highly dispersed and small Pt NPs compared to related Pt-based catalysts dispersed on plain SiC networks.[564] The authors showed that boron atoms incorporated

into the SiC lattice increased the material electrical conductivity while ensuring a higher and homogeneous Pt NP dispersion all over the carrier surface. Overall, their study highlighted the beneficial effects coming from the higher electrical conductivity of the as-prepared composites as well as the improved electrochemical performance of the composites due to the higher electrochemical surface area (ECSA) of their active phase. The same group recently reported on the alcohol electrooxidation activity of Pt NPs deposited on a silicon carbide encapsulated graphite (SiC/EG) composite support.[565] A comparison with commercial Pt/C unveiled better activity and durability of Pt/SiC/EG as well as higher electrochemical active surface area (ECSA) and CO poison tolerance. It was demonstrated that the incorporation of EG on SiC improved remarkably the carrier electrical conductivity while silicon carbide ensures high chemical and thermal stability. Finally, the porous structure of the SiC/EG network was claimed to favor a uniform Pt NP distribution thus enhancing the electrocatalytic activity.

Fu and co-workers have developed a novel and facile vapor deposition strategy to synthesize nanocomposites made of 17 nm SiC nanoparticles uniformly dispersed on graphitic carbon nanosheets (denoted as SiC/GC). Their protocol was successfully exploited in the preparation of Pt-decorated composites (10 wt % Pt-SiC/GC) exhibiting larger ECSA (147.1 m^2 g^{-1} for Pt-SiC/GC vs 61.9, 54.8, and 63.7 m^2 g^{-1} for Pt/GC, Pt/C(JM) and PtRu/C(JM), respectively), better stability, and superior CO stripping compared to Pt/C catalysts of the *state of the art*.[566] Remarkably, their Pt composite showed performance toward methanol electro-oxidation of 1585.3 A g^{-1} that was about 6.2 and 5.0 times higher than that observed with the commercial 20 wt % Pt/C (JM) and 30 wt % PtRu/C (JM) catalysts, respectively (Figure 59).

An interesting CNT-Ni/SiC composite was presented by the same authors as an effective and noble metal-free 3D hierarchically organized catalyst for the electrochemical methanol oxidation.[567] They proposed the growth of NiO flakes on SiC matrices to be converted *in situ* into Ni NPs by methane pyrolysis that act in turn as catalysts for the simultaneous growth (at the SiC surface) of Ni NP-decorated carbon nanotubes. The excellent electrochemical performance measured in the methanol oxidation with their noble metal-free 3D electrocatalyst was attributed to the uniform distribution and anchoring of Ni nanoparticles along with the good electrical conductivity of the CNTs/SiC composite.[567]
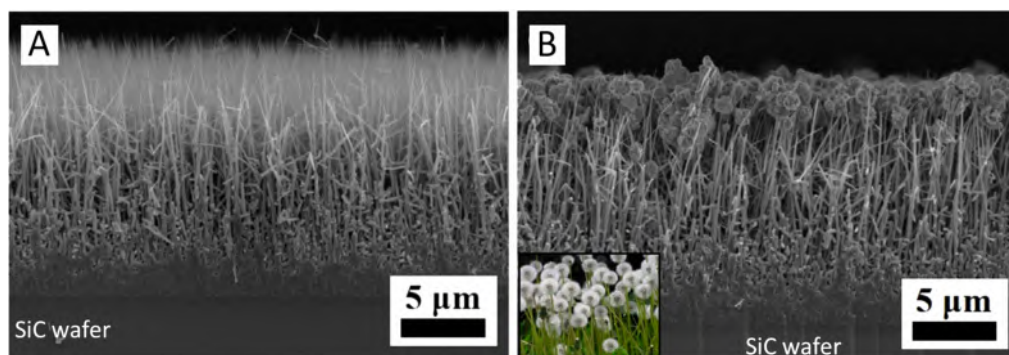
Figure 60. Scanning electron microscopy of (A) a cross section of the SiC wafer decorated with vertically aligned SiC nanowires (SiC NWs) and (B) a cross section of the VA SiC NWs on the SiC wafer after their Co_3O_4 functionalization. Adapted with permission from ref 571. Copyright 2017 Elsevier Ltd.

Water electrolysis is a fundamental electrochemical process where electrical energy is the driving force for chemical reactions: the hydrogen evolution reaction, HER (at the negatively charged cathode) and oxygen evolution reaction, OER (at the positively charged anode). The stoichiometry of the reaction is two volumes of hydrogen per one volume of oxygen. Pioneering works on water electrolysis were essentially based on acidic water solutions. Nowadays the new trend is focused on the use of alkaline electrolytes where cheaper electrocatalysts can be prepared, hence avoiding the use of costly materials and active phases necessary for surviving in more aggressive and oxidant acidic environments.[568]

As far as the use of SiC in electrocatalysts for water splitting is concerned, Nikiforov and co-workers first introduced the use of refractory SiC materials as supports for the active OER catalyst IrO_2 to be operated in the presence of phosphoric acid-containing electrolytes.[569] In spite of the poor electrical conduction of SiC, these authors demonstrated the existence of a positive support/IrO_2 interaction that allowed getting improved electrocatalytic performance with a lower IrO_2 content (80−90 wt %) supported on SiC compared to 100 wt % of unsupported IrO_2.[569] Because iridium is both expensive and scarce, its reduction at the anode of a water electrolyzer along with the choice of a support showing a good compromise between chemical stability and electronic conductivity (*i.e.* SiC) represented an important step forward toward the improvement of this catalytic technology also for other research teams.[570]

More recently, Maboudian et al. have reported on the surface engineering of a SiC wafer for the Ni-catalyzed CVD growth of vertically aligned SiC nanowires (SiC-NWs) and their successive electrodeposition coating with OER-active Co_3O_4 nanoclusters (on the top) and thin layers (on the sidewalls) to be employed as electrocatalysts under alkaline environments (Figure 60A).[571] Although SiC-NWs showed poor electrocatalytic activity, the Co_3O_4-functionalized material exhibited an impressively high activity in OER, much higher than that of the Co_3O_4-functionalized SiC electrode. Indeed, NW arrays acted as strong backing materials to withstand the vigorous OER while providing high surface area for Co_3O_4 and ensuring high interfacial contact between the electrode and electrolyte.[571]

3.4.1.3. SiC-Supported Electrocatalysts in Semicell Reductive Processes. An *in silico* study by Ganji and co-workers has recently reaffirmed the advantages of SiC networks as Pt supports for electrocatalysts[572] to be employed in one fundamental and kinetically sluggish semireaction of fuel cell technology: the oxygen reduction reaction (ORR).[573] They examined and compared the O_2 adsorption properties of Pt-decorated bidimensional hexagonal SiC supports with other Pt-decorated 2D materials such as graphene and boron nitrides.[572] They found that SiC-based catalysts exhibited a superior stability of the adsorbed Pt atoms together with a relatively weaker O_2 adsorption energy compared to their Pt−$C_{graphene}$ and Pt−BN counterparts. This theoretical study has highlighted the significant benefits raised from the use of SiC as the active-phase support in the process. Indeed, the stronger support-Pt NP interaction reduced the occurrence of the active-phase segregation/aggregation phenomena, while a weaker O_2 adsorption energy on Pt-SiC (−1.619 eV vs −2.840 eV and −2.790 eV of Pt−$C_{graphene}$ and Pt−BN, respectively) ensured an optimal catalyst turnover.

Viswanathan and collaborators came to similar conclusions already in 2008 by studying the electrochemical performance of Pt-based systems on ultrafine SiC supports for ORR.[574] These authors claimed the comparable performance of Pt-SiC catalysts in the process with respect to the commercial Pt/C (E-TEK) catalyst. They stressed the superior stability of the former by investigating the current density-time plots of the two catalytic systems at work and hence revealing the lower degradation activity of Pt/SiC.

A few years later, the Japanese team of Suzuki and co-workers described the preparation of silicon carbide-coated carbon black (SiC/C) as a robust and effective support for Pt NPs to be employed as the ORR electrocatalyst in a perchloric acid ($HClO_4$) solution.[575] They found that a thin (10 nm) SiC coating on carbon black maintained similar electrical and morphological properties of the latter, while improving the support resistance to environmental corrosion often observed for Pt NPs directly deposited on carbonaceous supports.

In the same years, a Chinese team and a Japanese team described independently the preparation of carbon/SiC nanocomposites as robust and durable supports for Pt-based ORR electrocatalysts to be employed in acid electrolyte solutions.[576,577] While the former reported on a prolonged acid-etching of nano-SiC particles for the generation of oxidized carbon shells at the SiC surface (O−C/SiC),[576] the latter described the preparation of ordered mesoporous carbon (OMC)-SiC nanocomposites containing nearly 10 wt % of SiC and featuring high surface areas (568 m^2/g) and well-defined mesopores (2.7 nm).[577] Pt-based electrocatalysts based on O−C/SiC or (OMC)-SiC nanocomposites showed superior
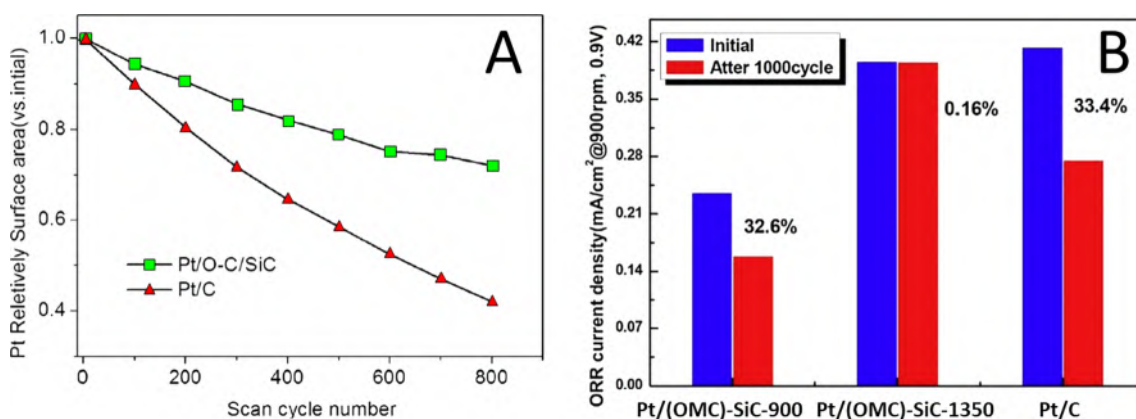
Figure 61. (A) Modification of catalysts' ECSA for Pt/O−C/SiC and Pt/C in ORR operated in a 0.5 M H_2SO_4 solution at a scan rate of 0.05 V/s. Reproduced with permission from ref 576. Copyright 2014 Hydrogen Energy Publications, LLC. (B) ORR current density changes measured on Pt/(OMC)-SiC 900, Pt/(OMC)-SiC-1350, and commercial Pt/C catalysts at 0.9 V and before and after 1000 cycles. Adapted with permission from ref 577. Copyright 2015 Elsevier Ltd.

stability (Figure 61A) and current density retention (Figure 61B) after accelerated durability tests (ADTs) due to the improved stabilization of Pt-NPs on the composites as well as to the inherently higher stability offered by the nano-SiC components.

A thermal annealing of a SiC substrate in vacuum at temperatures comprised between 1300 and 1600 °C has led the Japanese team of Watanabe et al. to generate few-layer graphene deposits on SiC with a thickness varying between 20 and 40 monolayers.[578] The subsequent electron-beam depositions of 1.5 nm-thick island-like Pt layers gave rise to effective and stable ORR electrocatalysts. The authors' conclusions in this work have suggested that an appropriate thickness of a low-defective graphene buffer (more electrically conductive) between the Pt layers and the SiC core was a crucial feature for developing effective Pt/graphene/SiC electrocatalysts for the process.[578]

As far as the development of Pt-free and SiC-based ORR electrocatalysts is concerned, several contributions described the electrochemical properties of metal-free systems, generally based on SiC composites in combination with light-element-doped carbon networks whose catalytic action will be outlined later (see section 4.1.4). Among Pt-free but transition-metal-promoted ORR electrocatalysts, Zang and co-workers described a N-doped amorphous carbon and titanium nitride particles supported on SiC as an excellent and stable ORR catalyst with superior tolerance to alcohol poisoning with respect to the classical Pt-based electrocatalyst.[579] They took advantage of the known inherent ability of N-doped carbon networks to perform ORR efficiently for joining them with the promising PEMFC properties of titanium nitride (TiN) as to acquire a NC-TiN/SiC hybrid with excellent activity and stability in ORR. In a simple two-step path, TiO_2 was deposited on SiC, and the composite underwent heating in the presence of melamine at 1000 °C under N_2 atmosphere. The formation of the NC phase reduced the TiN particles agglomeration while improving the electrical conductivity of the composite for a faster electron transport. The SiC core, with its mechanical strength and resistance under oxidative environments, was finally claimed to improve the catalyst stability.[579]

In the same years, Bao and Wang described the synthesis of a SiC core with a derived N-doped carbon shell (SiC@N−C)

on which iron nanoparticles encapsulated in a N-doped carbon network (Fe@N−C) were properly grown (Fe@N−C/SiC@N−C).[580] Besides the unique features of SiC matrices in ORR, they claimed the key role played by carbon shells on the catalyst durability in the electrocatalytic process. N−C shells prevented acid leaching of the active phase as well as the occurrence of oxidation and agglomeration phenomena of transition-metal NPs. Most importantly, the synergetic effect of N-doping in the carbon of encapsulated iron NPs was found to stimulate and enhance the inherent electrocatalytic activity of the composite.[581] Indeed, the Fe@N−C/SiC@N−C composite showed more positive onset potential (E_{on}) and enhanced limiting current density values (J) compared to the metal-free SiC@N−C and the Fe_3Si/SiC obtained by depositing iron on the plain SiC.[580]

As an additional study on this area of electrocatalysis, the theoretical work of Chen and collaborators has pointed out the positive promotion rising from nickel- or cobalt-doping of model $Si_{60}C_{60}$ nanocages.[582] The DFT investigation has unveiled that their atomic doping with Co or Ni largely reduced the adsorption energies of ORR species compared to the plain SiC cage matrix with a consequent positive catalyst turnover. As a matter of fact, these authors postulated improved ORR performance and detailed the presumed O_2 activation/reduction path on $Ni_1Si_{59}C_{60}$ and $Co_1Si_{59}C_{60}$ with the former resulting in the most active catalyst in the process.[582]

Finally, silicon carbide has been recently exploited also as a suitable support for molybdenum-based electrocatalysts for the hydrogen evolution reaction (HER). Yu et al. prepared a ternary system composed of $Mo_{3+2x}Si_3C_{0.6}$ ($x = 0.9−0.764$) embedded in an *in situ* generated SiC/C matrix. The high chemical inertness of the support together with the formation of a carbon-rich phase (that enhances the material electrical conductivity) significantly improves the charge transfer rate and the overall HER performance in acidic media.[583] More recently, Wang and co-workers developed MoS_2/SiC nanowire (NW) composites for fruitful application in HER.[584] Molybdenum disulfide is recognized as a promising HER catalytic material, but it suffers from low electrical conductivity, low active edge site exposure, and sluggish water dissociation kinetics.[585] On this ground, the coupling of MoS_2 with SiC NWs was found to overcome these limitations creating a
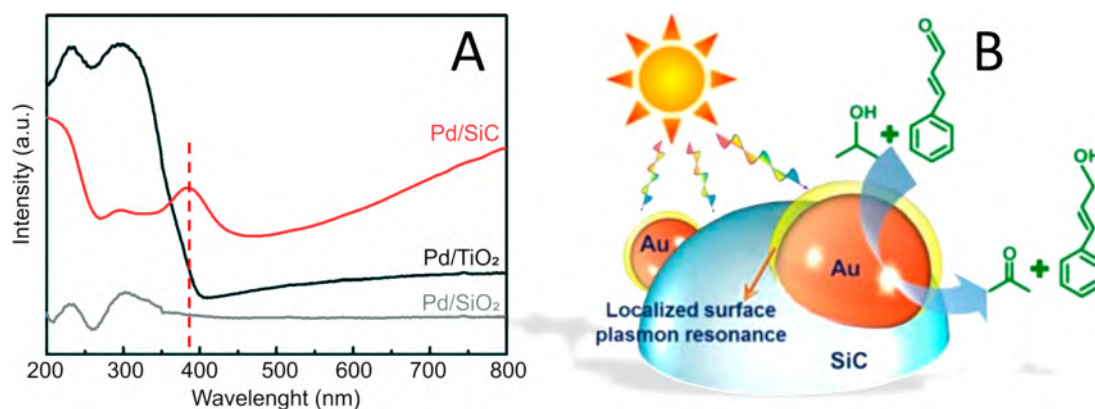
Figure 62. (A) UV−vis spectra of different Pd catalysts in comparison, showing the superior light absorption capacity of a SiC-based catalyst around 400 nm. Adapted with permission from ref 134. Copyright 2014 The Royal Society of Chemistry. (B) Proposed reaction sketch for a visible-light-promoted Au/SiC catalyst in the selective CAL hydrogenation to COL. Adapted with permission from ref 136. Copyright 2016 American Chemical Society.

beneficial synergistic effect and producing an excellent HER catalytic system with improved reaction kinetics (Tafel slope = 55 mV dec^{-1}). Indeed, the introduction of SiC nanocrystals was demonstrated to reduce the energy barrier associated with water dissociation, while the morphology of SiC NWs enhances both active edge sites exposure and charge transport.[584]

3.5. Photochemical Processes

Photocatalysis is receiving much research interest because of its potentialities in tackling many important energy and environmental challenges on a global level and in an economically sustainable manner. Light is an important energy source, and it has been employed in combination with selected semiconductor materials as the driving force of a number of photoinduced processes to be performed. H$_2$ generation,[586] water splitting,[587,588] CO$_2$ reduction,[589,590] environmental remediation,[591,592] and bacterial disinfection[593] are just a selection of the most representative photocatalyzed transformations. Recently, researchers have also introduced light in catalytic organic synthesis in order to promote chemical transformations under milder reaction conditions while avoiding undesired reaction paths.[594] The photocatalytic properties of a given semiconductor are dependent on its electronic structure, consisting of a filled valence band (VB) and an empty conduction band (CB). The energy required for electrons in VB to be promoted to the CB leaving behind a positive hole is called "band gap" (Eg). A photocatalytic process can occur only when all necessary thermodynamic requirements are satisfied. In a very simplified scheme, a photocalytic transformation can occur when electrons in VB are photo excited to its CB under a proper light irradiation with the energies of incident photons that need to be equal or higher than that of the semiconductor's band gap. Photogenerated electrons and holes can recombine quickly or migrate to the surface of the material, where they can induce redox reactions with adsorbed species. Photogenerated electrons in the CB promote reduction reactions when the semiconductor CB edge is more negative than the reduction potential of the adsorbed species. Holes act as oxidant when the VB edge is more positive than the oxidation potential of the adsorbed species.[595] β-SiC is an interesting semiconductor featured by a band gap of about 2.4 eV, which can be effectively employed to absorb visible light. Accordingly, it has

rapidly gained the interest of the scientific community hence growing its relevance in this area of catalysis as well.

The following sections aim at highlighting all main achievements in photocatalytic processes developed up to now and based on this kind of non-oxide semiconductors.

3.5.1. Synthesis of Fine Chemicals. As far as the use of semiconductor SiC matrices in fine chemical synthesis is concerned, the team of Guo and co-workers has decisively contributed to the development of this branch of photocatalysis. They first demonstrated that the use of SiC as the support for palladium NPs significantly fostered the catalyst performance in the hydrogenation of furan derivatives at ambient conditions and under visible-light irradiation.[134] They found that Pd/SiC showed a strong light absorption band around 400 nm wavelength where Pd catalysts supported on classical oxide-based materials exhibited very weak absorption bands (Figure 62A). Most importantly, they postulated that the metal−semiconductor heterojunction generated between metallic Pd NPs and the SiC surface (Mott−Schottky contact)[596] largely contributed to the promotion of the catalytic performance of their composite by fostering the quick transfer of the photogenerated electrons from SiC to Pd nanoparticles. Similarly, the same team referred to the highly efficient (TOF as high as 487 h^{-1}) and selective (>99%) cinnamaldehyde (CAL) hydrogenation to cinnamyl alcohol (COL) using SiC-supported Au NPs as the photocatalyst under visible-light irradiation at 20 °C in the presence of 2-isopropanol as a sacrificial source of active hydrogen (Figure 62B).[136] The authors attributed the excellent performance of the Au/SiC catalyst to its superior light absorption capacity around 400 nm wavelength as well as to the localized surface plasmon resonance effect (LSPR) of Au NPs approximatively located at 520 nm. They claimed the existence of a synergistic effect between the LSPR of Au NPs and the metal−semiconductor heterojunction at the SiC/Au NP interface upon exposure of their catalyst to visible light. In their model, photogenerated electrons migrated to the conduction band of SiC, leading to the formation of slightly positively charged sites on Au NP and electron-rich sites at the Au/SiC interface.

Accordingly, 2-propanol was oxidized on the positively charged Au sites with the generation of active hydrogen that reacted in turn with the C=O bond of CAL activated at the Au/SiC heterojunction to give the corresponding unsaturated alcohol (COL).[136]
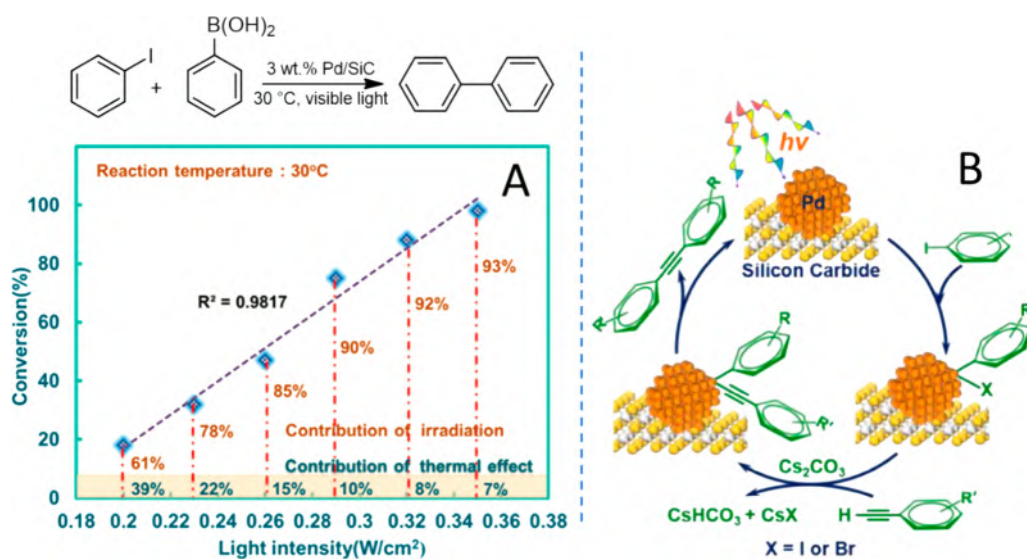
Figure 63. (A) Phenyl iodide conversion in the photocatalytic Suzuki–Miyaura cross-coupling promoted by a 3 wt % Pd/SiC as a function of the irradiation light intensity. Thermal and irradiation contributions to the process have been reported. Adapted with permission from ref 135. Copyright 2015 American Chemical Society (B) Mechanistic sketch for the photocatalytic Sonogashira cross-coupling of aryl halides and phenylacetylene over Pd/SiC. Adapted with permission from ref 137. Copyright 2017 Elsevier BV.

More recently the same team also reported on another challenging hydrogenation process using molecular H_2 and segregated Pd and Au NPs on SiC as a highly effective photocatalytic system for the nitroarenes' hydrogenation to anilines under ambient conditions and visible-light radiation.[139] Their study unveiled the existence of a synergistic effect between Pd and Au NPs on the semiconducting SiC. It was supposed to originate from the plasmonic electron injection of Au and the Pd/SiC heterojunction that changed the surface electronic properties of the semiconductor. Accordingly, hydrogen activated at Pd NPs and spilled over the SiC surface recombined with the N=O bonds of nitroarenes absorbed on SiC giving rise to the corresponding anilines chemoselectively and orthogonally to other reducible functional groups on the same molecule.[139] As a step forward in the nitroarenes' chemoselective hydrogenation to anilines, the Chinese team has recently described the bimetallic Pt_1–Fe_1/SiC photocatalyst for the highly efficient and selective *p*-nitrostyrene hydrogenation to 4-vinylaniline.[597] The introduction of Fe species was found to modify the adsorption way of the substrate on the catalyst active sites, making its vertical alignment (instead of parallel) as the preferential activation mode for the hydrogenation of the nitro group to occur selectively. In addition, the combination of Fe sites with a sacrificial electron donor (triethylamine–TEA) was used to consume the positively charged holes produced at the SiC surface, thus hampering the styrene double bond activation at its surface. As a matter of fact, they acquired a highly efficient and selective photocatalyst for the chemoselective reduction of nitro groups to amino groups also in the presence of easily reducible functionalities (C=C or C=O) on the same molecule.[597]

The SiC capacity to absorb visible-light radiation along with the continuous transfer of photogenerated electrons through the Mott–Schottky heterojunction of Pd/SiC composites has prompted these authors to investigate the ability of their photocatalysts to promote other fundamental transformations at the heart of modern organic synthesis. During the past decade, Guo and collaborators have reported on a series of

highly efficient and selective photocatalysts for the visible-light driven C–C cross-coupling. They demonstrated that the Pd/SiC photocatalyst,[135] eventually decorated with NiO nanodots,[598] was able to catalyze the Suzuki-Miyaura cross-coupling reaction in air at ambient conditions and upon visible-light irradiation. The authors postulated that electron-rich Pd NPs and positively charged holes at the semiconductor surface played different roles in process. While the former fostered the C–X bond cleavage, the latter activated C–B bonds on phenylboronic acids. Notably, they also highlighted the influence of the radiation intensity on the aryl halide conversion. Figure 63A refers to the linear increase of iodobenzene conversion with radiation intensity, using a 3 wt % Pd/SiC photocatalyst in the model cross-coupling reaction with boronic acid. A distinctive contribution to the process efficiency in terms of thermal vs irradiation effects was also presented.[135]

As far as the role of ultrafine NiO doping of the Pd/SiC catalyst is concerned, they found that nanodots favored a spontaneous electron transfer toward Pd NPs.[598] Accordingly, a higher electron density in the Pd sites made easier the activation/cleavage of less reactive aryl halides (*i.e.* Ar–Br or Ar–Cl) in the process, while holes left on the SiC support assisted again the cleavage of C–B bonds.

Following a conceptually similar strategy, these authors have also demonstrated the ability of their Pd/SiC photocatalyst to promote the Sonogashira reaction efficiently and selectively under copper and ligand-free conditions and upon visible-light irradiation (Figure 63B).[137] Once again, Pd NPs electronically enriched by the continuous transfer of photogenerated electrons from the semiconductor facilitated the cleavage of carbon–halogen bonds of aryl halides. Afterward, the final product was achieved by substitution reaction and reductive elimination.

More recently, they have also described SiC-supported Pd_3Cu_1 alloy NPs as a more efficient photocatalyst for the process suitable to operate the new C–C bond-forming reaction under milder and ligand-free operative conditions.[138] In both cases, they found a strong dependence of the process
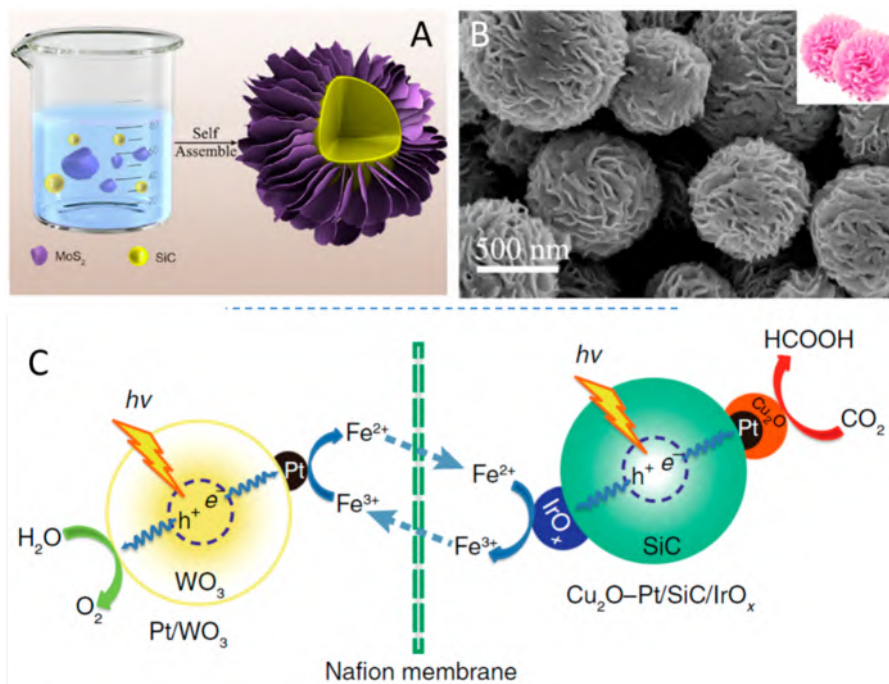
Figure 64. SiC@MoS$_2$ nanoflowers: (A) schematically synthetic process and (B) SEM images of SiC@MoS$_2$ nanoflowers. Adapted with permission from ref 604. Copyright 2018 American Chemical Society. (C) Artificial photocatalytic scheme for the efficient CO$_2$ reduction and O$_2$ evolution reaction at the two photoexcited catalysts operating within distinct reactive chambers separated by a proton exchange membrane. Adapted from ref 605. Springer Nature 2020 under [CC license 4.0] [https://creativecommons.org/licenses/by/4.0/].

rate from the light intensity and wavelength of irradiation light.[137,138]

Pd/SiC composites prepared on hierarchical SiC nanowires have also been proposed as effective photocatalysts for the borylation of aryl halides under mild conditions and upon visible-light irradiation.[599] Once again these authors have shown the potentiality of the photogenerated electrons on SiC and their subsequent transfer to supported metal nanoparticles for promoting the C−X bond cleavage under milder operational conditions compared to thermal protocols.

A photothermal process for alkanes, olefins, and oxygenated compounds generation from syngas (Fischer−Tropsch synthesis−FTS)[250] has finally been described by these authors with a 10 wt % Ru/SiC photocatalyst.[600] They have exploited the transfer of photogenerated electrons from SiC to metal NPs within another highly challenging catalytic transformation. Worthy of note, they unveiled the ability of electron-rich Ru NPs to strongly bind CO under typical FTS operational conditions hence increasing the process selectivity toward long-chain hydrocarbons and decreasing alkyl aldehydes hydrogenation almost to zero. Therefore, photochemically promoted FTS resulted in a higher aldehydes concentration among the oxygenated products in the reaction mixture, with respect to the more common alcohols.[600]

As far as photochemical CO$_2$ valorization processes are concerned, Li and co-workers first described the photocatalytic CO$_2$ reduction to methanol on Cu$_2$O modified β-SiC NPs.[601] Their pioneering work unveiled the superior performance of the Cu$_2$O/SiC composite under visible-light-irradiated conditions with respect to plain SiC or Cu$_2$O catalysts operated under identical conditions.

A few years later, Zhang, Wang, and co-workers reported on an original sol−gel protocol for the preparation of 3D, open mouth β-SiC hollow spheres, and their successful use as a

thermally, chemically stable, and metal-free photocatalyst to be employed under simulated solar light irradiation for the effective CO$_2$ conversion into CH$_4$ and O$_2$ in the presence of pure steam (eq 38).[602]

$$CO_2(g) + 2H_2O(g) \rightarrow CH_4(g) + 2O_2(g) \tag{38}$$
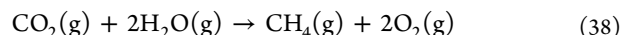
They described the hollow-sphere structure of the semiconductor as a crucial feature to allow multireflections of irradiated light in the interior SiC cavities, thus maximizing the material photocatalytic performance. On the same grounds, they also claimed improved catalyst performance with a stable CH$_4$ evolution when SiC hollow spheres were doped with a 2 wt % of Pt.[602] More recently, Han, Wang, and collaborators have described an intriguing synergistic effect between SiC nanosheets and ultrafine Pt NPs in the deep photoinduced CO$_2$ reduction to CH$_4$.[603] These authors found that ultrafine Pt NPs allowed harvesting photogenerated electrons from the SiC support, fostering an 8e$^-$ reduction path mainly with the subsequent increase of the process selectivity as well as the methane production rate.

In the search of more efficient and selective photocatalysts for carbon capture and utilization (CCU), Zhang, Wang, and Li have described a unique Z-scheme heterojunction between two distinct semiconductors with generation of SiC@MoS$_2$ nanoflowers, obtained by the judicious combination of a 3D SiC semiconductor core with 2D MoS$_2$ perpendicularly fixed petals (Figure 64A,B).[604] SiC@MoS$_2$ has shown excellent photocatalytic performance in the process (eq 38) upon visible-light excitation ($\lambda \geq$ 420 nm), listing important photocatalytic benefits resulting from its unique electronic and morphological features.[604] Recently, these authors have smartly proposed an artificial photosystem based on the rational combination of the Cu$_2$O−Pt/SiC/IrO$_x$ composite for CO$_2$ reduction with a Pt/WO$_3$ H$_2$O oxidation photo-

catalyst.[605] Both semiphotoreactions occurred under visible-light irradiation and took place within distinct reactive chambers separated by a proton exchange membrane (Figure 64C) but relayed each other by the Fe^{3+}/Fe^{2+} redox couple. The high efficiency and durability of this artificial system was ascribed to both the direct Z-scheme electronic structure of $Cu_2O−Pt/SiC/IrO_x$ as well as to the indirect Z-scheme of the spatially separated redox processes.[605]

In a very recent paper, Sun and co-workers exploited 3C-SiC for building an atomic Schottky junction via epitaxial growth of high-quality and uniform graphene layers.[606] The as-prepared material was demonstrated to promote charge carrier separation and transport, while the high conductivity of graphene avoids SiC surface photocorrosion and shuttles charged carriers to the deposited co-catalyst of choice. Different PEC cells were constructed using FeOOH or CoOOH deposited on graphene/SiC as photoanodes coupled with different metallic photocathodes and saturating the cathodic compartment with CO_2. An efficient CO_2 photo-reduction was achieved with all scrutinized cathodic materials showing different product distributions: CH_4 was observed using a Cu cathode, while Zn- or Bi-based electrodes produce mainly CO and HCOOH, respectively. Overall, the study unveiled the versatility of FeOOH- and CoOOH-supported graphene/SiC photoanodes for the photocatlytic production of solar fuels from CO_2.[606]

3.5.2. Photochemical Hydrogen Production.

Water splitting to form hydrogen and oxygen using solar energy in combination with a semiconductor photocatalyst is one of the most studied catalytic processes as it holds the potentiality of producing on a large scale a clean and sustainable energy fuel with a zero-carbon footprint impact. Indeed, the light-driven water splitting is expected to allow solar hydrogen to be highly competitive on cost and environmental impact bases with fossil fuel-derived hydrogen.[607−609] Accordingly, several research efforts have been devoted to select efficient semiconductor materials featuring by a relatively high band gap energy and suitable CB and VB positions.

As a non-oxide semiconductor, bare SiC powder has shown photocatalytic activity for splitting water and producing H_2.[610] However, the activity of bare SiC needs to be greatly promoted. Considerable efforts have been contributed to the development of SiC-based composite photocatalysts for efficient H_2 production. In 2002, the Khan group reported the activity of a p-type SiC (p-SiC) as a photocatode for water splitting in acidic medium.[611] In particular, the USA team investigated the influence of p-SiC surface treatments on the performance of a p-SiC/Pt cell. Herein, they demonstrated that SiC etching by aqua regia-HF followed by electro-deposition of Pt islets positively shifted the photocurrent onset potential because of an improved charge transfer rate at the p-SiC/solution interface. Moreover, the authors showed for the first time the possibility of increasing SiC activity combining a p-SiC photocathode with a stable n-TiO$_2$ photoanode for splitting water in an acidic medium without the need for any external bias potential. In spite of a large band position overlap between the semiconductors and their suitable values with respect to hydrogen and oxygen evolution reaction potentials, their "self driven" system suffered of low efficiency due to high band gap energies and a high recombination rate of photogenerated carriers.[611] In 2009, van Dorp et al. extended the study of 4H-SiC as a photocathode for water splitting in alkaline medium showing that a thin Pd layer electrodeposited

on p-SiC constituted an efficient material for hydrogen production, enhancing the activity of bare SiC.[612] This study contributed to consolidate among the scientific community the idea of SiC as a promising system to photochemically split water even if it was evident that the large band gap of 4H-SiC (3.26 eV) largely hampered its practical exploitation for hydrogen production with solar radiation. Much attention was then devoted to 3C-SiC featuring a band gap ($\approx$2.4 eV) more congenial to solar spectrum. Thus, several strategies have been developed to enhance the unsatisfied activity of bare SiC and achieve an efficient photocatalytic response toward water splitting.

Zhang et al. in 2012 reported a ternary system by coupling SiC with a large band gap semiconductor (TiO_2) and Cr^{3+} species in order to extend the material optical response range.[613] The authors demonstrated that the ternary $Cr_2O_3−SiC-TiO_2$ composites underwent a red-shift of absorption edges with increasing Cr^{3+} levels thus enhancing the separation efficiency of photogenerated carriers and ultimately improving H_2 production under visible light. A year later, other multicomponent photocatalytic systems with SiC as a key promoter for water splitting reaction were developed by the Li team.[614] In particular, they demonstrated that the addition of 1 wt % SiC to NiO_x/TiO_2 brings a 30% increase of hydrogen production with ethanol as the sacrificial reagent. Most importantly, because of the SiC narrow band gap, the ternary SiC (1 wt %)-NiO_x/TiO_2 was found to be responsive under visible light while NiO_x/TiO_2 was completely inactive. A further 70% increase of H_2 production was finally achieved with the addition of an IrO_2 co-catalyst on the surface of SiC. This further addition was found to boost the charge carrier transfer. In the same year, Guo and co-workers designed a flower-like $MoS_2−SiC$ hybrid material with the aim at combining the optimal properties of both semiconducting samples.[615] In spite of its moderate conductivity, molybdenum sulfide is a well-recognized catalyst for HER.[616] On the other hand, SiC not only exhibits a suitable band gap ($\approx$2.4 eV for β-SiC) and good electrical conductivity but also a distinctive HER activity. As a result, the $MoS_2−SiC$ hybrid material was able to enhance the adsorption and dissociation of water on exposed S and Si edges recognized as active sites.[615] The synergistic combination of the two semiconductor materials not only outperformed the HER activity of the benchmark Pt/C catalyst but were found to respond effectively to visible light producing a large photocurrent density. The Hatano team followed a different strategy to improve 3C-SiC photochemical activity. They proposed the introduction of variable amounts of nitrogen as lightweight dopant by low pressure chemical vapor deposition (LPCVD).[617] These authors observed a photocurrent increase upon nitrogen addition without the need for any external bias because of the longer lifetime of light-generated charge carriers. With the aim at improving the overall efficiency, Pt NPs were finally loaded on SiC as co-catalysts as to boost carrier transport and achieve higher incident photon-to-current efficiency (IPCE) in the visible-light range.[617]

Fang, Liu, and collaborators conceived in 2014 a hybrid SnO_2/SiC hollow sphere nanochain (HSNC) system exhibiting excellent activity and durability in the photocatalytic HER.[618] Due to ideal band gap energies and well-organized redox energy levels of CB and VB, the addition of SnO_2 to the non-oxide ceramic created a heterojunction able to efficiently separate charges thus leading to the simultaneous transfer of
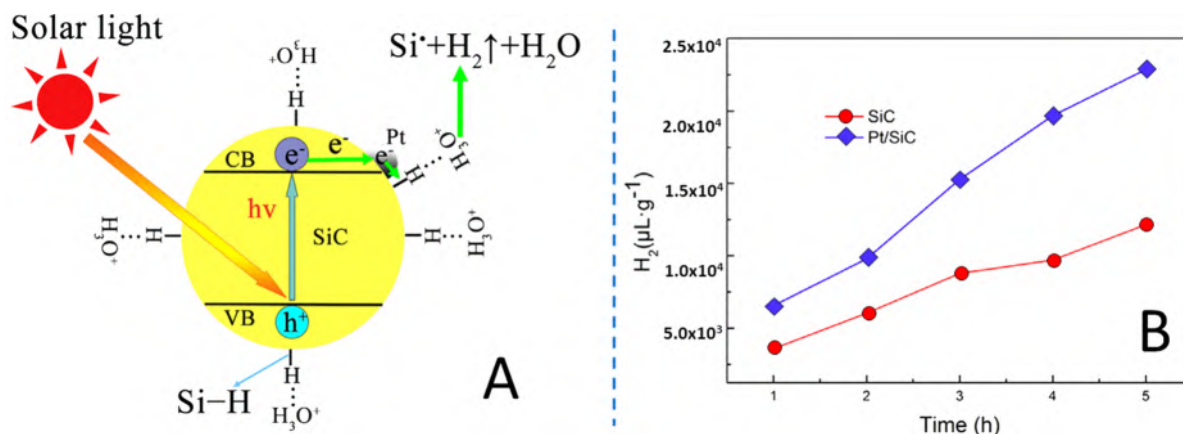
Figure 65. (A) Schematic illustration of the possible reaction mechanism for hydrogen evolution promoted by a Pt/SiC photocatalyst. (B) H_2 evolution rate of Pt/SiC NWs and bare SiC NWs. Adapted with permission from ref 619. Copyright 2014 Elsevier BV.

electrons from SiC to SnO_2 and of holes from SnO_2 to SiC. At the same time, the peculiar HSNC structure played a key role for a multidimensional electronic conduction.[618] Overall, the morphological and electronic properties of SnO_2/SiC HSNCs allowed an average hydrogen production rate as high as 825 μmol g^{-1} h^{-1}. In the same year, Chen and co-workers reported a SiC nanowire (NW) photocatalyst able to produce H_2 with an average evolution rate of 2432 mL g^{-1} h^{-1} under simulated sunlight irradiation.[619] A key step for the reaction to occur was identified in the interaction of H_3O^+ ions with the Si−H bond formed at the SiC surface (Figure 65A). With the addition of Pt NPs on SiC, the photogenerated electrons were transferred to the metal thus reducing the recombination rate of charges and accelerating the process (Figure 65B). In particular, the surrounding electrons of carbon atoms were quickly transferred to Si and Pt active sites thus breaking the Si−H···H_3O^+ bond and releasing H_2 efficiently. As a result, Pt/SiC NWs showed an average hydrogen production 88% higher with respect to bare SiC NWs.

The same group successively developed different photoelectrode composites where SiC NWs were combined with cheaper co-catalysts such as SnO_2[620] and metallic nickel.[621] In both cases, the authors found an enhancement in the hydrogen evolution rate with respect to bare SiC due to a synergistic effect between SiC and metals that improved their light-utilization capacity preventing the recombination of photoexcited electron−hole pairs. In particular, the hydrogen evolution rate of SnO_2/SiC NWs in acidic media was 4 times higher than that of pristine SiC NWs, while Ni NPs, due to their lower Fermi level, captured the photogenerated electrons in the conductive band of SiC nanowires with holes remaining in SiC VB. The fast transfer to Ni NPs restrained electron−hole pair recombination hence contributing to enhance the overall photocatalytic activity in an alkaline medium.

As an alternative approach, Yuan and co-workers focused on the morphological features of SiC-based composites and developed a series of CdS/SiC hybrid materials bearing different crystal lattices and studied the influence of these latter on the materials photocatalytic hydrogen production activity.[622−624] In their first report, these authors prepared a series of powdery composites made of micro-SiC and cubic CdS grains able to lower the surface activation energy of SiC. They found that the well-connected interfaces between SiC and CdS served as active sites, and the close contact between the two

components enhanced the light-utilization ability and the separation efficiency of the photoexcited carrier reaching hydrogen production as high as 555 μmol h^{-1} g^{-1}.[622] In a successive work, they replaced cubic CdS with hexagonal ones.[623] Hexagonal CdS resulted in being more uniformly distributed on the hexagonal SiC surface hence increasing the amount of absorbed light, the charge carrier lifetime, and shuttling electron flow between the two material components. They prepared two different SiC/CdS composites featured with different interfaces: hexagonal SiC/hexagonal CdS and hexagonal SiC/cubic CdS. Despite a similar band gap and potential values of the two types of CdS, the former combination displayed a 4-fold higher hydrogen evolution rate with respect to the latter. Moreover, the first class of composites resulted in a BET increase, stronger light adsorption, and a lower charge carrier recombination thus confirming that a lattice match played a pivotal role in the formation of efficient heterojunctions for improved photocatalytic performance.[624]

The same Chinese team reported in 2016 the synthesis of a new composite material prepared by the selective photodeposition of Pt NPs on Si atoms of micro-SiC particles.[625] The Pt−Si bond at the interface was demonstrated to act as an excellent transport channel for the electron transfer from SiC to Pt and thus for their ultimate use in water reduction. Moreover, the charge recombination was decreased producing a remarkable hydrogen production increase as high as 1367 μL h^{-1} g^{-1}, double that obtained on a Pt/SiC composite simply prepared by unselective impregnation. This work has contributed in confirming the role of Si atoms in SiC at the co-catalyst interface for photoelectron transfer. As a further step forward, the authors exploited the same synthetic approach to prepare ternary systems selectively depositing Pt and IrO_2[626] or MnO_2[627] NPs on selected hexagonal micro-SiC facets. In both cases, the spatial separation of the two co-catalysts allowed an efficient suppression of electron−hole recombination on SiC thus allowing a hydrogen production up to 2337 μL h^{-1} g^{-1}.[626] Starting from this result, the same group reported SiC surface decoration with Au NPs because of their known localized surface plasmon resonance (LSPR) effect that highly promoted the separation of photogenerated electrons and holes. This resonance was indeed suitable to excite Au NP electrons that become "hot" and transferred to a semiconductor under light irradiation hence boosting surface chemical reactions under milder conditions.[136,628] Overall,
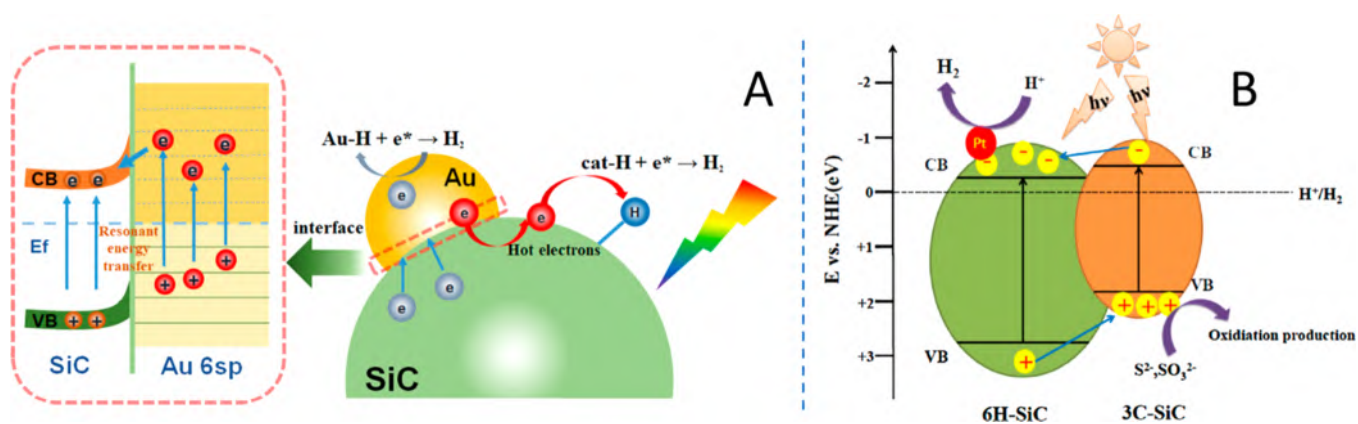
Figure 66. (A) Illustration of the photocatalytic mechanism for hydrogen production over Au/SiC. Adapted with permission from ref 629. Copyright 2018 Elsevier BV. (B) Schematic illustration of the possible mechanism for the charge separation and transition in the photocatalytic system. Adapted with permission from ref 636. Copyright 2017 Elsevier BV.

the LSPR effect and the accelerated water reduction rate on the SiC surface by hot electrons improved the photocatalytic hydrogen production up to 30-fold with respect to the pristine SiC (Figure 66A).[629]

Continuing in the exploration among SiC-noble metal composites for photocatalytic hydrogen production, Kato and co-workers prepared two different photocathodic materials with 3C-SiC and either Pt or Pd NPs as co-catalysts.[630] As expected, both metals were found to enhance the charge transfer from SiC to hydrogen with the highest energy conversion efficiency registered for the Pt co-catalyst.

However, it is still questionable if the Pt/SiC systems can photocatalytically split water. According to the results of Gao et al., commercial bare α-SiC powder with diameters 400−500 nm can photocatalytically split water, but the α-SiC powder with Pt loading cannot.[631] In other words, the Pt loading will suppress the photocatalytic activity of SiC for H_2 production from water. The similar conclusion was also obtained by Chen et al.[632] The latter found that the addition of methanol also decreased the photocatalytic activity of SiC for decomposition of water.

In recent years, Smith's team developed a series of hydrogen evolution photocatalysts based on amorphous SiC (a-SiC).[633,634] This latter constitutes an interesting p-type photocatode material due to its tunable band gap energy (1.8−2.1 eV) together with its high chemical stability. These authors coated a thin (25 nm) TiO_2 layer on a-SiC by atomic layer deposition and first created a hetero p-i-n junction. The as-obtained junction significantly increased the photovoltage leading to an efficient charge carrier collection for water reduction. The subsequent addition of a Ni−Mo co-catalyst favored a significant onset potential shift while showing a photocurrent density of 8.3 mA cm^{-2} at 0 V vs RHE that was remarkably higher than that registered with pure a-SiC (0.15 mA cm^{-2}) under acidic conditions.[633] Successively, the authors further increased the catalyst activity incorporating an ultrathin Ni film on TiO_2-coated a-SiC prior to Ni−Mo co-catalyst electrodeposition. This addition enhanced the number of active sites and prevented charge accumulation on the surface and hence reaching a photocurrent value as high as 14 mA cm^{-2} at 0 V vs RHE.[634] Following the consolidated idea of coupling p-SiC with n-TiO_2 to improve materials visible-light adsorption capacity, Singh and collaborators made use of β-SiC as a chemically inert, narrow band gap semiconductor to

construct a series of sulfate modified β-SiC/TiO_2 composites with high hydrogen photocatalytic evolution activity. The sulfate species were found to positively influence the photocatalytic activity narrowing the band gap and contributing to produce a bathochromic shift of optical absorbance. The heterojunction together with S doping were found to play a key role on both visible-light adsorption and harvesting as well as on suppressing the photogenerated electron−hole recombination.[635]

In an attempt to avoid expensive materials for a possible large-scale development of photocatalytic hydrogen production devices, Armstrong and co-workers prepared SiC NWs doped with iron.[637] These authors registered a light-driven hydrogen production up to 100-fold higher with respect to that of bare SiC because of a cooperative mechanism between Fe atoms and Si−OH groups on the SiC surface. They postulated that iron sites underwent proton-to-hydride cycles with the Si atoms providing permanent −OH ligands able to capture and transfer protons ultimately producing H_2. In a more recent paper, Yanand co-workers developed a photocatalytic material by recycling SiC present in the slurry wastes produced during wafer slicing in the photovoltaic industry.[636] They found that the recovered material was mainly composed of 3C- and 6H-SiC with a minor amount of silicon oxycarbides. This multicomponent semiconductor material was then loaded with Pt as the co-catalyst generating the considerable hydrogen rate of 129.7 μmol h^{-1} g^{-1}. As illustrated in Figure 66B, the photogenerated electrons were shuttled from the CB of 3C-SiC to the more negative 6H-SiC CB, while the excited holes were transferred from the lower VB of 6H-SiC to 3C-SiC. The copresence of two different SiC polytypes with different band gap energies was found to be beneficial for facilitating charge carriers separation and avoiding their recombination.

In 2015, Yuan et al. exploited micro-SiC powders for application in the overall water splitting process under visible-light irradiation.[638,639] They demonstrated that micro-SiC powders were suitable for enhancing the photocatalytic oxygen evolution reaction of $BiVO_4$ due to the efficient contact between the semiconducting materials and the exposure of SiC surface that boosted the electrons shuttling while decreasing charge recombination.[638] Successively, they decorated micro-SiC with Pt for hydrogen production and employed WO_3 particles for oxygen evolution by assembling a photocatalytic system for water splitting able to produce a stoichiometric

amount of H_2 and O_2 with a quantum yield efficiency of 0.021% at 420 nm. These authors found maximum photocatalytic activity at pH = 3 because at higher pH values the hydrogen reduction potential becomes more negative, thus reducing the potential difference with SiC CB and therefore mitigating the overall activity.[639] For the first time, micro-SiC was demonstrated to be a cheap, chemically stable, and efficient semiconductor material for promoting the overall water splitting process.

More recently, Sun and co-workers developed a 3C-SiC/NiO catalyst to be exploited as an efficient photoanode for water splitting. The authors evidenced the formation of a SiC/NiO p-n heterojunction able to promote the separation of photogenerated charge carriers while suppressing their recombination. The as-prepared material was found to remarkably enhance the water splitting activity with high photovoltage and photocurrent values with a decrease of the onset potential with respect to bare SiC.[640] The same group prepared later a Ni:FeOOH bimetallic co-catalyst deposited on cubic silicon carbide. The authors found that the limited photocatalytic activity observed for bare 3C-SiC was due to the short charge carrier diffusion length compared to the light penetration depth that hinders the charge separation. The addition of the metallic co-catalysts is able to overcome these limitations thus improving the overall photocatalytic water splitting.[641]

Very recently, Shuai and Qi's group performed a theoretical systematic investigation on the properties of a series of 2D GaN/SiC heterojunctions to be exploited for visible-light driven photocatalytic water splitting. Their investigation included SiC monolayers and bilayers coupled with GaN mono-, bi-, and trilayers. They demonstrated that the layers' number plays a key role in modulating the heterostructure band gap through interlayer interaction and lattice constant variation. Their study therefore provides a route to follow for the experimental synthesis of GaN/SiC materials for efficient water splitting.[642]

A completely different approach to produce hydrogen is represented by the hydrolysis of lightweight inorganic hydrides. Among them, ammonia borane (AB, NH_3BH_3) is considered as one of the most promising candidates because of its large hydrogen content (19.6 wt %) that allows a theoretical release of 3 mol of H_2 per AB. However, the low kinetics of AB hydrolysis makes imperative the development of appropriate catalysts to promote H_2 release.[425] Moving from previous reports on the photocatalytic AB hydrolysis by means of classical TiO_2-based materials,[643,644] Yan and co-workers simulated the photocatalyzed AB hydrolysis by constructing a bimetallic/SiC composite able to promote the hydrogen release.[645] In particular, these authors combined β-SiC with Cu and Co in order to tune the band gap of SiC and allow AB photocatalytic hydrolysis under visible-light irradiation. Indeed, the metal doping was demonstrated to reduce the β-SiC band gap thus bathochromically shifting its response to radiation and increasing the photocatalytic quantum efficiency of AB hydrolysis. Overall, DFT calculations from these authors demonstrated that the photochemical response of SiC could be synergistically combined with the catalytic activity of transition metals for boosting hydrogen release from AB.

3.5.3. Photodegradation of Organic Pollutants.
Removal of pollutants represents one main priority of our modern society due to its impact on both public health and the environment. On this ground, photocatalysis has been largely employed for air and wastewater treatments, and several research efforts have been devoted to the development of efficient semiconductor catalytic materials.[646,647] Among them, SiC-based composites with metals or TiO_2 offer unique morphological and photocatalytic properties that make them highly promising materials for application in these fields.

3.5.3.1. Removal of Pollutants from Air. Keller and Garin first reported on the use of SiC as a component for semiconductor photocatalytic systems to be exploited for air pollutant removal.[648] Taking methylethylketone (MEK) as a model volatile organic compound (VOC), they developed a ternary system composed of WO_3 supported on SiC-TiO_2. They found that SiC and WO_3 addition to TiO_2 remarkably enhances MEK photodegradation at room temperature with total mineralization to CO_2 and H_2O. If WO_3 surface acidity is claimed to play a trapping effect, the addition of SiC with its suitable band gap energy and energy level position was found to increase charge separation preventing their recombination.

More recently, Keller and co-workers took advantage of alveolar open-cell medium surface area β-SiC as a support for TiO_2 for gas-phase photodegradation of MEK.[649−651] With respect to more classical metallic foams, SiC offers several advantages such as high thermal and chemical stability allowing operation under severe reaction conditions and regeneration of the catalyst without any damage to the support. Moreover, SiC foams can be easily shaped "on-demand" depending on photoreactor geometry. Finally, the medium SSA is ideal for a suitable dispersion of the photoactive phase, and the high density of SiC oxygenated surface groups is optimal for titania anchoring. The authors found that β-SiC structured foams induce a beneficial effect on MEK photodegradation (both under conventional UV-A[651] or greener LED[650] as irradiation light source) due to their static mixer effect and their ability to enhance the amount of available TiO_2 per reactor volume unit. In this case, no synergistic photocatalytic effect was observed between the two semiconductors; therefore, β-SiC is just exploited as a support for the TiO_2 photoactive phase. On the contrary, Xie's group demonstrated the active role of SiC as the co-catalyst for pollutant degradation promoted by porous TiO_2/SiC films prepared by ball-milling and screen printing.[652] In particular, they tested the composite performance for degradation of toluene chosen as a model organic contaminant and found that SiC enhances the photodegradation activity of TiO_2 bringing it to complete mineralization. The SiC-TiO_2 heterojunction with its peculiar staggered energy bands allows photogenerated electrons to be shuttled from SiC CB to TiO_2 with holes following the opposite way from TiO_2 VB to SiC with an overall increase of photodegradation activity (Figure 67).

In a recent report, Wang and Zhao developed an efficient photocatalyst for NO removal under visible-light irradiation combining Ti_3C_2 MXene quantum dots and SiC. The authors demonstrated that the novel heterojunction catalyst exhibits 3.1 and 3.7 times higher activity with respect to bare Ti_3C_2 MXene and SiC, respectively. Several aspects are claimed to improve the photocatalytic degradation of NO such as the exposed Ti sites and the unique optical properties of SiC together with its thermal stability. Moreover, the formed heterojunction was found to efficiently adsorb visible light, boost charge transfer, and avoid their recombination.[653]

3.5.3.2. Removal of Organic Water Pollutants. Yamashita and co-workers first investigated the photodegradation activity of TiO_2−SiC composites for wastewater treatment.[654,655] The
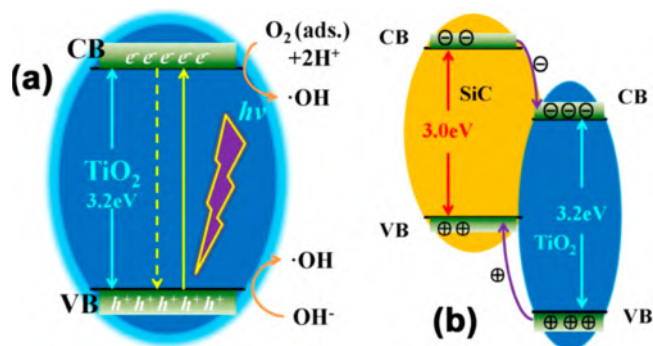
Figure 67. Schematic diagram of a photogenerated electron and hole reaction (a) and their transfer between SiC and TiO$_2$ (b). Reproduced with permission from ref 652. Copyright 2012 Elsevier B.V.

materials were prepared by calcination of TiC-SiC nanoparticles, obtained in turn by carbothermic reduction of SiO$_2$−TiO$_2$. The authors demonstrated that TiO$_2$ deposited on SiC outperforms both bare TiO$_2$ and the TiO$_2$−SiO$_2$ binary system in the photodegradation of diluted 2-propanol (Figure 68) due to the well-crystallized deposited TiO$_2$ phase and to the hydrophobic SiC surface.
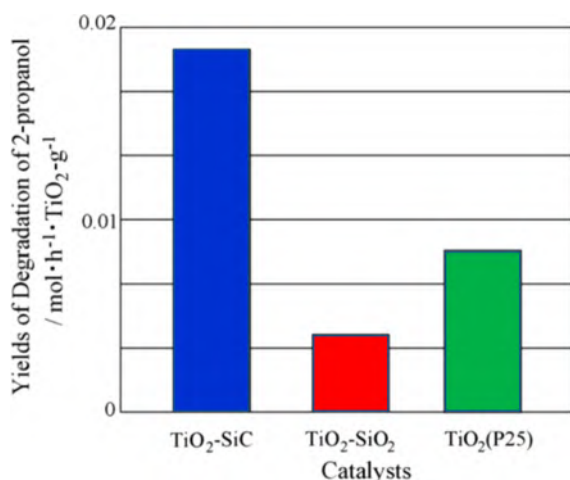
Figure 68. Photocatalytic reactivity normalized per weight of TiO$_2$ for 2-propanol diluted in water on TiO$_2$−SiC, TiO$_2$−SiO$_2$ photocatalyst, and commercial TiO$_2$ powder (P-25). Adapted with permission from ref 655. Copyright 2006 Elsevier B.V.

More recently, the same group prepared by hydrothermal synthesis a 1T/2H-MoS$_2$-phase hybrid coupled with SiC forming a heterojunction structure for 4-nitrophenol degradation. Silicon carbide was found to increase significantly the photocharge carrier level, visible-light response, and reaction rate thus improving the photocatalytic activity.[656]

A few years later, Rodriguez et al. confirmed the potentiality of TiO$_2$−SiC binary systems for photocatalytic applications evaluating their ability toward oxidation of aqueous ammonia,[657] but only in 2011, Robert's group exploited TiO$_2$ supported on medium surface area β-SiC showing their potential application for industrial reactors.[658] Taking the herbicide Diuron (3-(3,4-dichlorophenyl)-1,1-dimethyl-urea) as a model water contaminant, the authors investigated the photocatalytic activity of a TiO$_2$−SiC foam structured reactor working in a recirculation mode[649,659] demonstrating the

possibility to operate continuously for wastewater treatment with very low pressure drop phenomena. Moreover, the catalyst can be easily recovered and reused, and the SiC-based foams, other than offering a static mixer effect enhancing the molecules/active-phase contact, are prone to be adapted to any reactor geometry. Similar conclusions were drawn by the same group in collaboration with M'Bra, while studying the photocatalytic degradation of Paraquat herbicide (1,1′-dimethyl-4,4′-bipyridinium dichloride)[660,661] and Scala fungicide (Pyrimethanil)[662] promoted by TiO$_2$ NPs coated on β-SiC alveolar foams. Even if the kinetics is lower for the supported photocatalysts with respect to TiO$_2$ powder suspension, β-SiC support allows conduction of the photodegradation in continuous operational mode for several cycles without the need for any filtration step to separate the catalyst from treated water, thus opening to the large scale development of the process. Other than extending the applicability of their composite to the removal of natural organic matter (NOM) in treated water,[663] as a further step forward, Robert's group recently reported the direct synthesis of TiO$_2$-β-SiC composites prepared by a shape-memory replica method.[664,665] In particular, they incorporated TiO$_2$ powders directly in the slurry used for the transformation of polyurethane foams in the corresponding carbides, avoiding any successive step for TiO$_2$ immobilization on SiC. Even if the as-prepared materials result in being slightly less efficient in Diuron mineralization with respect to the classical TiO$_2$-supported β-SiC, they benefit in higher stability with a negligible titania release in water. Very recently, the same group reported a Ti-modified LaFeO$_3$ dual catalyst supported on β-SiC for a combined photocatalytic and photocatalytic wet peroxide oxidation (CWPO) mediated by H$_2$O$_2$ under a UV-A light source. Taking the removal of 4-chlorophenol from water as a model reaction, the authors demonstrated that their catalyst offers the advantages of both processes achieving full total organic carbon (TOC) conversion. Moreover, the β-SiC support allows the catalyst macroscopic shaping to overcome all technical issues related to powdery materials and ensures its easy recycling without activity loss.[666]

At odds to what was reported by Robert's group where SiC does not actively participate in the photocatalytic process, Juarez-Ramirez et al. showed a synergistic effect between TiO$_2$ and SiC semiconductors through the interaction of their respective CV and VB bearing ideal potential values. The composite demonstrated the reduction of the recombination rate of charge carriers thus enhancing the degradation of methylene blue and indigo carmine chosen as model water polluting dyes.[667] Following these conclusions, Hao's group prepared different TiO$_2$−SiC composites analyzing their photocatalytic activity in the degradation of the model 4-aminobenzenesulfonic acid (4-ABS). In particular, they loaded TiO$_2$ particles on both n- and p-type SiC foams showing a remarkable higher activity with the latter. The authors attributed the better performance to the formation of a p-n heterojunction that allows a higher charge separation and transfer thus increasing the material photodegradation activity.[668,669] Similar conclusions were drawn independently by Singh's and Tian's groups for Rhodamine B (Rh-B) and methylene blue degradation promoted by β-SiC-TiO$_2$ composites.[670,671] They found that the combination of the two semiconductors produces a p-n heterojunction that favors the separation of photogenerated charge carriers thus enhancing the photocatalytic degradation activity. Moreover,
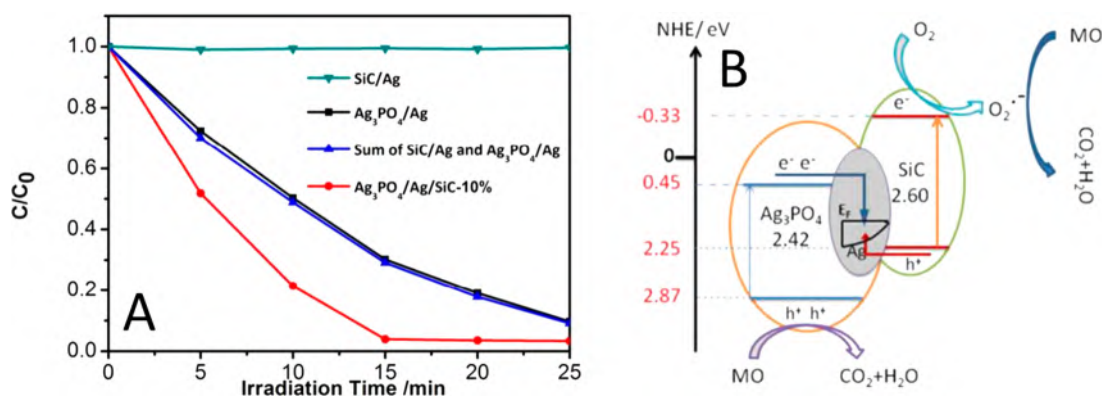
Figure 69. (A) Comparison of Ag$_3$PO$_4$/Ag/SiC-10% photocatalytic activity with that of the mixture of Ag$_3$PO$_4$/Ag and SiC/Ag with the same weight fraction of SiC on the degradation of MO under visible-light irradiation (>420 nm). (B) Schematic illustration of the photocatalytic mechanism of Ag$_3$PO$_4$/Ag/SiC under visible-light irradiation (>420 nm). Adapted with permission from ref 672. Copyright 2015 The Royal Society of Chemistry.

it was found that the narrow β-SiC band gap enlarges the TiO$_2$ light response from UV to the visible-light region.

Successively, Fang's group designed a series of Ag-based photocatalysts for visible-light-promoted dye degradation taking methyl orange (MO) as a model water contaminant.[672] In order to overcome classical drawbacks encountered with Ag$_3$PO$_4$ catalytic systems such as its partial solubility in aqueous solution that obviously limits its practical application and the absence of an electron acceptor that decreases its visible-light absorption capability, the authors designed a ternary hybrid Ag$_3$PO$_4$/Ag/SiC photocatalyst. This latter showed enhanced activity toward MO degradation with respect to both bare Ag$_3$PO$_4$/Ag and SiC/Ag (Figure 69A) due to an efficient electron−hole separation. As depicted in Figure 69B, Ag NPs act as a bridge for charge transmission producing a Z-scheme system. Upon visible-light excitation, electrons in the CB of Ag$_3$PO$_4$ are shuttled to Ag, and at the same time, holes on SiC VB are shifted to Ag producing a simultaneous charge transfer that contributes to their separation increasing the overall photocatalytic activity.

A similar synergistic effect between semiconductors was reported by Du et al. with yolk−shell Si/SiC@C@TiO$_2$ composites.[673] They showed that the TiO$_2$ and SiC/Si interface junction boosts photogenerated charge separation minimizing their recombination. Surface electrons are then captured by O$_2$ generating superoxide radicals responsible for organic dye degradation.

In the same year, Sivasamy's group developed a hybrid composite for photodegradation of phenols based on ZnO.[674] This latter is a wide band gap n-type semiconductor that is preferable with respect to the more commonly used TiO$_2$ due to its low cost and lower toxicity. However, ZnO suffers from low activity due to the fast electron−hole recombination rate that largely limits its photocatalytic response. The combination of ZnO with SiC was reported by authors to be able to double the activity of pure ZnO. Indeed, they showed that enhanced charge transfer mechanism in the ZnO-SiC hybrid material boosts OH radical formation for phenol degradation both under UV and visible-light radiation.

Yuan and co-workers highlighted the importance of spatial separation of SiC-supported Pt and IrO$_2$ co-catalysts for an efficient photodegradation activity of the model Rh-B contaminant. As already reported by them for application in H$_2$ production (see section 3.5.2), the authors showed that a selective deposition on SiC allows a spatial isolation among metal co-catalysts thus suppressing electron−hole recombination and enhancing the overall photocatalytic activity.[626]

More recently, Sarkar et al. deposited Ag NPs on spherical β-SiC creating a hierarchical Ag@SiC structure exploited for dye degradation and antibacterial activity.[675] Due to an intimate contact created by the homogeneous dispersion of Ag NPs on SiC, an effective charge transfer was observed thus bringing to significant photodegradation orange G and amido black 10B model water contaminants under UV-light irradiation. In addition, a strong antimicrobial activity was observed and attributed to the efficient charge transfer promoted by silver. Overall, the Schotty barrier formation at the Ag@SiC interface is claimed to enhance the photoactivity response of the developed binary hybrid compound.

Other than classical silver composites, other metal-SiC composites were recently developed for dye degradation. In particular, the SiC/SnO$_2$ composite[676] and BiOBr/SiC whisker[677] hybrids were exploited for MO and Rh-B degradation, respectively. In both cases, the formation of SiC/heterojunctions improved the photoinduced charge separation hence reducing electron/hole recombination and favoring the hybrid photodegradation activity.

4. SIC AND ITS COMPOSITES AS METAL-FREE CATALYSTS

Metals and metal oxides have been widely used as catalysts for a long time and in an almost indefinite number of relevant industrial processes. Their use has always been regarded as an obvious choice to activate target molecules and reduce the energy barriers associated with their conversion in a given process, hence accomplishing any transformation quickly and efficiently. On the other hand, metal-based catalysts can suffer from high costs, low selectivity, poor durability, and the susceptibility to gas poisoning other than holding a potentially negative impact on the environment. The last decades have witnessed tremendous progress in the development of more sustainable and green catalytic processes based on metal-free systems, particularly with respect to the replacement of PGMs with earth-abundant elements in challenging energy-related transformations and devices.[678]

This last section aims at providing a comprehensive overview on the use of SiC matrices as either supports or
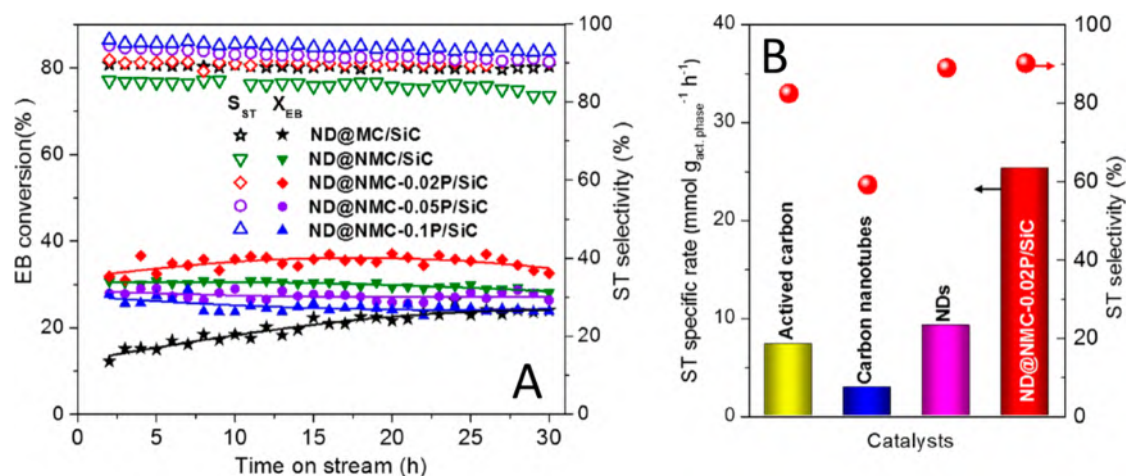
Figure 70. (A) EB conversion (%) and SE selectivity (%) in the EB ODH promoted by various carbon-based monoliths under identical experimental conditions. (B) Catalytic performance of different C-based materials in comparison to ND@NMC-0.02 P/SiC catalysts. Reproduced with permission from ref 687. Copyright 2020 Elsevier BV.

non-innocent active phases within a relatively wide number of catalytic transformations.

4.1. Synthesis of Fine Chemicals

4.1.1. Alkane Oxidation. Catalytic dehydrogenation of alkanes is one of the most promising routes for the production of value-added olefins.[679,680] Ethylbenzene (EB) dehydrogenation to styrene (SE) is very likely one of the most studied dehydrogenation processes operated under either oxidative (ODH−exothermic) or direct (DDH−endothermic) dehydrogenation conditions.[681]

Since the discovery that carbon nanotubes (CNTs) were promising heterogeneous catalysts for promoting the metal-free oxidative alkane dehydrogenation,[682−684] many efforts have been devoted to immobilizing CNTs on macroscopically shaped supports to be use in fixed-bed reactors. Such an approach was basically dictated by the need for solving practical limits of a class of nanomaterials generally produced in the form of powders. Their immobilization on selected macroscopically shaped carriers would have avoided classical pressure drop problems in fixed-bed reactors and could also have compensated the generation of local temperature gradients (hotspots) during the exothermic ODH (eq 39, R = alkyl, aryl).

$$RCH_2CH_3 + \tfrac{1}{2}O_2 \rightarrow RCH{=}CH_2 + H_2O \qquad (39)$$

$$C_6H_5CH_2CH_3 \rightarrow C_6H_5CH{=}CH_2 + H_2 \qquad (40)$$
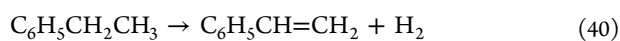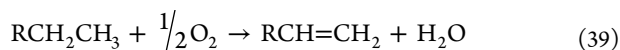
Su et al. first described the preparation of CNT/SiC monoliths featured by a uniform and stable CNT layer on the SiC foam surface.[685] The foam was selected in light of its high thermal conductivity and mechanical strength that made it an ideal choice for high-temperature and highly exothermic processes. CNTs were grown at the SiC surface starting from the washcoated material with an iron-containing layer exposed in turn to ethylene as the C source under CVD conditions. The resulting composite was used with success for the ODH reaction of 1-butene into butadiene with higher selectivity and product formation compared to the powdered CNT catalyst.[685] A conceptually similar approach was followed later by the same team for the preparation of a related SiC monolith composite featuring two different surface immobilized allotropic forms of carbon: CNT and nanodiamonds

(NDs).[686] These authors prepared a ND/CNT-SiC catalyst made of a uniform CNT layer of roughly 20 μm thickness at the SiC surface, employed for embedding ND aggregates as "fishes in a CNT net". The composite was then successfully tested as a metal-free catalyst in the model endothermic DDH of EB to SE (eq 40), showing improved performance with respect to the CNT/SiC monolith as well as pure commercial ND powders.[686]

As an additional step forward in the area of metal-free dehydrogenation catalysis, this team has more recently described the synthesis and application of a robust SiC foam monolith catalyst containing nanodiamond aggregates (NDs) coated in a P, N codoped mesoporous carbon matrix.[687] P, N codoping of the mesoporous C network was believed to enhance the density of active sites (N-doping) in the metal-free system for the improvement of EB conversion while inhibiting a deep EB oxidation (P-doping) to CO_x. At the same time, the monolith contributed to the high NDs utilization in the ODH and mitigated the pressure drop phenomena across the catalytic bed and the formation of local temperature gradients due to the process exothermicity. Accordingly, the selected SiC-based composite from this series (Figure 70A) showed a remarkable performance in the ODH and largely outperformed all other metal-free catalysts reported in the literature to date both in terms of process rate and SE selectivity (Figure 70B).

Pham-Huu and co-workers reported in the same years the preparation of macroscopic ND/β-SiC composites[688] including the use of a nitrogen-rich mesoporous carbon matrix (NMC) as a non-innocent glue between NDs and the foam.[689] Once again, open-cell SiC foam structures featured by high mechanical stability and good thermal conductivity were selected by these authors as ideal supports for NDs in the dehydrogenation process. The combination with a N-rich mesoporous C phase ensured highly dispersed ND fillers at the monolith surface. Their catalytic outcomes in the direct EB DH (DDH) have also unveiled the role of basicity of N-doped carbon glue on the mitigation of cracking side processes responsible for the catalyst coking/deactivation in the highly endothermic process.[689]

4.1.2. C−C and C−Halogen Bond-Forming Reactions. As far as the use of SiC as a C−C bond-forming reaction
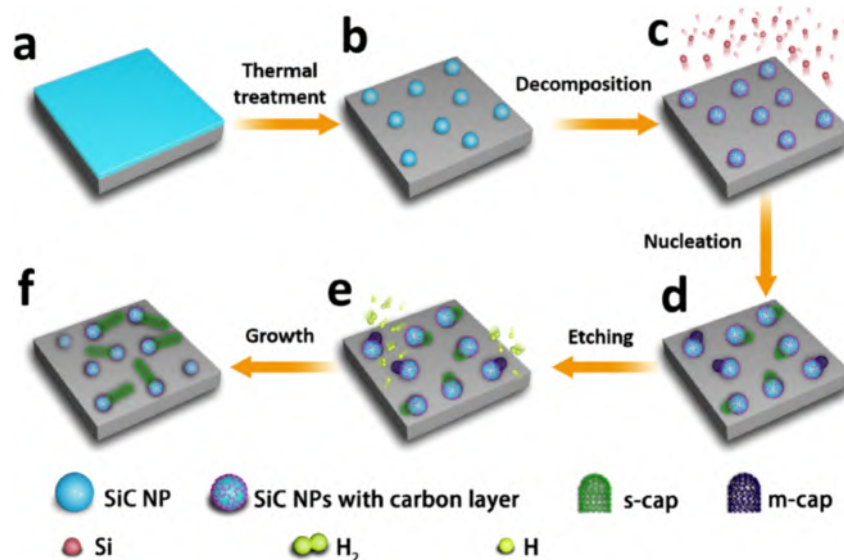
Figure 71. Reaction scheme for growing s-SWCNTs from SiC nanoparticles. (a) A layer of SiC deposited on a silicon substrate by sputtering. (b) Formation of SiC nanoparticles on the substrate by thermal treatment. (c) Sublimation of Si atoms from the surface of SiC nanoparticles. (d) Formation of m- and s-carbon caps on the SiC nanoparticles. (e) Selective removal of the m-caps. (f) Growth of s-SWCNTs. Reproduced with permission from ref 690. Copyright 2018 Elsevier Ltd.

catalyst is concerned, Hou, Liu, and collaborators have elegantly demonstrated the use of SiC nanoparticles as selective catalysts for the ultrapure growth of semiconducting single-wall carbon nanotubes (s-SWCNTs).[690] As illustrated by the reaction scheme proposed by these authors (Figure 71), s-SWCNTs nucleate from SiC nanoparticles after the surface depletion of Si atoms under thermal treatment and ultrahigh vacuum. Remaining surface C atoms originate carbon nano-caps with the more chemically active metallic ones (m-caps) being preferentially etched away under H_2 atmosphere, hence allowing high purity s-SWCNTs to be grown selectively by the CVD of ethanol.

Pan, Bao, and co-workers have pointed out the advantages of using SiC as an alternative solution to C nanostructures in the preparation of heterogeneous metal-free catalysts.

In a seminal contribution, this team has shown that reacting SiC with NH_3/CCl_4 under elevated temperatures caused the depletion of surface Si atoms and the reorganization of remaining C atoms in the form of light-heterodoped carbon layers.[691] The final textural properties and chemical composition of the composite were modulated on the basis of the selected operational conditions. Their SiC-derived composite was found to activate acetylene for the efficient and selective $C\equiv C$ bond hydrochlorination reaction as a robust and truly metal-free system. Additional studies and *in silico* simulations led these authors to claim the central role played by C sites neighboring pyrrolic nitrogen atoms in the C−N phase grown at the SiC surface as the active sites for the process to occur.[691,692]

4.1.3. Other Challenging Metal-Free Catalytic Processes Using SiC as Either a Support or Active Phase.
Silicon carbide nanotubes (SiCNTs) have received a great deal of interest since their synthesis in 2001,[460] particularly with respect to their ability to interact with small molecules and promote their conversion. Their structure and stability, including that of their light-heteroelement doped forms, have been thoroughly investigated by quantum chemical calculations,[693,694] and their comparison with more classical carbon

nanotubes has offered useful hints to highlight their unique chemicophysical properties. At odds with their purely C-based cousins, SiCNTs list different desirable physical and chemical properties, possess semiconducting properties, and exhibit a diameter-independent stability with an only weak dependence from their helicity.[695] Theoretical calculations have shown that small molecules such as H_2,[696] CO,[697] HCN,[697] NO,[698] and N_2O,[698] commonly physisorbed on CNTs, can be chemisorbed at the surface of SiCNTs with relatively large adsorption energies. As far as the potential catalytic applications of SiCNTs are concerned, theoretical predictions from Ding and co-workers have demonstrated the potentiality of SiCNTs as promising metal-free systems for the cleavage and conversion of N−H or O−H functionalities of ammonia and alcohols.[699] Due to the significant charge separation between silicon (electron deficient) and carbon (electron rich) atoms, these elements in SiC structures can also be regarded as Lewis acid−base pairs, respectively. Theoretical studies conducted by Sun et al. have shown that SiCNTs can take hydrogen atoms from ammonia borane (AB) through the interaction between protic and hydridic hydrogens of the exogenous molecule and the Lewis acid−base pair of the nanotube.[700]

A series of *in silico* studies from the Iranian team of Esrafili and co-workers have additionally provided useful hints to the comprehension of the inherent potentialities of SiC nano-structures as metal-free catalysts for the adsorption/activation and conversion of other challenging molecules: from the dehydrogenation of hydrazine[701] and methylamine[702] and the related hydrogen production up to the ammonia[703] and formamide[704] decomposition. These fundamental studies offer a clear overview on the future applications of these materials as sustainable metal-free systems in key processes at the heart of renewable energy technology. They certainly contribute to highlight the potentialities of a class of materials that have been not fully exploited from an experimental viewpoint yet.

An interesting example of practical application of the adsorption capacity of SiC structures toward selected
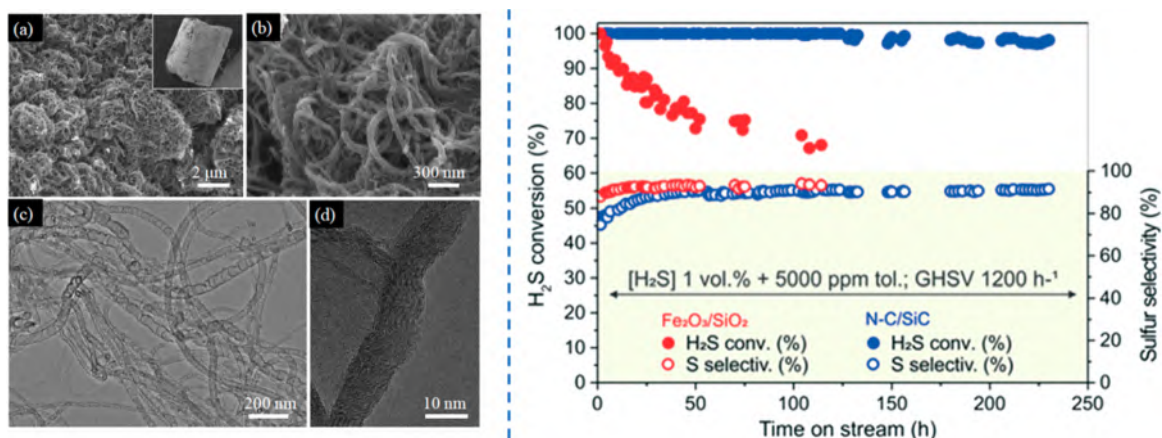
Figure 72. (left) SEM micrographs of a N-CNTs/SiC composite (a,b) showing high coverage of the SiC surface by the N-CNTs network. The inset in (a) refers to a digital photo of the SiC extrudate covered with N-doped carbon nanotubes. (c,d) TEM micrograph of N-CNTs at different magnifications, showing a bamboo-like morphology without any trace of an amorphous carbon. Reproduced with permission from ref 712. Copyright 2014 Dalian Institute of Chemical Physics, Chinese Academy of Sciences. Published by Elsevier BV. (light) Desulfurization tests on N−C/SiC and the benchmark Fe_2O_3/SiO_2 catalysts in comparison. Reaction conditions: H_2S: 1 vol % containing 5000 ppm (0.5 vol %) of toluene as aromatic contaminant; GHSVs: 1200 h^{-1}; O_2-to-H_2S ratio = 2.5, [H_2O] = 30 vol %, He (balance); reaction temperature = 210 °C. Reproduced from ref 713. The Royal Society of Chemistry 2020 under [CC BY-NC 3.0] [https://creativecommons.org/licenses/by-nc/3.0/].

molecules for their activation and conversion was reported by a Finnish team already in 1997.[705] These authors investigated the potentialities of a series of heterogeneous catalysts, including commercial grade silicon carbide, for the selective catalytic oxidation of NH_3 to N_2 in gasification gas. At odds with other catalysts such as dolomite or iron sinter for which the addition of oxidizers like O_2 and NO to the hot synthetic gasification gas resulted in an increase of NH_3 production, experiments with silicon carbide as catalyst at temperatures comprised between 700 and 800 °C revealed its preferential NH_3 oxidation to N_2. The reason for such a different behavior was generally ascribed to the generation of a porous silicon dioxide layer on SiC and its different capacity to adsorb gaseous species at its surface in the presence of a complex gas mixture such as that in the gasification gas.[705]

Other fundamental theoretical studies which appeared in the past few years have additionally pointed out the unique electronic properties of selected SiC morphologies and their inherent ability to activate and convert challenging molecules acting as metal-free catalysts for their oxidation or reduction. Independent *in silico* studies from a Chinese team[706] and an Indian[707] team have thoroughly discussed the ability of SiC monolayers to act as metal-free catalysts for CO oxidation and the relative reaction mechanisms. Density functional theory (DFT) computations have been finally performed by Zhao et al.[708] in order to explore the potentialities of layered SiC sheets as a metal-free catalyst for NO reduction. Their conclusions predict the superior catalytic performance of these plain SiC samples and provide a rational three-step mechanism of action in the process. More recently, Zeng and co-workers reported on metal-free SiC quantum dots (QDs) with respect to their ability to promote CO_2 hydrogenation to methanol. The authors demonstrated that the insertion of hydrophilic hydroxyl groups at SiC surface lowers the process activation energy and greatly enhances SiC QDs catalytic activity. In particular, −OH groups were found to be directly involved in the formation of HCOO* intermediates reducing the related energy barrier and thus facilitating CO_2 activation.[709]

Pham-Huu et al. have widely demonstrated the importance of SiC structures as inert and thermally stable supports for a

C−N active phase to be employed in the selective H_2S oxidation to elemental sulfur in sour gas tails.[710−715] Although SiC matrices mainly hold the role of refractory carriers for porous carbon networks in the form of N-doped systems as the active phase, they play a fundamental role in the catalyst shaping according to its downstream application. In particular, these authors have demonstrated the advantages of SiCs for the preparation of robust and durable hybrid organic−inorganic composites obtained from growing C deposits at the SiC surface both in the form of N-doped carbon nanotubes (N-CNTs)[710−712] (Figure 72 left) or porous N-doped C networks obtained from the CVD technique or the metal-free thermal treatment of selected C- and N-source building blocks,[713−715] respectively. Their metal-free systems have shown unique desulfurization performance in the H_2S selective oxidation to elemental sulfur even for catalytic processes operated under harsh reaction conditions [gas hourly space velocity (GHSV) close to those employed in industrial plants], in the presence of relatively high H_2S concentrations [0.5 vol % ≤ (H_2S) ≤ 2 vol %] or in the presence of contaminants such as heavy hydrocarbons and aromatics [*i.e.* benzene, toluene, and xylene (BTX) up to 20,000 ppm][713,714] commonly present in untreated natural gas streams. In addition to the excellent performance of their N−C phases with respect to benchmark metal-based catalysts of the *state of the art* (Figure 72 right), the macroscopic shaping allowed by the use of SiC has deeply contributed to the improvement of the final catalyst activity by maximizing the contact between the reactant and catalyst active phase, reducing problems linked to catalyst pressure drop in fixed-bed reactors, and largely solving all problems associated with the handling and transportation of nanoscopic active phases.

4.1.4. Electrocatalytic Processes with SiC-Based Metal-Free Catalysts. Salimi and collaborators first reported on the use of a SiC-modified glassy-carbon (GC) electrode for the development of a highly sensitive insulin amperometric detector.[716] Their seminal study demonstrated that the electrooxidation of this important hormone was successfully performed on the SiC-modified GC already on picomolar concentrations under flow conditions and without interfer-

ences from other co-oxidized compounds. At odds with classical GC electrodes, the oxidation of insulin at the GC electrode modified with SiC nanoparticles occurred indeed at reduced overpotentials. Moreover, the chemical stability and antifouling properties of the SiC modified electrode allowed these authors to develop a highly efficient electrochemical sensor suitable to operate under physiological conditions.[716]

Chu, Wu et al. reported an interesting study on the superior ability of ultrathin 3C-SiC nanocrystals (NCs) to dissociate water into −H and −OH fragments under weakly acidic conditions.[717] Their study highlighted the electrocatalytic properties of these nanocrystals officially acting as metal-free electrocatalysts for a fundamental process at the heart of renewable energy technology like the hydrogen evolution reaction (HER). Their fundamental finding in a key area of electrocatalysis was retrieved later by Shen and co-workers who proposed a rational atomic-scale mechanism to the process on the basis of quantum mechanical calculations.[718] These authors postulated the occurrence of a Volmer-Heyrovsky mechanism similar to that occurring with metals. Thus, an electron from a SiC nanocrystal reacted with a hydronium molecule (H_3O^+) (Heyrovsky reaction) adsorbed at a Si−H site hence generating H_2 and a coordinatively unsaturated Si atom. Afterward, the Volmer reaction follows and regenerates the Si−H bond.[718]

Density functional theory (DFT) calculations have demonstrated the potentialities of layered SiC sheets as an important class of cheap and sustainable catalytic materials to be employed as metal-free systems for another key and kinetically sluggish process at the heart of fuel cell technology: the oxygen reduction reaction (ORR). Zhu, Jiang et al. have predicted the ability of layered SiC sheets to play as effective ORR electrocatalysts in the place of Pt-based [Pt(111) surface] systems without suffering from any alteration of their performance in the presence of classical poisons for platinum (i.e. CO).[719] Their outcomes suggested that layered SiC existed as stable metal-free electrocatalysts for the process with high CO tolerance and with a lower energy activation barrier for the reaction RDS under alkaline media with respect to a Pt(111) surface.

As far as the practical application of metal-free and SiC-based electrocatalysts for the ORR is concerned, Wang and collaborators described the synthesis of a structural N-doped carbon/silicon carbide composite based on a nanoscale SiC core covered by a N-doped carbon shell. A nanoporous amorphous C layer was obtained from the acid etching of a nanocrystalline 3C-SiC powder, followed by its annealing in the presence of melanine (as C and N sources) under vacuum and high-temperature conditions.[720,721] The as-prepared composite was evaluated as a metal-free system in the electrocatalytic cathodic ORR showing high activity, stability, and resistance to alcohol crossover phenomena, typically responsible for the poisoning of Pt-based electrocatalysts in alcohol fuel cell devices.[720] Giambastiani, Pham-Huu, and co-workers came across similar conclusions by playing with SiC networks coated with a highly N-doped mesoporous carbon network grown through a simple soaking of the non-oxide samples in an aqueous solution of food-grade components followed by controlled drying/calcination/annealing treatments.[715] The choice of these authors of a SiC core instead of a more classical C-based nanocarrier for the catalytically active N-doped carbon shell was dictated by the superior resistance to electrochemical corrosion of the sp^3-bonded

network in the former with respect to the classical sp^2-bonded matrix in the latter.[722]

More recently, a Chinese team theoretically predicted the ability of SiC(111) to promote another challenging electrochemical process: molecular nitrogen reduction to NH_3. Starting from the known ability of boron to bind and activate N_2,[723] authors found that the polarized SiC(111) surface plays a similar dual donor−acceptor function with N_2, inducing its strong adsorption. Overall, adsorbed N_2 was found to be effectively reduced to ammonia on C-terminated SiC with low limiting potential values.[724]

4.1.5. Photochemical Processes with SiC-Based Metal-Free Catalysts.
Metal-free semiconductive photocatalysts include a series of nonmetal elements, such as carbon, silicon, nitrogen, and boron that have largely attracted the interest of the catalysis community.[725] Semiconductors of this type undergo less evident erosion phenomena and are cost-effective and sustainable materials for a relatively wide number of photocatalytic applications of relevance from an industrial viewpoint. Photogenerated electrons and holes in a semiconductor electrode can transfer to reactants in an electrolyte solution hence causing the photoassisted decomposition or synthesis of chemical compounds. Hereafter, we provide a comprehensive overview on the use of SiC networks as a metal-free semiconductor to be employed as a photoelectrode catalyst in two challenging processes: the CO_2 reduction to added value organic compounds and the hydrogen generation from water splitting reaction. An additional section dedicated to the photocatalytic degradation of organic pollutants will be also reported for the sake of completeness.

4.1.5.1. Photoassisted CO_2 Reduction Processes.
The Japanese team of Inoue and collaborators first reported on the excellent performance of photosensitive semiconductor powders, including SiC, for the photoelectrocatalytic reduction of CO_2 into variable reduction products (i.e. HCOOH, H_2CO, CH_3OH, and CH_4) starting from a water suspension of the plain powdery samples.[726] Their study highlighted that SiC photoexcitation provided methanol as the main CO_2 reduction product, with a productivity that was up to five times higher than that measured on other ultrapure semiconductors (WO_3, TiO_2, ZnO, CdS, GaP, and SiC) employed under identical conditions.

Many years later Gondal et al. came across similar conclusions by studying a laser-induced (355 nm) photocatalytic CO_2 reduction using commercially available 6H-SiC granules as a catalyst.[727] Most importantly, they got the highest photonic efficiency in methanol production with a complete process selectivity (100%) when the system was irradiated with a 355 nm wavelength UV laser with respect to the use of a xenon mercury (XeHg) broad band lamp as the light source. Indeed, with the latter, they found a reduced photonic efficiency and a selectivity as low as 50% of that obtained with the laser irradiation.[728] Kaci and co-workers reported later on the effects of SiC grain size and concentration on the ultimate photochemical conversion of CO_2 to MeOH under material UV light (365 nm) irradiation.[729]

In the same years, Wang et al. have also presented the use of microsized SiC granules recovered from silicon sludge wastes as effective photocatalysts for the CO_2 reduction and reductive coupling under UV−vis-IR irradiation (253−2000 nm) to afford HCOOH and CH_3COOH as main products, respectively.[730]
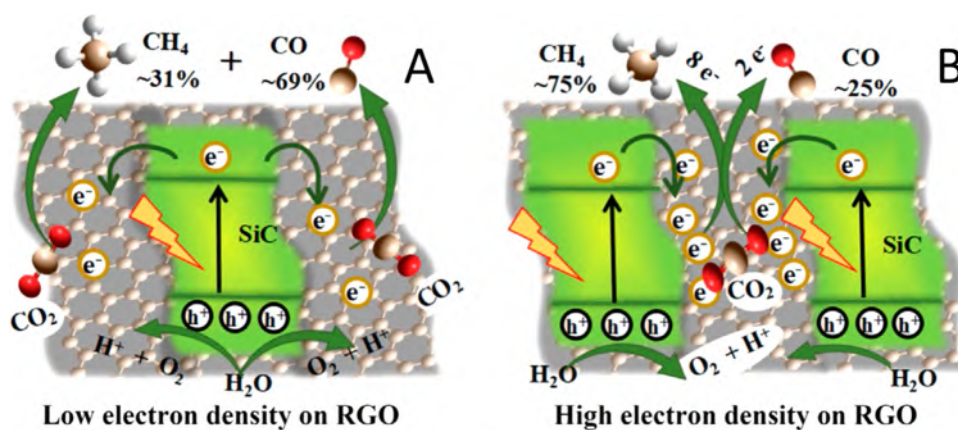
Figure 73. Photocatalytic generation of CH_4 or CO on samples with variable RGO heterojunction content. (A) Low electron density on RGO and (B) high electron density on RGO. Figures adapted with permission from ref 731. Copyright 2018 Wiley-VCH.

Wang and collaborators have described an interesting synthetic approach to the control of selectivity in SiC-based photoelectrocatalysts applied to CO_2 reduction.[731−733] They proposed the use of reduced graphene-oxide (RGO) as a sacrificial carbon template for the preparation of ultrathin SiC nanosheets (NSs) featured by high crystallinity and an intimate 2D/2D heterojunction with the C source. Their ultrathin SiC/RGO NSs allowed the fast transfer of photogenerated electrons from SiC to RGO thus resulting in an appreciable enhancement of the composite photocatalytic activity in CO_2 reduction as well as in preferential process selectivity toward CH_4. Such a high selectivity was basically ascribed to densely accumulated energetic electrons within RGO that foster the eight-electron process to occur while reducing the recombination of charge carriers. Most importantly, these authors realized that an appropriate balance of RGO in the SiC/RGO heterojunction was crucial for getting an effective catalyst for the CO_2-to-CH_4 conversion.[731] As Figure 73 shows, SiC/RGO heterojunctions were supposed to allow photogenerated electrons at SiC to quickly migrate on RGO for the subsequent CO_2 reduction step. However, a high RGO proportion in the SiC/RGO heterojunction would have shared sparse energetic electrons on RGO and favored the occurrence of a two-electron process mainly (CO generation). On the other hand, a low proportion of RGO would have translated in a dense accumulation of energetic electrons hence facilitating the eight-electron process to CH_4.

Very recently, the ability of metal-free SiC to reduce CO_2 to methane has been further investigated. While Lin theoretically predicted that the reaction is highly favored on the SiC(111) surface with respect to the hydroxylated counterpart,[734] Sun's group prepared 3C-SiC nanoparticles able to promote the CO_2 reaction with 90% methane selectivity.[735] They prepared their photocatalytic material on gram scale through powder ball-milling producing 3C-SiC NPs bearing an amorphous SiO_x outer shell and inducing abundant surface states. These latter are known to capture the photogenerated electrons thus avoiding charge recombination while silicon oxide preserves the 3C-SiC core from corrosion under visible light.

4.1.5.2. Photoassisted Water Splitting for H_2 Production. Photoelectrochemical properties of SiC have attracted the interest of scientists for a long time because of its unique electronic and chemicophysical properties.[736,737] Water splitting for hydrogen production is certainly one of the most studied processes also in light of developing sustainable and robust photocatalytic materials to be applied as metal-free systems to H_2 production. Moreover, the use of large band gap semiconductors like SiC makes clearer the distinction between valence (VB) and conduction (CB) bands whose gaps make these semiconductors chemically more stable than those featured by smaller band gaps.

In the early 1990s, Inowe and collaborators studied β-SiC powder without the deposition of any other metal or metal oxide species as a catalyst for the water decomposition under light irradiation.[610] These authors reported that hydrogen was produced at a constant rate from water upon the SiC exposure to a xenon lamp. They also found that photocatalytic activity started under material irradiation around 400 nm wavelength, and a drastic increase was observed around 350 nm. Several years later, Wang et al. came across similar conclusions by studying the photocatalytic water spilling promoted by visible-light-irradiated SiC fine powders.[738] They also found an important effect on the hydrogen productivity related to both the initial pH of the water solution (with an optimal productivity value reached at around pH = 12) and the addition of selected sacrificial reagents. Overall, different SiC polytypes 4H-, 6H-SiC and 3C-SiC have demonstrated band edge potentials suitable to split water under material light irradiation.[739,740]

A clear dependence of the H_2 production rate from the SiC surface properties and their morphology was described later from Guo and collaborators for a series of β-SiC samples in pure water and under visible-light irradiation.[741,742] The Chinese team demonstrated that an acid and oxidative treatment of β-SiC nanowires translated into more hydrophilic samples (compared to pristine materials) with a remarkable increase of the H_2 productivity in the water splitting.[741] They also argued on the role played by SiC morphology on their final photochemical performance. In a further contribution from this team, the authors compared three different SiC morphologies (whiskery, wormlike, and particulate) in the process and concluded the existence of a correlation between the specific surface areas of the samples, their morphology, and their hydrogen productivity in the water splitting.[742] She, Shi, and collaborators developed a synthetic protocol for the fabrication of oriented arrays of highly porous SiC NWs on silicon carriers by carbonization of the Si nanowire arrays. With their SiC nanowires featured with a high surface-to-volume ratio, the authors obtained highly stable and performing photocatalysts for the pure water splitting under UV
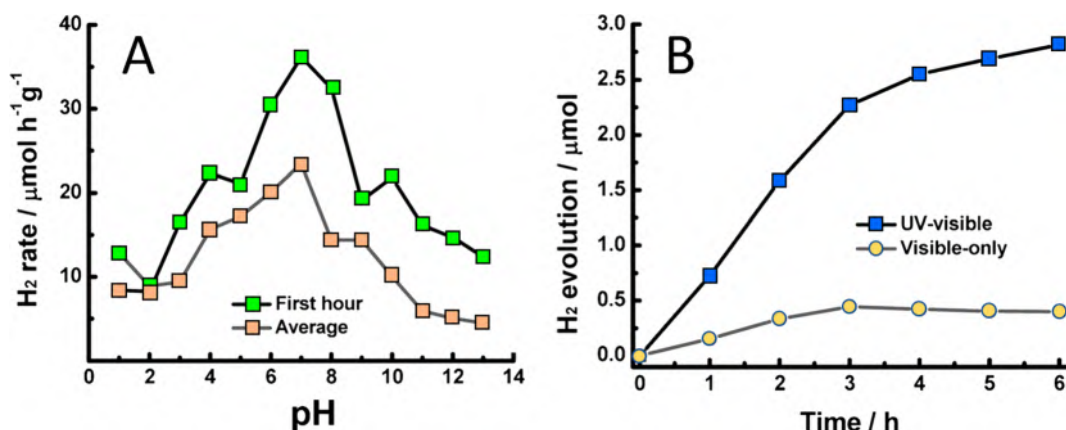
Figure 74. (A) pH dependence of the H_2 generation rate on SiC NPs within the first hour (■, green) and after 6 h (■, tan) on run (pH adjusted with HCl or NaOH). (B) H_2 generation using SiC nanoparticles under UV−visible light (■, blue) and visible light (●, yellow) from the simulated sunlight. Experimental conditions: 20.0 mg of SiC nanoparticles, 100 mL of pure water, 150 W Xe lamp solar simulator. Adapted with permission from ref 632. Copyright 2014 Wiley-VCH.
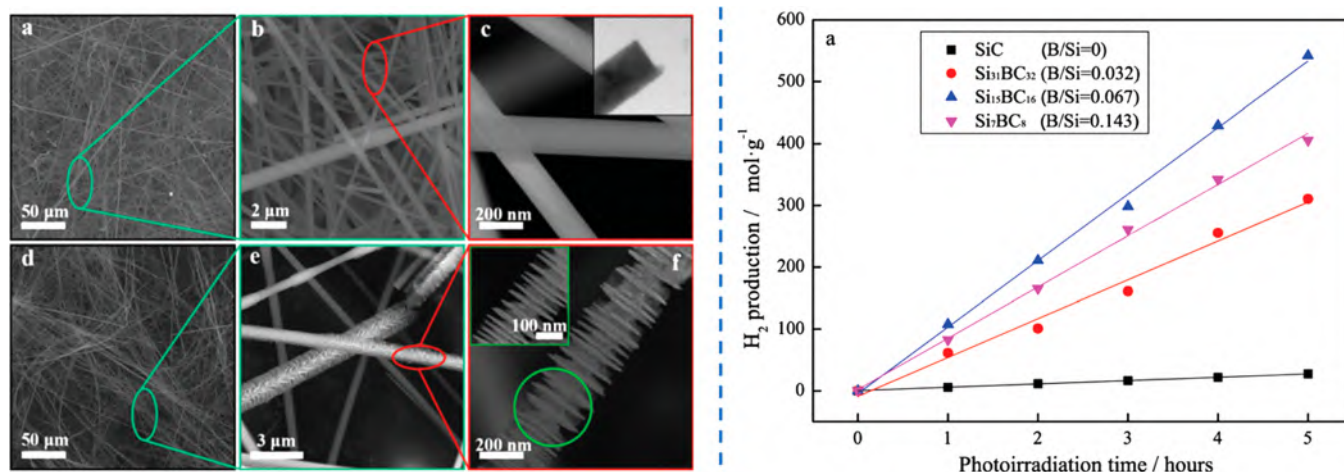
Figure 75. Left) SEM images of 3C-SiC (a−c) and B-doped 3C-SiC (b−d) samples recorded at different magnifications. Right) Photocatalytic hydrogen evolution performance over 3C-SiC and B_xSiC samples in comparison. Figures reproduced with permission from ref 751. Copyright 2015 The Royal Society of Chemistry.

irradiation.[743] Sun and co-workers more recently found that a preferential exposure of SiC carbon-face is detrimental for the process due to a substantial energy loss related to proton transfer. On the other hand, the preferential exposure of silicon favors the O−H bond breaking with a facile proton exchange thus improving the photocatalytic water oxidation activity.[744]

Partially in contrast with previous studies on the topic, Chen and collaborators have recently reported on the photocatalytic hydrogen generation of commercial β-SiC NPs in pure water, under simulated solar light irradiation with and without the assistance of sacrificial reagents or precious metal co-catalysts.[632] Their conclusions showed that SiC nanoparticles displayed the higher efficiency in hydrogen generation when the process was operated in pure and neutral water (Figure 74A). Moreover, both ultraviolet (UV) and visible-light regions were suitable to promote H_2 evolution on these NPs although a large part of their photocatalytic activity resulted from UV-light absorption (Figure 74B). Notably, the addition of sacrificial reagents (*i.e.* methanol) or the SiC surface decoration with Pt NPs resulted in any case into a decrease of the semiconductors photocatalytic activity.

Many efforts have been devoted during the past decade to the generation of hybrid 2D-2D or 1D-1D SiC-C-based composites featuring intimate heterojunctions for an enhanced separation of SiC photogenerated holes and electrons together with an increase of the composite visible-light absorption. Guo and co-workers reported on the synthesis of SiC-graphene composites by the simple chemical grafting between the properly amine-functionalized SiC sample and graphene-oxide (GO) followed by material reduction at 500 °C under a H_2 atmosphere.[745] In this way, the authors demonstrated the superior performance of their composite in the photocatalytic water splitting under visible-light irradiation. Indeed, the strong heterojunction at the interface between the two nanomaterials was supposed to facilitate the quick transfer of photogenerated electrons from SiC to graphene hence suppressing or strongly reducing their recombination with holes and accelerating reactions. Yuan and collaborators made use of a GO/SiC composite as a photocatalyst under visible-light irradiation for the simultaneous H_2 production and GO reduction.[746] As for the case reported above, heterojunction between the two materials was claimed to have a beneficial effect on the process with reduced-GO serving as an electron collector and

transporter to lengthen the lifetime of the charge carriers effectively. Graphite paper-supported 3C-SiC nanowire film was proposed by Chen as a promising electrode material for the production of high energy-storage devices and catalytic photoelectrodes for water splitting.[747] In the same years, Li, Feng, Li et al. demonstrated that the photocatalytic properties of a series of SiC-graphene sheets (SiC-GSs) composites to be applied as photocatalysts for the H_2 production were significantly affected by the morphology of the SiC active phase.[748] In accord with previous studies, they concluded that the enhanced photocatalytic activity of hybrid SiC-graphene composites was related to the crystallinity of the SiC phase, the composite specific surface area, its light-absorption capacity, and the nature of the intimate Schottky-type heterojunction between the conducting C phase and the SiC semiconducting one. The same team also reported on the preparation of 1D-1D hybrid composites by reacting multiwalled carbon nanotubes and silicon powder.[749] The crystalline MWCNT-SiC composite was studied in turn as a photocatalyst for H_2 production under visible-light irradiation and in the presence of sacrificial reagents showing enhanced photocatalytic activity due to the unique 1D-1D heterojunctions between the two phases and the increased visible-light absorption of the composite.

Following a similar concept, a novel organic–inorganic composite prepared from a net-like SiC nanowires framework and the conjugated poly(3,4-ethylenedioxythiophene) poly-(styrenesulfonate) copolymer (PEDOT/PSS) has been reported by Chen and Tang.[750] These authors referred to the photocatalytic properties of their composite and its improved H_2 production rate in solar water splitting basically ascribed to the efficient carriers separation of the PEDOT/PSS as a hole-transporting copolymer. Hou and collaborators described the straightforward preparation of B-doped 3C-SiC nanowires with a different B/Si ratio.[751] Using the carbothermal reduction method, they obtained originally shaped crystalline and finned microstructured nanowires with fins of about 100–200 nm in diameter and 10–20 nm in thickness (Figure 75 left). The authors proved the superior performance of their B-doped 3C-SiC NWs in the light-promoted H_2 production with respect to their undoped counterpart (3C-SiC) (Figure 75 right) and attributed the observed trend to combined effects such as the single crystalline nature and the properly tuned electronic structure of the B-doped networks as well as their finned-like morphology.[751] Yang replaced boron with nitrogen preparing N-doped 3C-SiC powder via single-step combustion.[752] The authors found that nitrogen insertion highly influences the photocatalytic activity doubling the hydrogen production rate with respect to bare SiC. In particular, nitrogen is claimed to tune band gap and form donor levels for trapping holes thus achieving low charge recombination rates and higher photocatalytic activity.

In the same years, Chen, Guo, and co-workers have pointed out the relevance of intrinsic properties of graphene in graphene/SiC composites to be applied as efficient photocatalysts for H_2 evolution.[753] Accordingly, epitaxially grown high-quality graphene layers were prepared on a 6H-SiC powder,[754] and the unique photocatalytic properties of the resulting composite were ascribed to the perfect graphene/SiC heterojunction in their core–shell structured particles. Indeed, the authors claimed that such an ideal graphene/SiC interphase allowed two inverse energy band configurations of

the Schottky to be created, which would serve as the transfer channels for photogenerated electrons and holes on the single core–shell particle.[753]

Wang, Lei, and co-workers have also proposed the synthesis of nanofibers constituted by a graphitic carbon core embedded in a mesoporous SiC network as valuable water splitting photocatalytic materials to be operated under both simulated solar and visible-light irradiation and in high-pH solution.[755] While the carbon core allowed the fast transfer of SiC photogenerated electrons and improved the material light absorption, hydroxyl anions from the alkaline environment simultaneously accelerated the hole trapping. Overall, their hybrid and metal-free composite resulted in an improvement of the photocatalytic activity in the process similarly to related outcomes presented later independently by Huang's[756] and Gondal's[757] groups. These authors reported on the superior photocatalytic performance of a graphitic carbon nitride (g-C_3N_4)/SiC composite prepared at a different SiC mass ratio by growing g-C_3N_4 directly at the SiC surface. The intimate and strong connection realized between g-C_3N_4 and SiC semiconductors, also favored by well-matched materials band positions, gave rise to a highly stable photocatalyst with improved H_2 productivity upon material exposure to visible-light irradiation. They concluded that the improved performance of g-C_3N_4/SiC was ascribed to the combined effect of the enhanced separation of photogenerated carriers along with the increased hydrophilic character of the composite.[756]

Han, Smith, and Smets chose hydrogenated amorphous silicon carbide (a-SiC:H) for developing a cost-effective and earth abundant photocatalytic material for hydrogen production.[758] a-SiC:H offers an easily tunable band gap and can be exploited as a photocathode for water splitting, but it suffers from low charge carrier separation efficiency and high overpotential values. The authors tried to tackle these main issues adopting different strategies. First, they introduced variable amounts of a boron dopant that were found to enhance the charge carrier collection, and then they integrated a-SiC:H with thin-film silicon photovoltaic junctions that were allowed to reach an anodic shift of overpotential values. In addition, the introduction of glass substrates with integrated microtextured photonic structures increased the material light collection efficiency. Overall, the as-prepared a-SiC:H-based photocathode was able to reach a photocurrent density of −5.1 mA cm^{-2} at 0 V vs RHE with a 2.1% photocathode efficiency.[758]

4.1.5.3. Photoassisted Degradation of Organic Pollutants. Photocatalysis also lists important environmental- and health-related applications in rapidly developing fields such as the treatment of liquid or gaseous effluents for the mineralization of organic pollutants or the disinfection of water and air. Nowadays, natural sunlight- or artificial light irradiated semiconductors for photocatalysis is one of the most promising environmental remediation tools. Among semiconductors, SiC represents a third-generation material with excellent properties that make it a promising photocatalyst to be used as such or in the form of metal-free composites for addressing conveniently several environmental concerns.

Zhang and co-workers first reported on the photodegradation of gaseous acetaldehyde (CH_3CHO) accompanied by the generation of CO_2, using UV-irradiated single-crystal β-SiC nanowires coated with an amorphous SiO_2 layer.[759] In the next series of metal-free photocatalysts applied to the mineralization of organic pollutants, Guo, Chen et al.
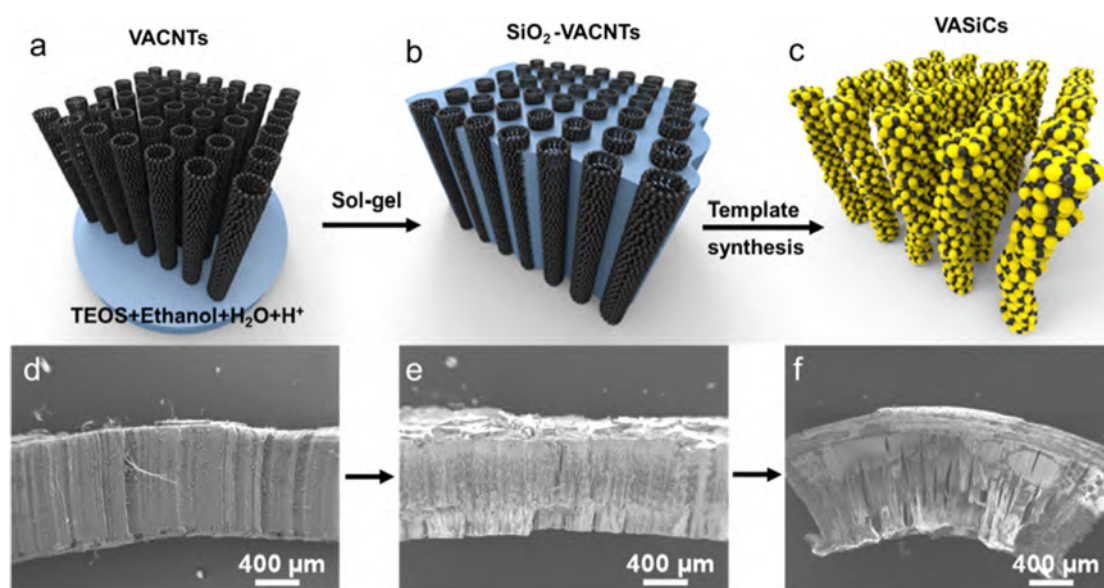
Figure 76. Schematic representation of VASiC NWs synthesis from a VACNT template. Reproduced with permission from ref 763. Copyright 2017 Elsevier B.V.

described the largely beneficial effects rising from functional graphene/SiC heterojunctions on the ultimate photodegradation performance of their composite.[760] Graphene-coated SiC nanoparticles exhibited up to a 100% increase in the photodegradation of Rhodamine B (Rh-B) under UV illumination with respect to the pristine SiC powder. The UK team of Hong and Grober argued on the superior electronic and mass transfer properties of uniformly aligned one-dimensional nanomaterials in energy[761,762] and environmental applications while preparing vertically aligned silicon carbide (VASiC) nanowire arrays to be employed as photocatalysts for the highly efficient Rhodamine B decomposition.[763] As shown in Figure 76, VASiC NWs were prepared from SiO$_2$ infiltrated vertically aligned multiwall carbon nanotubes (VACNTs) and Si powder by template synthesis at 1350 °C under inert atmosphere, followed by calcination at 900 °C in air. VASiC NWs possessed cubic crystal structure and showed strong light absorbance in the UV−vis range. Besides presenting good stability and recyclability in photocatalysis, they also showed remarkable photocatalytic degradation activity of Rh-B under UV−vis or visible-light irradiation without the addition of any co-catalyst.[763]

3C-SiC hierarchical nanowires with finned microstructure[764] and SiC hollow spheres[765] have been independently prepared by two Chinese teams and reported as photocatalysts with enhanced activity in the photodegradation of methylene blue (MB) as a pollutant in aqueous solutions under visible-light irradiation. In both cases, the presence of a surface SiO$_2$ layer was supposed to enhance the material catalytic performance by improving the light absorption and conversion efficiency, reducing electron−hole recombination and improving the nanowires hydrophilic character.[764,765]

Cao and co-workers have recently reported on the promising application of commercial SiC powder in the photocatalytic ozonation for the wastewater treatment and for the challenging mineralization of organic pollutants such as oxalic acid, *p*-hydroxybenzoic acid, and Penicillin G.[766] The moderate SiC photocatalytic degradation activity toward these pollutants together with its equally poor catalytic ozonation performance

was largely outperformed by the photocatalytic ozonation because of the very high CB position in this semiconductor. Indeed, the high efficiency of the photocatalytic ozonation promoted by SiC was ascribed to the ability of photogenerated electrons to reduce ozone and oxygen with the formation of free hydroxyl radicals as the main players in the degradation of organic pollutants.[766]

A series of SiC composites with graphitic carbon nitride (g-C$_3$N$_4$) were developed independently by different research groups and demonstrated to be highly efficient in the photodegradation of organic pollutants from wastewater.[767−770] The created heterojunction favors charge carrier transfer and separation thus providing longer carrier lifetimes and ultimately improving not only the composite photodegradation activity toward methyl orange (MO),[767,768] Rhodamine B (Rh-B),[768,770] and methylene blue[769] (MB) but also antibacterial activity.[769] Habibi-Yangjeh and co-workers prepared a ternary metal-free composite where carbon dots were added to SiC/g-C$_3$N$_4$ finding an improved visible-light adsorption, charge separation, and enhanced photodegradation activity of MB, Rh-B, fuchsine, and Congo red (CR).[771]

Finally, SiC-based composites were found to be active in photocatalytic dehalogenation. In particular, p-n SiC heterojunctions were proven to boost 98% of bromide release from brominated acetic acid and chloride formation from tri- and dichloroacetic acid.[772] More recently, Niu and co-workers designed a SiC/graphene hybrid able to decompose perfluorooctanoic acid under visible light. Electrons photogenerated on SiC are transferred to perfluoroalkyl groups exploiting conductivity of graphene and boosting the defluorination process.[773]

5. CONCLUDING REMARKS AND FUTURE PERSPECTIVES

The last decades have witnessed a steady increase of literature reports dedicated to the design of SiC-based catalysts, developing a portfolio covering a wide range of well-controlled porous structures with tailored surface properties. At the same

time, the benefits rising from the use of this non-oxide material have been demonstrated in several reactions, taking advantage of an unmatched combination of chemicophysical and morphological properties: stability under harsh chemical environments, chemical inertness, good thermal conductivity, and tunable surface chemistry as well as semiconductive nature. Although non-porous or macroporous SiC materials have been available on the market for a long time, their low specific surface area (usually <1 m^2/g) has deeply limited their industrial applications in catalysis. The production of SiC with high surface area on an industrial scale has taken more than a while, but its wide exploitation as support of heterogeneous catalysts has already started to become a reality.

The growing interest of the scientific community for high surface area SiCs and their composites has deeply contributed to boost their development and application in a series of challenging catalytic transformations. Numerous experimental evidence have shown that economically affordable process intensification in selected and highly demanding catalytic transformations is now possible with these materials. The industrial efficiency of SiC-based catalysts has been proven in process units where they ensure significant technical and economic benefits. This review describes the benefits of porous SiC matrices in the world of heterogeneous catalysis. It would like to take the readership across an inspiring "journey" on the broad potential of SiC networks, moving from their discovery to the modern applications in industrially relevant catalytic transformations.

The excellent thermal conductivity, chemical inertness, and mechanical resistance are certainly among the most striking features of these macro- and mesoporous samples, nowadays produced as hierarchically structured networks with controlled shape and size. Well-defined geometries combined with extended mechanical strength ensure stable and homogeneous distributions of the catalytic packing and pressure drop in fixed-bed reactors. Macroporosity avoids diffusional limitations of the kinetics, and mesoporosity allows high specific surface area and good metal active-phase dispersions. In addition, the good thermal conductivity of SiC mitigates the generation of temperature gradients within the reactor and local hotspots, improving the catalyst lifetime and its performance.

Despite SiC-based catalysts having been studied in the academic community for decades, there are several features that remain poorly exploited in catalysis or even unexplored at present:

- Chemical and mechanical resistance even under harsh and oxidizing environmental conditions.

- Medium thermal conductivity that prevents the generation of temperature gradients and hotspots in the catalytic bed with large benefits for the process performance and catalyst lifetime.

- The possibility to exploit less conventional heating schemes (*e.g.* microwaves) where SiC acts as an electromagnetic susceptor for the direct heat generation at the catalytic bed. Alternative non-contact heating techniques hold important implications on the catalytic performance and their rational exploitation is one of the emerging trends in contemporary heterogeneous catalysis.

- The easy and low-cost separation of the carrier from the catalyst active phase with the recovery and reuse of both at the end of the catalyst lifetime. Under this perspective,

SiC is a promising choice for the design of more sustainable catalytic processes.

- Semiconductive properties that open new horizons in photocatalysis, where the role of SiC is supposed to go largely beyond that of an innocent active-phase carrier.

- Properties and distributions of silicon and carbon vacancies on the surface of SiC, which play important roles for anchoring catalytically active components (usually nanoparticles of metals or metal oxides).

- Charge transferring between SiC and the catalytically active components supported on SiC, because the transferring would influence the reduction of SiC-supported oxides as well as the catalytic activity of metallic components, and produce new active regions on the surface of SiC.

- New *in situ* methods to characterize the adsorption of reactant molecules on SiC-based catalysts. For example, SiC materials have strong infrared absorption/emission characteristics, and these characteristics would cover the infrared signals of some adsorbed molecules; therefore, it is necessary to develop new *in situ* characterizations.

- Theoretical investigations, in particular *ab initio* and molecular dynamics studies, highlighting the role of SiC support in catalysis. In particular, mechanistic studies on reactant molecules adsorption modes, electronic transfer from SiC to active phases, and peculiar photo(electro)-chemical SiC intrinsic properties should be further investigated.

- Development of further synthetic protocols able to produce porous SiC materials with tailored morphological properties for target catalytic applications.

The variety of catalytic reactions reviewed in this contribution leaves little doubt on the answer to the question posed in our title. Our readers will draw their own conclusions on the importance of this non-oxide material in catalysis and its potentiality in catalytic processes to come.

After more than two decades of use of SiC in heterogeneous catalysis, the development of novel synthetic methodologies, and unexplored applications of these functional materials in various branches of catalysis, the search for more robust, cost-effective, and durable catalysts continues onward. This is also the result of a fruitful cooperation between tireless scientists engaged in the improvement of their catalytic processes and industrial producers or material developers who synthesize new functional SiCs with morphologies tailored for specific catalytic applications. The virtuous link between materials producers, catalysts manufacturers, and end users will invariably translate into a growing SiC demand already in the near future.

AUTHOR INFORMATION

Corresponding Authors

Giuliano Giambastiani − *Institute of Chemistry of OrganoMetallic Compounds, ICCOM-CNR and Consorzio INSTM, 50019 Florence, Italy; Institute of Chemistry and Processes for Energy, Environment and Health (ICPEES), ECPM, UMR 7515 of the CNRS-University of Strasbourg, 67087 Strasbourg, France;* ⊙ orcid.org/0000-0002-0315-3286; Email: giuliano.giambastiani@iccom.cnr.it, giambastiani@unistra.fr

Yuefeng Liu − *Dalian National Laboratory for Clean Energy (DNL), Dalian Institute of Chemical Physics, Chinese*

Academy of Sciences, 116023 Dalian, China; ◉ orcid.org/
0000-0001-9823-3811; Email: yuefeng.liu@dicp.ac.cn

Xiangyun Guo − *School of Petrochemical Engineering,
Changzhou University, Changzhou 213164, China;*
Email: xyguo@cczu.edu.cn

Cuong Pham-Huu − *Institute of Chemistry and Processes for
Energy, Environment and Health (ICPEES), ECPM, UMR
7515 of the CNRS-University of Strasbourg, 67087
Strasbourg, France;* Email: cuong.pham-huu@unistra.fr

Authors

Giulia Tuci − *Institute of Chemistry of OrganoMetallic
Compounds, ICCOM-CNR and Consorzio INSTM, 50019
Florence, Italy;* ◉ orcid.org/0000-0002-3411-989X

Andrea Rossin − *Institute of Chemistry of OrganoMetallic
Compounds, ICCOM-CNR and Consorzio INSTM, 50019
Florence, Italy;* ◉ orcid.org/0000-0002-1283-2803

Charlotte Pham − *SICAT SARL, 67000 Strasbourg, France*

Complete contact information is available at:
https://pubs.acs.org/10.1021/acs.chemrev.1c00269

Author Contributions

#G.T. and Y.L. contributed equally to the manuscript.

Notes

The authors declare the following competing financial interest(s): C.P. declares a financial interest in SiCAT SARL, a company that produces and commercializes silicon carbide samples.

Biographies

Giulia Tuci graduated *cum laude* in Chemistry in 2010 at the University of Pisa and received her Ph.D. in Chemical Science in 2015 from the University of Florence under the supervision of Dr. Giuliano Giambastiani. Since 2018, she holds a Researcher permanent position at the Institute of Chemistry of OrganoMetallic Compounds of the Italian National Research Council (ICCOM-CNR). Her current scientific activity mainly deals with the design and synthesis of novel technologically advanced materials for their exploitation in heterogeneous catalysis in the field of renewable energy technology, CO_2 capture and conversion, and for application in industrially relevant processes. She is the author of more than 60 scientific contributions in peer-reviewed journals (communications, full papers, and review articles) and 1 book chapter, and she has presented her scientific activity in more than 20 international congresses.

Yuefeng Liu received his Ph.D. degree in 2013 from the University of Strasbourg under the supervision of Dr. C. Pham-Huu and then performed his 2-year postdoctoral research at the Institute of Chemical and Processes for Energy, Environment and Health (ICPEES, UMR 7515 CNRS-University of Strasbourg). After a short stay at the Institute of Metal Research, Chinese Academy of Sciences (CAS), he is now an associate professor at the Dalian Institute of Chemical Physics, CAS. His research interests deal with the heterogeneous catalysis, environmental TEM, and the preparation and characterization of hybrid carbon nanomaterials (*i.e.* carbon nanotubes, graphene, and nanodiamond) and carbide-based catalysts for the application in clean energy and sustainable chemistry. He is author of more than 80 scientific papers in peer-reviewed journals.

Andrea Rossin received his Ph.D. in chemistry from Cardiff University (Wales, UK). After postdoctoral training at the UAB (Barcelona, Spain) in 2005, he moved to Florence to join the Institute of Chemistry of OrganoMetallic Compounds (ICCOM-CNR) in 2006

where he became permanent researcher in 2010. Since 2021 he holds the position of Senior Researcher in the same institute. His research interests are manifold: synthesis and characterization of metal−organic frameworks and coordination polymers, along with their applications in H_2/CO_2 adsorption, luminescence, magnetism, and heterogeneous catalysis; reactivity studies of ammonia−borane and amino−boranes as chemical hydrogen storage materials with transition-metal organometallics; and synthesis and reactivity studies of transition-metal hydrides. He is the author of more than 100 scientific papers and 1 book chapter on the topic of hydrogen.

Xiangyun Guo is now a professor at the School of Petrochemical Engineering in Changzhou University. He received his first degree from Peking University in 1990 and his Ph.D degree from the Institute of Coal Chemistry, Chinese Academy of Sciences (CAS) in 1996. Afterwards, he was awarded an Alexander von Humboldt Fellowship and went to Hamburg University of Technology for a research stay and then went to the University of Orleans for postdoc research. In 2001, he was chosen as a selectee of the Hundred-Talent Program (CAS) and promoted to a full professor position at the Institute of Coal Chemistry (CAS). In 2018, he moved to the present university. His research activity is mainly focused on the mass production and catalytic application of high surface area SiC material, and he has authored more than 150 scientific contributions in peer-reviewed journals.

Charlotte Pham is Research Director at SICAT SARL. After spending 10 years at ELF ATOCHEM and ATOFINA in the development of catalysts and catalytic processes, she joined SICAT when the company was just created with the goal to bring high surface area silicon carbides to the market. There, she led the scale-up of the production processes and diversified the SiC-based portfolio to answer specific features needed for the catalyst market. She has also designed and brought to commercial production a range of new porous carbon materials with high mesoporous volumes combined with an extended mechanical strength for well controlled pellet geometries. In parallel, she is permanently involved in several collaborations with both academic and industrial partners, including projects for noncatalytic uses of silicon carbide and carbon materials. She is the inventor of 22 international patents and an author of more than 30 scientific papers in peer-reviewed journals.

Giuliano Giambastiani is Research Director at the Institute of Chemistry of OrganoMetallic Compounds of the Italian National Research Council − ICCOM-CNR, and since 2018, he has held the same position at the Institut de chimie et procédés pour l'énergie, l'environnement et la santé (ICPEES) of the CNRS-University of Strasbourg (France) as a Laureate of the international call of the French presidency "*Make our Planet Great Again*". Among his honors, in 2016, he was awarded from the Chinese Academy of Sciences with the *Lee Hsun Research Award* on Materials Science in recognition of his contribution to material science and technology. His current scientific activity deals with catalysis (homogeneous and heterogeneous) and the preparation and characterization of technologically advanced catalytic materials and composites for processes at the heart of renewable energy technology. He is the author of more than 170 scientific contributions (communications, full papers, and reviews) in peer-reviewed journals, 3 books, 7 book chapters, and 14 patents (8 with international application−WO).

Cuong Pham-Huu obtained his Ph.D. in the group of Dr. Marc-Jacques Ledoux (catalytic processes and materials) in 1991. At present, he is the Research Director at the CNRS and a scientific member of the Institute of Chemistry and Processes for Energy, Environment and Health (ICPEES) of the CNRS. His research field is

focused on the synthesis of 1D and 2D carbon-based materials and silicon carbide along with hierarchical composites for use in the fields of energy and environment. He has received the CNRS Excellent Scientific award (2011) and the Lee Hsun Research Award on Materials Science from the Institute of Metal Research, Chinese Academy of Sciences (2015). He has (co)authored over 300 peer-reviewed scientific publications and about 50 patents with more than 15,000 citations (https://scholar.google.fr/citations?user=t-7F8s4AAAAJ&hl=fr).

ACKNOWLEDGMENTS

ABBREVIATIONS

4-ABS	4-aminobenzenesulfonic acid
4-CBA	4-carboxybenzaldehyde
AAL	acetaldehyde
AB	ammonia borane
ABD	atomic beam deposition
AC	activated carbon
ACR	acrolein
ADT	accelerated durability test
AHPCS	allylhydridopolycarbosilane
ALD	atom layer deposition
AOP	advanced oxidation processes
a-SiC	amorphous SiC
ATP	Attapulgite
β-SiC$_o$	preoxidized β-SiC
BA	benzylamine
BAL	benzaldehyde
BDO	1,4-butane-diol
BED	2-butene-1,4-diol
bioSiC	biomorphic SiC
BN	benzonitrile
BOL	benzyl alcohol
BTX	benzene, toluene, and xylene
BYD	2-butyne-1,4-diol
CAL	cinnamaldehyde
CatPOx	catalytic partial oxidation
CA$_x$	calcium aluminate
CB	conduction band
CCU	carbon capture and utilization
CDC	carbide-derived carbon
CHC	catalytic H$_2$ combustion
CNFs	carbon nanofibers
CNTs	carbon nanotubes
COL	cinnamyl alcohol
CR	Congo red
CRT	continuously regeneration trap
CSCR	combined steam and CO$_2$ reforming
CSTR	continuous stirred-tank reactor
CV	cyclic voltammetry
CVD	chemical vapor deposition
CVI	chemical vapor infiltration
CWPO	catalytic wet peroxide oxidation
DBA	dibenzylamine
DC	direct current
DDH	direct dehydrogenation
DF	direct foaming
DFT	density functional theory
DH	dehydrogenation
DMC	dimethyl carbonate
DME	dimethyl ether
DMFCs	direct methanol fuel cells
DP	deposition-precipitation method
DPF	diesel particulate filter
DR	dry reforming
DRM	dry methane reforming
EB	ethylbenzene
ECSA	electrochemical surface area
EG	encapsulated graphite
EISA	evaporation-induced self-assembly
FAL	furfural
FCs	fuel cells
FFR	feed flow rate
FOL	furfuryl alcohol
FTO	Fischer–Tropsch to olefins
FTS	Fischer–Tropsch synthesis
GC	glassy-carbon
GHSV	gas hourly space velocity
GO	graphene oxide
GSs	graphene sheets
GVL	γ-valerolactone
GWP	global warming potential
HC	hydrocarbons
HCAL	hydrocinnamaldehyde
HCOL	hydrocinnamyl alcohol
HDO	hydrodeoxygenation
HDS	hydrodesulfurization
HER	hydrogen evolution reaction
HFCs	hydrofluorocarbons
HFOs	hydrofluoroolefins
HRTEM	high resolution transmission electron microscopy
HSNC	hollow spheres nanochain
IPCE	incident photon-to-current efficiency
ITY	iron time yield
IWI	incipient wetness impregnation
LA	levulinic acid
LED	light-emitting diode
LPCE	liquid-phase catalytic exchange
LPCVD	low pressure chemical vapor deposition
LSPR	localized surface plasmon resonance
m-SiC	microsized SiC
MA	maleic anhydride
MB	methylene blue
MDA	methane dehydroaromatization
MEAs	membrane electrode assemblies
MEK	methylethylketone

MG	malachite green
MO	methyl orange
MOR	methanol oxidation reaction
MSR	methane steam reforming
MTG	methanol-to-gasoline
MTO	methanol-to-olefins
MTP	methanol-to-propylene
MW	microwave
MWCNT	multiwall carbon nanotubes
NDs	nanodiamonds
NGVs	natural gas vehicles
NWs	nanowires
nH-SiC	hexagonal SiC
NMC	nitrogen-rich mesoporous carbon
NOM	natural organic matter
NOR	Norfloxacin
nR-SiC	rhombohedral SiC
NPs	nanoparticles
n-SiC	nanosized SiC
NSs	nanosheets
OCF	open-cell foam
OCM	oxidative coupling of methane
ODH	oxidative dehydrogenation
ODS	oxidative desulfurization
OER	oxygen evolution reaction
OMC	ordered mesoporous carbon
ORR	oxygen reduction reaction
P/E	propylene to ethylene
P2G	power-to-gas
PAHs	polycyclic aromatic hydrocarbons
PCS	polycarbosilane
PCT	precipitation method
PEDOT	poly(3,4-ethylenedioxythiophene)
PEMFCs	polymer electrolyte membrane fuel cells
PGM	platinum group metals
PNP	p-nitrophenol
PODH	propane oxidative dehydrogenation
POM	partial oxidation of methane
PS	partial sintering
PSD	plasma sputtering deposition
p-SiC	p-type SiC
PSR	platelet structured milli-reactor
PSS	poly(styrenesulfonate)
PTFE	polytetrafluoroethylene
PVC	polyvinyl chloride
QDs	quantum dots
RDS	rate-determining step
RGO	reduced graphene-oxide
Rh-B	Rhodamine B
RM	replica method
ROS	reactive oxygen species
rWGS	reverse water−gas-shift
s.m.	suspension method
SCR	selective catalytic reduction
SE	styrene
SEM	scanning electron microscopy
SF-SiO$_2$	silica fume
SG	sol−gel
SiCNTs	silicon carbide nanotubes
SiC-OM	ordered mesoporous SiC
SLP	supported liquid phase
SMS	shape-memory synthesis
SNG	synthetic natural gas

SNW	SiC nanowhiskers
SOFCs	solid oxide fuel cells
SR	steam reforming
SRP	propane steam reforming
SSA	specific surface area
s-SWCNT	semiconducting single-wall carbon nanotubes
ST	sacrificial template
STY	space-time yield
TEA	triethylamine
TEAOH	tetraethylammonium hydroxide
TEM	transition electron microscopy
TEOS	tetraethoxysilane
TES	tetraethylorthosilicate
TOC	total organic carbon
TOF	turnover frequency
TOS	time on stream
TPABr	tetrapropylammonium bromide
TPAOH	tetrapropylammonium hydroxide
TPO	temperature-programmed oxidation
TUD	TU Delft
UV	ultraviolet
VA	vertically aligned
VACNTs	vertically aligned multiwall carbon nanotubes
VASiC	vertically aligned silicon carbide
VB	valence band
VCM	vinyl chloride monomers
VOCs	volatile organic compounds
VPO	vanadyl pyrophosphate
VPT	vapor-phase transport
w.i.	wet impregnation
WD	water detritiation
WGMR	water to glycerol molar ratio
WGS	water−gas shift
WHSV	weight hourly space velocity
YSZ	yttria-stabilized zirconia
ZFS	$ZnFe_2O_4$-α-Fe_2O_3/SiC foam

REFERENCES

(1) Ertl, G.; Knözinger, H.; Schüth, F.; Weitkamp, J. *Handbook of Heterogeneous Catalysis*, 2nd ed.; Wiley-VCH: Weinheim, Germany, 2008, DOI: 10.1002/9783527610044.

(2) Thomas, J. M.; Thomas, W. J. *Principles and Practice of Heterogeneous Catalysis*, 2nd ed.; Wiley-VCH: Weinheim, Germany, 2014; p 744.

(3) Chorkendorff, I.; Niemantsverdriet, J. W. *Concepts of Modern Catalysis and Kinetics*, 3rd ed.; Wiley-VCH Verlag GmbH & Co.: 2007; p 524.

(4) van Santen, R., Catalysis in Perspective: Historic Review. In *Catalysis: From Principles to Applications*, 1st ed.; Beller, M., Renken, A., van Santen, R., Eds.; Wiley-VCH Verlag GmbH & Co.: 2012; p 642.

(5) Farrauto, R. J.; Bartholomew, C. H. *Fundamentals of Industrial Catalytic Processes*, 1st ed.; Blackie Academic and Professional: 1997; p 58.

(6) Munnik, P.; de Jongh, P. E.; de Jong, K. P. Recent Developments in the Synthesis of Supported Catalysts. *Chem. Rev.* **2015**, *115*, 6687−6718.

(7) Pérez-Mayoral, E.; Calvino-Casilda, V.; Soriano, E. Metal-Supported Carbon-Based Materials: Opportunities and Challenges in the Synthesis of Valuable Products. *Catal. Sci. Technol.* **2016**, *6*, 1265−1291.

(8) Lam, E.; Luong, J. H. T. Carbon Materials as Catalyst Supports and Catalysts in the Transformation of Biomass to Fuels and Chemicals. *ACS Catal.* **2014**, *4*, 3393−3410.

(9) Liu, L.; Zhu, Y.-P.; Su, M.; Yuan, Z.-Y. Metal-Free Carbonaceous Materials as Promising Heterogeneous Catalysts. *ChemCatChem* **2015**, *7*, 2765−2787.

(10) Zhang, P.; Zhu, H.; Dai, S. Porous Carbon Supports: Recent Advances with Various Morphologies and Compositions. *ChemCatChem* **2015**, *7*, 2788−2805.

(11) Serp, P.; Machado, B. *Nanostructured Carbon Materials for Catalysis*; Royal Society of Chemistry: 2015; pp 1−45, DOI: 10.1039/9781782622567-00001.

(12) Benaddi, H.; Bandosz, T. J.; Jagiello, J.; Schwarz, J. A.; Rouzaud, J. N.; Legras, D.; Beguin, F. Surface Functionality and Porosity of Activated Carbons Obtained from Chemical Activation of Wood. *Carbon* **2000**, *38*, 669−674.

(13) Rezma, S.; Birot, M.; Hafiane, A.; Deleuze, H. Physically Activated Microporous Carbon from a New Biomass Source: Date Palm Petioles. *C. R. Chim.* **2017**, *20*, 881−887.

(14) Lenz e Silva, G.; Viana, C.; Domingues, D.; Vieira, F. *Risk Assessment and Health, Safety, and Environmental Management of Carbon Nanomaterials*; IntechOpen: 2020; p 1−21, DOI: 10.5772/intechopen.85485.

(15) A mesoporous carbon support combining high purity, well controlled macroscopic shape, high mechanical strength, and essentially a macro- and mesoporous nature (with very limited content of micropores) is now produced at a commercial scale with the name of "mesoC+". More information can be found at https://www.sicatcatalyst.com/products (accessed 2021-01-03).

(16) Mukasyan, A. S. Silicon Carbide. In *Concise Encyclopedia of Self-Propagating High-Temperature Synthesis*; Borovinskaya, I. P., Gromov, A. A., Levashov, E. A., Maksimov, Y. M., Mukasyan, A. S., Rogachev, A. S., Eds.; Elsevier Inc.: 2017; pp 336−338.

(17) Ledoux, M. J.; Pham-Huu, C. Silicon Carbide - a Novel Catalyst Support for Heterogeneous Catalysis. *CATTECH* **2001**, *5*, 226−246.

(18) Scheffler, F.; Claus, P.; Schimpf, S.; Lucas, M.; Scheffler, M. Heterogeneously Catalyzed Processes with Porous Cellular Ceramic Monoliths. In *Cellular Ceramics: Structure, Manufacturing, Properties and Applications*; Scheffler, M., Colombo, P., Eds.; Wiley-VCH Verlag GmbH & Co.: Weinheim, 2005; DOI: 10.1002/3527606696.ch5d.

(19) Colombo, P. In Praise of Pores. *Science* **2008**, *322*, 381−383.

(20) Scheffler, M.; Colombo, P. *Cellular Ceramics: Structure, Manufacturing Properties and Applications*; Wiley-VCH: Weinheim, 2005; p 670, DOI: 10.1002/3527606696 .

(21) Ohji, T.; Colombo, P.; Naito, M.; Garay, J. E.; Lin, H.-T. *Innovative Processing and Manufacturing of Advanced Ceramics and Composites II*; John Wiley & Sons: 2010; p 224 DOI: 10.1002/9781118771464.

(22) Ohji, T.; Fukushima, M. Macro-Porous Ceramics: Processing and Properties. *Int. Mater. Rev.* **2012**, *57*, 115−131.

(23) Manoj Kumar, B. V.; Kim, Y.-W. Processing of Polysiloxane-Derived Porous Ceramics: a Review. *Sci. Technol. Adv. Mater.* **2010**, *11*, 044303.

(24) Yoon, T. H.; Lee, H. J.; Yan, Y.; Kim, D. P. Fabrication of SiC-Based Ceramic Microstructures from Preceramic Polymers with Sacrificial Templates and Lithographic Tecniques - A Review. *Nippon Seramikkusu Kyokai Gakujutsu Ronbunshi* **2006**, *114*, 473−479.

(25) Eom, J.-H.; Kim, Y.-W.; Raju, S. Processing and Properties of Macroporous Silicon Carbide Ceramics: A Review. *J. Asian Ceram. Soc.* **2013**, *1*, 220−242.

(26) Roewer, G.; Herzog, U.; Trommer, K.; Müller, E.; Frühauf, S. Silicon Carbide - a Survey of Synthetic Approaches, Properties and Applications. In *High Performance Non-Oxide Ceramics I*; Springer: 2002; pp 59−135, DOI: 10.1007/3-540-45613-9_2.

(27) Nguyen, P.; Pham, C. Innovative Porous SiC-Based Materials: From Nanoscopic Understandings to Tunable Carriers Serving Catalytic Needs. *Appl. Catal., A* **2011**, *391*, 443−454.

(28) Duong-Viet, C.; Ba, H.; El-Berrichi, Z.; Nhut, J.-M.; Ledoux, M. J.; Liu, Y.; Pham-Huu, C. Silicon Carbide Foam as a Porous Support Platform for Catalytic Applications. *New J. Chem.* **2016**, *40*, 4285−4299.

(29) Ledoux, M. J.; Pham-Huu, C.; Chianelli, R. R. Catalysis with Carbides. *Curr. Opin. Solid State Mater. Sci.* **1996**, *1*, 96−100.

(30) Centi, G.; Perathoner, S. Catalysis: Role and Challenges for a Sustainable Energy. *Top. Catal.* **2009**, *52*, 948−961.

(31) Mühlhaeuser, O. On Carborundum. *J. Am. Chem. Soc.* **1893**, *15*, 411−414.

(32) Reproduced with permission from ref 31. Copyright 1893 American Chemical Society.

(33) Knacke, R. Carbonaceous compounds in interstellar dust. *Nature* **1977**, *269*, 132−134.

(34) Henning, T.; Mutschke, H. Formation and Spectroscopy of Carbides. *Spectrochim. Acta, Part A* **2001**, *57*, 815−824.

(35) Merino, P.; Svec, M.; Martinez, J. I.; Jelinek, P.; Lacovig, P.; Dalmiglio, M.; Lizzit, S.; Soukiassian, P.; Cernicharo, J.; Martin-Gago, J. A. Graphene Etching on SiC Grains as a Path to Interstellar Polycyclic Aromatic Hydrocarbons Formation. *Nat. Commun.* **2014**, *5*, 3054.

(36) Schlichting, J.; Riley, F. L. Silicon Carbide. In *Concise Encyclopedia of Advanced Ceramic Materials*; Brook, R. J., Ed.; Pergamon Press: 1991; pp 426−429, DOI: 10.1016/B978-0-08-034720-2.50117-9.

(37) Adler, J. Ceramic Diesel Particulate Filters. *Int. J. Appl. Ceram. Technol.* **2005**, *2*, 429−439.

(38) Pyzik, A. J.; Li, C. G. New Design of a Ceramic Filter for Diesel Emission Control Applications. *Int. J. Appl. Ceram. Technol.* **2005**, *2*, 440−451.

(39) Agrafiotis, C. C.; Mavroidis, I.; Konstandopoulos, A. G.; Hoffschmidt, B.; Stobbe, P.; Romero, M.; Fernandez-Quero, V. Evaluation of Porous Silicon Carbide Monolithic Honeycombs as Volumetric Receivers/Collectors of Concentrated Solar Radiation. *Sol. Energy Mater. Sol. Cells* **2007**, *91*, 474−488.

(40) Vogt, U. F.; Gyorfy, L.; Herzog, A.; Graule, T.; Plesch, G. Macroporous Silicon Carbide Foams for Porous Burner Applications and Catalyst Supports. *J. Phys. Chem. Solids* **2007**, *68*, 1234−1238.

(41) Wood, S.; Harris, A. T. Porous Burners for Lean-Burn Applications. *Prog. Energy Combust. Sci.* **2008**, *34*, 667−684.

(42) Pollmann, J.; Peng, X.; Wieferink, J.; Krüger, P. Adsorption of Hydrogen and Hydrocarbon Molecules on SiC(001). *Surf. Sci. Rep.* **2014**, *69*, 55−104.

(43) Wu, R.; Zhou, K.; Yue, C. Y.; Wei, J.; Pan, Y. Recent Progress in Synthesis, Properties and Potential Applications of SiC Nanomaterials. *Prog. Mater. Sci.* **2015**, *72*, 1−60.

(44) Sarkar, N.; Kim, I. J. Porous Ceramics. In *Advanced Ceramic Processing*; Mohamed, A., Ed.; IntechOpen: 2015; pp 55−84, DOI: 10.5772/61047. Available from: https://www.intechopen.com/books/advanced-ceramic-processing/porous-ceramics (accessed 2020-07-01).

(45) Gerhardt, R. *Properties and Applications of Silicon Carbide*; InTech: Rijeka, Croatia, 2011; 535pp, DOI: 10.5772/615.

(46) Deng, Z. Y.; She, J.; Inagaki, Y.; Yang, J. F.; Ohji, T.; Tanaka, Y. Reinforcement by Crack-Tip Blunting in Porous Ceramics. *J. Eur. Ceram. Soc.* **2004**, *24*, 2055−2059.

(47) Zhao, H. S.; Liu, Z. G.; Yang, Y.; Liu, X. X.; Zhang, K. H.; Li, Z. Q. Preparation and Properties of Porous Silicon Carbide Ceramics Through Coat-Mix and Composite Additives Process. *Trans. Nonferrous Met. Soc. China* **2011**, *21*, 1329−1334.

(48) Kingery, W. D.; Bowen, H. K.; Uhlman, D. R. *Introduction to Ceramics*; Wiley: New York, 1976; p 636.

(49) Jang, B.-K.; Sakka, Y. Thermophysical Properties of Porous SiC Ceramics Fabricated by Pressureless Sintering. *Sci. Technol. Adv. Mater.* **2007**, *8*, 655−659.

(50) Ledoux, M. J.; Hantzer, S.; Pham-Huu, C.; Guille, J.; Desaneaux, M.-P. New Synthesis and Uses of High-Specific-Surface SiC as a Catalytic Support that is Chemically Inert and Has High Thermal Resistance. *J. Catal.* **1988**, *114*, 176−185.

(51) Ledoux, M. J.; Guille, J.; Hantzer, S.; Dubots, D. Procédé de Production de Carbure de Silicium à Grande Surface Spécifique et Application à des Reactions Catalytiques à Temperature Elevée. US Pat. No. 4914070, 1988.

(52) Lacroix, M.; Dreibine, L.; de Tymowski, B.; Vigneron, F.; Edouard, E.; Bégin, D.; Nguyen, P.; Pham, C.; Savin-Poncet, S.; Luck, F.; et al. Silicon Carbide Foam Composite Containing Cobalt as a Highly Selective and Re-Usable Fischer–Tropsch Synthesis Catalyst. *Appl. Catal., A* **2011**, *397*, 62–72.

(53) van Santen, R. A.; Neurock, M. *Molecular Heterogeneous Catalysis: A Conceptual and Computational Approach*; Wiley-VCH Verlag GmbH & Co.: Weinheim, 2006; 474pp, DOI: 10.1002/9783527610846.

(54) Argyle, M. D.; Bartholomew, C. H. Heterogeneous Catalyst Deactivation and Regeneration: A Review. *Catalysts* **2015**, *5*, 145–269.

(55) Leroi, P.; Madani, B.; Pham-Huu, C.; Ledoux, M. J.; Savin-Poncet, S.; Bousquet, J. L. Ni/SiC: a Stable and Active Catalyst for Catalytic Partial Oxidation of Methane. *Catal. Today* **2004**, *91–92*, 53–58.

(56) Rostrup-Nielsen, J. R. New Aspects of Syngas Production and Use. *Catal. Today* **2000**, *63*, 159–164.

(57) Izhevskyi, V. A.; Genova, L. A.; Bressiani, J. C.; Bressiani, A. H. A. Review Article: Silicon Carbide. Structure, Properties and Processing. *Ceramica* **2000**, *46*, 4–13.

(58) Yazdi, G. R.; Iakimov, T.; Yakimova, R. Epitaxial Graphene on SiC: A Review of Growth and Characterization. *Crystals* **2016**, *6*, 53.

(59) Guinier, A.; Bokil, G. B.; Boll-Dornberger, K.; Cowley, J. M.; Durovic, S.; Jagodzinski, H.; Krishna, P.; De Wolff, P. M.; Zvyagin, B. B.; Cox, D. E.; et al. Nomenclature of Polytype Structures. *Acta Crystallogr., Sect. A: Found. Crystallogr.* **1984**, *40*, 399–404.

(60) Verma, A. R.; Krishna, P. *Polymorphism and Polytypism in Crystals*; John Wiley & Sons Inc.: New York, NY, USA, 1966; pp 665–666.

(61) Ramsdell, L. S. Studies on Silicon Carbide. *Am. Mineral.* **1947**, *32*, 64–82.

(62) Abderrazak, H.; Selmane, E.; Hmida, B. H. Silicon Carbide: Synthesis and Properties. In *Properties and Applications of Silicon Carbide*; Gerhardt, R., Ed.; InTech: Rijeka, Croatia, 2011; pp 361–388, DOI: 10.5772/15736.

(63) van Haeringen, W.; Bobbert, P. A.; Backes, W. H. On the Band Gap Variation in SiC Polytypes. *Phys. Status Solidi B* **1997**, *202*, 63–79.

(64) Ou, H.; Ou, Y.; Argyraki, A.; Schimmel, S.; Kaiser, M.; Wellmann, P.; Linnarsson, M. K.; Jokubavicius, V.; Sun, J.; Liljedahl, R.; et al. Advances in Wide Bandgap SiC for Optoelectronics. *Eur. Phys. J. B* **2014**, *87*, 58.

(65) Scace, R. I.; Slack, G. A. *Silicon Carbide - A High Temperature Semiconductor*; O'Connor, J. R., Smiltens, J., Eds.; Pergamon Press: Oxford, London, New York, Paris, 1960; p 24.

(66) Goldberg, Y.; Levinshtein, M. E.; Rumyantsev, S. L. *Properties of Advanced Semiconductor Materials GaN, AlN, SiC, BN, SiC, SiGe*; Levinshtein, M. E., Rumyantsev, S. L., Shur, M. S., Eds.; John Wiley & Sons, Inc.: New York, 2001; pp 93–148.

(67) Nilsson, O.; Mehling, H.; Horn, R.; Fricke, J.; Hofmann, R.; Muller, S. G.; Eckstein, R.; Hofmann, D. Determination of the Thermal Diffusivity and Conductivity of Monocrystalline Silicon Carbide (300–2300 K). *High Temp. - High Pressures* **1997**, *29*, 73–79.

(68) Kern, E. L.; Hamill, D. W.; Deem, H. W.; Sheets, H. D. Thermal Properties of β-Silicon Carbide from 20 to 2000°C. *Mater. Res. Bull.* **1969**, *4*, S25–S32.

(69) Fend, Z. C. *SiC Power Materials: Devices and Applications*; Springer-Verlag: Berlin Heidelberg, 2004; p 452, DOI: 10.1007/978-3-662-09877-6

(70) www.sicatcatalyst.com (accessed April, 2021).

(71) Wang, Q.; Wang, Y. Y.; Guo, X. Y. Biomorphic High-Performance Materials. *Progress in Chem.* **2007**, *19*, 1217–1222.

(72) Qian, J. M.; Wang, J. P.; Qiao, G. J.; Jin, Z. H. Preparation of Porous Ceramic with a Woodlike Structure by Sol-Gel and Carbothermal Reduction Processing. *J. Eur. Ceram. Soc.* **2004**, *24*, 3251–3259.

(73) Wang, Q.; Jin, G. Q.; Wang, D. H.; Guo, X. Y. Biomorphous Porous Silicon Carbide Prepared from Carbonized Millet. *Mater. Sci. Eng., A* **2007**, *459*, 1–6.

(74) Wang, Q.; Wang, D. H.; Jin, G. Q.; Wang, Y. Y.; Guo, X. Y. Biomorphous Porous SiC from Lotus Root. *Particuology* **2009**, *7*, 199–203.

(75) Li, X. K.; Liu, L.; Zhang, Y. X.; Shen, S. D.; Ge, S.; Ling, L. C. Synthesis of Nanometre Silicon Carbide Whiskers from Binary Carbonaceous Silica Aerogels. *Carbon* **2001**, *39*, 159–165.

(76) Jin, G.-Q.; Guo, X.-Y. Synthesis and Characterization of Mesoporous Silicon Carbide. *Microporous Mesoporous Mater.* **2003**, *60*, 207–212.

(77) Jin, G.-Q.; Liang, P.; Guo, X.-Y. Novel Method for Synthesis of Silicon Carbide Nanowires. *J. Mater. Sci. Lett.* **2003**, *22*, 767–770.

(78) Guo, X.-Y.; Jin, G.-Q. Pore-Size Control in the Sol-Gel Synthesis of Mesoporous Silicon Carbide. *J. Mater. Sci.* **2005**, *40*, 1301–1303.

(79) Dawes, S. B.; Senaratne, S. Synthesis of Ordered Mesoporous Carbon-Silicon Nanocomposites. US 7,910,082 B2, 2011.

(80) Parmentier, J.; Patarin, J.; Dentzer, J.; Vix-Guterl, C. Formation of SiC via Carbothermal Reduction of a Carbon-Containing Mesoporous MCM-48 Silica Phase: a New Route to Produce High Surface Area SiC. *Ceram. Int.* **2002**, *28*, 1–7.

(81) Krawiec, P.; Weidenthaler, C.; Kaskel, S. SiC/MCM-48 and SiC/SBA-15 Nanocomposite Materials. *Chem. Mater.* **2004**, *16*, 2869–2880.

(82) Yan, J.; Wang, A.; Kim, D.-P. Preparation of Ordered Mesoporous SiC from Preceramic Polymer Templated by Nano-porous Silica. *J. Phys. Chem. B* **2006**, *110*, 5429–5433.

(83) Shi, Y. F.; Meng, Y.; Chen, D. H.; Cheng, S. J.; Chen, P.; Yang, H. F.; Wan, Y.; Zhao, D. Y. Highly Ordered Mesoporous Silicon Carbide Ceramics with Large Surface Areas and High Stability. *Adv. Funct. Mater.* **2006**, *16*, 561–567.

(84) Nishihora, R. K.; Rachadel, P. R.; Quadri, M. G. N.; Hotza, D. Manufacturing Porous Ceramic Materials by Tape Casting-A Review. *J. Eur. Ceram. Soc.* **2018**, *38*, 988–1001.

(85) Jana, D. C.; Sundararajan, G.; Chattopadhyay, K. Effect of Porosity on Structure, Young's Modulus, and Thermal Conductivity of SiC Foams by Direct Foaming and Gel Casting. *J. Am. Ceram. Soc.* **2017**, *100*, 312–322.

(86) Studart, A. R.; Gonzenbach, U. T.; Tervoort, E.; Gauckler, L. J. Processing Routes to Macroporous Ceramics: A Review. *J. Am. Ceram. Soc.* **2006**, *89*, 1771–1789.

(87) Alison, L.; Menasce, S.; Bouville, F.; Tervoort, E.; Mattich, I.; Ofner, A.; Studart, A. R. 3D Printing of Sacrificial Templates into Hierarchical Porous Materials. *Sci. Rep.* **2019**, *9*, 409.

(88) Baux, A.; Goillot, A.; Jacques, S.; Heisel, C.; Rochais, D.; Charpentier, L.; David, P.; Piquero, T.; Chartier, T.; Chollon, G. Synthesis and Properties of Macroporous SiC Ceramics Synthesized by 3D Printing and Chemical Vapor Infiltration/Deposition. *J. Eur. Ceram. Soc.* **2020**, *40*, 2834–2854.

(89) Harlin, M. E.; Krause, A. O. I.; Heinrich, B.; Pham-Huu, C.; Ledoux, M. J. Part II. Dehydrogenation of *n*-Butane over Carbon Modified MoO₃ Supported on SiC. *Appl. Catal., A* **1999**, *185*, 311–322.

(90) Xu, J.; Liu, Y.-M.; Xue, B.; Li, Y.-X.; Cao, Y.; Fan, K.-N. A Hybrid Sol-Gel Synthesis of Mesostructured SiC with Tunable Porosity and Its Application as a Support for Propane Oxidative Dehydrogenation. *Phys. Chem. Chem. Phys.* **2011**, *13*, 10111–10118.

(91) Ledoux, M. J.; Crouzet, C.; Pham-Huu, C.; Turines, V.; Kourtakis, K.; Mills, P. L.; Lerouz, J. J. High-Yield Butane to Maleic Anhydride Direct Oxidation on Vanadyl Pyrophosphate Supported on Heat-Conductive Materials: β-SiC, Si₃N₄, and BN. *J. Catal.* **2001**, *203*, 495–508.

(92) Shcherban, N. D.; Diyuk, E. A.; Sydorchuk, V. V. Synthesis and Catalytic Activity of Vanadium Phosphorous Oxides Systems Supported on Silicon Carbide for the Selective Oxidation of n-Butane to Maleic Anhydride. *React. Kinet., Mech. Catal.* **2019**, *126*, 975–985.

(93) Wang, Y.; Ma, F.; Chen, S.; Chen, F.; Lu, W. M. Performance of Mo-V-Te-P Catalysts Supported on the SiC for Propane Selective Oxidation to Acrolein. *Chin. Chem. Lett.* **2011**, *22*, 1321−1325.

(94) Mars, P.; van Krevelen, D. W. Oxidations Carried Out by Means of Vanadium Oxide Catalysts. *Chem. Eng. Sci.* **1954**, *3*, 41−59.

(95) Chen, L.; Liang, J.; Lin, H.; Weng, W.; Wan, H.; Védrine, J. C. MCM41 and Silica Supported MoVTe Mixed Oxide Catalysts for Direct Oxidation of Propane to Acrolein. *Appl. Catal., A* **2005**, *293*, 49−55.

(96) Yi, X.; Sun, X.; Zhang, X.; Huang, C.; Weng, W.; Wan, H. Highly Dispersed MoVTeNbO/SiO₂ Catalysts Prepared by the Sol-Gel Method for Selective Oxidation of Propane to Acrolein. *Catal. Commun.* **2009**, *10*, 1591−1594.

(97) Holmberg, J.; Häggblad, R.; Andersson, A. A Study of Propane Ammoxidation on Mo−V−Nb−Te-Oxide Catalysts Diluted with Al₂O₃, SiO₂, and TiO₂. *J. Catal.* **2006**, *243*, 350−359.

(98) Nguyen, T. T.; Burel, L.; Nguyen, D. L.; Pham-Huu, C.; Millet, J. M. M. Catalytic Performance of MoVTeNbO Catalyst Supported on SiC Foam in Oxidative Dehydrogenation of Ethane and Ammoxidation of Propane. *Appl. Catal., A* **2012**, *433−434*, 41−48.

(99) Solsona, B.; Vázquez, M. I.; Ivars, F.; Dejoz, A.; Concepción, P.; Nieto, J. M. L. Selective Oxidation of Propane and Ethane on Diluted Mo-V-Nb-Te Mixed-Oxide Catalysts. *J. Catal.* **2007**, *252*, 271−280.

(100) López-Medina, R.; Golinska, H.; Ziolek, M.; Guerrero-Pérez, M. O.; Bañares, M. A. Surface Active Sites in Alumina-Supported MoVNbTeO Oxide Catalysts. *Catal. Today* **2010**, *158*, 139−145.

(101) Baca, M.; Aouine, M.; Dubois, J. L.; Millet, J. M. M. Synergetic Effect Between Phases in MoVTe(Sb)NbO Catalysts Used for the Oxidation of Propane into Acrylic Acid. *J. Catal.* **2005**, *233*, 234−241.

(102) Carrero, C. A.; Burt, S. P.; Huang, F.; Venegas, J. M.; Love, A. M.; Mueller, P.; Zhu, H.; Grant, J. T.; Mathison, R.; Hanraham, M. P.; et al. Supported Two- and Three-Dimensional Vanadium Oxide Species on the Surface of *β*-SiC. *Catal. Sci. Technol.* **2017**, *7*, 3707−3714.

(103) Ramirez, A.; Hueso, J. L.; Abian, M.; Alzueta, M. U.; Mallada, R.; Santamaria, J. Escaping Undesired Gas-Phase Chemistry: Microwave-Driven Selectivity Enhancement in Heterogeneous Catalytic Reactors. *Sci. Adv.* **2019**, *5*, No. eaau9000.

(104) Ramirez, A.; Hueso, J. L.; Mallada, R.; Santamaria, J. Microwave-Activated Structured Reactors to Maximize Propylene Selectivity in the Oxidative Dehydrogenation of Propane. *Chem. Eng. J.* **2020**, *393*, 124746.

(105) Bawaked, S.; Dummer, N. F.; Bethell, D.; Knight, D. W.; Hutchings, G. J. Solvent-Free Selective Epoxidation of Cyclooctene Using Supported Gold Catalysts: an Investigation of Catalyst Re-Use. *Green Chem.* **2011**, *13*, 127−134.

(106) Hughes, M. D.; Xu, Y.-J.; Jenkins, P.; McMorn, P.; Landon, P.; Enache, D. I.; Carley, A. F.; Attard, G. A.; Hutchings, G. J.; King, F.; et al. Tunable Gold Catalysts for Selective Hydrocarbon Oxidation under Mild Conditions. *Nature* **2005**, *437*, 1132−1135.

(107) Jiang, R.; Jiao, Y.; Xie, Y.; Yang, Z.; Zhang, J. SiC Foam Based Structured Catalyst for Process Intensification in Oxidative Dehydrogenation of 1-Butene to Butadiene. *Chem. Eng. Process.* **2019**, *137*, 108−115.

(108) Guo, Z.; Liu, B.; Zhang, Q. H. Recent Advances in Heterogeneous Selective Oxidation Catalysis for Sustainable Chemistry. *Chem. Soc. Rev.* **2014**, *43*, 3480−3524.

(109) Zhao, L.; Kong, L.; Liu, C.; Wang, Y.; Dai, L. AgCu/SiC-Powder: A Highly Stable and Active Catalyst for Gas-Phase Selective Oxidation of Alcohols. *Catal. Commun.* **2017**, *98*, 1−4.

(110) Zhao, G.; Fan, S.; Pan, X.; Chen, P.; Liu, Y.; Lu, Y. Reaction-Induced Self-Assembly of CoO@Cu₂O Nanocomposites In Situ onto SiC-Foam for Gas-Phase Oxidation of Bioethanol to Acetaldehyde. *ChemSusChem* **2017**, *10*, 1380−1384.

(111) Li, M.-Y.; Lu, W.-D.; He, L.; Schüth, F.; Lu, A.-H. Tailoring the Surface Structure of Silicon Carbide Support for Copper Catalyzed Ethanol Dehydrogenation. *ChemCatChem* **2019**, *11*, 481−487.

(112) Wang, P.; Xu, L.; Zhu, J.; Gao, K.; Zhang, Y.; Wang, J. Reaction Induced Robust PdₓBiᵧ/SiC Catalyst for the Gas Phase Oxidation of Monopolistic Alcohols. *RSC Adv.* **2020**, *10*, 42564−42569.

(113) Mishra, G.; Behera, G. C.; Singh, S. K.; Parida, K. Facile Synthesis and Synergetic Interaction of VPO/*β*-SiC Composites toward Solvent-Free Oxidation of Methanol to Formaldehyde. *ACS Omega* **2020**, *5*, 22808−22815.

(114) Li, X.; Pan, X.; Zhou, Y.; Bao, X. Modulation of the Textures and Chemical Nature of C-SiC as the Support of Pd for Liquid Phase Hydrogenation. *Carbon* **2013**, *57*, 34−41.

(115) Zhou, Y.; Li, X.; Pan, X.; Bao, X. A Highly Active and Stable Pd-TiO₂/CDC-SiC Catalyst for Hydrogenation of 4-Carboxybenzaldehyde. *J. Mater. Chem.* **2012**, *22*, 14155−14159.

(116) Tie, K.; Pan, X.; He, L.; Li, P.; Yu, T.; Bao, X. Pd Supported on NC@SiC as an Efficient and Stable Catalyst for 4-Carboxybenzaldehyde Hydrogenation. *Catal. Commun.* **2018**, *110*, 79−82.

(117) Yao, R.; Li, J.; Wu, P.; Li, X. The Superior Performance of a Pt Catalyst Supported on Nanoporous SiC-C Composites for Liquid-Phase Selective Hydrogenation of Cinnamaldehyde. *RSC Adv.* **2016**, *6*, 81211−81218.

(118) Wang, G.; Yao, R.; Xin, H.; Guan, Y.; Wu, P.; Li, X. At Room Temperature in Water: Efficient Hydrogenation of Furfural to Furfuryl Alcohol with a Pt/SiC-C Catalyst. *RSC Adv.* **2018**, *8*, 37243−37253.

(119) Yu, Z.; Tian, H.; Sun, K.; Shao, Y.; Zhang, L.; Zhang, S.; Duan, P.; Liu, Q.; Niu, S.; Dong, D.; et al. Impacts of Externally Added Brønsted and Lewis Acid on Conversion of Furfural to Cyclopentanone over Ni/SiC Catalyst. *Mol. Catal.* **2020**, *496*, 111187.

(120) Min, Q.; Li, K.; Jiang, C.; Xu, W.; Yang, Z.; Zhang, J. Selective Hydrogenation of Cinnamaldehyde over a Rotating Stirrer Reactor Made of SiC Foam Supported Al₂O₃ and Pt Catalysts. *Catal. Commun.* **2016**, *83*, 62−65.

(121) Li, K.; Jiao, Y.; Yang, Z.; Zhang, J. A Comparative Study of Ni/Al₂O₃−SiC Foam Catalysts and Powder Catalysts for the Liquid-Phase Hydrogenation of Benzaldehyde. *J. Mater. Sci. Technol.* **2019**, *35*, 159−167.

(122) Wang, J.; Wang, Y.; Tong, X.; Wang, Y.; Jin, G.; Guo, X. Highly Active Ir/SiC Catalyst for Aqueous Hydrogenation of Levulinic Acid to *γ*-Valerolactone. *Catal. Commun.* **2020**, *139*, 105971.

(123) Wang, J.; Zhu, S.; Wang, Y.; Wang, Y.; Jin, G.; Tong, X.; Guo, X. Enhanced Activity of Ru-Ir Nanoparticles over SiC for Hydrogenation of Levulinic Acid at Room-Temperature. *Mater. Res. Bull.* **2021**, *135*, 111128.

(124) Díez-Ramírez, J.; Díaz, J. A.; Sánchez, P.; Dorado, F. Optimization of the Pd/Cu Ratio in Pd-Cu-Zn/SiC Catalysts for the CO₂ Hydrogenation to Methanol at Atmospheric Pressure. *J. CO2 Util.* **2017**, *22*, 71−80.

(125) Díez-Ramírez, J.; Díaz, J. A.; Dorado, F.; Sánchez, P. Kinetics of the Hydrogenation of CO₂ to Methanol at Atmospheric Pressure Using a Pd-Cu-Zn/SiC Catalyst. *Fuel Process. Technol.* **2018**, *173*, 173−181.

(126) Halim, N. S. A.; Zabidi, N. A. M.; Tasfy, S. F. H.; Shaharun, M. S. Morphology and Performance of Cu/ZnO Based Catalyst: Comparison Between Al₂O₃ and SiC Support. *AIP Conf. Proc.* **2016**, *1787*, 030008−1.

(127) Berthet, A.; Thomann, A. L.; Cadete Santos Aires, F. J.; Brun, M.; Deranlot, C.; Bertolini, J. C.; Rozenbaum, J. P.; Brault, P.; Andreazza, P. Comparison of Pd/(Bulk SiC) Catalysts Prepared by Atomic Beam Deposition and Plasma Sputtering Deposition: Characterization and Catalytic Properties. *J. Catal.* **2000**, *190*, 49−59.

(128) Garcia Cervantes, G.; Cadete Santos Aires, F. J.; Bertolini, J. C. Compared Properties of Pd on Thermo-Conductor Supports (SiC, Si₃N₄) and Pd on Oxide Supports (Al₂O₃, SiO₂) for the 1,3-Butadiene Hydrogenation Reaction. *J. Catal.* **2003**, *214*, 26−32.

(129) Zhang, H.; Cao, J.; Wu, B.; Dai, W.; Chen, Z.; Ma, M. An Alumina-Coated, Egg-Shell Pd/*α*-Al₂O₃@SiC Catalyst with Enhanced

Ethylene Selectivity in the Selective Hydrogenation of Acetylene. *RSC Adv.* **2016**, *6*, 57174−57182.

(130) Guo, Z.; Liu, Y.; Liu, Y.; Chu, W. Promising SiC Support for Pd Catalyst in Selective Hydrogenation of Acetylene to Ethylene. *Appl. Surf. Sci.* **2018**, *442*, 736−741.

(131) Shu, M.; Shi, C.; Yu, J.; Chen, X.; Liang, C.; Si, R. Efficient Selective Hydrogenation of 2-Butyne-1,4-diol to 2-Butene-1,4-diol by Silicon Carbide Supported Platinum Catalyst. *Catal. Sci. Technol.* **2020**, *10*, 327−331.

(132) Truong-Phuoc, L.; Truong-Huu, T.; Nguyen-Dinh, L.; Baaziz, W.; Romero, T.; Edouard, D.; Begin, D.; Janowska, I.; Pham-Huu, C. Silicon Carbide Foam Decorated with Carbon Nanofibers as Catalytic Stirrer in Liquid-Phase Hydrogenation Reactions. *Appl. Catal., A* **2014**, *469*, 81−88.

(133) Li, P.; Wang, Y.; Wang, Y.; Jin, G.; Guo, X.-Y.; Tong, X. Silicon Carbide Supported Palladium-Iridium Bimetallic Catalysts for Efficient Selective Hydrogenation of Cinnamaldehyde. *Chin. J. Chem.* **2020**, *38*, 367−371.

(134) Jiao, Z. F.; Guo, X. N.; Zhai, Z. Y.; Jin, G. Q.; Wang, X. M.; Guo, X. Y. The Enhanced Catalytic Performance of Pd/SiC for the Hydrogenation of Furan Derivatives at Ambient Temperature under Visible Light Irradiation. *Catal. Sci. Technol.* **2014**, *4*, 2494−2498.

(135) Jiao, Z. F.; Zhai, Z. Y.; Guo, X. N.; Guo, X. Y. Visible-Light-Driven Photocatalytic Suzuki-Miyaura Coupling Reaction on Mott-Schottky-type Pd/SiC Catalyst. *J. Phys. Chem. C* **2015**, *119*, 3238−3243.

(136) Hao, C. H.; Guo, X. N.; Pan, Y. T.; Chen, S.; Jiao, Z. F.; Yang, H.; Guo, X. Y. Visible-Light-Driven Selective Photocatalytic Hydrogenation of Cinnamaldehyde over Au/SiC Catalysts. *J. Am. Chem. Soc.* **2016**, *138*, 9361−9364.

(137) Wang, B.; Guo, X. N.; Jin, G. Q.; Guo, X. Y. Visible-Light-Enhanced Photocatalytic Sonogashira Reaction over Silicon Carbide Supported Pd Nanoparticles. *Catal. Commun.* **2017**, *98*, 81−84.

(138) Wang, B.; Wang, Y. Y.; Li, J. Z.; Guo, X. N.; Bai, G. L.; Tong, X. L.; Jin, G. Q.; Guo, X. Y. Photocatalytic Sonogashira Reaction over Silicon Carbide Supported Pd-Cu Alloy Nanoparticles under Visible Light Irradiation. *Catal. Sci. Technol.* **2018**, *8*, 3357−3362.

(139) Hao, C. H.; Guo, X. N.; Sankar, M.; Yang, H.; Ma, B.; Zhang, Y. F.; Tong, X. L.; Jin, G. Q.; Guo, X. Y. Synergistic Effect of Segregated Pd and Au Nanoparticles on Semiconducting SiC for Efficient Photocatalytic Hydrogenation of Nitroarenes. *ACS Appl. Mater. Interfaces* **2018**, *10*, 23029−23036.

(140) Zheng, Y.; Zheng, Y.; Li, Z.; Yu, H.; Wang, R.; Wei, K. Preparations of C/SiC Composites and Their Use as Supports for Ru Catalyst in Ammonia Synthesis. *J. Mol. Catal. A: Chem.* **2009**, *301*, 79−83.

(141) Nghiem, Q. D.; Kim, D. P. Direct Preparation of High Surface Area Mesoporous SiC-Based Ceramic by Pyrolysis of a Self-Assembled Polycarbosilane-block-Polystyrene Diblock Copolymer. *Chem. Mater.* **2008**, *20*, 3735−3739.

(142) Rider, D. A.; Liu, K.; Eloi, J. C.; Vanderark, L.; Yang, L.; Wang, J. Y.; Grozea, D.; Lu, Z. H.; Russel, T. R.; Manners, I. Nanostructured Magnetic Thin Films from Organometallic Block Copolymers: Pyrolysis of Self-Assembled Polystyrene-block-poly-(ferrocenylethylmethylsilane). *ACS Nano* **2008**, *2*, 263−270.

(143) Nghiem, Q. D.; Kim, D. P.; Kim, S. O. Well-Ordered Nanostructure SiC Ceramic Derived from Self-Assembly of Polycarbosilane-Block-Poly(methyl methacrylate) Diblock Copolymer. *J. Nanosci. Nanotechnol.* **2008**, *8*, 5527−5531.

(144) Temple, K.; Kulbaba, K.; Power-Billard, K. N.; Manners, I.; Leach, K. A.; Xu, T.; Russel, T. M.; Hawker, C. J. Spontaneous Vertical Ordering and Pyrolytic Formation of Nanoscopic Ceramic Patterns from Poly(styrene-*b*-ferrocenylsilane). *Adv. Mater.* **2003**, *15*, 297−300.

(145) Zaheer, M.; Hermannsdorfer, J.; Kretschmer, W. P.; Motz, G.; Kempe, R. Robust Heterogeneous Nickel Catalysts with Tailored Porosity for the Selective Hydrogenolysis of Aryl Ethers. *ChemCatChem* **2014**, *6*, 91−95.

(146) Eckardt, M.; Zaheer, M.; Kempe, R. Nitrogen-Doped Mesoporous SiC Materials with Catalytically Active Cobalt Nano-particles for the Efficient and Selective Hydrogenation of Nitroarenes. *Sci. Rep.* **2018**, *8*, 2567.

(147) Baumler, C.; Bauer, C.; Kempe, R. The Synthesis of Primary Amines through Reductive Amination Employing an Iron Catalyst. *ChemSusChem* **2020**, *13*, 3110−3114.

(148) Schönauer, T.; Thomä, S. L. J.; Kaiser, L.; Zobel, M.; Kempe, R. General Synthesis of Secondary Alkylamines by Reductive Alkylation of Nitriles by Aldehydes and Ketones. *Chem. - Eur. J.* **2021**, *27*, 1609−1614.

(149) Jiao, Z.-F.; Zhao, J.-X.; Guo, X.-N.; Tong, X.-L.; Zhang, B.; Jin, G.-Q.; Qin, Y.; Guo, X.-Y. Turning the Product Selectivity of Nitrile Hydrogenation from Primary to Secondary Amines by Precise Modification of Pd/SiC Catalysts using NiO Nanodots. *Catal. Sci. Technol.* **2019**, *9*, 2266−2272.

(150) Kang, J.; He, S.; Zhou, W.; Shen, Z.; Li, Y.; Chen, M.; Zhang, Q.; Wang, Y. Single-Pass Transformation of Syngas into Ethanol with High Selectivity by Triple Tandem Catalysis. *Nat. Commun.* **2020**, *11*, 827.

(151) Rachmady, W.; Vannice, M. A. Acetic Acid Hydrogenation over Supported Platinum Catalysts. *J. Catal.* **2000**, *192*, 322−334.

(152) Guo, Z.; Lim, S. H.; Chu, W.; Liu, Y.; Borgna, A. Highly Efficient SiC-Supported Ni-Based Catalysts with Enhanced Recycle Stability for One-Pot Cellobiose Hydrolytic Hydrogenation to Hexitols. *ACS Sustainable Chem. Eng.* **2020**, *8*, 10747−10755.

(153) Qin, Y.; Li, R.; Mi, W.; Shi, W.; Lu, B.; Tong, X. Phenol Hydrogenation to Cyclohexanol on a Novel Pd$_7$P$_3$/SiC Catalyst with High Activity and Selectivity. *Diamond Relat. Mater.* **2021**, *111*, 108163.

(154) Winé, G.; Tessonnier, J. P.; Pham-Huu, C.; Ledoux, M. J. Beta Zeolite Supported on a Macroscopic Pre-Shaped SiC as a High Performance Catalyst for Liquid-Phase Benzoylation. *Chem. Commun.* **2002**, 2418−2419.

(155) Winé, G.; Matta, J.; Tessonnier, J.-P.; Pham-Huu, C.; Ledoux, M. J. Beta Zeolite Supported on Silicon Carbide for Friedel-Crafts Fixed-Bed Reactions. *Chem. Commun.* **2003**, 530−531.

(156) Winé, G.; Tessonnier, J. P.; Rigolet, S.; Marichal, C.; Ledoux, M. J.; Pham-Huu, C. Beta Zeolite Supported on a *β*-SiC Foam Monolith: A Diffusionless Catalyst for Fixed-Bed Friedel-Crafts Reactions. *J. Mol. Catal. A: Chem.* **2006**, *248*, 113−120.

(157) Winé, G.; Pham-Huu, C.; Ledoux, M. J. Acylation of Anisole by Acetic Anhydride Catalysed by BETA Zeolite Supported on Pre-Shaped Silicon Carbide. *Catal. Commun.* **2006**, *7*, 768−772.

(158) Winé, G.; Ledoux, M. J.; Pham-Huu, C. Supported BETA Zeolite on Preshaped *β*-SiC as Clean Friedel-Crafts Liquid-Phase Catalyst. *Top. Catal.* **2007**, *45*, 111−116.

(159) Winé, G.; El Berrichi, Z.; Pham-Huu, C. BETA Zeolite Supported on Silicon Carbide for Friedel-Crafts Fixed-Bed Reactions. *J. Mol. Catal. A: Chem.* **2007**, *278*, 64−71.

(160) Winé, G.; Vanhaecke, E.; Ivanova, S.; Ziessel, R.; Pham-Huu, C. Microwave Heating Effects on Acylation of Anisole, Catalyzed by BEA Zeolite Supported on *β*-SiC. *Catal. Commun.* **2009**, *10*, 477−480.

(161) Cui, Y.; Guo, X.; Wang, Y.; Guo, X. Carbonylative Suzuki Coupling Reactions of Aryl Iodides with Arylboronic Acids over Pd/SiC. *Chin. J. Catal.* **2015**, *36*, 322−327.

(162) Asahara, H.; Kuribayashi, Y.; Wang, P.; Kobiro, K.; Nishiwaki, N. An Effect of Microwave Irradiation on Pd/SiC Catalyst for Prolonging the Catalytic Life. *Curr. Microw. Chem.* **2014**, *1*, 142−147.

(163) Kremsner, J. M.; Kappe, C. O. Silicon Carbide Passive Heating Elements in Microwave-Assisted Organic Synthesis. *J. Org. Chem.* **2006**, *71*, 4651−4658.

(164) Portela, R.; Marinkovic, J. M.; Logemann, M.; Schörner, M.; Zahrtman, N.; Eray, E.; Haumann, M.; García-Suárez, E. J.; Wessling, M.; Ávila, P. Monolithic SiC Supports with Tailored Hierarchical Porosity for Molecularly Selective Membranes and Supported Liquid-Phase Catalysis. *Catal. Today* **2020**, DOI: 10.1016/j.cattod.2020.06.045.

(165) Moulijn, J. A.; Kreutzer, M. T.; Nijhuis, T. A.; Kapteijn, F. Chapter 5 - Monolithic Catalysts and Reactors: High Precision with Low Energy Consumption. In *Advances in Catalysis*; Bruce, C. G., Helmut, K., Eds.; Adv. Catal. Academic Press: 2011; pp 249−327, DOI: 10.1016/B978-0-12-387772-7.00005-8.

(166) Logemann, M.; Marinkovic, J. M.; Schörner, M.; García-Suárez, E. J.; Hecht, C.; Franke, R.; Wessling, M.; Riisager, A.; Fehrmann, R.; Haumann, M. Continuous Gas-Phase Hydroformylation of But-1-ene in a Membrane Reactor by Supported Liquid Phase (SLP) Catalysis. *Green Chem.* 2020, 22, 5691−5700.

(167) Marinkovic, J. M.; Benders, S.; Garcia-Suarez, E. J.; Weiß, A.; Gundlach, C.; Haumann, M.; Kuppers, M.; Blumich, B.; Fehrmann, R.; Riisager, A. Elucidating the Ionic Liquid Distribution in Monolithic SILP Hydroformylation Catalysts by Magnetic Resonance Imaging. *RSC Adv.* 2020, 10, 18487−18495.

(168) Corma, A.; Melo, F. V.; Sauvanaud, L.; Ortega, F. Light Cracked Naphtha Processing: Controlling Chemistry for Maximum Propylene Production. *Catal. Today* 2005, 107−108, 699−706.

(169) Diercks, R.; Arndt, J.-D.; Freyer, S.; Geier, R.; Machhammer, O.; Schwartze, J.; Volland, M. Raw Material Changes in the Chemical Industry. *Chem. Eng. Technol.* 2008, 31, 631−637.

(170) Wang, S.; Zhu, Z. H. Catalytic Conversion of Alkanes to Olefins by Carbon Dioxide Oxidative Dehydrogenation - A Review. *Energy Fuels* 2004, 18, 1126−1139.

(171) Ivanova, S.; Louis, B.; Madani, B.; Tessonnier, J. P.; Ledoux, M. J.; Pham-Huu, C. ZSM-5 Coatings on β-SiC Monoliths: Possible New Structured Catalyst for the Methanol-to-Olefins Process. *J. Phys. Chem. C* 2007, 111, 4368−4374.

(172) Ivanova, S.; Louis, B.; Ledoux, M.-J.; Pham-Huu, C. Autoassembly of Nanofibrous Zeolite Crystals via Silicon Carbide Substrate Self-Transformation. *J. Am. Chem. Soc.* 2007, 129, 3383−3391.

(173) Ivanova, S.; Lebrun, C.; Vanhaecke, E.; Pham-Huu, C.; Louis, B. Influence of the Zeolite Synthesis Route on Its Catalytic Properties in the Methanol to Olefin Reaction. *J. Catal.* 2009, 265, 1−7.

(174) Gu, L.; Ma, D.; Yao, S.; Liu, X.; Han, X.; Shen, W.; Bao, X. Template-Synthesized Porous Silicon Carbide as an Effective Host for Zeolite Catalysts. *Chem. - Eur. J.* 2009, 15, 13449−13455.

(175) Gu, L.; Ma, D.; Hu, G.; Wu, J.; Wang, H.; Sun, C.; Yao, S.; Shen, W.; Bao, X. Fabrication and Catalytic Tests of MCM-22/Silicon Carbide Structured Catalysts. *Dalton Trans.* 2010, 39, 9705−9710.

(176) Kosinov, N.; Hensen, E. J. M. Reactivity, Selectivity, and Stability of Zeolite-Based Catalysts for Methane Dehydroaromatization. *Adv. Mater.* 2020, 32, 2002565.

(177) Julian, I.; Ramirez, H.; Hueso, J. L.; Mallada, R.; Santamaria, J. Non-Oxidative Methane Conversion in Microwave-Assisted Structured Reactors. *Chem. Eng. J.* 2019, 377, 119764.

(178) Jiao, Y.; Jiang, C.; Yang, Z.; Liu, J.; Zhang, J. Synthesis of Highly Accessible ZSM-5 Coatings on SiC Foam Support for MTP Reaction. *Microporous Mesoporous Mater.* 2013, 181, 201−207.

(179) Jiao, Y.; Yang, X.; Jiang, C.; Tian, C.; Yang, Z.; Zhang, J. Hierarchical ZSM-5/SiC Nano-Whisker/SiC Foam Composites: Preparation and Application in MTP Reactions. *J. Catal.* 2015, 332, 70−76.

(180) Jiao, Y.; Jiang, C.; Yang, Z.; Zhang, J. Controllable Synthesis of ZSM-5 Coatings on SiC Foam Support for MTP Application. *Microporous Mesoporous Mater.* 2012, 162, 152−158.

(181) Jiao, Y.; Xu, S.; Jiang, C.; Perdjon, M.; Fan, X.; Zhang, J. MFI Zeolite Coating with Intrazeolitic Aluminum (Acidic) Gradient Supported on SiC Foams to Improve the Methanol-to-Propylene (MTP) Reaction. *Appl. Catal., A* 2018, 559, 1−9.

(182) Jiao, Y.; Fan, X.; Perdjon, M.; Yang, Z.; Zhang, J. Vapor-Phase Transport (VPT) Modification of ZSM-5/SiC Foam Catalyst Using TPAOH Vapor to Improve the Methanol-to-Propylene (MTP) Reaction. *Appl. Catal., A* 2017, 545, 104−112.

(183) Liao, Z.; Xu, T.; Jiang, Y.; Jiang, B.; Wang, J.; Yang, Y.; Jiao, Y.; Yang, Z.; Zhang, J. Methanol to Propylene over Foam SiC-Supported ZSM-5 Catalyst: Performance of Multiple Reaction-Regeneration Cycles. *Ind. Eng. Chem. Res.* 2019, 58, 27−33.

(184) Torres Galvis, H. M.; Bitter, J. H.; Khare, C. B.; Ruitenbeek, M.; Dugulan, A. I.; de Jong, K. P. Supported Iron Nanoparticles as Catalysts for Sustainable Production of Lower Olefins. *Science* 2012, 335, 835−838.

(185) Galadima, A.; Muraza, O. Revisiting the Oxidative Coupling of Methane to Ethylene in the Golden Period of Shale Gas: A Review. *J. Ind. Eng. Chem.* 2016, 37, 1−13.

(186) Ji, S.-F.; Xiao, T. C.; Li, S.-b.; Xu, C.-z.; Hou, R.-l.; Coleman, K. S.; Green, M. L. H. The Relationship Between the Structure and the Performance of Na-W-Mn/SiO₂ Catalysts for the Oxidative Coupling of Methane. *Appl. Catal., A* 2002, 225, 271−284.

(187) Liu, H.; Yang, D.; Gao, R.; Chen, L.; Zhang, S.; Wang, X. A Novel Na₂WO₄−Mn/SiC Monolithic Foam Catalyst with Improved Thermal Properties for the Oxidative Coupling of Methane. *Catal. Commun.* 2008, 9, 1302−1306.

(188) Yildiz, M.; Simon, U.; Otremba, T.; Aksuc, Y.; Kailasam, K.; Thomas, A.; Schomäcker, R.; Arndt, S. Support Material Variation for the Mn$_x$O$_y$-Na₂WO₄/SiO₂ Catalyst. *Catal. Today* 2014, 228, 5−14.

(189) Serres, T.; Aquino, C.; Mirodatos, C.; Schuurman, Y. Influence of the Composition/Texture of Mn-Na-W Catalysts on the Oxidative Coupling of Methane. *Appl. Catal., A* 2015, 504, 509−518.

(190) Wang, H.; Schmack, R.; Paula, B.; Albrecht, M.; Sokolov, S.; Rümmler, S.; Kondratenko, E. V.; Kraehnert, R. Porous Silicon Carbide as a Support for Mn/Na/W/SiC Catalyst in the Oxidative Coupling of Methane. *Appl. Catal., A* 2017, 537, 33−39.

(191) Kim, J.; Park, L.-H.; Ha, J.-M.; Park, E. D. Oxidative Coupling of Methane over Mn₂O₃-Na₂WO₄/SiC Catalysts. *Catalysts* 2019, 9, 363.

(192) Sigaeva, S. S.; Temerev, V. L.; Shlyapin, D. A.; Tsyrulnikov, P. G. Pyrolysis of Methane on Resistive MgO/SiC Catalyst. *Russ. J. Appl. Chem.* 2017, 90, 1939−1943.

(193) Sigaeva, S. S.; Shlyapin, D. A.; Temerev, V. L.; Tsyrulnikov, P. G. Pyrolysis of Methane on a Resistive ZrO₂/SiC Catalyst. *Russ. J. Appl. Chem.* 2019, 92, 1258−1265.

(194) Yin, H. M.; Ding, Y. J.; Luo, H. Y.; Zhu, H. J.; He, D. P.; Xiong, J. M.; Lin, L. W. Influence of Iron Promoter on Catalytic Properties of Rh-Mn-Li/SiO₂ for CO Hydrogenation. *Appl. Catal., A* 2003, 243, 155−164.

(195) Yin, H.; Ding, Y.; Luo, H.; Yan, L.; Wang, T.; Lin, L. The Performance of C₂ Oxygenates Synthesis from Syngas over Rh-Mn-Li-Fe/SiO₂ Catalysts with Various Rh Loadings. *Energy Fuels* 2003, 17, 1401−1406.

(196) Han, L.; Mao, D.; Yu, J.; Guo, Q.; Lu, G. C₂-Oxygenates Synthesis through CO Hydrogenation on SiO₂-ZrO₂ Supported Rh-Based Catalyst: The Effect of Support. *Appl. Catal., A* 2013, 454, 81−87.

(197) Chen, W.; Ding, Y.; Xue, F.; Song, X.; Ning, L. Highly Efficient β-SiC-Supported 0.5% Rh-Based Catalyst for CO Hydrogenation to C₂ Oxygenates. *Catal. Commun.* 2016, 85, 44−47.

(198) Ci, L.; Bai, J. Novel Micro/Nanoscale Hybrid Reinforcement: Multiwalled Carbon Nanotubes on SiC Particles. *Adv. Mater.* 2004, 16, 2021−2024.

(199) Shahi, F.; Pasha, M. A.; Hosseini, A. A.; Arabshahi, Z. S. Synthesis of MWCNTs Using Monometallic and Bimetallic Combinations of Fe, Co and Ni Catalysts Supported on Nanometric SiC via TCVD. *J. Nanostruct.* 2015, 5, 87−95.

(200) Ci, L. J.; Zhao, Z. G.; Bai, J. B. Direct Growth of Carbon Nanotubes on the Surface of Ceramic Fibers. *Carbon* 2005, 43, 883−886.

(201) Ci, L.; Ryu, Z.; Jin-Phillipp, N. Y.; Rühle, M. Carbon Nanotubes/SiC Whiskers Composite Prepared by CVD Method. *Diamond Relat. Mater.* 2007, 16, 531−536.

(202) Xie, S.; Jin, G.-Q.; Meng, S.; Wang, Y.-W.; Qin, Y.; Guo, X.-Y. Microwave Absorption Properties of In Situ Grown CNTs/SiC Composites. *J. Alloys Compd.* 2012, 520, 295−300.

(203) Tsubota, T.; Matsuo, H.; Murakami, N.; Ohno, T.; Yajima, H. Synthesis of Nanofibrous Carbon with Herringbone Structure on Ni-

Supported SiC Particles Using Hot CVD Apparatus. *Diamond Relat. Mater.* **2014**, *48*, 104−109.

(204) Cao, A.; Veedu, V.; Li, X.; Yao, Z.; Ghasemi-Nejhad, M. N.; Ajayan, P. M. Multifunctional Brushes Made from Carbon Nanotubes. *Nat. Mater.* **2005**, *4*, 540−545.

(205) Cambaz, Z. G.; Yushin, G.; Osswald, S.; Mochalin, V.; Gogotsi, Y. Noncatalytic Synthesis of Carbon Nanotubes, Graphene and Graphite on SiC. *Carbon* **2008**, *46*, 841−849.

(206) Rebmann, G.; Keller, V.; Ledoux, M. J.; Keller, N. Cu−Y Zeolite Supported on Silicon Carbide for the Vapour Phase Oxidative Carbonylation of Methanol to Dimethyl Carbonate. *Green Chem.* **2008**, *10*, 207−213.

(207) King, S. T. Reaction Mechanism of Oxidative Carbonylation of Methanol to Dimethyl Carbonate in Cu−Y Zeolite. *J. Catal.* **1996**, *161*, 530−538.

(208) Ivanova, S.; Vanhaecke, E.; Dreibine, L.; Louis, B.; Pham, C.; Pham-Huu, C. Binderless HZSM-5 Coating on β-SiC for Different Alcohols Dehydration. *Appl. Catal., A* **2009**, *359*, 151−157.

(209) Ivanova, S.; Vanhaecke, E.; Louis, B.; Libs, S.; Ledoux, M.-J.; Rigolet, S.; Marichal, C.; Pham, C.; Luck, F.; Pham-Huu, C. Efficient Synthesis of Dimethyl Ether over HZSM-5 Supported on Medium-Surface-Area β-SiC Foam. *ChemSusChem* **2008**, *1*, 851−857.

(210) Liu, Y.; Podila, S.; Nguyen, D. L.; Edouard, D.; Nguyen, P.; Pham, C.; Ledoux, M.-J.; Pham-Huu, C. Methanol Dehydration to Dimethyl Ether in a Platelet Milli-Reactor Filled with H-ZSM5/SiC Foam Catalyst. *Appl. Catal., A* **2011**, *409−410*, 113−121.

(211) Elamin, M. M.; Muraza, O.; Malaibari, Z.; Ba, H.; Nhut, J.-M.; Pham-Huu, C. Microwave Assisted Growth of SAPO-34 on β-SiC Foams for Methanol Dehydration to Dimethyl Ether. *Chem. Eng. J.* **2015**, *274*, 113−122.

(212) Wang, Y.; Guo, X.; Lü, M.; Zhai, Z.; Wang, Y.; Guo, X. Cu_2O/ SiC as Efficient Catalyst for Ullmann Coupling of Phenols with Aryl Halides. *Chin. J. Catal.* **2017**, *38*, 658−664.

(213) Mishra, G.; Behera, G. C.; Singh, S. K.; Parida, K. M. Liquid Phase Esterification of Acetic Acid over WO_3 Promoted β-SiC in a Solvent Free System. *Dalton Trans.* **2012**, *41*, 14299−14308.

(214) Martin, C.; Solana, G.; Malet, P.; Rives, V. Nb_2O_5-Supported WO_3: a Comparative Study with WO_3/Al_2O_3. *Catal. Today* **2003**, *78*, 365−376.

(215) Pérez-Cadenas, A. F.; Moreno-Castilla, C.; Maldonado-Hódar, F. J.; Fierro, J. L. G. Tungsten Oxide Catalysts Supported on Activated Carbons: Effect of Tungsten Precursor and Pretreatment on Dispersion, Distribution, and Surface Acidity of Catalysts. *J. Catal.* **2003**, *217*, 30−37.

(216) Jiménez-Morales, I.; Santamaría-González, J.; Maireles-Torres, P.; Jiménez-López, A. Zirconium Doped MCM-41 Supported WO_3 Solid Acid Catalysts for the Esterification of Oleic Acid with Methanol. *Appl. Catal., A* **2010**, *379*, 61−68.

(217) Gao, X.; Ding, Q.; Wu, Y.; Jiao, Y.; Zhang, J.; Li, X.; Li, H. Kinetic Study of Esterification over Structured ZSM-5-Coated Catalysts Based on Fluid Flow Situations in Macrocellular Foam Materials. *React. Chem. Eng.* **2020**, *5*, 485−494.

(218) Yang, X.; Jiang, C.; Yang, Z.; Zhang, J. Hydrochlorination of Acetylene Using SiC Foam Supported Structured C/Au Catalysts. *J. Mater. Sci. Technol.* **2014**, *30*, 434−440.

(219) Wypych, G. *PVC Degradation & Stabilization*, 3rd ed.; ChemTec Publishing: 2015; 488pp, DOI: 10.1016/C2014-0-01988-0.

(220) Indarto, A.; Palguandi, J. *Syngas: Production, Applications and Environmental Impact*; Indarto, A., Palguandi, J., Eds.; Nova Science Publishers: 2012; p 365.

(221) Choudhary, V. R.; Uphade, B. S.; Mamman, A. S. Oxidative Conversion of Methane to Syngas over Nickel Supported on Commercial Low Surface Area Porous Catalyst Carriers Precoated with Alkaline and Rare Earth Oxides. *J. Catal.* **1997**, *172*, 281−293.

(222) Sun, W.-Z.; Jin, G.-Q.; Guo, X.-Y. Partial Oxidation of Methane to Syngas over Ni/SiC Catalysts. *Catal. Commun.* **2005**, *6*, 135−139.

(223) Wang, Q.; Sun, W.-Z.; Jin, G.-Q.; Wang, Y.-Y.; Guo, X.-Y. Biomorphic SiC Pellets as Catalyst Support for Partial Oxidation of Methane to Syngas. *Appl. Catal., B* **2008**, *79*, 307−312.

(224) Shang, R.; Wang, Y.; Jin, G.; Guo, X.-Y. Partial Oxidation of Methane over Nickel Catalysts Supported on Nitrogen-Doped SiC. *Catal. Commun.* **2009**, *10*, 1502−1505.

(225) Li, C.; Xu, H.; Hou, S.; Sun, J.; Meng, F.; Ma, J.; Tsubaki, N. SiC Foam Monolith Catalyst for Pressurized Adiabatic Methane Reforming. *Appl. Energy* **2013**, *107*, 297−303.

(226) Wei, Q.; Yang, G.; Yoneyama, Y.; Vitidsant, T.; Tsubaki, N. Designing a Novel $Ni-Al_2O_3$-SiC Catalyst with a Stereo Structure for the Combined Methane Conversion Process to Effectively Produce Syngas. *Catal. Today* **2016**, *265*, 36−44.

(227) Wei, Q.; Yang, G.; Gao, X.; Yamane, N.; Zhang, P.; Liu, G.; Tsubaki, N. Ni/Silicalite-1 Coating Being Coated on SiC Foam: A Tailor-Made Monolith Catalyst for Syngas Production Using a Combined Methane Reforming Process. *Chem. Eng. J.* **2017**, *327*, 465−473.

(228) Garcia-Vargas, J. M.; Valverde, J. L.; de Lucas-Consuegra, A.; Gomez-Monedero, B.; Dorado, F.; Sanchez, P. Methane Tri-Reforming over a Ni/β-SiC-Based Catalyst: Optimizing the Feedstock Composition. *Int. J. Hydrogen Energy* **2013**, *38*, 4524−4532.

(229) García-Vargas, J. M.; Valverde, J. L.; Díez, J.; Sánchez, P.; Dorado, F. Influence of Alkaline and Alkaline-Earth Cocations on the Performance of Ni/β-SiC Catalysts in the Methane Tri-Reforming Reaction. *Appl. Catal., B* **2014**, *148−149*, 322−329.

(230) García-Vargas, J. M.; Valverde, J. L.; Díez, J.; Sánchez, P.; Dorado, F. Preparation of Ni−Mg/β-SiC Catalysts for the Methane Tri-Reforming: Effect of the Order of Metal Impregnation. *Appl. Catal., B* **2015**, *164*, 316−323.

(231) García-Vargas, M.; Valverde, J. L.; Díez, J.; Dorado, F.; Sanchez, P. Catalytic and Kinetic Analysis of the Methane Tri-Reforming over a Ni-Mg/β-SiC Catalyst. *Int. J. Hydrogen Energy* **2015**, *40*, 8677−8687.

(232) Song, C.; Pan, W. Tri-Reforming of Methane: a Novel Concept for Catalytic Production of Industrially Useful Synthesis Gas with Desired H_2/CO Ratios. *Catal. Today* **2004**, *98*, 463−484.

(233) García-Vargas, J. M.; Valverde, J. L.; de Lucas-Consuegra, A.; Gómez-Monedero, B.; Sánchez, P.; Dorado, F. Precursor Influence and Catalytic Behaviour of Ni/CeO_2 and Ni/SiC Catalysts for the Tri-Reforming Process. *Appl. Catal., A* **2012**, *431−432*, 49−56.

(234) Kim, J.-H.; Suh, D. J.; Park, T.-J.; Kim, K.-L. Effect of Metal Particle Size on Coking During CO_2 Reforming of CH_4 over Ni-Alumina Aerogel Catalysts. *Appl. Catal., A* **2000**, *197*, 191−200.

(235) Christensen, K. O.; Chen, D.; Lødeng, R.; Holmen, A. Effect of Supports and Ni Crystal Size on Carbon Formation and Sintering During Steam Methane Reforming. *Appl. Catal., A* **2006**, *314*, 9−22.

(236) García-Vargas, J. M.; Valverde, J. L.; Dorado, F.; Sánchez, P. Influence of the Support on the Catalytic Behaviour of Ni Catalysts for the Dry Reforming Reaction and the Tri-Reforming Process. *J. Mol. Catal. A: Chem.* **2014**, *395*, 108−116.

(237) Nguyen, D. L.; Leroi, P.; Ledoux, M. J.; Pham-Huu, C. Influence of the Oxygen Pretreatment on the CO_2 Reforming of Methane on Ni/β-SiC Catalyst. *Catal. Today* **2009**, *141*, 393−396.

(238) Kim, A. R.; Lee, H. Y.; Lee, D. H.; Kim, B.-W.; Chung, C.-H.; Moon, D. J.; Jang, E. J.; Pang, C.; Bae, J. W. Combined Steam and CO_2 Reforming of CH_4 on $LaSrNiO_x$ Mixed Oxides Supported on Al_2O_3-Modified SiC Support. *Energy Fuels* **2015**, *29*, 1055−1065.

(239) Kim, S. M.; Woo, S. I. Sustainable Production of Syngas from Biomass-Derived Glycerol by Steam Reforming over Highly Stable Ni/SiC. *ChemSusChem* **2012**, *5*, 1513−1522.

(240) Encinar, J. M.; Gonzalez, J. F.; Rodriguez-Reinares, A. Biodiesel from Used Frying Oil. Variables Affecting the Yields and Characteristics of the Biodiesel. *Ind. Eng. Chem. Res.* **2005**, *44*, 5491−5499.

(241) Pagliaro, M.; Ciriminna, R.; Kimura, H.; Rossi, M.; Della Pina, C. From Glycerol to Value-Added Products. *Angew. Chem., Int. Ed.* **2007**, *46*, 4434−4440.

(242) Jiao, Y.; Ou, X.; Zhang, J.; Fan, X. Structured ZSM-5 Coated SiC Foam Catalysts for Process Intensification in Catalytic Cracking of n-Hexane. *React. Chem. Eng.* **2019**, *4*, 427−435.

(243) Dabbawala, A. A.; Vaithilingam, B. V.; Mittal, H.; Al Wahedi, Y.; Khan, S.; Joseph, T.; Singaravel, G.; Morin, S.; Berthod, M.; Alhassan, S. M. Synthesis and Catalytic Performance of Zeolite-Y Supported on Silicon Carbide in n-Heptane Cracking. *Appl. Catal., A* **2020**, *608*, 117866.

(244) Xie, Q.; Li, S.; Gong, R.; Zheng, G.; Wang, Y.; Xu, P.; Duan, Y.; Yu, S.; Lu, M.; Ji, W.; et al. Microwave-Assisted Catalytic Dehydration of Glycerol for Sustainable Production of Acrolein over a Microwave Absorbing Catalyst. *Appl. Catal., B* **2019**, *243*, 455−462.

(245) Mahmoudi, H.; Mahmoudi, M.; Doustdar, O.; Jahangiri, H.; Tsolakis, A.; Gu, S.; Wyszynski, M. L. A Review of Fischer−Tropsch Synthesis Process, Mechanism, Surface Chemistry and Catalyst Formulation. *Biofuels Eng.* **2017**, *2*, 11−31.

(246) Yang, J.; Ma, W.; Chen, D.; Holmen, A.; Davis, B. H. Fischer−Tropsch Synthesis: A Review of the Effect of CO Conversionon Methane Selectivity. *Appl. Catal., A* **2014**, *470*, 250−260.

(247) Dry, M. E. High Quality Diesel via the Fischer−Tropsch Process - a Review. *J. Chem. Technol. Biotechnol.* **2002**, *77*, 43−50.

(248) Dry, M. E. The Fischer−Tropsch Process: 1950−2000. *Catal. Today* **2002**, *71*, 227−241.

(249) Steynberg, A. P. Introduction to Fischer−Tropsch Technology. In *Studies in Surface Science and Catalysis*; Steynberg, A., Dry, M., Eds.; Elsevier B.V.: 2004; pp 1−63, DOI: 10.1016/S0167-2991(04)80458-0.

(250) Wood, D. A.; Nwaoha, C.; Towler, B. F. Gas-to-Liquids (GTL): A Review of an Industry Offering Several Routes for Monetizing Natural Gas. *J. Nat. Gas Sci. Eng.* **2012**, *9*, 196−208.

(251) Zhong, M.; Guo, Y.; Wang, J.; Ma, Z.; Xia, M.; Chen, C.; Jia, L.; Hou, B.; Li, D. The Fischer−Tropsch Synthesis Performance over Cobalt Supported on Silicon-Based Materials: the Effect of Thermal Conductivity of the Support. *Catal. Sci. Technol.* **2019**, *9*, 3482−3492.

(252) de Klerk, A.; Maitlis, P. M. Chapter 4 - What Can We Do with Fischer−Tropsch Products? In *Greener Fischer−Tropsch Processes for Fuels and Feedstocks*; de Klerk, A., Maitlis, P. M., Eds.; Wiley-VCH Verlag & Co. KGaA: Hoboken, 2013; pp 81−106, DOI: 10.1002/9783527656837.ch4.

(253) Philippe, R.; Lacroix, M.; Dreibine, L.; Pham-Huu, C.; Edouard, D.; Savin, S.; Luck, F.; Schweich, D. Effect of Structure and Thermal Properties of a Fischer−Tropsch Catalyst in a Fixed Bed. *Catal. Today* **2009**, *147S*, S305−S312.

(254) Zhu, X.; Lu, X.; Liu, X.; Hildebrandt, D.; Glasser, D. Heat Transfer Study with and without Fischer−Tropsch Reaction in a Fixed Bed Reactor with TiO₂, SiO₂, and SiC Supported Cobalt Catalysts. *Chem. Eng. J.* **2014**, *247*, 75−84.

(255) de la Osa, A. R.; De Lucas, A.; Romero, A.; Valverde, J. L.; Sánchez, P. Influence of the Catalytic Support on the Industrial Fischer−Tropsch Synthetic Diesel Production. *Catal. Today* **2011**, *176*, 298−302.

(256) Koo, H.-M.; Lee, B. S.; Park, M.-J.; Moon, D. J.; Roh, H.-S.; Bae, J. W. Fischer−Tropsch Synthesis on Cobalt/Al₂O₃-Modified SiC Catalysts: Effect of Cobalt-Alumina Interactions. *Catal. Sci. Technol.* **2014**, *4*, 343−351.

(257) Lee, B.; Koo, H. M.; Park, M.-J.; Lim, B.; Moon, D. J.; Yoon, K. J.; Bae, J. W. Deactivation Behavior of Co/SiC Fischer−Tropsch Catalysts by Formation of Filamentous Carbon. *Catal. Lett.* **2013**, *143*, 18−22.

(258) de la Osa, A. R.; De Lucas, A.; Díaz-Maroto, J.; Romero, A.; Valverde, J. L.; Sánchez, P. FTS Fuels Production over Different Co/SiC Catalysts. *Catal. Today* **2012**, *187*, 173−182.

(259) de la Osa, A. R.; de Lucas, A.; Sánchez-Silva, L.; Díaz-Maroto, J.; Valverde, J. L.; Sánchez, P. Performing the Best Composition of Supported Co/SiC Catalyst for Selective FTS Diesel Production. *Fuel* **2012**, *95*, 587−598.

(260) de la Osa, A. R.; Romero, A.; Díez-Ramírez, J.; Valverde, J. L.; Sánchez, P. Influence of a Zeolite-Based Cascade Layer on Fischer−

Tropsch Fuels Production over Silicon Carbide Supported Cobalt Catalyst. *Top. Catal.* **2017**, *60*, 1082−1093.

(261) Lillebø, A.; Havik, S.; Blekkan, E. A.; Holmen, A. Fischer−Tropsch Synthesis on SiC-Supported Cobalt Catalysts. *Top. Catal.* **2013**, *56*, 730−736.

(262) Rane, S.; Borg, Ø.; Yang, J.; Rytter, E.; Holmen, A. Effect of Alumina Phases on Hydrocarbon Selectivity in Fischer−Tropsch Synthesis. *Appl. Catal., A* **2010**, *388*, 160−167.

(263) Díaz, J. A.; Calvo-Serrano, M.; de la Osa, A. R.; García-Minguillán, A. M.; Romero, A.; Giroir-Fendler, A.; Valverde, J. L. β-Silicon Carbide as a Catalyst Support in the Fischer−Tropsch Synthesis: Influence of the Modification of the Support by a Pore Agent and Acidic Treatment. *Appl. Catal., A* **2014**, *475*, 82−89.

(264) Li, Z.; Wu, J.; Wu, L. Effect of Zr, Ca and Mn as Promoters on the Co/SiC Catalysts for the Fischer−Tropsch Synthesis. *React. Kinet., Mech. Catal.* **2017**, *122*, 887−900.

(265) de Tymowski, B.; Liu, Y.; Meny, C.; Lefèvre, C.; Begin, D.; Nguyen, P.; Pham, C.; Edouard, D.; Luck, F.; Pham-Huu, C. Co−Ru/SiC impregnated with ethanol as an effective catalyst for the Fischer−Tropsch synthesis. *Appl. Catal., A* **2012**, *419−420*, 31−40.

(266) Liu, Y.; Edouard, D.; Nguyen, L. D.; Begin, D.; Nguyen, P.; Pham, C.; Pham-Huu, C. High Performance Structured Platelet Milli-Reactor Filled with Supported Cobalt Open Cell SiC Foam Catalyst for the Fischer−Tropsch Synthesis. *Chem. Eng. J.* **2013**, *222*, 265−273.

(267) Noh, Y. S.; Lee, K.-Y.; Moon, D. J. Studies on the Fischer−Tropsch Synthesis over RuCo/SiC-Al₂O₃ Structured Catalyst. *Catal. Today* **2020**, *348*, 157−165.

(268) Solomonik, I. G.; Gryaznov, K. O.; Skoka, V. F.; Mordkovich, V. Z. Formation of Surface Cobalt Structures in SiC Supported Fischer−Tropsch Catalysts. *RSC Adv.* **2015**, *5*, 78586−78597.

(269) Lee, J. S.; Jung, J. S.; Moon, D. J. The Effect of Cobalt Loading on Fischer−Tropsch Synthesis over Silicon Carbide Supported Catalyst. *J. Nanosci. Nanotechnol.* **2015**, *15*, 396−399.

(270) de la Osa, A. R.; Romero, A.; Dorado, F.; Valverde, J. L.; Sánchez, P. Influence of Cobalt Precursor on Efficient Production of Commercial Fuels over FTS Co/SiC Catalyst. *Catalysts* **2016**, *6*, 98.

(271) Song, H.; Zhao, Q.; Zhou, X.; Cao, Z.; Luo, M. Selection of Highly Active and Stable Co Supported SiC Catalyst for Fischer−Tropsch Synthesis: Effect of the Preparation Method. *Fuel* **2018**, *229*, 144−150.

(272) Romar, H.; Lillebø, A. H.; Tynjala, P.; Hu, T.; Holmen, A.; Blekkan, E. A.; Lassi, U. Characterisation and Catalytic Fischer−Tropsch Activity of Co−Ru and Co−Re Catalysts Supported on γ-Al₂O₃, TiO₂ and SiC. *Top. Catal.* **2015**, *58*, 887−895.

(273) Borg, Ø.; Dietzel, P. D. C.; Spjelkavik, A. I.; Tveten, E. Z.; Walmsley, J. C.; Diplas, S.; Eri, S.; Holmen, A.; Rytter, E. Fischer−Tropsch Synthesis: Cobalt Particle Size and Support Effects on Intrinsic Activity and Product Distribution. *J. Catal.* **2008**, *259*, 161−164.

(274) Romar, H.; Lillebø, A. H.; Tynjälä, P.; Hu, T.; Holmen, A.; Blekkan, E. A.; Lassi, U. H₂-TPR, XPS and TEM Study of the Reduction of Ru and Re promoted Co/γ-Al₂O₃, Co/TiO₂ and Co/SiC Catalysts. *J. Mater. Sci. Res.* **2016**, *5*, 33−43.

(275) Liu, Y.; de Tymowski, B.; Vigneron, F.; Florea, I.; Ersen, O.; Meny, C.; Nguyen, P.; Pham, C.; Luck, F.; Pham-Huu, C. Titania-Decorated Silicon Carbide-Containing Cobalt Catalyst for Fischer−Tropsch Synthesis. *ACS Catal.* **2013**, *3*, 393−404.

(276) Liu, Y.; Florea, I.; Ersen, O.; Pham-Huu, C.; Meny, C. Silicon Carbide Coated with TiO₂ with Enhanced Cobalt Active Phase Dispersion for Fischer−Tropsch Synthesis. *Chem. Commun.* **2015**, *51*, 145−148.

(277) Florea, I.; Liu, Y.; Ersen, O.; Meny, C.; Pham-Huu, C. Microstructural Analysis and Energy-Filtered TEM Imaging to Investigate the Structure-Activity Relationship in Fischer−Tropsch Catalysts. *ChemCatChem* **2013**, *5*, 2610−2620.

(278) Jalama, K.; Kabuba, J.; Xiong, H. F.; Jewell, L. L. Co/TiO₂ Fischer−Tropsch Catalyst Activation by Synthesis Gas. *Catal. Commun.* **2012**, *17*, 154−159.

CO

(279) Lualdi, M.; Di Carlo, G.; Logdberg, S.; Jaras, S.; Boutonnet, M.; La Parola, V.; Liotta, L. F.; Ingo, G. M.; Venezia, A. M. Effect of Ti and Al Addition via Direct Synthesis to SBA-15 as Support for Cobalt Based Fischer−Tropsch Catalysts. *Appl. Catal., A* **2012**, *443−444*, 76−86.

(280) Venezia, A. M.; La Parola, V.; Liotta, L. F.; Pantaleo, G.; Lualdi, M.; Boutonnet, M.; Järås, S. Co/SiO₂ Catalysts for Fischer−Tropsch Synthesis; Effect of Co Loading and Support Modification by TiO₂. *Catal. Today* **2012**, *197*, 18−23.

(281) Yu, L.; Liu, X.; Fang, Y.; Wang, C.; Sun, Y. Highly Active Co/SiC Catalysts with Controllable Dispersion and Reducibility for Fischer−Tropsch Synthesis. *Fuel* **2013**, *112*, 483−488.

(282) Trepanier, M.; Tavasoli, A.; Dalai, A. K.; Abatzoglou, N. Co, Ru and K Loadings Effects on the Activity and Selectivity of Carbon Nanotubes Supported Cobalt Catalyst in Fischer−Tropsch Synthesis. *Appl. Catal., A* **2009**, *353*, 193−202.

(283) Borg, O.; Hammer, N.; Eri, S.; Lindvag, O. A.; Myrstad, R.; Blekkan, E. A.; Rønning, M.; Rytter, E.; Holmen, A. Fischer−Tropsch Synthesis over Un-Promoted and Re-Promoted gamma-Al₂O₃ Supported Cobalt Catalysts with Different Pore Sizes. *Catal. Today* **2009**, *142*, 70−77.

(284) Gnanamani, M. K.; Ribeiro, M. C.; Ma, W. P.; Shafer, W. D.; Jacobs, G.; Graham, U. M.; Davis, B. H. Fischer−Tropsch Synthesis: Metal-Support Interfacial Contact Governs Oxygenates Selectivity over CeO₂ Supported Pt-Co Catalysts. *Appl. Catal., A* **2011**, *393*, 17−23.

(285) Karaca, H.; Safonova, O. V.; Chambrey, S.; Fongarland, P.; Roussel, P.; Griboval-Constant, A.; Lacroix, M.; Khodakov, A. Y. Structure and Catalytic Performance of Pt-Promoted Alumina Supported Cobalt Catalysts under Realistic Conditions of Fischer−Tropsch Synthesis. *J. Catal.* **2011**, *277*, 14−26.

(286) Gnanamani, M. K.; Shafer, W. D.; Sparks, D. E.; Davis, B. H. Fischer−Tropsch Synthesis: Effect of CO₂ Containing Syngas over Pt Promoted Co/gamma-Al₂O₃ and K-Promoted Fe Catalysts. *Catal. Commun.* **2011**, *12*, 936−939.

(287) Piao, Y.; Jiang, Q.; Li, H.; Matsumoto, H.; Liang, J.; Liu, W.; Pham-Huu, C.; Liu, Y.; Wang, F. Identify Zr Promotion Effects in Atomic Scale for Co-Based Catalysts in Fischer−Tropsch Synthesis. *ACS Catal.* **2020**, *10*, 7894−7906.

(288) Labuschagne, J.; Meyer, R.; Chonco, Z. H.; Botha, J. M.; Moodley, D. J. Application of Water-Tolerant Co/β-SiC Catalysts in Slurry Phase Fischer−Tropsch Synthesis. *Catal. Today* **2016**, *275*, 2−10.

(289) Wang, M.; Guo, S.; Li, Z.; Ma, Z.; Wang, J.; Hou, B.; Jia, L.; Li, D. The Role of SiOₓCᵧ in the Catalytic Performance of Co/SiC Catalysts for Fischer−Tropsch Synthesis. *Fuel* **2019**, *241*, 669−675.

(290) Wang, D.; Chen, C.; Wang, J.; Jia, L.; Hou, B.; Li, D. Silicon Carbide Supported Cobalt for Fischer−Tropsch Synthesis: Probing into the Cause of the Intrinsic Excellent Catalytic Performance. *RSC Adv.* **2015**, *5*, 98900−98903.

(291) Wang, M.; Guo, S.; Xia, M.; Wang, J.; Ma, Z.; Hou, B.; Jia, L.; Li, D. The Role of Co-ZrO₂ Interfacial Sites in Promoting Catalytic Performance of Co/SiC Catalyst for Fischer−Tropsch Synthesis. *J. Energy Inst.* **2020**, *93*, 2355−2361.

(292) Alvarado Rupflin, L.; Van Rensburg, H.; Zanella, M.; Carrington, E. J.; Vismara, R.; Grigoropoulos, A.; Manning, T. D.; Claridge, J. B.; Katsoulidis, A. P.; Tooze, R. P.; et al. High-Throughput Discovery of Hf Promotion on the Stabilisation of hcp Co and Fischer−Tropsch Activity. *J. Catal.* **2021**, *396*, 315−323.

(293) Iablokov, V.; Alekseev, S. A.; Gryn, S.; Bezverkhyy, I.; Zaitsev, V.; Kovarik, L.; Visart de Bocarme, T.; Kruse, N. , Superior Fischer−Tropsch Performance of Uniform Cobalt Nanoparticles Deposited into Mesoporous SiC. *J. Catal.* **2020**, *383*, 297−303.

(294) Jiang, F.; Zhang, M.; Liu, B.; Xu, Y.; Liu, X. Insights into the Influence of Support and Potassium or Sulfur Promoter on Iron-Based Fischer−Tropsch Synthesis: Understanding the Control of Catalytic Activity, Selectivity to Lower Olefins, and Catalyst Deactivation. *Catal. Sci. Technol.* **2017**, *7*, 1245−1265.

(295) Oschatz, M.; Lamme, W. S.; Xie, J.; Dugulan, A. I.; de Jong, K. P. Ordered Mesoporous Materials as Supports for Stable Iron Catalysts in the Fischer−Tropsch Synthesis of Lower Olefins. *ChemCatChem* **2016**, *8*, 2846−2852.

(296) Geng, S.; Jiang, F.; Xu, Y.; Liu, X. Iron-Based Fischer−Tropsch Synthesis for the Efficient Conversion of Carbon Dioxide into Isoparaffins. *ChemCatChem* **2016**, *8*, 1303−1307.

(297) Bozell, J. J. Connecting Biomass and Petroleum Processing with a Chemical Bridge. *Science* **2010**, *329*, 522−523.

(298) Huber, G. W.; Iborra, S.; Corma, A. Synthesis of Transportation Fuels from Biomass: Chemistry, Catalysts, and Engineering. *Chem. Rev.* **2006**, *106*, 4044−4098.

(299) Zhang, Z.; Song, J.; Han, B. Catalytic Transformation of Lignocellulose into Chemicals and Fuel Products in Ionic Liquids. *Chem. Rev.* **2017**, *117*, 6834−6880.

(300) Li, C.; Zhao, X.; Wang, A.; Huber, G. W.; Zhang, T. Catalytic Transformation of Lignin for the Production of Chemicals and Fuels. *Chem. Rev.* **2015**, *115*, 11559−11624.

(301) Bridgwater, A. V. Review of Fast Pyrolysis of Biomass and Product Upgrading. *Biomass Bioenergy* **2012**, *38*, 68−94.

(302) Zhou, C.-H.; Xia, X.; Lin, C.-X.; Tong, D.-S.; Beltramini, J. Catalytic Conversion of Lignocellulosic Biomass to Fine Chemicals and Fuels. *Chem. Soc. Rev.* **2011**, *40*, 5588−5617.

(303) Nokkosmaki, M. I.; Kuoppala, E. T.; Leppamaki, E. A.; Krause, A. O. I. Catalytic Conversion of Biomass Pyrolysis Vapours with Zinc Oxide. *J. Anal. Appl. Pyrolysis* **2000**, *55*, 119−131.

(304) Chen, Y.; Wang, F.; Jia, Y.; Yang, N.; Zhang, X. One-Step Ethanolysis of Lignin into Small-Molecular Aromatic Hydrocarbons over Nano-SiC Catalyst. *Bioresour. Technol.* **2017**, *226*, 145−149.

(305) Qiu, S.; Li, M.; Huang, Y.; Fang, Y. Catalytic Hydrotreatment of Kraft Lignin over NiW/SiC: Effective Depolymerization and Catalyst Regeneration. *Ind. Eng. Chem. Res.* **2018**, *57*, 2023−2030.

(306) Czernik, S.; Bridgwater, A. Overview of Applications of Biomass Fast Pyrolysis Oil. *Energy Fuels* **2004**, *18*, 590−598.

(307) Zhou, N.; Liu, S.; Zhang, Y.; Fan, L.; Cheng, Y.; Wang, Y.; Liu, Y.; Chen, P.; Ruan, R. Silicon Carbide Foam Supported ZSM-5 Composite Catalyst for Microwave Assisted Pyrolysis of Biomass. *Bioresour. Technol.* **2018**, *267*, 257−264.

(308) Jiang, L.; Wang, Y.; Dai, L.; Yu, Z.; Yang, Q.; Yang, S.; Jiang, D.; Ma, Z.; Wu, Q.; Zhang, B.; et al. Co-Pyrolysis of Biomass and Soapstock in a Downdraft Reactor Using a Novel ZSM-5/SiC Composite Catalyst. *Bioresour. Technol.* **2019**, *279*, 202−208.

(309) Jiang, L.; Wang, Y.; Dai, L.; Yu, Z.; Wu, Q.; Zhao, Y.; Liu, Y.; Ruan, R.; Ke, L.; Peng, Y.; et al. Integrating Pyrolysis and Ex-Situ Catalytic Reforming by Microwave Heating to Produce Hydrocarbon-Rich Bio-Oil from Soybean Soapstock. *Bioresour. Technol.* **2020**, *302*, 122843.

(310) Yu, Z.; Jiang, L.; Wang, Y.; Li, Y.; Ke, L.; Yang, Q.; Peng, Y.; Xu, J.; Dai, L.; Wu, Q.; et al. Catalytic Pyrolysis of Woody Oil over SiC Foam-MCM41 Catalyst for Aromatic-Rich Bio-Oil Production in a Dual Microwave System. *J. Cleaner Prod.* **2020**, *255*, 120179.

(311) Yu, Z.; Wang, Y.; Jiang, L.; Dai, L.; Liu, Y.; Ruan, R.; Wen, P.; Zhao, Y.; Duan, D.; Zou, R.; et al. Conversion of Woody Oil into Bio-Oil in a Downdraft Reactor Using a Novel Silicon Carbide Foam Supported MCM41 Composite Catalyst. *RSC Adv.* **2019**, *9*, 19729−19739.

(312) Borges, F. C.; Du, Z.; Xie, Q.; Trierweiler, J. O.; Cheng, Y.; Wan, Y.; Liu, Y.; Zhu, R.; Lin, X.; Chen, P. Fast Microwave Assisted Pyrolysis of Biomass Using Microwave Absorbent. *Bioresour. Technol.* **2014**, *156*, 267−274.

(313) Wang, W.; Wang, M.; Li, X.; Cai, L.; Shi, S. Q.; Duan, C.; Ni, Y. Microwave-Assisted Catalytic Cleavage of C−C Bond in Lignin Models by Bifunctional Pt/CDC-SiC. *ACS Sustainable Chem. Eng.* **2020**, *8*, 38−43.

(314) Götz, M.; Lefebvre, J.; Mörs, F.; Koch, A. M.; Graf, F.; Bajohr, S.; Reimert, R.; Kolb, T. Renewable Power-to-Gas: A Technological and Economic Review. *Renewable Energy* **2016**, *85*, 1371−1390.

(315) Su, X.; Xu, J.; Liang, B.; Duan, H.; Hou, B.; Huang, Y. Catalytic Carbon Dioxide Hydrogenation to Methane: A Review of Recent Studies. *J. Energy Chem.* **2016**, *25*, 553−565.

(316) Ronsch, S.; Schneider, J.; Matthischke, S.; Schluter, M.; Gotz, M.; Lefebre, J.; Prabhakaran, P.; Bajohr, S. Review on Methanation-From Fundamentals to Current Projects. *Fuel* **2016**, *166*, 276−296.

(317) Aziz, M. A. A.; Jalil, A. A.; Triwahyono, S.; Ahmad, A. CO$_2$ Methanation over Heterogeneous Catalysts: Recent Progress and Future Prospects. *Green Chem.* **2015**, *17*, 2647−2663.

(318) Frontera, P.; Macario, M.; Ferraro, M.; Antonucci, P. Supported Catalysts for CO$_2$ Methanation: A Review. *Catalysts* **2017**, *7*, 59.

(319) Zhi, G.; Guo, X.; Wang, Y.; Jin, G.; Guo, X. Effect of La$_2$O$_3$ Modification on the Catalytic Performance of Ni/SiC for Methanation of Carbon Dioxide. *Catal. Commun.* **2011**, *16*, 56−59.

(320) Yu, Y.; Jin, G.; Wang, Y.; Guo, X.-Y. Synthesis of Natural Gas from CO Methanation over SiC Supported Ni-Co Bimetallic Catalysts. *Catal. Commun.* **2013**, *31*, 5−10.

(321) Yu, Y.; Jin, G.-Q.; Wang, Y.-Y.; Guo, X.-Y. Synthetic Natural Gas from CO Hydrogenation over Silicon Carbide Supported Nickel Catalysts. *Fuel Process. Technol.* **2011**, *92*, 2293−2298.

(322) Song, L.; Yu, Y.; Wang, X.; Jin, G.; Wang, Y.; Guo, X.-Y. The Influence of a Second Metal on the Ni/SiC Catalyst for the Methanation of Syngas. *Hwahak Konghak* **2014**, *52*, 678−687.

(323) Zhang, G.; Sun, T.; Peng, J.; Wang, S.; Wang, S. A Comparison of Ni/SiC and Ni/Al$_2$O$_3$ Catalyzed Total Methanation for Production of Synthetic Natural Gas. *Appl. Catal., A* **2013**, *462−463*, 75−81.

(324) Zhang, G.; Peng, J.; Sun, T.; Wang, S. Effects of Oxidation Extent of the SiC Surface on the Performance of Ni/SiC Methanation Catalysts. *Chin. J. Catal.* **2013**, *34*, 1745−1755.

(325) Petersen, E. M.; Rao, R. G.; Vance, B. C.; Tessonnier, J.-P. SiO$_2$/SiC Supports with Tailored Thermal Conductivity to Reveal the Effect of Surface Temperature on Ru-Catalyzed CO$_2$ Methanation. *Appl. Catal., B* **2021**, *286*, 119904.

(326) Jin, G.; Gu, F.; Liu, Q.; Wang, X.; Jia, L.; Xu, G.; Zhong, Z.; Su, F. Highly Stable Ni/SiC Catalyst Modified by Al$_2$O$_3$ for CO Methanation Reaction. *RSC Adv.* **2016**, *6*, 9631−9639.

(327) Sun, J.; Feng, Q.; Liu, Q.; Ji, S.; Fang, Y.; Peng, X.; Wang, Z.-j. An Al$_2$O$_3$-Coated SiC-Supported Ni Catalyst with Enhanced Activity and Improved Stability for Production of Synthetic Natural Gas. *Ind. Eng. Chem. Res.* **2018**, *57*, 14899−14909.

(328) Yuan, Q.; Yin, A.-X.; Luo, C.; Sun, L.-D.; Zhang, Y.-W.; Duan, W.-T.; Liu, H.-C.; Yan, C.-H. Facile Synthesis for Ordered Mesoporous γ-Aluminas with High Thermal Stability. *J. Am. Chem. Soc.* **2008**, *130*, 3465−3472.

(329) Morris, S. M.; Fulvio, P. F.; Jaroniec, M. Ordered Mesoporous Alumina-Supported Metal Oxides. *J. Am. Chem. Soc.* **2008**, *130*, 15210−15216.

(330) Wang, Y.; Xu, Y.; Liu, Q.; Sun, J.; Ji, S.; Wang, Z.-j. Enhanced Low-Temperature Activity for CO$_2$ Methanation over NiMgAl/SiC Composite Catalysts. *J. Chem. Technol. Biotechnol.* **2019**, *94*, 3780−3786.

(331) Frey, M.; Edouard, D.; Roger, A.-C. Optimization of Structured Cellular Foam-Based Catalysts for Low-Temperature Carbon Dioxide Methanation in a Platelet Milli-Reactor. *C. R. Chim.* **2015**, *18*, 283−292.

(332) Frey, M.; Romero, T.; Roger, A.-C.; Edouard, D. An Intensification of the CO$_2$ Methanation Reaction: Effect of Carbon Nanofiber Network on the Hydrodynamic, Thermal and Catalytic Properties of Reactors Filled with Open Cell Foams. *Chem. Eng. Sci.* **2019**, *195*, 271−280.

(333) Frey, M.; Romero, T.; Roger, A.-C.; Edouard, D. Open Cell Foam Catalysts for CO$_2$ Methanation: Presentation of Coating Procedures and *In Situ* Exothermicity Reaction Study by Infrared Thermography. *Catal. Today* **2016**, *273*, 83−90.

(334) Liu, S.-S.; Jin, Y.-Y.; Han, Y.; Zhao, J.; Ren, J. Highly Stable and Coking Resistant Ce Promoted Ni/SiC Catalyst towards High

Temperature CO Methanation. *Fuel Process. Technol.* **2018**, *177*, 266−274.

(335) Han, X.; Zhao, C.; Sun, W.; Han, B.; Han, Y.; Ren, J. A Density Functional Theory Study of CO Methanation Mechanism on Ni$_4$/SiC Catalyst. *Comput. Mater. Sci.* **2018**, *153*, 399−408.

(336) Li, L.; Zheng, J.; Liu, Y.; Wang, W.; Huang, Q.; Chu, W. Impacts of SiC Carrier and Nickel Precursor of NiLa/support Catalysts for CO$_2$ Selective Hydrogenation to Synthetic Natural Gas (SNG). *ChemistrySelect* **2017**, *2*, 3750−3757.

(337) Li, J.-W.; Song, Q.; Li, J.-B.; Yang, S.-C.; Gao, Y.-S.; Wang, Q.; Yu, F. La-Enhanced Ni Nanoparticles Highly Dispersed on SiC for Low Temperature CO Methanation Performance. *Rare Met.* **2021**, *40*, 1753−1761.

(338) Le, T. A.; Kang, J. K.; Park, E. D. CO and CO$_2$ Methanation over Ni/SiC and Ni/SiO$_2$ Catalysts. *Top. Catal.* **2018**, *61*, 1537−1544.

(339) Song, Q.; Zhai, X.; Yu, F.; Li, J.; Ren, X.; Zhang, H.; Zhu, M.; Dai, B.; Ge, G.; Zhang, J. Defect-Rich Nickel Nanoparticles Supported on SiC Derived from Silica Fume with Enhanced Catalytic Performance for CO Methanation. *Catalysts* **2019**, *9*, 295.

(340) Borgschulte, A.; Gallandat, N.; Probst, B.; Suter, R.; Callini, E.; Ferri, F.; Arroyo, Y.; Erni, R.; Geerlings, H.; Züttel, A. Sorption Enhanced CO$_2$ Methanation. *Phys. Chem. Chem. Phys.* **2013**, *15*, 9620−9625.

(341) Borgschulte, A.; Callini, E.; Stadie, N.; Arroyo, Y.; Rossell, M. D.; Erni, R.; Geerlings, H.; Züttel, A.; Ferri, D. Manipulating the Reaction Path of the CO$_2$ Hydrogenation Reaction in Molecular Sieves. *Catal. Sci. Technol.* **2015**, *5*, 4613−4621.

(342) Borgschulte, A.; Delmelle, R.; Duarte, R. B.; Heel, A.; Boillat, P.; Lehmann, E. Water Distribution in a Sorption Enhanced Methanation Reactor by Time Resolved Neutron Imaging. *Phys. Chem. Chem. Phys.* **2016**, *18*, 17217−17223.

(343) Delmelle, R.; Duarte, R. B.; Franken, T.; Burnat, D.; Holzer, L.; Borgschulte, A.; Heel, A. Development of Improved Nickel Catalysts for Sorption Enhanced CO$_2$ Methanation. *Int. J. Hydrogen Energy* **2016**, *41*, 20185−20191.

(344) Delmelle, R.; Terreni, J.; Remhof, A.; Heel, A.; Proost, J.; Borgschulte, A. Evolution of Water Diffusion in a Sorption-Enhanced Methanation Catalyst. *Catalysts* **2018**, *8*, 341.

(345) Zhang, R.; Chen, H.; Mu, Y.; Chansai, S.; Ou, X.; Hardacre, C.; Jiao, Y.; Fan, X. Structured Ni@NaA Zeolite Supported on Silicon Carbide Foam Catalysts for Catalytic Carbon Dioxide Methanation. *AIChE J.* **2020**, *66*, e17007.

(346) Subramani, V.; Sharma, P.; Zhang, L.; Liu, K. Catalytic Steam Reforming Technology for the Production of Hydrogen and Syngas. In *Hydrogen and Syngas Production and Purification Technologies*; Liu, K., Song, C., Subramani, V., Eds.; American Institute of Chemical Engineers: 2009; pp 14−126, DOI: 10.1002/9780470561256.ch2.

(347) Speight, J. *Natural Gas; A Basic Handbook*, 2nd ed.; Gulf Professional Publishing: 2018; p 462, DOI: 10.1016/C2015-0-02190-6 .

(348) Vozniuk, O.; Tanchoux, N.; Millet, J.-M.; Albonetti, S.; Di Renzo, F.; Cavani, F. Spinel Mixed Oxides for Chemical-Loop Reforming: From Solid State to Potential Application. In *Horizons in Sustainable Industrial Chemistry and Catalysis*; Albonetti, S., Perathoner, S., Quadrelli, E. A., Eds.; Elsevier: 2019; Vol. *178*, pp 281−302, DOI: 10.1016/B978-0-444-64127-4.00014-8.

(349) Bradford, M. C. J.; Vannice, M. A. CO$_2$ Reforming of CH$_4$. *Catal. Rev.: Sci. Eng.* **1999**, *41*, 1−42.

(350) Lavoie, J.-M. Review on Dry Reforming of Methane, a Potentially more Environmentally-Friendly Approach to the Increasing Natural Gas Exploitation. *Front. Chem.* **2014**, *2*, 81.

(351) Worner, A.; Tamme, R. CO$_2$ Reforming of Methane in a Solar Driven Volumetric Receiver-Reactor. *Catal. Today* **1998**, *46*, 165−174.

(352) Kodama, T.; Moriyama, T.; Shimoyama, T.; Gokon, N.; Andou, H.; Satou, N. Ru/Ni−Mg−O Catalyzed SiC-Foam Absorber for Solar Reforming Receiver-Reactor. *J. Sol. Energy Eng.* **2006**, *128*, 318−325.

(353) Gokon, N.; Yamawaki, Y.; Nakazawa, D.; Kodama, T. Ni/MgO-Al$_2$O$_3$ and Ni-Mg-O Catalyzed SiC Foam Absorbers for High Temperature Solar Reforming of Methane. *Int. J. Hydrogen Energy* **2010**, *35*, 7441−7453.

(354) Liu, H.; Li, S.; Zhang, S.; Wang, J.; Zhou, G.; Chen, L.; Wang, X. Catalytic Performance of Novel Ni Catalysts Supported on SiC Monolithic Foam in Carbon Dioxide Reforming of Methane to Synthesis Gas. *Catal. Commun.* **2008**, *9*, 51−54.

(355) Liu, H.; Li, S.; Zhang, S.; Chen, L.; Zhou, G.; Wang, J.; Wang, X. Catalytic Performance of Monolithic Foam Ni/SiC Catalyst in Carbon dioxide Reforming of Methane to Synthesis Gas. *Catal. Lett.* **2008**, *120*, 111−115.

(356) Aw, M. S.; Zorko, M.; Djinovic, P.; Pintar, P. Insights into Durable NiCo Catalysts on β-SiC/CeZrO$_2$ and γ-Al$_2$O$_3$/CeZrO$_2$ Advanced Supports Prepared from Facile Methods for CH$_4$-CO$_2$ Dry Reforming. *Appl. Catal., B* **2015**, *164*, 100−112.

(357) Silva, C. G.; Passos, F. B.; da Silva, V. T. Influence of the Support on the Activity of a Supported Nickel-Promoted Molybdenum Carbide Catalyst for Dry Reforming of Methane. *J. Catal.* **2019**, *375*, 507−518.

(358) Guo, P.-F.; Jin, G.-Q.; Guo, C.-X.; Wang, Y.-Y.; Tong, X.-L.; Guo, X.-Y. Effects of Yb$_2$O$_3$ Promotor on the Performance of Ni/SiC Catalysts in CO$_2$ Reforming of CH$_4$. *J. Fuel Chem. Technol.* **2014**, *42*, 719−726.

(359) Wang, B.; Jin, G.-Q.; Wang, Y.-Y.; Guo, X.-Y. Ni-Sm/SiC Catalysts Prepared by Hydrothermal Method for Carbon Dioxide Reforming of Methane. *J. Fuel Chem. Technol.* **2016**, *44*, 1473−1478.

(360) Zhang, Z.; Zhao, G.; Bi, G.; Guo, Y.; Xie, J. Monolithic SiC-Foam Supported Ni-La$_2$O$_3$ Composites for Dry Reforming of Methane with Enhanced Carbon Resistance. *Fuel Process. Technol.* **2021**, *212*, 106627.

(361) Zou, J.; Mu, X.; Zhao, W.; Rukundo, P.; Wang, Z.-J. Improved Catalytic Activity of SiC Supported Ni Catalysts for CO$_2$ Reforming of Methane via Surface Functionalizations. *Catal. Commun.* **2016**, *84*, 116−119.

(362) Guo, Y.; Zou, J.; Shi, X.; Rukundo, P.; Wang, Z.-J. A Ni/CeO$_2$−CDC-SiC Catalyst with Improved Coke Resistance in CO$_2$ Reforming of Methane. *ACS Sustainable Chem. Eng.* **2017**, *5*, 2330−2338.

(363) Gao, X.; Liu, G.; Wei, Q.; Yang, G.; Masaki, M.; Peng, X.; Yang, R.; Tsubaki, N. Carbon Nanofibers Decorated SiC Foam Monoliths as the Support of Anti-Sintering Ni Catalyst for Methane Dry Reforming. *Int. J. Hydrogen Energy* **2017**, *42*, 16547−16556.

(364) Hoffmann, C.; Plate, P.; Steinbrück, A.; Kaskel, S. Nanoporous Silicon Carbide as Nickel Support for the Carbon Dioxide Reforming of Methane. *Catal. Sci. Technol.* **2015**, *5*, 4174−4183.

(365) Li, H.; Qiu, Y.; Wang, C.; Huang, X.; Xiao, T.; Zhao, Y. Nickel Catalysts Supported on Ordered Mesoporous SiC Materials for CO$_2$ Reforming of Methane. *Catal. Today* **2018**, *317*, 76−85.

(366) Zhan, H.-j.; Shi, X.-y.; Hi, X.; Zhao, N. Highly Coke-Resistant Ordered Mesoporous Ni/SiC with Large Surface Areas in CO$_2$ Reforming of CH$_4$. *J. Fuel Chem. Technol.* **2019**, *47*, 942−948.

(367) Zhang, F.; Song, Z.; Zhu, J.; Liu, L.; Sun, J.; Zhao, X.; Mao, Y.; Wang, W. Process of CH$_4$-CO$_2$ Reforming over Fe/SiC Catalyst under Microwave Irradiation. *Sci. Total Environ.* **2018**, *639*, 1148−1155.

(368) Zhang, F.; Song, Z.; Zhu, J.; Sun, J.; Zhao, X.; Mao, Y.; Liu, L.; Wang, W. Factors Iinfluencing CH$_4$-CO$_2$ Reforming Reaction over Fe Catalyst Supported on Foam Ceramics under Microwave Irradiation. *Int. J. Hydrogen Energy* **2018**, *43*, 9495−9502.

(369) de Dios García, I.; Stankiewicz, A.; Nigar, H. Syngas Production via Microwave-Assisted Dry Reforming of Methane. *Catal. Today* **2021**, *362*, 72−80.

(370) Rostrup-Nielsen, J. R. Catalytic Steam Reforming. In *CATALYSIS Science and Technology*; Anderson, J. R., Boudart, M., Eds.; Springer-Verlag: Berlin, Heidelberg, New York, Tokyo, 1984; Vol. *5*, pp 3−110, DOI: 10.1007/978-3-642-93247-2_1.

(371) Basile, F.; Del Gallo, P.; Fornasari, G.; Gary, D.; Rosetti, V.; Vaccari, A. SiC as Stable High Thermal Conductive Catalyst for

(372) Halabi, M. H.; Van der Schaaf, J.; Cobden, P. D.; Schouten, J. C. Reactor Modeling of Sorption-Enhanced Autothermal Reforming of Methane. Part I: Performance Study of Hydrotalcite and Lithium Zirconate-Based Processes. *Chem. Eng. J.* **2011**, *168*, 883−888.

(373) Palma, V.; Ricca, A.; Ciambelli, P. Monolith and Foam Catalysts Performances in ATR of Liquid and Gaseous Fuels. *Chem. Eng. J.* **2012**, *207−208*, 577−586.

(374) Palma, V.; Martino, M.; Meloni, E.; Ricca, A. Novel Structured Catalysts Configuration for Intensification of Steam Reforming of Methane. *Int. J. Hydrogen Energy* **2017**, *42*, 1629−1638.

(375) Palma, V.; Ricca, A.; Martino, M.; Meloni, E. Innovative Catalytic Systems for Methane Steam Reforming Intensification. *Chem. Eng. Trans.* **2016**, *52*, 301−306.

(376) Palma, V.; Ricca, A.; Martino, M.; Meloni, E. Innovative Structured Catalytic Systems for Methane Steam Reforming Intensification. *Chem. Eng. Process.* **2017**, *120*, 207−215.

(377) Palma, V.; Ricca, A.; Meloni, E.; Miccio, M.; Martino, M.; Ciambelli, P. Methane Steam Reforming Intensification: Experimental and Numerical Investigations on Monolithic Catalysts. *Chem. Eng. Trans.* **2015**, *43*, 919−924.

(378) Noh, Y. S.; Lee, K.-Y.; Moon, D. J. Hydrogen Production by Steam Reforming of Methane over Nickel Based Structured Catalysts Supported on Calcium Aluminate Modified SiC. *Int. J. Hydrogen Energy* **2019**, *44*, 21010−21019.

(379) Park, K. S.; Son, M.; Park, M.-J.; Kim, D. H.; Kim, J. H.; Park, S. H.; Choi, J.-H.; Bae, J. W. Adjusted Interactions of Nickel Nanoparticles with Cobalt-Modified MgAl$_2$O$_4$-SiC for an Enhanced Catalytic Stability During Steam Reforming of Propane. *Appl. Catal., A* **2018**, *549*, 117−133.

(380) AlSabban, B.; Falivene, L.; Kozlov, S. M.; Aguilar-Tapia, A.; Ould-Chikh, S.; Hazemann, J.-L.; Cavallo, L.; Basset, J.-M.; Takanabe, K. In-Operando Elucidation of Bimetallic CoNi Nanoparticles During High-Temperature CH$_4$/CO$_2$ Reaction. *Appl. Catal., B* **2017**, *213*, 177−189.

(381) Ruckenstein, E.; Wang, H. Y. Carbon Deposition and Catalytic Deactivation during CO$_2$ Reforming of CH$_4$ over Co/γ-Al$_2$O$_3$ Catalysts. *J. Catal.* **2002**, *205*, 289−293.

(382) Sá, S.; Silva, H.; Brandão, L.; Sousa, J. M.; Mendes, A. Catalysts for Methanol Steam Reforming - A Review. *Appl. Catal., B* **2010**, *99*, 43−57.

(383) Chen, Y.; Wang, Y.; Xu, H.; Xiong, G. Hydrogen Production Capacity of Membrane Reformer for Methane Steam Reforming near Practical Working Conditions. *J. Membr. Sci.* **2008**, *322*, 453−459.

(384) Tosti, S.; Basile, A.; Borgognoni, F.; Capaldo, V.; Cordiner, S.; Cave, S. D.; Gallucci, F.; Rizzello, C.; Santucci, A.; Traversa, E. Low Temperature Ethanol Steam Reforming in a Pd-Ag Membrane Reactor: Part 1: Ru-Based Catalyst. *J. Membr. Sci.* **2008**, *308*, 250−257.

(385) Olah, G. A.; Goeppert, A.; Prakash, G. K. S. In *Beyond Oil and Gas: The Methanol Economy*, 2nd ed.; Wiley-VCH Verlag GmbH & Co. KGaA: Weinheim, 2006; 334pp, DOI: 10.1002/9783527627806.

(386) Tomoda, A.; Mikami, D.; Azuma, N.; Ueno, A. Methanol Steam Reforming over Cu/SiC Catalysts. *J. Adv. Sci.* **2001**, *13*, 414−417.

(387) Fukahori, S.; Koga, H.; Kitaoka, T.; Tomoda, A.; Suzuki, R.; Wariishi, H. Hydrogen Production from Methanol Using a SiC Fiber-Containing Paper Composite Impregnated with Cu/ZnO Catalyst. *Appl. Catal., A* **2006**, *310*, 138−144.

(388) Liao, M.; Guo, C.; Guo, W.; Hu, T.; Qin, H.; Gao, P.; Xiao, H. Hydrogen Production in Microreactor Using Porous SiC Ceramic with a Pore-in-Pore Hierarchical Structure as Catalyst Support. *Int. J. Hydrogen Energy* **2020**, *45*, 20922−20932.

(389) Guo, W.; Hu, T.; Qin, H.; Gao, P.; Xiao, H. Preparation and In Situ Reduction of Ni/SiCxOy Catalysts Supported on Porous SiC

Ceramic for Ethanol Steam Reforming. *Ceram. Int.* **2021**, *47*, 13738−13744.

(390) Patil, N.; Mishra, N. K.; Saed, M. A.; Green, M. J.; Wilhite, B. A. Radio Frequency Driven Heating of Catalytic Reactors for Portable Green Chemistry. *Adv. Sustainable Syst.* **2020**, *4*, 2000095.

(391) Wang, W.; Tuci, G.; Duong-Viet, C.; Liu, Y.; Rossin, A.; Luconi, L.; Nhut, J.-M.; Nguyen, D. L.; Pham-Huu, C.; Giambastiani, G. Induction Heating: an Enabling Technology for the Heat Management in Catalytic Processes. *ACS Catal.* **2019**, *9*, 7921−7935.

(392) Monnerat, B.; Kiwi-Minsker, L.; Renken, A. Hydrogen Production by Catalytic Cracking of Methane over Nickel Gauze under Periodic Reactor Operation. *Chem. Eng. Sci.* **2001**, *56*, 633−639.

(393) Valdés-López, V. F.; Mason, T.; Shearing, P. R.; Brett, D. J. L. Carbon Monoxide Poisoning and Mitigation Strategies for Polymer Electrolyte Membrane Fuel Cells - A Review. *Prog. Energy Combust. Sci.* **2020**, *79*, 100842.

(394) Church, T. L.; Fallani, S.; Liu, J.; Zhao, M.; Harris, A. T. Novel Biomorphic Ni/SiC Catalysts that Enhance Cellulose Conversion to Hydrogen. *Catal. Today* **2012**, *190*, 98−106.

(395) Zhang, Y.; Song, Z.; Yan, Y.; Zhao, X.; Sun, J.; Mao, Y.; Wang, W. Performance of Fe/SiC Catalysts for Cracking of Toluene under Microwave Irradiation. *Int. J. Hydrogen Energy* **2018**, *43*, 7227−7236.

(396) Sengodan, S.; Lan, R.; Humphreys, J.; Du, D.; Xu, W.; Wang, H.; Tao, S. Advances in Reforming and Partial Oxidation of Hydrocarbons for Hydrogen Production and Fuel Cell Applications. *Renewable Sustainable Energy Rev.* **2018**, *82*, 761−780.

(397) Liao, M.; Chen, Y.; Cheng, Z.; Wang, C.; Luo, X.; Bu, E.; Jiang, Z.; Liang, B.; Shu, R.; Song, Q. Hydrogen Production from Partial Oxidation of Propane: Effect of SiC Addition on Ni/Al$_2$O$_3$ Catalyst. *Appl. Energy* **2019**, *252*, 113435.

(398) Liao, M.; Wang, C.; Bu, E.; Chen, Y.; Cheng, Z.; Luo, X.; Shu, R.; Wu, J. Efficient Hydrogen Production from Partial Oxidation of Propane over SiC Doped Ni/Al$_2$O$_3$ Catalyst. *Energy Procedia* **2019**, *158*, 1772−1779.

(399) Wang, C.; Liao, M.; Bu, E.; Jiang, Z.; Chen, Y.; Cheng, Z.; Luo, X.; Liang, B.; Shu, R.; Song, Q. Effective Hydrogen Production from Partial Oxidation of Propane over Composite Ni/Al$_2$O$_3$-SiC Catalyst. *Int. J. Hydrogen Energy* **2019**, *44*, 680−693.

(400) Sawatmongkhon, B.; Theinnoi, K.; Wongchang, T.; Haoharn, C.; Wongkhorsub, C.; Tsolakis, A. Hydrogen Production via the Catalytic Partial Oxidation of Ethanol on a Platinum−Rhodium Catalyst: Effect of the Oxygen-to-Ethanol Molar Ratio and the Addition of Steam. *Energy Fuels* **2019**, *33*, 6742−6753.

(401) Li, X.; Wang, F.; Pan, X.; X, B. Rh/CeO$_2$-SiC as a Catalyst in Partial Oxidation of Ethanol for Hydrogen Production (*in Chinese*). *Chin. J. Catal.* **2013**, *34*, 257−262.

(402) Bockris, J. O. M. The Hydrogen Economy: Its History. *Int. J. Hydrogen Energy* **2013**, *38*, 2579−2588.

(403) Haruta, M.; Sano, H. Catalytic Combustion of Hydrogen I - Its Role in Hydrogen Utilization System and Screening of Catalyst Materials. *Int. J. Hydrogen Energy* **1981**, *6*, 601−608.

(404) Sanap, K. K.; Varma, S.; Waghmode, S. B.; Bharadwaj, S. R. Supported Pt Nanoparticles for the Hydrogen Mitigation Application. *Int. J. Hydrogen Energy* **2014**, *39*, 15142−15155.

(405) Fernández, A.; Arzac, G. M.; Vogt, U. F.; Hosoglu, F.; Borgschulte, A.; Jiménez de Haroa, M. C.; Montes, O.; Züttel, A. Investigation of a Pt Containing Washcoat on SiC Foam for Hydrogen Combustion Applications. *Appl. Catal., B* **2016**, *180*, 336−343.

(406) Arzac, G. M.; Montes, O.; Fernández, A. Pt-Impregnated Catalysts on Powdery SiC and Other Commercial Supports for the Combustion of Hydrogen under Oxidant Conditions. *Appl. Catal., B* **2017**, *201*, 391−399.

(407) Arzac, G. M.; Ramırez-Rico, J.; Gutierrez-Pardo, A.; Jimenez de Haro, M. C.; Hufschmidt, D.; Martınez-Fernandez, J.; Fernandez, A. Monolithic Supports Based on Biomorphic SiC for the Catalytic Combustion of Hydrogen. *RSC Adv.* **2016**, *6*, 66373−66384.

(408) Karagiannakis, G.; Agrafiotis, C. C.; Zygogianni, A.; Pagkoura, C.; Konstandopoulos, A. G. Hydrogen Production via Sulfur-Based Thermochemical Cycles: Part 1: Synthesis and Evaluation of Metal Oxide-Based Candidate Catalyst Powders for the Sulfuric Acid Decomposition Step. *Int. J. Hydrogen Energy* **2011**, *36*, 2831−2844.

(409) Lin, S. S.; Flaherty, R. Design Studies of the Sulfur Trioxide Decomposition Reactor for the Sulfur Cycle Hydrogen Production Process. *Int. J. Hydrogen Energy* **1983**, *8*, 589−596.

(410) Giaconia, A.; Sau, S.; Felici, C.; Tarquini, P.; Karagiannakis, G.; Pagkoura, C.; Agrafiotis, C.; Konstandopoulos, A. G.; Thomey, D.; de Oliveira, L.; et al. Hydrogen Production via Sulfur-Based Thermochemical Cycles: Part 2: Performance Evaluation of Fe$_2$O$_3$-Based Catalysts for the Sulfuric Acid Decomposition Step. *Int. J. Hydrogen Energy* **2011**, *36*, 6496−6509.

(411) Karagiannakis, G.; Agrafiotis, C. C.; Pagkoura, C.; Konstandopoulos, A. G.; Thomey, D.; de Oliveira, L.; Roeb, M.; Sattler, C. Hydrogen Production via Sulfur-Based Thermochemical Cycles: Part 3: Durability and Post-Characterization of Silicon Carbide Honeycomb Substrates Coated with Metal Oxide-Based Candidate Catalysts for the Sulfuric Acid Decomposition Step. *Int. J. Hydrogen Energy* **2012**, *37*, 8190−8203.

(412) Zhang, P.; Su, T.; Chen, Q. H.; Wang, L. J.; Chen, S. Z.; Xu, J. M. Catalytic Decomposition of Sulfuric Acid on Composite Oxides and Pt/SiC. *Int. J. Hydrogen Energy* **2012**, *37*, 760−764.

(413) Yang, H.; Zhang, Y.; Zhou, J.; Wang, Z.; Liu, J.; Cen, K. Study on CuO-CeO$_2$/SiC Catalysts in the Sulfur-Iodine Cycle for Hydrogen Production. *Int. J. Energy Res.* **2016**, *40*, 1062−1072.

(414) Kubo, S.; Futakawa, M.; Ioka, I.; Onuki, K.; Yamaguchi, A. Corrosion Resistance of Structural Materials in High Temperature Aqueous Sulfuric Acids in Thermochemical Water Splitting Iodine-Sulfur Process. *Int. J. Hydrogen Energy* **2013**, *38*, 6577−6585.

(415) Yang, H.; Zhang, Y.; Zhou, J.; Wang, Z.; Liu, J.; Cen, K. Influence of Calcination Temperature on CuO-CeO$_2$/SiC Catalysts for SO$_3$ Decomposition in the Sulfur-Iodine Cycle for Hydrogen Production. *Int. J. Hydrogen Energy* **2016**, *41*, 3339−3348.

(416) Soto-Dıaz, O.; Orozco-Mena, R. E.; Roman-Aguirre, M.; Romero-Paredes, H.; Camacho-Davila, A. A.; Ramos-Sanchez, V. H. Metal Sulfate Decomposition Using Green Pd-Based Catalysts Supported on γAl$_2$O$_3$ and SiC: A Common Step in Sulfur-Family Thermochemical Cycles. *Int. J. Hydrogen Energy* **2019**, *44*, 12309−12314.

(417) Lee, S. Y.; Jung, H.; Kim, W. J.; Shul, Y. G.; Jung, K.-D. Sulfuric Acid Decomposition on Pt/SiC-Coated-Alumina Catalysts for SI Cycle Hydrogen Production. *Int. J. Hydrogen Energy* **2013**, *38*, 6205−6209.

(418) Khan, H. A.; Jung, K.-D. Preparation Scheme of Active Pt/SiC Catalyst and Its Phase Changes During Sulfuric Acid Decomposition to Produce Hydrogen in the SI Cycle. *Catal. Lett.* **2017**, *147*, 1931−1940.

(419) Khan, H. A.; Natarajan, P.; Jung, K.-D. Stabilization of Pt at the Inner Wall of Hollow Spherical SiO$_2$ Generated from Pt/Hollow Spherical SiC for Sulfuric Acid Decomposition. *Appl. Catal., B* **2018**, *231*, 151−160.

(420) Noh, S.-C.; Lee, S. Y.; Shul, Y. G.; Jung, K.-D. Sulfuric Acid Decomposition on the Pt/n-SiC Catalyst for SI Cycle to Produce Hydrogen. *Int. J. Hydrogen Energy* **2014**, *39*, 4181−4188.

(421) Khan, H. A.; Natarajan, P.; Jung, K.-D. Synthesis of Pt/Mesoporous SiC-15 and Its Catalytic Performance for Sulfuric Acid Decomposition. *Catal. Today* **2018**, *303*, 25−32.

(422) Tomar, S.; Gangwar, S.; Kondamudi, K.; Upadhyayula, S. SO$_3$ Decomposition over β-SiC and SiO$_2$ Supported CuFe$_2$O$_4$: A Stability and Kinetic Study. *Int. J. Hydrogen Energy* **2020**, *45*, 21287−21296.

(423) Pathak, S.; Saini, S.; Kondamudi, K.; Upadhyayula, S.; Bhattacharya, S. Insights into Enhanced Stability and Activity of Silica Modified SiC Supported Iron Oxide Catalyst in Sulfuric Acid Decomposition. *Appl. Catal., B* **2021**, *284*, 119613.

(424) Salameh, C.; Bruma, A.; Malo, S.; Demirci, U. B.; Miele, P.; Bernard, S. Monodisperse Platinum Nanoparticles Supported on Highly Ordered Mesoporous Silicon Nitride Nanoblocks: Superior

Catalytic Activity for Hydrogen Generation from Sodium Borohydride. *RSC Adv.* **2015**, *5*, 58943−58951.

(425) Luconi, L.; Tuci, G.; Giambastiani, G.; Rossin, A.; Peruzzini, M. H$_2$ Production from Lightweight Inorganic Hydrides Catalyzed by 3d Transition Metals. *Int. J. Hydrogen Energy* **2019**, *44*, 25746−25776.

(426) Lale, A.; Wasan, A.; Kumar, R.; Miele, P.; Demirci, U. B.; Bernard, S. Organosilicon Polymer-Derived Mesoporous 3D Silicon Carbide, Carbonitride and Nitride Structures as Platinum Supports for Hydrogen Generation by Hydrolysis of Sodium Borohydride. *Int. J. Hydrogen Energy* **2016**, *41*, 15477−15488.

(427) Okura, K.; Miyazaki, K.; Muroyama, H.; Matsui, T.; Eguchi, K. Ammonia Decomposition over Ni Catalysts Supported on Perovskite-Type Oxides for the On-Site Generation of Hydrogen. *RSC Adv.* **2018**, *8*, 32102−32110.

(428) Pinzón, M.; Romero, A.; de Lucas Consuegra, A.; de la Osa, A. R.; Sánchez, P. Hydrogen Production by Ammonia Decomposition over Ruthenium Supported on SiC Catalyst. *J. Ind. Eng. Chem.* **2021**, *94*, 326−335.

(429) Jie, X.; Gonzalez-Cortes, S.; Xiao, T.; Wang, J.; Yao, B.; Slocombe, D. R.; Al-Megren, H. A.; Dilworth, J. R.; Thomas, J. M.; Edwards, P. P. Rapid Production of High-Purity Hydrogen Fuel through Microwave-Promoted Deep Catalytic Dehydrogenation of Liquid Alkanes with Abundant Metals. *Angew. Chem., Int. Ed.* **2017**, *56*, 10170−10173.

(430) Hansen, S.; Mirkouei, A.; Diaz, L. A. A Comprehensive State-of-Technology Review for Upgrading Bio-Oil to Renewable or Blended Hydrocarbon Fuels. *Renewable Sustainable Energy Rev.* **2020**, *118*, 109548.

(431) Pham-Huu, C.; Del Gallo, P.; Peschiera, E.; Ledoux, M. J. *n*-Hexane and *n*-Heptane Isomerization at Atmospheric and Medium Pressure on MoO$_3$-Carbon-Modified Supported on SiC and γ-Al$_2$O$_3$. *Appl. Catal., A* **1995**, *132*, 77−96.

(432) Del Gallo, P.; Pham-Huu, C.; Bouchy, C.; Estournes, C.; Ledoux, M. J. Effect of the Total Activation Pressure on the Structural and Catalytic Performance of the SiC Supported MoO$_3$-Carbon-Modified Catalyst for the *n*-Heptane Isomerization. *Appl. Catal., A* **1997**, *156*, 131−149.

(433) Pham-Huu, C.; Bouchy, C.; Dintzer, T.; Ehret, G.; Estournes, C.; Ledoux, M. J. High Surface Area Silicon Carbide Doped with Zirconium for Use as Catalyst Support. Preparation, Characterization and Catalytic Application. *Appl. Catal., A* **1999**, *180*, 385−397.

(434) York, A. P. E.; Pham-Huu, C.; Del Gallo, P.; Ledoux, M. J. Molybdenum Oxycarbide Hydrocarbon Isomerization Catalysts: Cleaner Fuels for the Future. *Catal. Today* **1997**, *35*, 51−57.

(435) Campelo, J. M.; Lafont, E.; Marinas, J. M. Hydroisomerization and Hydrocracking of n-Heptane on Pt/SAPO-5 and Pt/SAPO-11 Catalysts. *J. Catal.* **1995**, *156*, 11−18.

(436) Blekkan, E. A.; Pham-Huu, C.; Guille, J.; Ledoux, M. J. Isomerization of n-Heptane on an Oxygen-Modified Molybdenum Carbide Catalyst. *Ind. Eng. Chem. Res.* **1994**, *33*, 1657−1664.

(437) Ou, X.; Wu, C.; Shi, K.; Hardacre, C.; Zhang, J.; Jiao, Y.; Fan, X. Structured ZSM-5/SiC Foam Catalysts for Bio-Oils Upgrading. *Appl. Catal., A* **2020**, *599*, 117626.

(438) Zhu, Q.; Wang, Y.; Wang, L.; Yang, Z.; Wang, L.; Meng, X.; Xiao, F.-S. Solvent-Free Crystallization of ZSM-5 Zeolite on SiC Foam as a Monolith Catalyst for Biofuel Upgrading. *Chin. J. Catal.* **2020**, *41*, 1118−1124.

(439) de Souza, W. F.; Guimarães, I. R.; Guerreiro, M. C.; Oliveira, L. C. A. Catalytic Oxidation of Sulfur and Nitrogen Compounds from Diesel Fuel. *Appl. Catal., A* **2009**, *360*, 205−209.

(440) Song, C. An Overview of New Approaches to Deep Desulfurization for Ultra-Clean Gasoline, Diesel Fuel and Jet Fuel. *Catal. Today* **2003**, *86*, 211−263.

(441) Muzic, M.; Sertic-Bionda, K. Alternative Processes for Removing Organic Sulfur Compounds from Petroleum Fractions. *Chem. Biochem. Eng. Q.* **2013**, *27*, 101−108.

(442) Mjalli, F. S.; Ahmed, O. U.; Al-Wahaibi, T.; Al-Wahaibi, Y.; AlNashef, I. M. Deep Oxidative Desulfurization of Liquid Fuels. *Rev. Chem. Eng.* **2014**, *30*, 337−378.

(443) Kim, J. H.; Ma, X.; Zhou, A.; Song, C. Ultra-Deep Desulfurization and Denitrogenation of Diesel Fuel by Selective Adsorption over Three Different Adsorbents: A Study on Adsorptive Selectivity and Mechanism. *Catal. Today* **2006**, *111*, 74−83.

(444) Bakar, W. A. W. A.; Ali, R.; Abdul Kadir, A. A.; Wan Mokhtar, W. N. A. Effect of Transition Metal Oxides Catalysts on Oxidative Desulfurization of Model Diesel. *Fuel Process. Technol.* **2012**, *101*, 78−84.

(445) Zhu, W.; Li, H.; Jiang, X.; Yan, Y.; Lu, J.; Xia, J. Oxidative Desulfurization of Fuels Catalyzed by Peroxotungsten and Peroxomolybdenum Complexes in Ionic Liquids. *Energy Fuels* **2007**, *21*, 2514−2516.

(446) Afsharpour, M.; Amraee, A. R. Synthesis of Bio-inspired N-doped SiC and Investigation of Its Synergetic Effects on Mo Catalysts in Oxidative Desulfurization Reaction. *Mol. Catal.* **2017**, *436*, 285−293.

(447) Khomand, E.; Afsharpour, M. Green Synthesis of Nano-structured SiCs by Using Natural Biopolymers (Guar, Tragacanth, Arabic, and Xanthan Gums) for Oxidative Desulfurization of Model Fuel. *Int. J. Environ. Sci. Technol.* **2019**, *16*, 2359−2372.

(448) Seifikar Gomi, L.; Afsharpoura, M.; Lianos, P. Novel Porous SiO$_2$@SiC Core-Shell Nanospheres Functionalized with an Amino Hybrid of WO$_3$ as an Oxidative Desulfurization Catalyst. *J. Ind. Eng. Chem.* **2020**, *89*, 448−457.

(449) Seifikar Gomi, L.; Afsharpour, M. Porous MoO$_3$@SiC Hallow Nanosphere Composite as an Efficient Oxidative Desulfurization Catalyst. *Appl. Organomet. Chem.* **2019**, *33*, No. e4830.

(450) Wieckowska, J. Catalytic and Adsorptive Desulphurization of Gases. *Catal. Today* **1995**, *24*, 405−465.

(451) Eow, J. S. Recovery of Sulfur from Sour Acid Gas: A Review of the Technology. *Environ. Prog.* **2002**, *21*, 143−162.

(452) Piéplu, A.; Saur, O.; Lavalley, J. C.; Legendre, O.; Nédez, C. Claus Catalysis and H$_2$S Selective Oxidation. *Catal. Rev.: Sci. Eng.* **1998**, *40*, 409−450.

(453) Zhang, X.; Tang, Y.; Qu, S.; Da, J.; Hao, Z. H$_2$S-Selective Catalytic Oxidation: Catalysts and Processes. *ACS Catal.* **2015**, *5*, 1053−1067.

(454) van den Brink, P. J.; Terörde, R. J. A. M.; Moors, J. H.; van Dillen, A. J.; Geus, J. W. *New Developments Selective Oxidation by Heterogeneous Catalysis*; Studies in Surface Science and Catalysis; Ruiz, P., Delmon, B., Eds.; Elsevier: Amsterdam, 1992; Vol. 72, p 123, DOI: 10.1016/S0167-2991(08)61665-1.

(455) Keller, N.; Pham-Huu, C.; Crouzet, C.; Ledoux, M. J.; Savin-Poncet, S.; Nougayrede, J.-B.; Bousquet, J. Direct Oxidation of H$_2$S into S. New Catalysts and Processes Based on SiC Support. *Catal. Today* **1999**, *53*, 535.

(456) Keller, N.; Pham-Huu, C.; Estournes, C.; Ledoux, M. J. Low-Temperature Selective Oxidation of Hydrogen Sulfide into Elemental Sulfur on a NiS$_2$/SiC Catalyst. *Catal. Lett.* **1999**, *61*, 151−155.

(457) Ledoux, M. J.; Pham-Huu, C.; Keller, N.; Nougayrède, J.-B.; Savin-Poncet, S.; Bousquet, J. Selective Oxidation of H$_2$S in Claus Tail-Gas over SiC Supported NiS$_2$ Catalyst. *Catal. Today* **2000**, *61*, 157−163.

(458) Keller, N.; Pham-Huu, C.; Ledoux, M. J. Continuous Process for Selective Oxidation of H$_2$S over SiC-Supported Iron Catalysts into Elemental Sulfur above Its Dewpoint. *Appl. Catal., A* **2001**, *217*, 205−217.

(459) Keller, N.; Vieira, R.; Nhut, J.-M.; Pham-Huu, C.; Ledoux, M. J. New Catalysts Based on Silicon Carbide Support for Improvements in the Sulfur Recovery. Silicon Carbide as Support for the Selective H$_2$S Oxidation. *J. Braz. Chem. Soc.* **2005**, *16*, 202−209.

(460) Pham-Huu, C.; Keller, N.; Ehret, G.; Ledoux, M. J. The First Preparation of Silicon Carbide Nanotubes by Shape Memory Synthesis and Their Catalytic Potential. *J. Catal.* **2001**, *200*, 400−410.

(461) Keller, N.; Pham-Huu, C.; Estournès, C.; Ledoux, M. J. Low Temperature Use of SiC-Supported NiS$_2$-Based Catalysts for Selective H$_2$S Oxidation Role of SiC Surface Heterogeneity and Nature of the Active Phase. *Appl. Catal., A* **2002**, *234*, 191−205.

(462) Duong-Viet, C.; Nguyen-Dinh, L.; Liu, Y.; Tuci, G.; Giambastiani, G.; Pham-Huu, C. Nickel Sulfides Decorated SiC Foam for the Low Temperature Conversion of H_2S into Elemental Sulfur. *Molecules* **2018**, *23*, 1528.

(463) Nguyen, P.; Edouard, D.; Nhut, J.-M.; Ledoux, M. J.; Pham, C.; Pham-Huu, C. High Thermal Conductive β-SiC for Selective Oxidation of H_2S: A New Support for Exothermal Reactions. *Appl. Catal., B* **2007**, *76*, 300−310.

(464) Nguyen, P.; Nhut, J.-M.; Edouard, D.; Pham, C.; Ledoux, M. J.; Pham-Huu, C. Fe_2O_3/β-SiC: A New High Efficient Catalyst for the Selective Oxidation of H_2S into Elemental Sulfur. *Catal. Today* **2009**, *141*, 397−402.

(465) Moradi, M.; Daryan, J. T.; Mohamadalizadeh, A. Response Surface Modeling of H_2S Conversion by Catalytic Oxidation Reaction over Catalysts Based on SiC Nanoparticles using Box−Behnken Experimental Design. *Fuel Process. Technol.* **2013**, *109*, 163−171.

(466) Manisalidis, I.; Stavropoulou, E.; Stavropoulos, A.; Bezirtzoglou, E. Environmental and Health Impacts of Air Pollution: A Review. *Front. Public Health.* **2020**, *8*, 14.

(467) Oi-Uchisawa, J.; Obuchi, A.; Enomoto, R.; Xu, J.; Nanba, T.; Liu, S.; Kushiyama, S. Oxidation of Carbon Black over Various Pt/MO_x/SiC Catalysts. *Appl. Catal., B* **2001**, *32*, 257−268.

(468) Oi-Uchisawa, J.; Obuchi, A.; Wang, S.; Nanba, T.; Ohi, A. Catalytic Performance of Pt/MO_x Loaded over SiC-DPF for Soot Oxidation. *Appl. Catal., B* **2003**, *43*, 117−129.

(469) Oi-Uchisawa, J.; Obuchi, A.; Wang, S.; Nanba, T.; Ohi, A. Performance of Pt Catalysts Supported on SiC-DPF. In *Science and Technology in Catalysis*; Anpo, M., Onaka, M., Yamashita, H., Eds.; Elsevier Science: 2002; Vol. *145*, pp 465−466, DOI: 10.1016/S0167-2991(03)80262-8.

(470) Setiabudi, A.; Makkee, M.; Moulijn, J. A. An Optimal NO_x Assisted Abatement of Diesel Soot in an Advanced Catalytic Filter Design. *Appl. Catal., B* **2003**, *42*, 35−45.

(471) Pesant, L.; Matta, J.; Garin, F.; Ledoux, M. J.; Bernhardt, P.; Pham, C.; Pham-Huu, C. A High-Performance Pt/β-SiC Catalyst for Catalytic Combustion of Model Carbon Particles (CPs). *Appl. Catal., A* **2004**, *266*, 21−27.

(472) Pesant, L.; Matta, J.; Pham-Huu, C.; Garin, F.; Bernhardt, P.; Pham, C.; Ledoux, M. J. Catalytic Combustion of Model Carbon Particles (CPs) over Pt/β-SiC Catalyst. *Top. Catal.* **2004**, *30/31*, 281−286.

(473) Quiles-Dıaz, S.; Gimenez-Manogil, J.; Garcıa-Garcıa, A. Catalytic Performance of CuO/$Ce_{0.8}Zr_{0.2}O_2$ Loaded onto SiC-DPF in NO_x-Assisted Combustion of Diesel Soot. *RSC Adv.* **2015**, *5*, 17018−17029.

(474) Orihuela, M. P.; Miceli, P.; Ramírez-Rico, J.; Fino, D.; Chacartegui, R. Ceria-Based Catalytic Coatings on Biomorphic Silicon Carbide: A System for Soot Oxidation with Enhanced Properties. *Chem. Eng. J.* **2021**, *415*, 128959.

(475) Fan, Y. V.; Perry, S.; Klemeš, J. J.; Lee, C. T. A Review on Air Emissions Assessment: Transportation. *J. Cleaner Prod.* **2018**, *194*, 673−684.

(476) Al Soubaihi, M. R.; Saoud, K. M.; Dutta, J. Critical Review of Low-Temperature CO Oxidation and Hysteresis Phenomenon on Heterogeneous Catalysts. *Catalysts* **2018**, *8*, 660.

(477) Singh, S. K.; Parida, K. M.; Mohanty, B. C.; Rao, S. B. High Surface Area Silicon Carbide from Rice Husk: A Support Material for Catalysts. *React. Kinet. Catal. Lett.* **1995**, *54*, 29−34.

(478) Shen, X.-N.; Zheng, Y.; Zhan, Y.-Y.; Cai, G.-H.; Xiao, Y.-H. Synthesis of Porous SiC and Application in the CO Oxidation Reaction. *Mater. Lett.* **2007**, *61*, 4766−4768.

(479) Vershinin, N. N.; Bakaev, V. A.; Berestenko, V. I.; Efimov, O. N.; Kurkin, E. N.; Kabachkov, E. N. Synthesis and Properties of a Platinum Catalyst Supported on Plasma Chemical Silicon Carbide. *High Energy Chem.* **2017**, *51*, 46−50.

(480) Xi, K.; Wang, Y.; Jiang, K.; Xie, J.; Zhou, Y.; Lu, H. Support Interaction of Pt/CeO_2 and Pt/SiC Catalysts Prepared by Nano Platinum Colloid Deposition for CO Oxidation. *J. Rare Earths* **2020**, *38*, 376−383.

(481) Ishchenko, O. V.; Silenko, P. M.; Zakharova, T. M.; Yatsimirskii, A. V.; Shlapak, A. M.; Tsapyuk, G. G. Catalytic Systems Based on Multicomponent Oxides of 3d-Metals and Si-Containing Carriers for CO Oxidation Reaction. *Powder Metall. Met. Ceram.* **2012**, *50*, 662−670.

(482) Barbato, P. S.; Di Benedetto, A.; Landi, G.; Lisi, L. CuO/CeO_2 Based Monoliths for CO Preferential Oxidation in H_2-Rich Streams. *Chem. Eng. J.* **2015**, *279*, 983−993.

(483) Velders, G. J. M.; Fahey, D. W.; Daniel, J. S.; McFarland, M.; Andersen, S. O. The Large Contribution of Projected HFC Emissions to Future Climate Forcing. *Proc. Natl. Acad. Sci. U. S. A.* **2009**, *106*, 10949−10954.

(484) Baker, A. W.; Bonniface, D.; Klapotke, T. M.; Nicol, I.; Scott, J. D.; Scott, W. D. S.; Spence, R. R.; Watson, M. J.; Webb, G.; Winfield, J. M. Catalytic Fluorination of Trichloroethene by Anhydrous Hydrogen Fluoride in the Presence of Fluorinated Chromia under Static Conditions. *J. Fluorine Chem.* **2000**, *102*, 279−284.

(485) Liu, Z. H.; Qi, Q.; Yan, Y. J.; Zhang, H.; Liu, X. J.; Luo, H. J.; Huang, Z. R. Effect of Residual Phase and Grain Size on Corrosion Resistance of SiC Ceramics in Mixed HF-HNO_3 Acid Solution. *J. Inorg. Mater.* **2016**, *31*, 661−666.

(486) Watari, K. Evaluation of Thermal Conductivity of Grains and Fillers by Using Thermoreflectance Technique-Si_3N_4, AlN. *J. Ceram. Soc. Jpn.* **2014**, *122*, 967−970.

(487) Lu, J.; Han, W.; Yu, W.; Liu, Y.; Yang, H.; Liu, B.; Tang, H.; Li, Y. Thermally Conductive SiC as Support of Aluminum Fluoride for the Catalytic Dehydrofluorination Reaction. *Catal. Commun.* **2020**, *142*, 106033.

(488) Choudhary, T. V.; Banerjee, S.; Choudhary, V. R. Catalysts for Combustion of Methane and Lower Alkanes. *Appl. Catal., A* **2002**, *234*, 1−23.

(489) Méthivier, C.; Béguin, B.; Brun, M.; Massardier, J.; Bertolini, J. C. Pd/SiC Catalysts; Characterization and Catalytic Activity for the Methane Total Oxidation. *J. Catal.* **1998**, *173*, 374−382.

(490) Nhut, J.-M.; Pesant, L.; Keller, N.; Pham-Huu, C.; Ledoux, M.-J. Pd/SiC Exhaust Gas Catalyst for Heavy-Duty Engines: Improvement of Catalytic Performances by Controlling the Location of the Active Phase on the Support. *Top. Catal.* **2004**, *30/31*, 353−358.

(491) Guo, X.-N.; Shang, R.-J.; Wang, D.-H.; Jin, G.-Q.; Guo, X.-Y.; Tu, K. N. Avoiding Loss of Catalytic Activity of Pd Nanoparticles Partially Embedded in Nanoditches in SiC Nanowires. *Nanoscale Res. Lett.* **2010**, *5*, 332−337.

(492) Guo, X.; Brault, P.; Zhi, G.; Caillard, A.; Jin, G.; Guo, X. Structural Evolution of Plasma-Sputtered Core Shell Nanoparticles for Catalytic Combustion of Methane. *J. Phys. Chem. C* **2011**, *115*, 24164−24171.

(493) Guo, X.; Zhi, G.; Yan, X.; Jin, G.; Guo, X.; Brault, P. Methane Combustion over Pd/ZrO_2/SiC, Pd/CeO_2/SiC, and Pd/$Zr_{0.5}Ce_{0.5}O_2$/SiC Catalysts. *Catal. Commun.* **2011**, *12*, 870−874.

(494) Marin, P.; Ordonez, S.; Diez, F. V. Performance of Silicon-Carbide Foams as Supports for Pd-Based Methane Combustion Catalysts. *J. Chem. Technol. Biotechnol.* **2012**, *87*, 360−367.

(495) Litto, R.; Nien, T.; Hayes, R. E.; Mmbaga, J. P.; Votsmeier, M. Parametric Study of a Recuperative Catalytic Converter. *Catal. Today* **2012**, *188*, 106−112.

(496) Thompson, C. R.; Marín, P.; Díez, F. V.; Ordóñez, S. Evaluation of the Use of Ceramic Foams as Catalyst Supports for Reverse-Flow Combustors. *Chem. Eng. J.* **2013**, *221*, 44−54.

(497) Ercolino, G.; Stelmachowski, P.; Specchia, S. Catalytic Performance of Pd/Co_3O_4 on SiC and ZrO_2 Open Cell Foams for Process Intensification of Methane Combustion in Lean Conditions. *Ind. Eng. Chem. Res.* **2017**, *56*, 6625−6636.

(498) Moncada Quintero, C. W.; Ercolino, G.; Poozhikunnath, A.; Maric, R.; Specchia, S. Analysis of Heat and Mass Transfer Limitations for the Combustion of Methane Emissions on PdO/Co_3O_4 Coated on Ceramic Open Cell Foams. *Chem. Eng. J.* **2021**, *405*, 126970.

(499) Hoffmann, C.; Biemelt, T.; Lohe, M. R.; Rümmeli, M. H.; Kaskel, S. Nanoporous and Highly Active Silicon Carbide Supported CeO$_2$-Catalysts for the Methane Oxidation Reaction. *Small* **2014**, *10*, 316−322.

(500) Koshikawa, H.; Nakanishi, S.; Hashimoto, K.; Kamiya, K. Catalytic Methane Combustion over Iron/Nitrogen Doped Silicon Carbide. *RSC Adv.* **2016**, *6*, 85559−85563.

(501) Skalska, K.; Miller, J. S.; Ledakowicz, S. Trends in NO$_x$ Abatement: A Review. *Sci. Total Environ.* **2010**, *408*, 3976−3989.

(502) Pérez-Ramírez, J.; Kapteijn, F.; Schöffel, K.; Moulijn, J. A. Formation and Control of N$_2$O in Nitric Acid Production: Where Do We Stand Today? *Appl. Catal., B* **2003**, *44*, 117−151.

(503) Zheng, J.; Meyer, S.; Köhler, K. Abatement of Nitrous Oxide by Ruthenium Catalysts: Influence of the Support. *Appl. Catal., A* **2015**, *505*, 44−51.

(504) Klegova, A.; Inayat, A.; Indyka, P.; Gryboś, J.; Sojka, Z.; Pacultová, K.; Schwieger, W.; Volodarskaja, A.; Kuśtrowski, P.; Rokicińska, A.; et al. Cobalt Mixed Oxides Deposited on the SiC Open-Cell Foams for Nitrous Oxide Decomposition. *Appl. Catal., B* **2019**, *255*, 117745.

(505) Brüggemann, T. C.; Keil, F. J. Theoretical Investigation of the Mechanism of the Selective Catalytic Reduction of Nitric Oxide with Ammonia on H-Form Zeolites. *J. Phys. Chem. C* **2008**, *112*, 17378−17387.

(506) Topsøe, N.-Y. Mechanism of the Selective Catalytic Reduction of Nitric Oxide by Ammonia Elucidated by In Situ On-Line Fourier Transform Infrared Spectroscopy. *Science* **1994**, *265*, 1217−1219.

(507) Bai, S.; Zhao, J.; Wang, L.; Zhu, Z. SO$_2$-Promoted Reduction of NO with NH$_3$ over Vanadium Molecularly Anchored on the Surface of Carbon Nanotubes. *Catal. Today* **2010**, *158*, 393−400.

(508) Bai, S.; Wang, Z.; Li, H.; Xu, X.; Liu, M. SO$_2$ Promotion in NH$_3$-SCR Reaction over V$_2$O$_5$/SiC Catalyst at Low Temperature. *Fuel* **2017**, *194*, 36−41.

(509) Yuan, Q.; Zhang, Z.; Yu, N.; Dong, B. Cu-ZSM-5 Zeolite Supported on SiC Monolith with Enhanced Catalytic Activity for NH$_3$-SCR. *Catal. Commun.* **2018**, *108*, 23−26.

(510) Heidenreich, S. Hot Gas Filtration - a Review. *Fuel* **2013**, *104*, 83−94.

(511) Han, F.; Zhong, Z.; Zhang, F.; Xing, W.; Fan, Y. Preparation and Characterization of SiC Whisker-Reinforced SiC Porous Ceramics for Hot Gas Filtration. *Ind. Eng. Chem. Res.* **2015**, *54*, 226−232.

(512) Shen, W.; Liu, Y.; Yan, B.; Wang, J.; He, P.; Zhou, C.; Huo, X.; Zhang, W.; Xu, G.; Ding, Q. Cement Industry of China: Driving Force, Environment Impact and Sustainable Development. *Renewable Sustainable Energy Rev.* **2017**, *75*, 618−628.

(513) Choi, J.-H.; Kim, J.-H.; Bak, Y.-C.; Amal, R.; Scott, J. D. Pt-V$_2$O$_5$-WO$_3$/TiO$_2$ Catalysts Supported on SiC Filter for NO Reduction at Low Temperature. *Korean J. Chem. Eng.* **2005**, *22*, 844−851.

(514) Kim, Y. A.; Choi, J. H.; Scott, J.; Chiang, K.; Amal, R. Preparation of High Porous Pt−V$_2$O$_5$−WO$_3$/TiO$_2$/SiC Filter for Simultaneous Removal of NO and Particulates. *Powder Technol.* **2008**, *180*, 79−85.

(515) Kim, J. H.; Choi, J. H.; Phule, A. D. Development of High Performance Catalytic Filter of V$_2$O$_5$-WO$_3$/TiO$_2$ Supported-SiC for NO$_x$ Reduction. *Powder Technol.* **2018**, *327*, 282−290.

(516) Pan, B.; Chen, J.; Zhang, F.; Zhang, B.; Li, D.; Zhong, Z.; Xing, W. Porous TiO$_2$ Aerogel-Modified SiC Ceramic Membrane Supported MnO$_x$ Catalyst for Simultaneous Removal of NO and Dust. *J. Membr. Sci.* **2020**, *611*, 118366.

(517) Li, W. B.; Wang, J. X.; Gong, H. Catalytic Combustion of VOCs on Non-Noble Metal Catalysts. *Catal. Today* **2009**, *148*, 81−87.

(518) Yang, C.; Miao, G.; Pi, Y.; Xia, Q.; Wu, J.; Li, Z.; Xiao, J. Abatement of Various Types of VOCs by Adsorption/Catalytic Oxidation: A Review. *Chem. Eng. J.* **2019**, *370*, 1128−1153.

(519) Benaissa, M.; Pham-Huu, C.; Werckmann, J.; Crouzet, C.; Ledoux, M. J. A Sub-Nanometer Structural Study of Pt-Rh Catalysts Supported on Ce-Doped SiC. *Catal. Today* **1995**, *23*, 283−298.

(520) Yang, J.; Xu, W.; He, C.; Huang, Y.; Zhang, Z.; Wang, Y.; Hu, L.; Xia, D.; Shu, D. One-Step Synthesis of Silicon Carbide Foams Supported Hierarchical Porous Sludge-Derived Activated Carbon as Efficient Odor Gas Adsorbent. *J. Hazard. Mater.* **2018**, *344*, 33−41.

(521) Yang, J.; Zhang, Q.; Zhang, F.; Xia, D.; Liu, H.; Tian, S.; Sun, L.; Shu, D.; He, C.; Run, S. Three-Dimensional Hierarchical Porous Sludge-Derived Carbon Supported on Silicon Carbide Foams as Effective and Stable Fenton-Like Catalyst for Odorous Methyl Mercaptan Elimination. *J. Hazard. Mater.* **2018**, *358*, 136−144.

(522) Thomas, N.; Dionysiou, D. D.; Pillai, S. C. Heterogeneous Fenton Catalysts: A Review of Recent Advances. *J. Hazard. Mater.* **2021**, *404*, 124082.

(523) Li, L.; Zhang, F.; Zhong, Z.; Zhu, M.; Jiang, C.; Hu, J.; Xing, W. Novel Synthesis of a High-Performance Pt/ZnO/SiC Filter for the Oxidation of Toluene. *Ind. Eng. Chem. Res.* **2017**, *56*, 13857−13865.

(524) Piumetti, M.; Bensaid, S.; Andana, T.; Russo, N.; Pirone, R.; Fino, D. Cerium-Copper Oxides Prepared by Solution Combustion Synthesis for Total Oxidation Reactions: From Powder Catalysts to Structured Reactors. *Appl. Catal., B* **2017**, *205*, 455−465.

(525) Sandra, F.; Ballestero, A.; NGuyen, V. L.; Tsampas, M. N.; Vernoux, P.; Balan, C.; Iwamoto, Y.; Demirci, U. B.; Miele, P.; Bernard, S. Silicon Carbide-Based Membranes with High Soot Particle Filtration Efficiency, Durability and Catalytic Activity for CO/HC Oxidation and Soot Combustion. *J. Membr. Sci.* **2016**, *501*, 79−92.

(526) Atwater, J. E.; Akse, J. R.; McKinnis, J. A.; Thompson, J. O. Aqueous Phase Heterogeneous Catalytic Oxidation of Trichloroethylene. *Appl. Catal., B* **1996**, *11*, L11−L18.

(527) Akse, J. R.; Atwater, J. E. Deep Oxidation of Aqueous Organics over a Silicon Carbide-Activated Carbon Supported Platinum−Ruthenium Bimetallic Catalyst. *Top. Catal.* **2005**, *33*, 51−57.

(528) Atwater, J. E.; Akse, J. R.; Rodarte, J. M.; Thompson, J. O.; Wang, T.-C.; Hurley, J. A. Silicon Carbide Coated Granular Activated Carbon: a Robust Support for Low Temperature Aqueous Phase Oxidation Catalysts. *Carbon* **1997**, *35*, 1678−1679.

(529) Atwater, J. E.; Akse, J. R.; Wang, T.-C.; Kimura, S.; Johnson, D. C. Preparation of Silicon-Carbide-Coated Activated Carbon Using a High-Temperature Fluidized Bed Reactor. *Chem. Eng. Sci.* **2001**, *56*, 2685−2693.

(530) Obermayer, D.; Gutmann, B.; Kappe, C. O. Microwave Chemistry in Silicon Carbide Reaction Vials: Separating Thermal from Non Thermal Effects. *Angew. Chem., Int. Ed.* **2009**, *48*, 8321−8324.

(531) Gao, J.; Yang, S.; Li, N.; Meng, L.; Wang, F.; He, H.; Sun, C. Rapid Degradation of Azo Dye Direct Black BN by Magnetic MgFe$_2$O$_4$-SiC under Microwave Radiation. *Appl. Surf. Sci.* **2016**, *379*, 140−149.

(532) Mao, Y.; Yang, S.; Xue, C.; Zhang, M.; Wang, W.; Song, Z.; Zhao, X.; Sun, J. Rapid Degradation of Malachite Green by CoFe$_2$O$_4$-SiC Foam under Microwave Radiation. *R. Soc. Open Sci.* **2018**, *5*, 180085.

(533) Li, H.; Chen, J.; Hou, H.; Pan, H.; Ma, X.; Yang, J.; Wang, L.; Crittenden, J. C. Sustained Molecular Oxygen Activation by Solid Iron Doped Silicon Carbide under Microwave Irradiation: Mechanism and Application to Norfloxacin Degradation. *Water Res.* **2017**, *126*, 274−284.

(534) Pan, H.; Hou, H.; Shi, Y.; Li, H.; Chen, J.; Wang, L.; Crittenden, J. C. High Catalytic Oxidation of As(III) by Molecular Oxygen over Fe-Loaded Silicon Carbide with MW Activation. *Chemosphere* **2018**, *198*, 537−545.

(535) Chen, J.; Pan, H.; Hou, H.; Li, H.; Yang, J.; Wang, L. High Efficient Catalytic Degradation of PNP over Cu-Bearing Catalysts with Microwave Irradiation. *Chem. Eng. J.* **2017**, *323*, 444−454.

(536) Sun, J.; Xia, G.; Yang, W.; Hu, Y.; Shen, W. Microwave-Assisted Method to Degrade Phenol Using Persulfate or Hydrogen

Peroxide Catalyzed by Cu-Bearing Silicon Carbide. *Water Sci. Technol.* **2020**, *82* (4), 704−714.

(537) Rueda Márquez, J. J.; Levchuk, I.; Sillanpää, M. Application of Catalytic Wet Peroxide Oxidation for Industrial and Urban Wastewater Treatment: A Review. *Catalysts* **2018**, *8*, 673.

(538) Ou, X.; Pilitsis, F.; Jiao, Y.; Zhang, Y.; Xu, S.; Jennings, M.; Yang, Y.; Taylor, S. F. R.; Garforth, A.; Zhang, H.; et al. Hierarchical Fe-ZSM-5/SiC Foam Catalyst as the Foam Bed Catalytic Reactor (FBCR) for Catalytic Wet Peroxide Oxidation (CWPO). *Chem. Eng. J.* **2019**, *362*, 53−62.

(539) Ou, X.; Pilitsis, F.; Xu, N.; Taylor, S. F. R.; Warren, J.; Garforth, A.; Zhang, J.; Hardacre, C.; Jiao, Y.; Fan, X. On Developing Ferrisilicate Catalysts Supported on Silicon Carbide (SiC) Foam Catalysts for Continuous Catalytic Wet Peroxide Oxidation (CWPO) Reactions. *Catal. Today* **2020**, *356*, 631−640.

(540) Quintanilla, A.; Casas, J. A.; Miranzo, P.; Osendi, M. I.; Belmonte, M. 3D-Printed Fe-Doped Silicon Carbide Monolithic Catalysts for Wet Peroxide Oxidation Processes. *Appl. Catal., B* **2018**, *235*, 246−255.

(541) He, J.; Wang, H.; Xiao, C.; Li, J.; Chen, P.; Hou, J. Preparation and Performance of Pt/PTFE/Foam SiC as a Hydrophobic Catalyst for LPCE. *Fusion Eng. Des.* **2016**, *113*, 269−274.

(542) Whittingham, M. S.; Savinell, R. F.; Zawodzinski, T. Introduction: Batteries and Fuel Cells. *Chem. Rev.* **2004**, *104*, 4243−4244.

(543) Sazali, N.; Salleh, W. N. W.; Jamaludin, A. S.; Razali, M. N. M. New Perspectives on Fuel Cell Technology: A Brief Review. *Membranes* **2020**, *10*, 99.

(544) Pérez, L. C.; Brandão, L.; Sousa, J. M.; Mendes, A. Segmented Polymer Electrolyte Membrane Fuel Cells - A Review. *Renewable Sustainable Energy Rev.* **2011**, *15*, 169−185.

(545) Stambouli, A. B.; Traversa, E. Solid Oxide Fuel Cells (SOFCs): a Review of an Environmentally Clean and Efficient Source of Energy. *Renewable Sustainable Energy Rev.* **2002**, *6*, 433−455.

(546) Li, X.; Faghri, A. Review and Advances of Direct Methanol Fuel Cells (DMFCs) Part I: Design, Fabrication, and Testing with High Concentration Methanol Solutions. *J. Power Sources* **2013**, *226*, 223−240.

(547) Honji, A.; Marl, T.; Hishinuma, Y.; Kurita, K. Platinum Supported on Silicon Carbide as Fuel Cell Electrocatalyst. *J. Electrochem. Soc.* **1988**, *135*, 917−918.

(548) Lv, H.; Mu, S.; Cheng, N.; Pan, M. Nano-Silicon Carbide Supported Catalysts for PEM Fuel Cells with High Electrochemical Stability and Improved Performance by Addition of Carbon. *Appl. Catal., B* **2010**, *100*, 190−196.

(549) Passalacqua, E.; Antonucci, P. L.; Vivaldi, M.; Patti, A.; Antonucci, V.; Giordano, N.; Kinoshita, K. The Influence of Pt on the Electrooxidation Behaviour of Carbon in Phosphoric Acid. *Electrochim. Acta* **1992**, *37*, 2725−2730.

(550) Roen, L. M.; Paik, C. H.; Jarvi, T. D. Electrocatalytic Corrosion of Carbon Support in PEMFC Cathodes. *Electrochem. Solid-State Lett.* **2004**, *7*, A19−A22.

(551) Niu, J. J.; Wang, J. N. Synthesis of Macroscopic SiC Nanowires at the Gram Level and Their Electrochemical Activity with Pt Loadings. *Acta Mater.* **2009**, *57*, 3084−3090.

(552) Zhang, Y.; Zang, J.; Dong, L.; Cheng, X.; Zhao, Y.; Wang, Y. A Ti-Coated Nano-SiC Supported Platinum Electrocatalyst for Improved Activity and Durability in Direct Methanol Fuel Cells. *J. Mater. Chem. A* **2014**, *2*, 10146−10153.

(553) Zang, J.; Dong, L.; Jia, Y.; Pan, H.; Gao, Z.; Wang, Y. Core-Shell Structured SiC@C Supported Platinum Electrocatalysts for Direct Methanol Fuel Cells. *Appl. Catal., B* **2014**, *144*, 166−173.

(554) Dhiman, R.; Johnson, E.; Skou, E. M.; Morgen, P.; Andersen, S. M. SiC Nanocrystals as Pt Catalyst Supports for Fuel Cell Applications. *J. Mater. Chem. A* **2013**, *1*, 6030−6036.

(555) Andersen, S. M.; Larsen, M. J. Performance of the Electrode Based on Silicon Carbide Supported Platinum Catalyst for Proton Exchange Membrane Fuel Cells. *J. Electroanal. Chem.* **2017**, *791*, 175−184.

(556) Dhiman, R.; Stamatin, S. N.; Andersen, S. M.; Morgen, P.; Skou, E. M. Oxygen Reduction and Methanol Oxidation Behaviour of SiC Based Pt Nanocatalysts for Proton Exchange Membrane Fuel Cells. *J. Mater. Chem. A* **2013**, *1*, 15509−15516.

(557) Stamatin, S. N.; Speder, J.; Dhiman, R.; Arenz, M.; Skou, E. M. Electrochemical Stability and Postmortem Studies of Pt/SiC Catalysts for Polymer Electrolyte Membrane Fuel Cells. *ACS Appl. Mater. Interfaces* **2015**, *7*, 6153−6161.

(558) Lobato, J.; Zamora, H.; Plaza, J.; Canizares, P.; Rodrigo, M. A. Enhancement of High Temperature PEMFC Stability Using Catalysts Based on Pt Supported on SiC Based Materials. *Appl. Catal., B* **2016**, *198*, 516−524.

(559) Lobato, J.; Zamora, H.; Plaza, J.; Rodrigo, M. A. Composite Titanium Silicon Carbide as a Promising Catalyst Support for High-Temperature Proton-Exchange Membrane Fuel Cell Electrodes. *ChemCatChem* **2016**, *8*, 848−854.

(560) Tong, X.; Dong, L.; Jin, G.; Wang, Y.; Guo, X.-Y. Electrocatalytic Performance of Pd Nanoparticles Supported on SiC Nanowires for Methanol Oxidation in Alkaline Media. *Fuel Cells* **2011**, *11*, 907−910.

(561) Dai, H.; Chen, Y.; Lin, Y.; Xu, G.; Yang, C.; Tong, Y.; Guo, L.; Chen, G. A New Metal Electrocatalysts Supported Matrix: Palladium Nanoparticles Supported Silicon Carbide Nanoparticles and Its Application for Alcohol Electrooxidation. *Electrochim. Acta* **2012**, *85*, 644−649.

(562) Fang, L.; Huang, X.-P.; Vidal-Iglesias, F.-J.; Liu, Y.-P.; Wang, X.-L. Preparation, Characterization and Catalytic Performance of a Novel Pt/SiC. *Electrochem. Commun.* **2011**, *13*, 1309−1312.

(563) Hu, M.-S.; Kuo, C.-C.; Wu, C.-T.; Chen, C.-W.; Ang, P. K.; Loh, K. P.; Chen, K.-H.; Chen, L.-C. The Production of SiC Nanowalls Sheathed with a Few Layers of Strained Graphene and Their Use in Heterogeneous Catalysis and Sensing Applications. *Carbon* **2011**, *49*, 4911−4919.

(564) Dong, L.-L.; Tong, X.-L.; Wang, Y.-Y.; Jin, G.-Q.; Guo, X.-Y. Boron-Doped Silicon Carbide Supported Pt Catalyst for Methanol Electrooxidation. *J. Fuel Chem. Technol.* **2014**, *42*, 845−850.

(565) Dong, L.; Wang, Y.; Tong, X.; Lei, T. Silicon Carbide Encapsulated Graphite Nanocomposites Supported Pt Nanoparticles as High-Performance Catalyst for Methanol and Ethanol Oxidation Reaction. *Diamond Relat. Mater.* **2020**, *104*, 107739.

(566) Wang, L.; Zhao, L.; Yu, P.; Tian, C.; Sun, F.; Feng, H.; Zhou, W.; Wang, J.; Fu, H. Silica Direct Evaporation: a Size-Controlled Approach to SiC/Carbon Nanosheet Composites as Pt Catalyst Supports for Superior Methanol Electrooxidation. *J. Mater. Chem. A* **2015**, *3*, 24139−24147.

(567) Xie, S.; Tong, X.-L.; Jin, G.-Q.; Qin, Y.; Guo, X.-Y. CNT−Ni/SiC Hierarchical Nanostructures: Preparation and Their Application in Electrocatalytic Oxidation of Methanol. *J. Mater. Chem. A* **2013**, *1*, 2104−2109.

(568) Schmidt, O.; Gambhir, A.; Staffell, I.; Hawkes, A.; Nelson, J.; Few, S. Future Cost and Performance of Water Electrolysis: An Expert Elicitation Study. *Int. J. Hydrogen Energy* **2017**, *42*, 30470−30492.

(569) Nikiforov, A. V.; Tomas Garcıa, A. L.; Petrushina, I. M.; Christensen, E.; Bjerrum, N. J. Preparation and Study of IrO$_2$/SiCeSi Supported Anode Catalyst for High Temperature PEM Steam Electrolysers. *Int. J. Hydrogen Energy* **2011**, *36*, 5797−5805.

(570) Polonský, J.; Mazúr, P.; Paidar, M.; Bouzek, K. Investigation of *β*-SiC as an Anode Catalyst Support for PEM Water Electrolysis. *J. Solid State Electrochem.* **2014**, *18*, 2325−2332.

(571) Lee, C.-P.; Luna, L. E.; DelaCruz, S.; Ortaboy, S.; Rossi, F.; Salviati, G.; Carraro, C.; Maboudian, R. Hierarchical Cobalt Oxide-Functionalized Silicon Carbide Nanowire Array for Efficient and Robust Oxygen Evolution Electro-Catalysis. *Mater. Today Energy* **2018**, *7*, 37−43.

(572) Darvish Ganji, M.; Agheb, R.; Ganji, H. D.; Ashrafian, S. First Principles Computational Investigation on the Possibility of Pt-Decorated SiC Hexagonal Sheet as a Suitable Material for Oxygen Reduction Reaction. *J. Phys. Chem. Solids* **2016**, *88*, 47−53.

(573) Kulkarni, A.; Siahrostami, S.; Patel, A.; Nørskov, J. K. Understanding Catalytic Activity Trends in the Oxygen Reduction Reaction. *Chem. Rev.* **2018**, *118*, 2302−2312.

(574) Rao, C. V.; Singh, S. K.; Viswanathan, B. Electrochemical Performance of Nano-SiC Prepared in Thermal Plasma. *Indian J. Chem.* **2008**, *47A*, 1619−1625.

(575) Suzuki, S.; Onodera, T.; Kawaji, J.; Mizukami, T.; Morishima, M.; Yamaga, K. Improvement in Stability of Carbon Support for Platinum Catalyst by Applying Silicon Carbide Coating. *J. Power Sources* **2013**, *223*, 79−85.

(576) Dong, L.; Zang, J.; Su, J.; Jia, Y.; Wang, Y.; Lu, J.; Xu, X. Oxidized Carbon/nano-SiC Supported Platinum Nanoparticles as Highly Stable Electrocatalyst for Oxygen Reduction Reaction. *Int. J. Hydrogen Energy* **2014**, *39*, 16310−16317.

(577) You, D. J.; Jin, X.; Kim, J. H.; Jin, S.-A.; Lee, S.; Choi, K. H.; Baek, W. J.; Pak, C.; Kim, J. M. Development of Stable Electrochemical Catalysts Using Ordered Mesoporous Carbon/Silicon Carbide Nanocomposites. *Int. J. Hydrogen Energy* **2015**, *40*, 12352−12361.

(578) Watanabe, M.; Moon, J.; Tanabe, T.; Todoroki, N.; Wadayama, T. Oxygen Reduction Reaction Properties of Dry-Process-Synthesized Pt/graphene/SiC(0001) Model Catalyst Surfaces. *ECS Trans.* **2018**, *86*, 525−530.

(579) Jia, Y.; Wang, Y.; Dong, L.; Huang, J.; Zhang, Y.; Su, J.; Zang, J. A Hybrid of Titanium Nitride and Nitrogen-Doped Amorphous Carbon Supported on SiC as a Noble Metal-Free Electrocatalyst for Oxygen Reduction Reaction. *Chem. Commun.* **2015**, *51*, 2625−2628.

(580) Li, J.; Wang, J.; Gao, D.; Li, X.; Miao, S.; Wang, G.; Bao, X. Silicon Carbide-Supported Iron Nanoparticles Encapsulated in Nitrogen-Doped Carbon for Oxygen Reduction Reaction. *Catal. Sci. Technol.* **2016**, *6*, 2949−2954.

(581) Wang, J.; Wang, G. X.; Miao, S.; Jiang, X. L.; Li, J. Y.; Bao, X. H. Synthesis of Fe/Fe₃C Nanoparticles Encapsulated in Nitrogen-Doped Carbon with Single-Source Molecular Precursor for the Oxygen Reduction Reaction. *Carbon* **2014**, *75*, 381−389.

(582) Chen, X.; Sun, F.; Chang, J. Cobalt or Nickel Doped SiC Nanocages as Efficient Electrocatalyst for Oxygen Reduction Reaction: A Computational Prediction. *J. Electrochem. Soc.* **2017**, *164*, F616−F619.

(583) Feng, Y.; Yu, Z.; Schuch, J.; Tao, S.; Wiehl, L.; Fasel, C.; Jaegermann, W.; Riedel, R. Nowotny Phase $Mo_{3+2x}Si_3C_{0.6}$ Dispersed in a Porous SiC/C Matrix: A Novel Catalyst for Hydrogen Evolution Reaction. *J. Am. Ceram. Soc.* **2020**, *103*, 508−519.

(584) Peng, K.; Zhou, J.; Gao, H.; Wang, J.; Wang, H.; Su, L.; Wan, P. Emerging One-/Two-Dimensional Heteronanostructure Integrating SiC Nanowires with MoS_2 Nanosheets for Efficient Electrocatalytic Hydrogen Evolution. *ACS Appl. Mater. Interfaces* **2020**, *12*, 19519−19529.

(585) Li, Y.; Zhang, Y.; Tong, X.; Wang, X.; Zhang, L.; Xia, X.; Tu, J. Recent Progress on the Phase Modulation of Molybdenum Disulphide/Diselenide and Their Applications in Electrocatalysis. *J. Mater. Chem. A* **2021**, *9*, 1418−1428.

(586) Chen, X.; Shen, S.; Guo, L.; Mao, S. S. Semiconductor-Based Photocatalytic Hydrogen Generation. *Chem. Rev.* **2010**, *110*, 6503−6570.

(587) Kudo, A.; Miseki, Y. Heterogeneous Photocatalyst Materials for Water Splitting. *Chem. Soc. Rev.* **2009**, *38*, 253−278.

(588) Li, X.; Yu, J.; Low, J.; Fang, Y.; Xiao, J. Engineering Heterogeneous Semiconductors for Solar Water Splitting. *J. Mater. Chem. A* **2015**, *3*, 2485−2534.

(589) Appel, A. M.; Bercaw, J. E.; Bocarsly, A. B.; Dobbek, H.; DuBois, D. L.; Dupuis, M.; Ferry, J. G.; Fujita, E.; Hille, R.; Kenis, P. J. A.; et al. Frontiers, Opportunities, and Challenges in Biochemical and Chemical Catalysis of CO_2 Fixation. *Chem. Rev.* **2013**, *113*, 6621−6658.

(590) Marszewski, M.; Cao, S.; Yu, J.; Jaroniec, M. Semiconductor-Based Photocatalytic CO_2 Conversion. *Mater. Horiz.* **2015**, *2*, 261−278.

(591) Hoffmann, M.; Martin, S.; Choi, W.; Bahnemann, D. Environmental Applications of Semiconductor Photocatalysis. *Chem. Rev.* **1995**, *95*, 69−96.

(592) Di Paola, A.; Garcia-Lopez, E.; Marci, G.; Palmisano, L. A Survey of Photocatalytic Materials for Environmental Remediation. *J. Hazard. Mater.* **2012**, *211*, 3−29.

(593) Pelaez, M.; Nolan, N. T.; Pillai, S. C.; Seery, M. K.; Falaras, P.; Kontos, A. G.; Dunlop, P. S. M.; Hamilton, J. W. J.; Byrne, J. A.; O'Shea, K.; et al. A Review on the Visible Light Active Titanium Dioxide Photocatalysts for Environmental Applications. *Appl. Catal., B* **2012**, *125*, 331−349.

(594) Sarina, S.; Waclawik, E. R.; Zhu, H. Y. Photocatalysis on Supported Gold and Silver Nanoparticles under Ultraviolet and Visible Light Irradiation. *Green Chem.* **2013**, *15*, 1814−1833.

(595) Melchionna, M.; Fornasiero, P. Updates on the Roadmap for Photocatalysis. *ACS Catal.* **2020**, *10*, 5493−5501.

(596) Li, X. H.; Baar, M.; Blechert, S.; Antonietti, M. Facilitating Room-Temperature Suzuki Coupling Reaction with Light: Mott-Schottky Photocatalyst for C-C Coupling. *Sci. Rep.* **2013**, *3*, 1743.

(597) Hou, D.-F.; Jiao, Z.-F.; Liang, Z.-P.; Wang, Y.-W.; Guo, X.-N.; Guo, X.-Y. Selectivity Control of Pt/SiC Catalysts for Photo-thermocatalytic Hydrogenation of 3-Nitrostyrene. *Appl. Surf. Sci.* **2020**, *526*, 146616.

(598) Jiao, Z.-F.; Tian, Y.-M.; Zhang, B.; Hao, C.-H.; Qiao, Y.; Wang, Y.-X.; Qin, Y.; Radius, U.; Braunschweig, H.; Marder, T. B.; et al. High Photocatalytic Activity of a NiO Nanodot-Decorated Pd/SiC Catalyst for the Suzuki-Miyaura Cross-Coupling of Aryl Bromides and Chlorides in Air under Visible Light. *J. Catal.* **2020**, *389*, 517−524.

(599) Jiao, Z.-F.; Zhao, J.-X.; Guo, X.-N.; Guo, X.-Y. Photocatalytic C−X Borylation of Aryl Halides by Hierarchical SiC Nanowire-Supported Pd Nanoparticles. *Chin. J. Catal.* **2020**, *41*, 357−363.

(600) Liang, Z.-P.; Hou, D.-F.; Jiao, Z.-F.; Guo, X.-N.; Tong, X.-L.; Guo, X.-Y. Aldehydes Rather than Alcohols in Oxygenated Products from Light-Driven Fischer−Tropsch Synthesis over Ru/SiC Catalysts. *Catal. Sci. Technol.* **2019**, *9*, 4629−4632.

(601) Li, H.; Lei, Y.; Huang, Y.; Fang, Y.; Xu, Y.; Zhu, L.; Li, X. Photocatalytic Reduction of Carbon Dioxide to Methanol by Cu_2O/SiC Nanocrystallite under Visible Light Irradiation. *J. Nat. Gas Chem.* **2011**, *20*, 145−150.

(602) Wang, Y.; Zhang, L.; Zhang, X.; Zhang, Z.; Tong, Y.; Li, F.; Wu, J. C.-S.; Wang, X. Openmouthed β-SiC Hollow-Sphere with Highly Photocatalytic Activity for Reduction of CO_2 with H_2O. *Appl. Catal., B* **2017**, *206*, 158−167.

(603) Han, C.; Wang, B.; Wu, N.; Shen, S.; Wang, Y. Deep and Selective Photoreduction of CO_2 to CH_4 over Ultrafine Pt Nanoparticles-Decorated SiC Nanosheets. *Appl. Surf. Sci.* **2020**, *515*, 145952.

(604) Wang, Y.; Zhang, Z.; Zhang, L.; Luo, Z.; Shen, J.; Lin, H.; Long, J.; Wu, J. C.-S.; Fu, X.; Wang, X.; et al. Visible-Light Driven Overall Conversion of CO_2 and H_2O to CH_4 and O_2 on 3D-SiC@2D-MoS_2 Heterostructure. *J. Am. Chem. Soc.* **2018**, *140*, 14595−14598.

(605) Wang, Y.; Shang, X.; Shen, J.; Zhang, Z.; Wang, D.; Lin, J.; Wu, J. C.-S.; Fu, X.; Wang, X.; Li, C. Direct and Indirect Z-Scheme Heterostructure-Coupled Photosystem Enabling Cooperation of CO_2 Reduction and H_2O Oxidation. *Nat. Commun.* **2020**, *11*, 3043.

(606) Li, H.; Shi, Y.; Shang, H.; Wang, W.; Lu, J.; Zakharov, A. A.; Hultman, L.; Uhrberg, R. I. G.; Syväjärvi, M.; Yakimova, R.; et al. Atomic-Scale Tuning of Graphene/Cubic SiC Schottky Junction for Stable Low-Bias Photoelectrochemical Solar-to-Fuel Conversion. *ACS Nano* **2020**, *14*, 4905−4915.

(607) Fajrina, N.; Tahir, M. A Critical Review in Strategies to Improve Photocatalytic Water Splitting towards Hydrogen Production. *Int. J. Hydrogen Energy* **2019**, *44*, 540−577.

(608) Wang, Q.; Domen, K. Particulate Photocatalysts for Light-Driven Water Splitting: Mechanisms, Challenges, and Design Strategies. *Chem. Rev.* **2020**, *120*, 919−985.

(609) Maeda, K.; Domen, K. Photocatalytic Water Splitting: Recent Progress and Future Challenges. *J. Phys. Chem. Lett.* **2010**, *1*, 2655−2661.

(610) Nariki, Y.; Inoue, Y.; Tanaka, K. Production of Ultra Fine SiC Powder from SiC bulk by Arc-Plasma Irradiation under Different Atmospheres and Its Application to Photocatalysts. *J. Mater. Sci.* **1990**, *25*, 3101−3104.

(611) Akikusa, J.; Khan, S. U. M. Photoelectrolysis of Water to Hydrogen in p-SiC/Pt and p-SiC/n-TiO$_2$ Cells. *Int. J. Hydrogen Energy* **2002**, *27*, 863−870.

(612) van Dorp, D. H.; Hijnen, N.; Di Vece, M.; Kelly, J. J. SiC: A Photocathode for Water Splitting and Hydrogen Storage. *Angew. Chem., Int. Ed.* **2009**, *48*, 6085−6088.

(613) Zhang, Y.; Xu, Y.; Li, T.; Wang, Y. Preparation of Ternary Cr$_2$O$_3$-SiC-TiO$_2$ Composites for the Photocatalytic Production of Hydrogen. *Particuology* **2012**, *10*, 46−50.

(614) Li, Y.; Yu, Z.; Meng, J.; Li, Y. Enhancing the Activity of a SiC-TiO$_2$ Composite Catalyst for Photo-Stimulated Catalytic Water Splitting. *Int. J. Hydrogen Energy* **2013**, *38*, 3898−3904.

(615) Guo, X.; Tong, X.; Wang, Y.; Chen, C.; Jin, G.; Guo, X.-Y. High Photoelectrocatalytic Performance of a MoS$_2$-SiC Hybrid Structure for Hydrogen Evolution Reaction. *J. Mater. Chem. A* **2013**, *1*, 4657−4661.

(616) Ge, P. Y.; Scanlon, M. D.; Peljo, P.; Bian, X. J.; Vubrel, H.; O'Neill, A.; Coleman, J. N.; Cantoni, M.; Hu, X. L.; Kontturi, K.; et al. Hydrogen Evolution across Nano-Schottky Junctions at Carbon Supported MoS$_2$ Catalysts in Biphasic Liquid Systems. *Chem. Commun.* **2012**, *48*, 6484.

(617) Tae Song, J.; Mashiko, H.; Kamiya, M.; Nakamine, Y.; Ohtomo, A.; Iwasaki, T.; Hatano, M. Improved Visible Light Driven Photoelectrochemical Properties of 3C-SiC Semiconductor with Pt Nanoparticles for Hydrogen Generation. *Appl. Phys. Lett.* **2013**, *103*, 213901.

(618) Zhou, X.; Liu, Y.; Li, X.; Gao, Q.; Liu, X.; Fang, Y. Topological Morphology Conversion towards SnO$_2$/SiC Hollow Sphere Nano-chains with Efficient Photocatalytic Hydrogen Evolution. *Chem. Commun.* **2014**, *50*, 1070−1073.

(619) Wang, M.; Chen, J.; Liao, X.; Liu, Z.; Zhang, J.; Gao, L.; Li, Y. Highly Efficient Photocatalytic Hydrogen Production of Platinum Nanoparticle-Decorated SiC Nanowires under Simulated Sunlight Irradiation. *Int. J. Hydrogen Energy* **2014**, *39*, 14581−14587.

(620) Liao, X.; Chen, J.; Wang, M.; Liu, Z.; Ding, L.; Li, Y. Enhanced Photocatalytic and Photoelectrochemical Activities of SnO$_2$/SiC Nanowire Heterostructure Photocatalysts. *J. Alloys Compd.* **2016**, *658*, 642−648.

(621) Jiang, M.; Liu, Z.; Ding, L.; Chen, J. Facile Fabrication and Efficient Photoelectrochemical Water-Splitting Activity of Electro-deposited Nickel/SiC Nanowires Composite Electrode. *Catal. Commun.* **2017**, *96*, 46−49.

(622) Peng, Y.; Guo, Z.; Yang, J.; Wang, D.; Yuan, W. Enhanced Photocatalytic H$_2$ Evolution over Micro-SiC by Coupling with CdS under Visible Light Irradiation. *J. Mater. Chem. A* **2014**, *2*, 6296−6300.

(623) Peng, Y.; Guo, Z.; Wang, D.; Pan, N.; Yuan, W. Heterogeneous Nucleation of CdS to Enhance Visible-Light Photo-catalytic Hydrogen Evolution of SiC/CdS Composite. *Appl. Phys. Lett.* **2015**, *107*, No. 012102.

(624) Peng, Y.; Han, G.; Wang, D.; Wang, K.; Guo, Z.; Yang, J.; Yuan, W. Improved H$_2$ Evolution under Visible Light in Heterostructured SiC/CdS Photocatalyst: Effect of Lattice Match. *Int. J. Hydrogen Energy* **2017**, *42*, 14409−14417.

(625) Wang, D.; Peng, Y.; Wang, Q.; Pan, N.; Guo, Z.; Yuan, W. High-Efficient Photo-Electron Transport Channel in SiC Constructed by Depositing Co-catalysts Selectively on Specific Surface Sites for Visible-Light H$_2$ Production. *Appl. Phys. Lett.* **2016**, *108*, 161601.

(626) Wang, D.; Wang, W.; Wang, Q.; Guo, Z.; Yuan, W. Spatial Separation of Pt and IrO$_2$ Co-catalysts on SiC Surface for Enhanced Photocatalysis. *Mater. Lett.* **2017**, *201*, 114−117.

(627) Wang, D.; Liu, N.; Guo, Z.; Wang, W.; Guo, L.; Yuan, W.; Chen, X. Hexagonal SiC with Spatially Separated Active Sites on Polar and Nonpolar Facets Achieving Enhanced Hydrogen Production from Photocatalytic Water Reduction. *Phys. Chem. Chem. Phys.* **2018**, *20*, 4787−4792.

(628) Chen, H.; Shao, L.; Li, Q.; Wang, J. Gold Nanorods and Their Plasmonic Properties. *Chem. Soc. Rev.* **2013**, *42*, 2679−2724.

(629) Wang, D.; Huang, L.; Guo, Z.; Han, X.; Liu, C.; Wang, W.; Yuan, W. Enhanced Photocatalytic Hydrogen Production over Au/SiC for Water Reduction by Localized Surface Plasmon Resonance Effect. *Appl. Surf. Sci.* **2018**, *456*, 871−875.

(630) Ichikawa, N.; Kato, M.; Ichimura, M. The Enhanced Performance of 3C-SiC Photocathodes for the Generation of Hydrogen through the Use of Co-catalysts. *Appl. Phys. Lett.* **2016**, *109*, 153904.

(631) Gao, Y. T. *Photocatalytic Properties of SiC Under Visible Light Irradiation*; A graduation thesis of Tianjin University: 2006.

(632) Zhang, Y.; Xia, T.; Wallenmeyer, P.; Harris, C. X.; Peterson, A. A.; Corsiglia, G. A.; Murowchick, J.; Chen, X. Photocatalytic Hydrogen Generation from Pure Water using Silicon Carbide Nanoparticles. *Energy Technol.* **2014**, *2*, 183−187.

(633) Digdaya, I. A.; Han, L.; Buijs, T. W. F.; Zeman, M.; Dam, B.; Smets, A. H. M.; Smith, W. A. Extracting Large Photovoltages from a-SiC Photocathodes with an Amorphous TiO$_2$ Front Surface Field Layer for Solar Hydrogen Evolution. *Energy Environ. Sci.* **2015**, *8*, 1585−1593.

(634) Digdaya, I. A.; Perez Rodriguez, P.; Ma, M.; Adhyaksa, G. W. P.; Garnett, E. C.; Smets, A. H. M.; Smith, W. A. Engineering the Kinetics and Interfacial Energetics of Ni/Ni−Mo Catalyzed Amorphous Silicon Carbide Photocathodes in Alkaline Media. *J. Mater. Chem. A* **2016**, *4*, 6842−6852.

(635) Mishra, G.; Parida, K. M.; Singh, S. K. Facile Fabrication of S-TiO$_2$/β-SiC Nanocomposite Photocatalyst for Hydrogen Evolution under Visible Light Irradiation. *ACS Sustainable Chem. Eng.* **2015**, *3*, 245−253.

(636) Zhang, Y.; Hu, Y.; Zeng, H.; Zhong, L.; Liu, K.; Cao, H.; Li, W.; Yan, H. Silicon Carbide Recovered from Photovoltaic Industry Waste as Photocatalysts for Hydrogen Production. *J. Hazard. Mater.* **2017**, *329*, 22−29.

(637) Wang, Z.; Armstrong, A. Catalysis of Solar Hydrogen Production by Iron Atoms on the Surface of Fe-Doped Silicon Carbide. *Catal. Sci. Technol.* **2016**, *6*, 7038−7041.

(638) Wang, D.; Guo, Z.; Peng, Y.; Yuan, W. A Simple Route to Significant Enhancement of Photocatalytic Water Oxidation on BiVO$_4$ by Heterojunction with SiC. *Chem. Eng. J.* **2015**, *281*, 102−108.

(639) Wang, D.; Guo, Z.; Peng, Y.; Yuan, W. Visible Light Induced Photocatalytic Overall Water Splitting over Micro-SiC Driven by the Z-Scheme System. *Catal. Commun.* **2015**, *61*, 53−56.

(640) Jian, J.; Shi, Y.; Ekeroth, S.; Keraudy, J.; Syväjärvi, M.; Yakimova, R.; Helmersson, U.; Sun, J. A Nanostructured NiO/Cubic SiC p-n Heterojunction Photoanode for Enhanced Solar Water Splitting. *J. Mater. Chem. A* **2019**, *7*, 4721−4728.

(641) Jian, J.-X.; Jokubavicius, V.; Syväjärvi, M.; Yakimova, R.; Sun, J. Nanoporous Cubic Silicon Carbide Photoanodes for Enhanced Solar Water Splitting. *ACS Nano* **2021**, *15*, 5502−5512.

(642) Peng, B.; Xu, L.; Zeng, J.; Qi, X.; Yang, Y.; Ma, Z.; Huang, X.; Wang, L.-L.; Shuai, C. Layer-Dependent Photocatalysts of GaN/SiC Based Multilayer van der Waals Heterojunctions for Hydrogen Evolution. *Catal. Sci. Technol.* **2021**, *11*, 3059−3069.

(643) Pant, B.; Pant, H. R.; Park, M.; Liu, Y. N.; Choi, J. W.; Barakat, N. A.; Kim, H. Y. Electrospun CdS-TiO$_2$ Doped Carbon Nanofibers for Visible-Light-Induced Photocatalytic Hydrolysis of Ammonia Borane. *Catal. Commun.* **2014**, *50*, 63−68.

(644) Nirmala, R.; Kim, H. Y.; Yi, C.; Barakat, N. A. M.; Navamathavan, R.; Newehy, M. Electrospun Nickel Doped Titanium Dioxide Nanofibers as an Effective Photocatalyst for the Hydrolytic Dehydrogenation of Ammonia Borane. *Int. J. Hydrogen Energy* **2012**, *37*, 10036−10045.

(645) Li, H.; Yan, Y.; Feng, S.; Zhu, Y.; Chen, Y.; Fan, H.; Zhang, L.; Yang, Z. Transition Metal Tuned Semiconductor Photocatalyst CuCo/β-SiC Catalyze Hydrolysis of Ammonia Borane to Hydrogen Evolution. *Int. J. Hydrogen Energy* **2019**, *44*, 8307−8314.

(646) Koe, W. S.; Lee, J. W.; Chong, W. C.; Pang, Y. L.; Sim, L. C. An Overview of Photocatalytic Degradation: Photocatalysts, Mechanisms, and Development of Photocatalytic Membrane. *Environ. Sci. Pollut. Res.* **2020**, *27*, 2522−2565.

(647) Rueda-Marquez, J. J.; Levchuk, I.; Ibañez, P. F.; Sillanpää, M. A Critical Review on Application of Photocatalysis for Toxicity Reduction of Real Wastewaters. *J. Cleaner Prod.* **2020**, *258*, 120694.

(648) Keller, V.; Garin, F. Photocatalytic Behavior of a New Composite Ternary System: WO$_3$/SiC-TiO$_2$. Effect of the Coupling of Semiconductors and Oxides in Photocatalytic Oxidation of Methylethylketone in the Gas Phase. *Catal. Commun.* **2003**, *4*, 377−383.

(649) Kouamé, A. N.; Masson, R.; Robert, D.; Keller, N.; Keller, V. β-SiC Foams as a Promising Structured Photocatalytic Support for Water and Air Detoxification. *Catal. Today* **2013**, *209*, 13−20.

(650) Doss, N.; Bernhardt, P.; Romero, T.; Masson, R.; Keller, V.; Keller, N. Photocatalytic Degradation of Butanone (Methylethylketone) in a Small-Size TiO$_2$/β-SiC Alveolar Foam LED Reactor. *Appl. Catal., B* **2014**, *154−155*, 301−308.

(651) Masson, R.; Keller, V.; Keller, N. β-SiC Alveolar Foams as a Structured Photocatalytic Support for the Gas Phase Photocatalytic Degradation of Methylethylketone. *Appl. Catal., B* **2015**, *170−171*, 301−311.

(652) Zou, T.; Xie, C.; Liu, Y.; Zhang, S.; Zou, Z.; Zhang, S. Full Mineralization of Toluene by Photocatalytic Degradation with Porous TiO$_2$/SiC Nanocomposite Film. *J. Alloys Compd.* **2013**, *552*, 504−510.

(653) Wang, H.; Zhao, R.; Hu, H.; Fan, X.; Zhang, D.; Wang, D. 0D/2D Heterojunctions of Ti$_3$C$_2$ MXene QDs/SiC as an Efficient and Robust Photocatalyst for Boosting the Visible Photocatalytic NO Pollutant Removal Ability. *ACS Appl. Mater. Interfaces* **2020**, *12*, 40176−40185.

(654) Nishida, Y.; Omichi, T.; Katayama, I.; Yamashita, H. Photocatalytic Degradation of 2-Propanol Diluted in Water with TiO$_2$ Photocatalyst Deposited on SiC. *e-J. Surf. Sci. Nanotechnol.* **2005**, *3*, 311−313.

(655) Yamashita, H.; Nishida, Y.; Yuan, S.; Mori, K.; Narisawa, M.; Matsumura, Y.; Ohmichi, T.; Katayama, I. Design of TiO$_2$-SiC Photocatalyst Using TiC-SiC Nano-Particles for Degradation of 2-Propanol Diluted in Water. *Catal. Today* **2007**, *120*, 163−167.

(656) Zhang, Y.; Kuwahara, Y.; Mori, K.; Yamashita, H. Construction of Hybrid MoS$_2$ Phase Coupled with SiC Heterojunctions with Promoted Photocatalytic Activity for 4-Nitrophenol Degradation. *Langmuir* **2020**, *36*, 1174−1182.

(657) Rodriguez, P.; Meille, V.; Pallier, S.; Al Sawah, M. A. Deposition and Characterisation of TiO$_2$ Coatings on Various Supports for Structured (Photo)catalytic Reactors. *Appl. Catal., A* **2009**, *360*, 154−162.

(658) Kouamé, N. A.; Robert, D.; Keller, V.; Keller, N.; Pham, C.; Nguyen, P. Preliminary Study of the Use of β-SiC Foam as a Photocatalytic Support for Water Treatment. *Catal. Today* **2011**, *161*, 3−7.

(659) Kouamé, N. A.; Robert, D.; Keller, V.; Keller, N.; Pham, C.; Nguyen, P. TiO$_2$/β-SiC Foam-Structured Photoreactor for Continuous Wastewater Treatment. *Environ. Sci. Pollut. Res.* **2012**, *19*, 3727−3734.

(660) M'Bra, I. C.; Atheba, G. P.; Robert, D.; Drogui, P.; Trokourey, A. Photocatalytic Degradation of Paraquat Herbicide Using a Fixed Bed Reactor Containing TiO$_2$ Nanoparticles Coated onto β-SiC Alveolar Foams. *Am. J. Anal. Chem.* **2019**, *10*, 171−184.

(661) Marien, C. B. D.; Le Pivert, M.; Azaïs, A.; M'Bra, I. C.; Drogui, P.; Dirany, A.; Robert, D. Kinetics and Mechanism of Paraquat's Degradation: UV-C Photolysis vs UV-C Photocatalysis with TiO$_2$/SiC Foams. *J. Hazard. Mater.* **2019**, *370*, 164−171.

(662) M'Bra, I. C.; García-Muñoz, P.; Drogui, P.; Keller, N.; Trokourey, A.; Robert, D. Heterogeneous Photodegradation of Pyrimethanil and Its Commercial Formulation with TiO$_2$ Immobilized on SiC Foams. *J. Photochem. Photobiol., A* **2019**, *368*, 1−6.

(663) Ayekoe, C. Y. P.; Robert, D.; Gone, L. D. Combination of Coagulation-Flocculation and Heterogeneous Photocatalysis for Improving the Removal of Humic Substances in Real Treated Water from Agbô River (Ivory-Coast). *Catal. Today* **2017**, *281*, 2−13.

(664) Rico-Santacruz, M.; García-Muñoz, P.; Keller, V.; Batail, N.; Pham, C.; Robert, D.; Keller, N. Alveolar TiO$_2$-β-SiC Photocatalytic Composite Foams with Tunable Properties for Water Treatment. *Catal. Today* **2019**, *328*, 235−242.

(665) Rico-Santacruz, M.; García-Muñoz, P.; Marchal, C.; Batail, N.; Pham, C.; Robert, D.; Keller, N. Coating-Free TiO$_2$@β-SiC Alveolar Foams as a Ready-to-Use Composite Photocatalyst with Tunable Adsorption Properties for Water Treatment. *RSC Adv.* **2020**, *10*, 3817−3825.

(666) García-Muñoz, P.; Fresno, F.; Lefevre, C.; Robert, D.; Keller, N. Ti-Modified LaFeO$_3$/β-SiC Alveolar Foams as Immobilized Dual Catalysts with Combined Photo-Fenton and Photocatalytic Activity. *ACS Appl. Mater. Interfaces* **2020**, *12*, 57025−57037.

(667) Gómez-Solís, C.; Juárez-Ramírez, I.; Moctezuma, E.; Torres-Martínez, L. M. Photodegradation of Indigo Carmine and Methylene Blue Dyes in Aqueous Solution by SiC-TiO$_2$ Catalysts Prepared by Sol-Gel. *J. Hazard. Mater.* **2012**, *217−218*, 194−199.

(668) Hao, D.; Yang, Z.; Jiang, C.; Zhang, J. Photocatalytic Activities of TiO$_2$ Coated on Different Semiconductive SiC Foam Supports. *J. Mater. Sci. Technol.* **2013**, *29*, 1074−1078.

(669) Hao, D.; Yang, Z.; Jiang, C.; Zhang, J. Synergistic Photocatalytic Effect of TiO$_2$ Coatings and p-Type Semiconductive SiC Foam Supports for Degradation of Organic Contaminant. *Appl. Catal., B* **2014**, *144*, 196−202.

(670) Mishra, G.; Parida, K. M.; Singh, S. K. Solar Light Driven Rhodamine B Degradation over Highly Active β-SiC-TiO$_2$ Nanocomposite. *RSC Adv.* **2014**, *4*, 12918−12928.

(671) Yang, J.; Feng, J.; Li, W.; Chen, X.; Liu, X.; Ruan, J.; Qiu, R.; Xiong, Y.; Tian, S. A Resource-Utilization Way of the Waste Printed Circuit Boards to Prepare Silicon Carbide Nanoparticles and Their Photocatalytic Application. *J. Hazard. Mater.* **2019**, *373*, 640−648.

(672) Chen, Z.; Bing, F.; Liu, Q.; Zhang, Z.; Fang, X. Novel Z-Scheme Visible-Light-Driven Ag$_3$PO$_4$/Ag/SiC Photocatalysts with Enhanced Photocatalytic Activity. *J. Mater. Chem. A* **2015**, *3*, 4652−4658.

(673) Liu, M.-P.; Su, T.; Sun, L.; Du, H.-B. Facile Preparation of Yolk-Shell Structured Si/SiC@C@TiO$_2$ Nanocomposites as Highly Efficient Photocatalysts for Degrading Organic Dye in Wastewater. *RSC Adv.* **2016**, *6*, 4063−4069.

(674) Meenakshi, G.; Sivasamy, A.; Suganya Josephine, G. A.; Kavithaa, S. Preparation, Characterization and Enhanced Photocatalytic Activities of Zinc Oxide Nano Rods/Silicon Carbide Composite under UV and Visible Light Irradiations. *J. Mol. Catal. A: Chem.* **2016**, *411*, 167−178.

(675) Adhikari, S.; Eswar, N. K.; Sangita, S.; Sarkar, D.; Madras, G. Investigation of Nano Ag-decorated SiC Particles for Photoelectrocatalytic Dye Degradation and Bacterial Inactivation. *J. Photochem. Photobiol., A* **2018**, *357*, 118−131.

(676) Zhang, T.; Dai, Z.; Liang, B.; Mu, Y. Facile Synthesis of SnO$_2$/SiC Nanosheets for Photocatalytic Degradation of MO. *J. Inorg. Organomet. Polym. Mater.* **2021**, *31*, 303−310.

(677) Hou, Z.-H.; Chen, J.-P.; Xie, L.-J.; Wei, X.-X.; Guo, S.-Q.; Chen, M.-C. Design of BiOBr Nanosheets Decorated SiC Whisker Hybrid Structure with Enhanced Photocatalytic Performance. *Appl. Surf. Sci.* **2021**, *543*, 148779.

(678) Liu, X.; Dai, L. Carbon-Based Metal-Free Catalysts. *Nat. Rev. Mater.* **2016**, *1*, 16064.

(679) Cavani, F.; Trifirò, F. Alternative Processes for the Production of Styrene. *Appl. Catal., A* **1995**, *133*, 219−239.

(680) Meyers, R. A. In *Handbook of Petrochemicals Production Processes*; McGraw-Hill Handbooks: New York, 2005; pp 11.3−11.34.

(681) STYROLUTION In *Global Styrene Market, Key Factors Influencing the Future Landscape, Platts Global Aromatics Conference, Seoul, South Korea.* https://www.platts.com/IM.Platts.Content/ProductsServices/ConferenceandEvents/2013/ga001/presentations/27Sept_10.00_%20Steve%20Harrington.pdf (accessed March, 2021).

(682) Su, D. S.; Maksimova, N.; Delgado, J. J.; Keller, N.; Mestl, G.; Ledoux, M. J.; Schlogl, R. Nanocarbons in Selective Oxidative Dehydrogenation Reaction. *Catal. Today* **2005**, *102−103*, 110−114.

(683) Zhang, J.; Liu, X.; Blume, R.; Zhang, A.; Schlogl, R.; Su, D. S. Surface-Modified Carbon Nanotubes Catalyze Oxidative Dehydrogenation of n-Butane. *Science* **2008**, *322*, 73−77.

(684) Zhang, J.; Su, D. S.; Zhang, A.; Wang, D.; Schlogl, R.; Hébert, C. Nanocarbon as Robust Catalyst: Mechanistic Insight into Carbon-Mediated Catalysis. *Angew. Chem., Int. Ed.* **2007**, *46*, 7319−7323.

(685) Yuan, H.; Sun, Z.; Liu, H.; Zhang, B.; Chen, C.; Wang, H.; Yang, Z.; Zhang, J.; Wei, F.; Su, D. S. Immobilizing Carbon Nanotubes on SiC Foam as a Monolith Catalyst for Oxidative Dehydrogenation Reactions. *ChemCatChem* **2013**, *5*, 1713−1717.

(686) Liu, H.; Diao, J.; Wang, Q.; Gu, S.; Chen, T.; Miao, C.; Yang, W.; Su, D. S. A Nanodiamond/CNT-SiC Monolith as a Novel Metal Free Catalyst for Ethylbenzene Direct Dehydrogenation to Styrene. *Chem. Commun.* **2014**, *50*, 7810−7812.

(687) Feng, L.; Liu, Y.; Jiang, Q.; Liu, W.; Wu, K.-H.; Ba, H.; Pham-Huu, C.; Yange, W.; Su, D. S. Nanodiamonds @ N, P Co-Modified Mesoporous Carbon Supported on Macroscopic SiC Foam for Oxidative Dehydrogenation of Ethylbenzene. *Catal. Today* **2020**, *357*, 231−239.

(688) Ba, H.; Liu, Y.; Mu, X.; Doh, W.-H.; Nhut, J.-M.; Granger, P.; Pham-Huu, C. Macroscopic Nanodiamonds/β-SiC Composite as Metal-Free Catalysts for Steam-Free Dehydrogenation of Ethylbenzene to Styrene. *Appl. Catal., A* **2015**, *499*, 217−226.

(689) Ba, H.; Luo, J.; Liu, Y.; Duong-Viet, C.; Tuci, G.; Giambastiani, G.; Nhut, J.-M.; Nguyen-Dinh, L.; Ersen, O.; Su, D. S.; et al. Macroscopically Shaped Monolith of Nanodiamonds@ Nitrogen-Enriched Mesoporous Carbon Decorated SiC as a Superior Metal-Free Catalyst for the Styrene Production. *Appl. Catal., B* **2017**, *200*, 343−350.

(690) Cheng, M.; Wang, B.-W.; Hou, P.-X.; Li, J.-C.; Zhang, F.; Luan, J.; Cong, H.-T.; Liu, C.; Cheng, H.-M. Selective Growth of Semiconducting Single-Wall Carbon Nanotubes Using SiC as a Catalyst. *Carbon* **2018**, *135*, 195−201.

(691) Li, X.; Pan, X.; Yu, L.; Ren, P.; Wu, X.; Sun, L.; Jiao, F.; Bao, X. Silicon Carbide-Derived Carbon Nanocomposite as a Substitute for Mercury in the Catalytic Hydrochlorination of Acetylene. *Nat. Commun.* **2014**, *5*, 3688.

(692) Li, X.; Li, P.; Pan, X.; Ma, H.; Bao, X. Deactivation Mechanism and Regeneration of Carbon Nanocomposite Catalyst for Acetylene Hydrochlorination. *Appl. Catal., B* **2017**, *210*, 116−120.

(693) Choudhary, S.; Qureshi, S. Theoretical Study on the Effect of Dopant Positions and Dopant Density on Transport Properties of a BN Co-Doped SiC Nanotube. *Phys. Lett. A* **2013**, *377*, 430−435.

(694) Khodadad, M.; Baizaee, S. M.; Yuonesi, M.; Kahnouji, H. First-Principles Study of Structural and Electronic Properties of Lithium Doped SiC Nanotubes. *Phys. E* **2014**, *59*, 139−143.

(695) Zhao, M.; Xia, Y.; Li, F.; Zhang, R. Q.; Lee, S.-T. Strain Energy and Electronic Structures of Silicon Carbide Nanotubes: Density Functional Calculations. *Phys. Rev. B: Condens. Matter Mater. Phys.* **2005**, *71*, No. 085312.

(696) Mpourmpakis, G.; Froudakis, G. E.; Lithoxoos, G. P.; Samios, J. SiC Nanotubes: A Novel Material for Hydrogen Storage. *Nano Lett.* **2006**, *6*, 1581−1583.

(697) Wu, R. Q.; Yang, M.; Lu, Y. H.; Feng, Y. P.; Huang, Z. G.; Wu, Y. Q. Silicon Carbide Nanotubes As Potential Gas Sensors for CO and HCN Detection. *J. Phys. Chem. C* **2008**, *112*, 15985−15988.

(698) Gao, G.; Kang, H. S. First Principles Study of NO and NNO Chemisorption on Silicon Carbide Nanotubes and Other Nanotubes. *J. Chem. Theory Comput.* **2008**, *4*, 1690−1697.

(699) Zhao, J.-x.; Xiao, B.; Ding, Y.-h. Theoretical Prediction of the N-H and O-H Bonds Cleavage Catalyzed by the Single-Walled Silicon Carbide Nanotube. *J. Phys. Chem. C* **2009**, *113*, 16736−16740.

(700) Cao, F.; Sun, H. Theoretical Study on the Possibility of Using Silicon Carbide Nanotubes as Dehydrogenation Catalysts for Ammonia-Borane. *RSC Adv.* **2012**, *2*, 7561−7568.

(701) Esrafili, M. D.; Teymurian, V. M.; Nurazar, R. Catalytic Dehydrogenation of Hydrazine on Silicon-Carbide Nanotubes: A DFT Study on the Kinetic Issue. *Surf. Sci.* **2015**, *632*, 118−125.

(702) Esrafili, M. D.; Nurazar, R. Hydrogen Generation from Methylamine Using Silicon Carbide Nanotubes as a Dehydrogenation Catalyst: A Density Functional Theory Study. *J. Mol. Graphics Modell.* **2015**, *55*, 41−47.

(703) Esrafili, M. D.; Nurazar, R. Catalytic Decomposition of Ammonia over Silicon-Carbide Nanotube: a DFT Study. *Struct. Chem.* **2015**, *26*, 799−807.

(704) Esrafili, M. D.; Nurazar, R.; Masumi, V. Adsorption and Decomposition of Formamide over Zigzag (n,0) Silicon-Carbide Nanotubes (n = 5−7): Investigation of Curvature Effects. *Surf. Sci.* **2015**, *637−638*, 69−76.

(705) Leppalahti, J.; Koljonen, T.; Hupa, M.; Kilpinen, P. Selective Catalytic Oxidation of NH_3 in Gasification Gas. 1. Effect of Iron Sinter and Dolomite on the Reactions of NH_3, NO, and O_2 in Gasification Gas. *Energy Fuels* **1997**, *11*, 30−38.

(706) Wang, N.; Tian, Y.; Zhao, J.; Jin, P. CO Oxidation Catalyzed by Silicon Carbide (SiC) Monolayer: A Theoretical Study. *J. Mol. Graphics Modell.* **2016**, *66*, 196−200.

(707) Sinthika, S.; Vala, S. T.; Kawazoe, Y.; Thapa, R. CO Oxidation Prefers the Eley-Rideal or Langmuir-Hinshelwood Pathway: Monolayer vs Thin Film of SiC. *ACS Appl. Mater. Interfaces* **2016**, *8*, 5290−5299.

(708) Feng, J. W.; Liu, Y. J.; Zhao, J. x. Layered SiC Sheets: A Promising Metal-Free Catalyst for NO Reduction. *J. Mol. Graphics Modell.* **2015**, *60*, 132−141.

(709) Peng, Y.; Wang, L.; Luo, Q.; Cao, Y.; Dai, Y.; Li, Z.; Li, H.; Zheng, X.; Yan, W.; Yang, J.; et al. Molecular-Level Insight into How Hydroxyl Groups Boost Catalytic Activity in CO_2 Hydrogenation into Methanol. *Chem.* **2018**, *4*, 613−625.

(710) Chizari, K.; Deneuve, A.; Ersen, O.; Florea, I.; Liu, Y.; Edouard, D.; Janowska, I.; Begin, D.; Pham-Huu, C. Nitrogen-Doped Carbon Nanotubes as a Highly Active Metal-Free Catalyst for Selective Oxidation. *ChemSusChem* **2012**, *5*, 102−108.

(711) Cuong, D.-V.; Truong-Phuoc, L.; Tran-Thanh, T.; Nhut, J.-M.; Nguyen-Dinh, L.; Janowska, I.; Begin, D.; Pham-Huu, C. Nitrogen-Doped Carbon Nanotubes Decorated Silicon Carbide as a Metal-Free Catalyst for Partial Oxidation of H_2S. *Appl. Catal., A* **2014**, *482*, 397−406.

(712) Duong-Viet, C.; Ba, H.; Liu, Y.; Truong-Phuoc, L.; Nhut, J.-M.; Pham-Huu, C. Nitrogen-Doped Carbon Nanotubes on Silicon Carbide as a Metal-Free Catalyst. *Chin. J. Catal.* **2014**, *35*, 906−913.

(713) Duong-Viet, C.; Nhut, J.-M.; Truong-Huu, T.; Tuci, G.; Nguyen-Dinh, L.; Liu, Y.; Pham, C.; Giambastiani, G.; Pham-Huu, C. A Nitrogen-Doped Carbon-Coated Silicon Carbide as a Robust and Highly Efficient Metal-Free Catalyst for Sour Gas Desulfurization in the Presence of Aromatics as Contaminants. *Catal. Sci. Technol.* **2020**, *10*, 5487−5500.

(714) Duong-Viet, C.; Nhut, J.-M.; Truong-Huu, T.; Tuci, G.; Nguyen-Dinh, L.; Pham, C.; Giambastiani, G.; Pham-Huu, C. Tailoring Properties of Metal-Free Catalysts for the Highly Efficient Desulfurization of Sour Gases under Harsh Conditions. *Catalysts* **2021**, *11*, 226.

(715) Ba, H.; Liu, Y.; Truong-Phuoc, L.; Duong-Viet, C.; Mu, X.; Doh, W. H.; Tran-Thanh, T.; Baaziz, W.; Nguyen-Dinh, L.; Nhut, J.-M.; et al. A Highly N-Doped Carbon Phase "Dressing" of Macroscopic Supports for Catalytic Applications. *Chem. Commun.* **2015**, *51*, 14393−14396.

(716) Salimi, A.; Mohamadi, L.; Hallaj, R.; Soltanian, S. Electrooxidation of Insulin at Silicon Carbide Nanoparticles Modified Glassy Carbon Electrode. *Electrochem. Commun.* **2009**, *11*, 1116−1119.

(717) He, C.; Wu, X.; Shen, J.; Chu, P. K. High-Efficiency Electrochemical Hydrogen Evolution Based on Surface Autocatalytic Effect of Ultrathin 3C-SiC Nanocrystals. *Nano Lett.* **2012**, *12*, 1545–1548.

(718) Shen, X.; Pantelides, S. T. Atomic-Scale Mechanism of Efficient Hydrogen Evolution at SiC Nanocrystal Electrodes. *J. Phys. Chem. Lett.* **2013**, *4*, 100–104.

(719) Zhang, P.; Xiao, B. B.; Hou, X. L.; Zhu, Y. F.; Jiang, Q. Layered SiC Sheets: A Potential Catalyst for Oxygen Reduction Reaction. *Sci. Rep.* **2015**, *4*, 3821.

(720) Pan, H.; Zang, J.; Dong, L.; Li, X.; Wang, Y.; Wang, Y. Synthesis of Shell/Core Structural Nitrogen-Doped Carbon/Silicon Carbide and Its Electrochemical Properties as a Cathode Catalyst for Fuel Cells. *Electrochem. Commun.* **2013**, *37*, 40–44.

(721) Pan, H.; Zang, J.; Li, X.; Wang, Y. One-Pot Synthesis of Shell/Core Structural N-Doped Carbide-Derived Carbon/SiC Particles as Electrocatalysts for Oxygen Reduction Reaction. *Carbon* **2014**, *69*, 630–633.

(722) Zang, J.; Wang, Y.; Bian, L.; Zhang, J.; Meng, F.; Zhao, Y.; Lu, R.; Qu, X.; Ren, S. Graphene Growth on Nanodiamond as a Support for a Pt Electrocatalyst in Methanol Electro-Oxidation. *Carbon* **2012**, *50*, 3032–3038.

(723) Liu, C.; Li, Q.; Wu, C.; Zhang, J.; Jin, Y.; MacFarlane, D. R.; Sun, C. Single-Boron Catalysts for Nitrogen Reduction Reaction. *J. Am. Chem. Soc.* **2019**, *141*, 2884–2888.

(724) Zheng, M.; Li, Y.; Ding, K.; Zhang, Y.; Chen, W.; Lin, W. Nitrogen Fixation on Metal-Free SiC(111) Polar Surfaces. *J. Mater. Chem. A* **2020**, *8*, 7412–7421.

(725) Huang, C.; Chen, C.; Zhang, M.; Lin, L.; Ye, X.; Lin, S.; Antonietti, M.; Wang, X. Carbon-Doped BN Nanosheets for Metal-Free Photoredox Catalysis. *Nat. Commun.* **2015**, *6*, 7698.

(726) Inoue, T.; Fujishima, A.; Konishi, S.; Honda, K. Photoelectrocatalytic Reduction of Carbon Dioxide in Aqueous Suspensions of Semiconductor Powders. *Nature* **1979**, *277*, 637–638.

(727) Gondal, M. A.; Ali, M.; Chang, X. F.; Shen, K.; Xu, Q.; Yamani, Z. H. Pulsed Laser-Induced Photocatalytic Reduction of Greenhouse Gas CO_2 into Methanol: A Value-Added Hydrocarbon Product over SiC. *J. Environ. Sci. Health, Part A: Toxic/Hazard. Subst. Environ. Eng.* **2012**, *47*, 1571–1576.

(728) Gondal, M. A.; Ali, M. A.; Dastageer, M. A.; Chang, X. CO_2 Conversion into Methanol Using Granular Silicon Carbide (α6H-SiC): A Comparative Evaluation of 355 nm Laser and Xenon Mercury Broad Band Radiation Sources. *Catal. Lett.* **2013**, *143*, 108–117.

(729) Azzouz, F.; Kacia, S.; Bozetine, I.; Keffous, A.; Trari, M.; Belhousse, S.; Aissiou-Bouanik, S. Photochemical Conversion of CO_2 into Methyl Alcohol Using SiC Micropowder under UV Light. *Acta Phys. Pol., A* **2017**, *132*, 479–483.

(730) Yang, T.-C.; Chang, F.-C.; Peng, C.-Y.; Wang, H. P.; Wei, Y.-L. Photocatalytic Reduction of CO_2 with SiC Recovered from Silicon Sludge Wastes. *Environ. Technol.* **2015**, *36*, 2987–2990.

(731) Han, C.; Lei, Y.; Wang, B.; Wang, Y. In Situ-Fabricated 2D/2D Heterojunctions of Ultrathin SiC/Reduced Graphene Oxide Nanosheets for Efficient CO_2 Photoreduction with High CH_4 Selectivity. *ChemSusChem* **2018**, *11*, 4237–4245.

(732) Han, C.; Wang, B.; Wu, C.; Shen, S.; Zhang, X.; Sun, L.; Tian, Q.; Lei, Y.; Wang, Y. Ultrathin SiC Nanosheets with High Reduction Potential for Improved CH_4 Generation from Photocatalytic Reduction of CO_2. *ChemistrySelect* **2019**, *4*, 2211–2217.

(733) Han, C.; Lei, Y.; Wang, B.; Whu, C.; Zhang, X.; Shen, S.; Sun, L.; Tian, Q.; Feng, Q.; Wang, Y. The Functionality of Surface Hydroxyls on Selective CH_4 Generation from Photoreduction of CO_2 over SiC Nanosheets. *Chem. Commun.* **2019**, *55*, 1572–1575.

(734) Zheng, M.; Li, Y.; Ding, K.; Zhang, Y.; Chen, W.; Lin, W. The Sources of Hydrogen Affect the Productivity and Selectivity of CO_2 Photoreduction on SiC. *Appl. Surf. Sci.* **2021**, *538*, 148010.

(735) Li, H.; Sun, J. Highly Selective Photocatalytic CO_2 Reduction to CH_4 by Ball-Milled Cubic Silicon Carbide Nanoparticles under Visible-Light Irradiation. *ACS Appl. Mater. Interfaces* **2021**, *13*, 5073–5078.

(736) Lauermann, I.; Memming, R.; Meissner, D. Electrochemical Properties of Silicon Carbide. *J. Electrochem. Soc.* **1997**, *144*, 73–80.

(737) Bockris, J. O. M.; Uosaki, K. The Rate of the Photoelectrochemical Generation of Hydrogen at p-Type Semiconductors. *J. Electrochem. Soc.* **1977**, *124*, 1348–1355.

(738) Gao, Y.; Wang, Y.; Wang, Y. Photocatalytic Hydrogen Evolution from Water on SiC under Visible Light Irradiation. *React. Kinet. Catal. Lett.* **2007**, *91*, 13–19.

(739) Yasuda, T.; Kato, M.; Ichimura, M.; Hatayama, T. SiC Photoelectrodes for a Self-Driven Water-Splitting Cell. *Appl. Phys. Lett.* **2012**, *101*, No. 053902.

(740) Ichikawa, N.; Ichimura, M.; Kato, M. Improved Performance of 3C-SiC Photocathodes by Using a pn Junction. *Int. J. Hydrogen Energy* **2017**, *42*, 22698–22703.

(741) Hao, J.-Y.; Wang, Y.-Y.; Tong, X.-L.; Jin, G.-Q.; Guo, X.-Y. Photocatalytic Hydrogen Production over Modified SiC Nanowires under Visible Light Irradiation. *Int. J. Hydrogen Energy* **2012**, *37*, 15038–15044.

(742) Hao, J.-Y.; Wang, Y.-Y.; Tong, X.-L.; Jin, G.-Q.; Guo, X.-Y. SiC Nanomaterials with Different Morphologies for Photocatalytic Hydrogen Production under Visible Light Irradiation. *Catal. Today* **2013**, *212*, 220–224.

(743) Liu, H.; She, G.; Mu, L.; Shi, W. Porous SiC Nanowire Arrays as Stable Photocatalyst for Water Splitting under UV Irradiation. *Mater. Res. Bull.* **2012**, *47*, 917–920.

(744) Li, H.; Shang, H.; Shi, Y.; Yakimova, R.; Syväjärvi, M.; Zhang, L.; Sun, J. Atomically Manipulated Proton Transfer Energizes Water Oxidation on Silicon Carbide Photoanodes. *J. Mater. Chem. A* **2018**, *6*, 24358–24366.

(745) Wang, Y.; Guo, X.; Dong, L.; Jin, G.; Wang, Y.; Guo, X.-Y. Enhanced Photocatalytic Performance of Chemically Bonded SiC-Graphene Composites for Visible-Light-Driven Overall Water Splitting. *Int. J. Hydrogen Energy* **2013**, *38*, 12733–12738.

(746) Yang, J.; Zeng, X.; Chen, L.; Yuan, W. Photocatalytic Water Splitting to Hydrogen Production of Reduced Graphene Oxide/SiC under Visible Light. *Appl. Phys. Lett.* **2013**, *102*, No. 083101.

(747) Chen, J.; Zhang, J.; Wang, M.; Gao, L.; Li, Y. SiC Nanowire Film Grown on the Surface of Graphite Paper and Its Electrochemical Performance. *J. Alloys Compd.* **2014**, *605*, 168–172.

(748) Zhou, X.; Gao, Q.; Li, X.; Liu, Y.; Zhang, S.; Fang, Y.; Li, J. Ultra-Thin SiC Layer Covered Graphene Nanosheets as Advanced Photocatalysts for Hydrogen Evolution. *J. Mater. Chem. A* **2015**, *3*, 10999–11005.

(749) Zhou, X.; Li, X.; Gao, Q.; Yuan, J.; Wen, J.; Fang, Y.; Liu, W.; Zhang, S.; Liu, Y. Metal-Free Carbon Nanotube-SiC Nanowire Heterostructures with Enhanced Photocatalytic H_2 Evolution under Visible Light Irradiation. *Catal. Sci. Technol.* **2015**, *5*, 2798–2806.

(750) Liao, X.; Liu, Z.; Ding, L.; Chen, J.; Tang, W. Photoelectrocatalytic Activity of Flexible PEDOT–PSS/Silicon Carbide Nanowire Films. *RSC Adv.* **2015**, *5*, 99143–99147.

(751) Yang, T.; Chang, X.; Chen, J.; Chou, K.-C.; Hou, X. B-Doped 3C-SiC Nanowires with a Finned Microstructure for Efficient Visible Light-Driven Photocatalytic Hydrogen Production. *Nanoscale* **2015**, *7*, 8955–8961.

(752) Liu, W.; Li, Q.; Yang, X.; Chen, X.; Xu, X. Synthesis and Characterization of N-Doped SiC Powder with Enhanced Photocatalytic and Photoelectrochemical Performance. *Catalysts* **2020**, *10*, 769.

(753) Lu, W.; Wang, D.; Guo, L.; Jia, Y.; Ye, M.; Huang, J.; Li, Z.; Peng, Y.; Yuan, W.; Chen, X. Bipolar Carrier Transfer Channels in Epitaxial Graphene/SiC Core–Shell Heterojunction for Efficient Photocatalytic Hydrogen Evolution. *Adv. Mater.* **2015**, *27*, 7986–7991.

(754) Lu, W.; Guo, L.; Jia, Y.; Guo, Y.; Li, Z.; Lin, J.; Huang, J.; Wang, W. Significant Enhancement in Photocatalytic Activity of High Quality SiC/Graphene Core-Shell Heterojunction with Optimal Structural Parameters. *RSC Adv.* **2014**, *4*, 46771–46779.

(755) Wang, B.; Wang, Y.; Lei, Y.; Wu, N.; Gou, Y.; Han, C.; Xie, S.; Fang, D. Mesoporous Silicon Carbide Nanofibers with *In Situ*

Embedded Carbon for Co-Catalyst Free Photocatalytic Hydrogen Production. *Nano Res.* **2016**, *9*, 886−898.

(756) Wang, B.; Zhang, J.; Huang, F. Enhanced Visible Light Photocatalytic H$_2$ Evolution of Metal-Free g-C$_3$N$_4$/SiC Heterostructured Photocatalysts. *Appl. Surf. Sci.* **2017**, *391*, 449−456.

(757) Baig, U.; Khan, A.; Gondal, M. A.; Dastageer, M. A.; Akhtar, S. Single-Step Synthesis of Silicon Carbide Anchored Graphitic Carbon Nitride Nanocomposite Photo-Catalyst for Efficient Photoelectrochemical Water Splitting under Visible-Light Irradiation. *Colloids Surf., A* **2021**, *611*, 125886.

(758) Han, L.; Digdaya, I. A.; Buijs, T. W. F.; Abdi, F. F.; Huang, Z.; Liu, R.; Dam, B.; Zeman, M.; Smith, W. A.; Smets, A. H. M. Gradient Dopant Profiling and Spectral Utilization of Monolithic Thin-Film Silicon Photoelectrochemical Tandem Devices for Solar Water Splitting. *J. Mater. Chem. A* **2015**, *3*, 4155−4162.

(759) Zhou, W.; Yan, L.; Wang, Y.; Zhang, Y. SiC Nanowires: A Photocatalytic Nanomaterial. *Appl. Phys. Lett.* **2006**, *89*, No. 013105.

(760) Zhu, K.; Guo, L.; Lin, J.; Hao, W.; Shang, J.; Jia, Y.; Chen, L.; Jin, S.; Wang, W.; Chen, X. Graphene Covered SiC Powder as Advanced Photocatalytic Material. *Appl. Phys. Lett.* **2012**, *100*, No. 023113.

(761) Krishnamoorthy, T.; Thavasi, V.; Ramakrishna, S. A First Report on the Fabrication of Vertically Aligned Anatase TiO$_2$ Nanowires by Electrospinning: Preferred Architecture for Nanostructured Solar Cells. *Energy Environ. Sci.* **2011**, *4*, 2807−2812.

(762) Evanoff, K.; Khan, J.; Balandin, A. A.; Magasinski, A.; Ready, W. J.; Fuller, T. F.; Yushin, G. Towards Ultrathick Battery Electrodes: Aligned Carbon Nanotube - Enabled Architecture. *Adv. Mater.* **2012**, *24*, 533−537.

(763) Hong, J.; Meysami, S. S.; Babenko, V.; Huang, C.; Luanwuthi, S.; Acapulco, J.; Holdway, P.; Grant, P. S.; Grobert, N. Vertically-Aligned Silicon Carbide Nanowires as Visible-Light-Driven Photocatalysts. *Appl. Catal., B* **2017**, *218*, 267−276.

(764) Zhang, J.; Chen, J.; Xin, L.; Wang, M. Hierarchical 3C-SiC Nanowires as Stable Photocatalyst for Organic Dye Degradation under Visible Light Irradiation. *Mater. Sci. Eng., B* **2014**, *179*, 6−11.

(765) Haibo, O.; Jianfeng, H.; Xierong, Z.; Liyun, C.; Cuiyan, L.; Xinbo, X.; Jie, F. Visible-Light Photocatalytic Activity of SiC Hollow Spheres Prepared by a Vapor-Solid Reaction of Carbon Spheres and Silicon Monoxide. *Ceram. Int.* **2014**, *40*, 2619−2625.

(766) Xie, Y.; Yang, J.; Chen, Y.; Liu, X.; Zhao, H.; Yao, Y.; Cao, H. Promising Application of SiC without Co-Catalyst in Photocatalysis and Ozone Integrated Process for Aqueous Organics Degradation. *Catal. Today* **2018**, *315*, 223−229.

(767) Xu, H.; Gan, Z.; Zhou, W.; Ding, Z.; Zhang, X. A Metal-Free 3C-SiC/g-C$_3$N$_4$ Composite with Enhanced Visible Light Photocatalytic Activity. *RSC Adv.* **2017**, *7*, 40028−40033.

(768) Chang, F.; Zheng, J.; Wang, X.; Xu, Q.; Deng, B.; Hu, X.; Liu, X. Heterojuncted Non-Metal Binary Composites Silicon Carbide/g-C$_3$N$_4$ with Enhanced Photocatalytic Performance. *Mater. Sci. Semicond. Process.* **2018**, *75*, 183−192.

(769) Baig, U.; Gondal, M. A.; Ansari, M. A.; Dastageer, M. A.; Sajid, M.; Falath, W. S. Rapid Synthesis and Characterization of Advanced Ceramic-Polymeric Nanocomposites for Efficient Photocatalytic Decontamination of Hazardous Organic Pollutant under Visible Light and Inhibition of Microbial Biofilm. *Ceram. Int.* **2021**, *47*, 4737−4748.

(770) Yang, J.; Peng, Y.; Yang, B.; Li, P. Enhanced Photocatalytic Degradation of Rhodamine B over Metal Free SiC/C$_3$N$_4$ Heterostructure under Visible Light Irradiation. *Mater. Res. Express* **2018**, *5*, No. 085511.

(771) Asadzadeh-Khaneghah, S.; Habibi-Yangjeh, A.; Asl, M. S.; Ahmadi, Z.; Ghosh, S. Synthesis of Novel Ternary g-C$_3$N$_4$/SiC/C-Dots Photocatalysts and Their Visible-Light-Induced Activities in Removal of Various Contaminants. *J. Photochem. Photobiol., A* **2020**, *392*, 112431.

(772) Schnabel, C.; Wörner, M.; Gonzalez, B.; del Olmo, I.; Braun, A. M. Photoelectrochemical Characterization of p- and n-Doped Single Crystalline Silicon Carbide and Photoinduced Reductive Dehalogenation of Organic Pollutants at p-Doped Silicon Carbide. *Electrochim. Acta* **2001**, *47*, 719−727.

(773) Huang, D.; Yin, L.; Niu, J. Photoinduced Hydrodefluorination Mechanism of Perfluorooctanoic Acid by the SiC/graphene Catalyst. *Environ. Sci. Technol.* **2016**, *50*, 5857−5863.